1984

Mechanisms Of Thermal And Photochemical Reactions Of Organoplatinum Complexes

Ross Henry Hill

CANADIAN THESES ON MICROFICHE

I.S.B.N.

THESES CANADIENNES SUR MICROFICHE

National Library of Canada
Collections Development Branch

Canadian Theses on
Microfiche Service

Ottawa, Canada
K1A 0N4

Bibliothèque nationale du Canada
Direction du developpement des collections

Service des thèses canadiennes
sur microfiche

NOTICE

The quality of this microfiche is heavily dependent upon the quality of the original thesis submitted for microfilming. Every effort has been made to ensure the highest quality of reproduction possible.

If pages are missing, contact the university which granted the degree.

Some pages may have indistinct print especially if the original pages were typed with a poor typewriter ribbon or if the university sent us a poor photocopy.

Previously copyrighted materials (journal articles, published tests, etc.) are not filmed.

AVIS

La qualité de cette microfiche dépend grandement de la qualité de la thèse soumise au microfilmage. Nous avons tout fait pour assurer une qualité supérieure de reproduction.

S'il manque des pages, veuillez communiquer avec l'université qui a conféré le grade.

La qualité d'impression de certaines pages peut laisser à désirer, surtout si les pages originales ont été dactylographiées à l'aide d'un ruban usé ou si l'université nous a fait parvenir une photocopie de mauvaise qualité.

Les documents qui font déjà l'objet d'un droit d'auteur (articles de revue, examens publiés, etc.) ne sont pas microfilmés.

THIS DISSERTATION
HAS BEEN MICROFILMED
EXACTLY AS RECEIVED

LA THÈSE A ÉTÉ
MICROFILMÉE TELLE QUE
NOUS L'AVONS REÇUE

NL-339 (r. 82/08)

Canada

MECHANISMS OF THERMAL AND PHOTOCHEMICAL REACTIONS OF ORGANOPLATINUM COMPLEXES

by

ROSS H. HILL

Department of Chemistry

Submitted in partial fulfillment

of the requirements for the degree of

Doctor of Philosophy

Faculty of Graduate Studies

The University of Western Ontario

London, Ontario

April, 1984

ABSTRACT

This thesis describes investigations into a variety of thermal and photochemical reactions of organoplatinum complexes.

The mechanism of reaction of tertiary phosphine ligands, L, with $[Pt_2H_2(\mu\text{-}H)(\mu\text{-}dppm)_2]^+$ (dppm = bis(diphenylphosphino)methane)to give $[Pt_2HL(\mu\text{-}dppm)_2]^+$ and H_2 has been studied. The reaction has been shown to proceed through an intermediate, $[Pt_2H_2(\mu\text{-}H)L(\mu\text{-}dppm)_2]^+$, from which intramolecular hydrogen loss occurs. Kinetic studies of the reaction yielded equilibrium constants for intermediate formation, and rate constants for the overall reaction. From these data at a variety of temperatures, activation parameters were obtained and a reaction coordinate energy level diagram for the reductive elimination reaction was constructed. The elimination of H_2 from $[Pt_2H(\mu\text{-}H)Me(\mu\text{-}dppm)_2]^+$ was also studied and found to occur in the same manner. A correlation between the equilibrium constants, for formation of the intermediate and the overall rate constants for reductive elimination was observed, and indicated that the rate of hydrogen loss from the intermediates, $[Pt_2H_2(\mu\text{-}H)L(\mu\text{-}dppm)_2]^+$ and $[Pt_2H(\mu\text{-}H)MeL(\mu\text{-}dppm)_2]^+$, are similar. This explains the much lower reactivity towards reduction of $[Pt_2(\mu\text{-}H)Me_2(\mu\text{-}dppm)_2]^+$ which does not form an intermediate, $[Pt_2(\mu\text{-}H)Me_2L(\mu\text{-}dppm)_2]^+$, in detectable concentrations.

The photochemically induced reductive elimination of hydrogen from $[Pt_2H_2(\mu\text{-}H)(\mu\text{-}dppm)_2]^+$ was also studied. The loss of hydrogen occurs with a quantum yield of .81 (in acetonitrile solution) and .57 (in pyridine solution) to give $[Pt_2H(L)(\mu\text{-}dppm)_2]^+$ (L = solvent). The reaction was found to be intramolecular and is initiated from a singlet

excited state. The photochemical reductive elimination of H_2 from $[Pt_2HMe(\mu\text{-}H)(\mu\text{-}dppm)_2]^+$ and CH_4 from $[Pt_2(\mu\text{-}H)Me_2(\mu\text{-}dppm)_2]^+$ was found to occur in an analogous fashion although with slightly lower quantum yields, (.37 and .34 in acetonitrile respectively; .21 and .30 in pyridine respectively). Photolysis of the complex $[Pt_2Me_3(\mu\text{-}dppm)_2]^+$ in pyridine leads to fragmentation to $[PtMe_2(dppm)]$ and $[PtMe(Py)(dppm)]^+$ with a quantum yield of 0.6. In contrast, photolysis in acetonitrile, acetone or methylene chloride gave reductive elimination of ethane, with quantum yields of 0.1, 1.2±0.3 and 1.0±0.1 respectively. In the case of photolysis in acetonitrile or acetone the product was $[Pt_2HL(\mu\text{-}dppm)_2]^+$ (L = solvent). In methylene chloride, further reactions with solvent and starting material produced $[Pt_2(\mu\text{-}Cl)Me_2(\mu\text{-}dppm)_2]^+$.

The photochemically induced β-elimination reaction of $[Pt_2Et_3(\mu\text{-}dppm)_2]^+$ and $[Pt_2Et(dppm)(\mu\text{-}dppm)_2]^+$ were also studied. The photolysis of $[Pt_2Et_3(\mu\text{-}dppm)_2]^+$ led to the loss of ethylene producing $[Pt_2(\mu\text{-}H)Et_2(\mu\text{-}dppm)_2]^+$. The reaction was very efficient (we estimate a quantum yield greater than 0.5). However, the production of colored impurities precluded a quantum yield measurement. Photolysis of $[Pt_2Et(dppm)(\mu\text{-}dppm)_2]^+$ led to the formation of ethane and $[Pt_2H(dppm)(\mu\text{-}dppm)_2]^+$, with a quantum yield of 5.3×10^{-4}. This quantum yield was insensitive to deuterium substitution of the ethyl group (CH_2CD_3) or to addition of free dppm.

The thermally induced β-elimination of ethane from $[Pt_2Et(dppm)(\mu\text{-}dppm)_2]^+$ was also studied. The reaction followed first order kinetics and the rate constant, $2.0\pm0.3 \times 10^{-5}\ s^{-1}$ at 100°C, was independent of added free dppm or isotope substitution. The rate of the β-elimination reaction did increase in the presence of O_2, yielding

a first order rate constant of $8.5\pm.3 \times 10^{-5}$ s^{-1} at 64°C.

The mechanism of photochemically initiated oxidative addition of isopropyl iodide to $[PtMe_2(phen)]$ (phen = 1,10-phenanthroline) was investigated. The reaction was found to be initiated by a $(d \rightarrow \pi^*)$ triplet excited state abstracting an iodine from isopropyl iodide. The resultant species, $[PtMe_2I(phen)]$, then abstracts a second iodine atom, thus producing, overall, one mole of $[PtMe_2I_2(phen)]$ and two moles of free isopropyl radical per initiation sequence. The oxidative addition product, $[PtMe_2(^iPr)I(phen)]$, was then formed by a chain reaction involving $^iPr\cdot$ attack on $[PtMe_2(phen)]$ producing $[PtMe_2{}^iPr(phen)]$ which abstracted an iodine atom from ^iPrI to regenerate $^iPr\cdot$ and produce $[PtMe_2(^iPr)I(phen)]$. The chain termination step was found to be attack of free isopropyl radical on either the phenanthroline or methyl group of the starting complex, $[PtMe_2(phen)]$. The rate constants for excited state decay to ground state, iodine atom abstraction by the excited state of the complex, and isopropyl radical attack on $[PtMe_2(phen)]$, leading to both propagation and termination of the chain sequence, have been determined.

A brief investigation of the catalysis of the water gas shift reaction by $[Pt_2H_2(\mu\text{-}H)(\mu\text{-}dppm)]^+$ was also undertaken. The rate of the catalysis was found to be first order in initial concentration of $[Pt_2H_2(\mu\text{-}H)(\mu\text{-}dppm)_2]^+$, at a pressure of 7.5 atmospheres CO. Under these conditions, the turnover rate was found to be 3.0±.2 mol H_2 (or CO_2) $(mol[Pt_2H_2(\mu\text{-}H)(\mu\text{-}dppm)_2]^+)^{-1}$ h^{-1}. The turnover rate was found to increase with decreasing carbon monoxide pressure (a rate of 25.2 mol H_2 (or CO_2) $(mol[Pt_2H_2(\mu\text{-}H)(\mu\text{-}dppm)_2]^+)^{-1}$ h^{-1} was found at a pressure of .13 atm CO.). The kinetics of the catalysis are found to be consistent

with the presence of two active catalysts in the catalytic mixture. The complexes present in the catalytic mixture were investigated. In the presence of oxygen, the complex, $[Pt_4(\mu\text{-}CO)_2(\mu\text{-}dppm)_3(Ph_2PCH_2P(O)Ph_2)]$, was recovered. In the absence of oxygen a yellow cluster was recovered. The structure of this complex has not yet been determined.

ACKNOWLEDGEMENT

I would like to express my appreciation and gratitude to Professor R.J. Puddephatt, who always had time, and a considerable amount of patience, to guide and encourage me throughout the course of this work.

I also wish to acknowledge the influence of Professor P. de Mayo who offered both advice and criticism in many helpful discussions.

I would also like to thank J. Stilborn, J. Taylor, Dr. M. Thomson, Dr. J. Stothers, Dr. P.A.W. Dean, Dr. A.K. Azam, and Dr. M.P. Brown for their contributions and assistance.

The financial support given by both the University and NSERC is gratefully acknowledged.

I also wish to thank Ms. S. Tamowski for her skilled preparation of this manuscript.

TABLE OF CONTENTS

LIST OF TABLES

LIST OF FIGURES

ABBREVIATIONS

dppm	bis(diphenylphosphino)methane, P⁀P
phen	1,10-phenanthroline, N⁀N
diars	1,2-bis(dimethylarsino)benzene
γ-picoline	$4\text{-}MeC_5H_4N$
Me	methyl
Et	ethyl
^{i}Pr	isopropyl
Ph	phenyl
ISC	INTER SYSTEM CROSSING
S	singlet
T	triplet
DMPO	5,5-Dimethyl-1-pyrroline-1-oxide

CHAPTER 1

Introduction

1. Introduction

Platinum, and its chemistry, have been central to the development of current principles in both inorganic and organometallic chemistry. To give the reader an appreciation of this, a brief historical sketch of platinum chemistry will be included in this chapter. This will be followed by a description of the oxidation states and coordination geometries which have been observed in the compounds of platinum. The next section will deal with reactions in organometallic chemistry. This will not be an exhaustive survey but an introduction to the reactions studied in this thesis.

The next section will describe, in general terms, the object of this thesis. Because of the general nature of this section a more specific introduction will precede each chapter.

This thesis is, for the most part, a study of the chemistry of a system of binuclear platinum compounds linked by the ligand dppm. As this area is relatively new, a brief description of the associated chemistry will be given at the end of this chapter.

At this juncture I should also point out that, for the purpose of this thesis, I shall define organometallic chemistry to include metal hydrides. The reason for this inclusion is the similarity of the reactions associated with M-H and M-C sigma bonds. A more utilitarian justification is the importance of metal-hydride intermediates in catalysis. For this reason a better understanding of metal-hydride chemistry is expected to have its largest impact in the general field of organometallic chemistry.

1.1 Historical Sketch[1]

Reports of platinum entered Europe from the New World as early as the 16th century. The interest in platinum was partially due to the inability of the Spanish to melt the metal. In fact the earliest known reference to platinum, by Julius Caesar Scaliger, describes it as "... a substance which it has not hitherto been possible to melt by fire or by any of the Spanish arts."

Although isolated Indians were able to work the metal into jewelry, in Europe it was considered valueless. In fact one of the earliest uses of platinum was to adulterate gold, a process which eventually led the King of Spain to ban its importation. In spite of this, samples of platinum entered the European scientific community and were a subject of intense interest in the 18th century. Early in the 19th century the other noble metals in native platinum were separated and identified. The chemistry of platinum was now developing quite rapidly.

The first major scientific contribution founded on platinum chemistry was the observation of catalysis by H. Davy and later E. Davy, although neither grasped the significance of the discovery. It was, however, these reports which led J.W. Döbereiner, who may be termed the founder of the study of catalysis, to undertake his own studies. Shortly thereafter Döbereiner reported the catalysis, by platinum, of the conversion of alcohol to acetic acid followed closely by his reports of the catalytic combination of H_2 and O_2 to produce water. These reports stimulated much activity and it was less than 10 years later, in 1831, that the first patent of catalytic processes was granted to P. Phillips for the manufacture of H_2SO_4 by passing SO_2

and air over finely divided platinum.

It is also notable that the synthesis of the first organo-transition metal compound, reported by W.C. Zeise in 1831, was of a platinum complex, $K[PtCl_3(C_2H_4)]$. The chemistry of platinum also played a significant role in the development of coordination chemistry. It was through the study of ammonia compounds predominantly of cobalt and platinum that eventually led to Werner's coordination theory for which he won the Nobel prize in 1913.

The chemistry of platinum was a subject of intense interest in the early 20th century as the trans-effect was studied in platinum(II) complexes. As theory developed, an appreciation of the application of organoplatinum chemistry to catalysis has made platinum one of the most thoroughly studied transition metals.

1.2 Oxidation States and Stereochemistry of Platinum Complexes

We can define the oxidation state of a metal as the formal charge remaining on the metal after all ligands have been removed in their closed shell configurations and all metal-metal bonds are homolytically cleaved. Platinum complexes have been found in all oxidation states from zero to six.

Table 1.1 gives some examples of platinum complexes in each of these oxidation states.

1.3 Reactions of Organoplatinum Complexes

This thesis is concerned primarily with the mechanisms of the β-elimination (equation 1.1), reductive elimination (equation 1.2), and oxidative addition (equation 1.3) reactions.[9]

$$L_n,M^n\text{-}CH_2CH^*R_2 \rightarrow L_n,M^n\text{-}H^* + CH_2CR_2 \qquad \ldots(1.1)$$

TABLE 1.1

Platinum Oxidation States

Oxidation State	Coordination Number	Geometry	Compound	Ref.
0	4	Tetrahedral	$[Pt(PF_3)_4]$	2
	3	Distorted trigonal planar	$[Pt(PPh_3)_3]$	3
	2	Linear	$[Pt(PPh^tBu_2)_2]$	4
I	4	Square planar	$[Pt_2(CNMe)_6]^{2+}$	5
II	6	Octahedral	$[Pt(NO)Cl_5]^{2-}$	6
	5	Trigonal bipyramidal	$[Pt(SnCl_3)_5]^{3-}$	6
	4	Square planar	$K_2[PtCl_4]$	6
III	6	Octahedral	$[Pt_2Me_4(\mu\text{-}OC(CF_3)\text{-}O)_2(\gamma\text{-picoline})_2]$	7
IV	6	Octahedral	$K_2\underline{fac}\text{-}[Pt(NO_2)_3Cl_3]$	8
V	6	Octahedral	$[Xe\Gamma][PtF_6]$	6
VI	6	Octahedral	$[PtF_6]$	6

$$L_n,M^nAB \rightarrow L_n,M^{n-2} + AB \qquad ...(1.2)$$

$$L_n,M^n + AB \rightarrow L_n,M^{n+2}AB \qquad ...(1.3)$$

The latter two reactions involve a change of two in both oxidation state and coordination number. In platinum, which has its three most common oxidation states ((0), (II) and (IV)) separated by two, a wide variety of oxidative addition and reductive elimination reactions are known.

As both the β-elimination and reductive-elimination reactions studied in this thesis are from binuclear complexes a brief survey of mechanisms encountered in mononuclear complexes is given in section 1.3.1 and 1.3.2.

The oxidative addition reaction studied in chapter 6 involves the platinum(II) complex $[PtMe_2(phen)]$ and its reaction with iso-propyliodide. A brief survey of mechanisms of oxidative addition reactions is included in the introduction to chapter 6.

1.3.1 The β-Elimination Reaction

The β-elimination reaction is most easily illustrated by considering the reaction of trans-$[C_2H_5PtCl(PPh_3)_2]$, equation (1.4).[10]

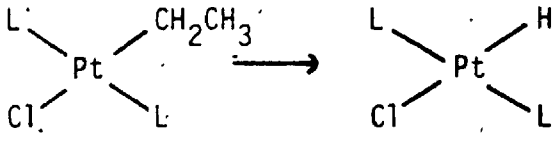

$$+ \ C_2H_4 \qquad ...(1.4)$$

As can be seen, the net reaction involves transfer of a β-hydrogen from the alkyl chain to the platinum and loss of ethylene. In this case the reaction may be reversed by treatment with ethylene.

A more common situation in platinum(II) chemistry, in which the platinum hydride species is unstable, is illustrated by the decomposition of $[Pt(C_4H_9)_2(PPh_3)_2]$ (Scheme 1.1).[11,12] The evidence for this mechanism is as follows. n-Butane and 1-butene were formed in a 1:1 ratio. The rate of the reaction was decreased in the presence of excess phosphine. The reaction was shown to be intramolecular by a mixture of $[Pt(CH_2CD_2CH_2CH_3)_2(PPh_3)_2]$ and $[Pt(n\text{-}C_8H_7)_2(PPh_3)_2]$; the octane formed showed no deuterium incorporation.

In the absence of added phosphine, the dissociation of PPh_3 was found to be rate determining whereas, in the presence of excess phosphine, reductive elimination was found to be the rate limiting step.

The importance of β-elimination as a decomposition pathway is illustrated by the much higher thermal stability of methylplatinum(II) complexes, where no β-hydrogens exist, compared with ethyl and higher n-alkyl complexes.[13,14] Recently, evidence has been collected which indicates that, following the creation of a vacant coordination site, β-elimination occurs with near zero activation energy[15] in some systems. This is consistent with the observed chemistry of platinum(II) where the β-elimination has been found to precede or follow the rate limiting step; it has not yet been identified as the rate limiting step.

The β-elimination reaction may also be initiated photochemically. One example of this involves the thermally stable thorium complex $[Th(\mu^5\text{-}C_5H_5)_3(i\text{-}C_3H_7)]$.[16] Photolysis leads to the production of equimolar propylene and propane. The authors interpreted this in terms of β-elimination of hydride followed by reductive elimination of propane (equation (1.5)).

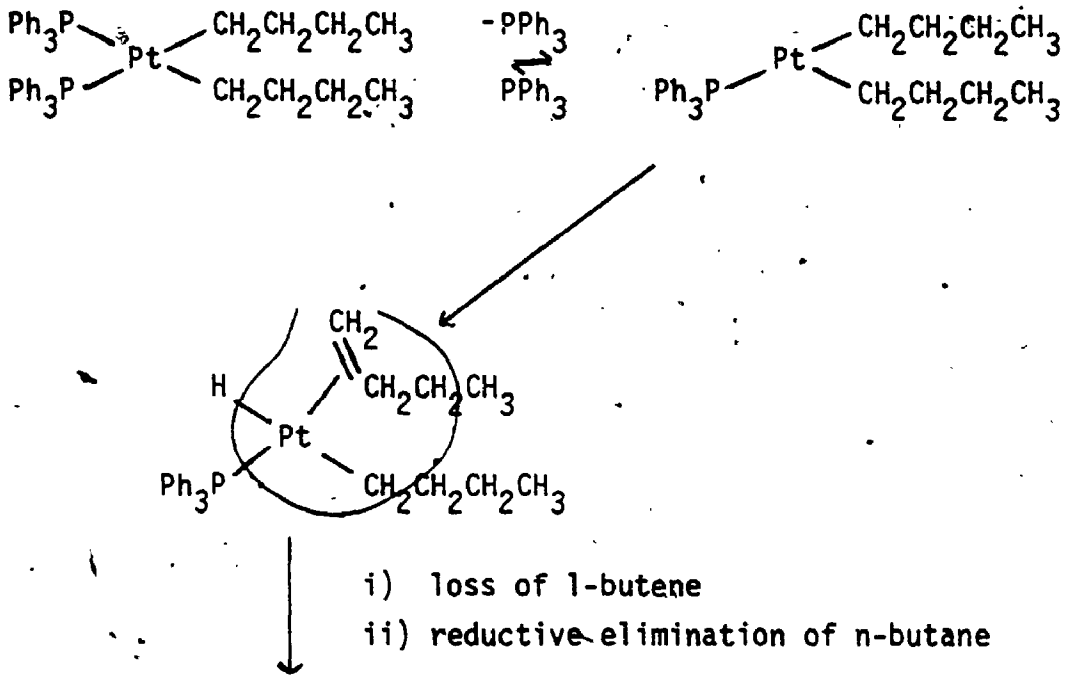

$$CH_2 = CHCH_2CH_3 + CH_3CH_2CH_2CH_3 + Pt^0 + PPh_3$$

Scheme 1.1

$$2[Th(\eta^5\text{-}C_5H_5)_3(i\text{-}C_3H_7)] \xrightarrow{h\nu} CH_2CHCH_3 + Th(\eta^5\text{-}C_5H_5)_3$$

$$+$$

$$(\eta^5\text{-}C_5H_5)_3Th(C_3H_7)(H)$$

$$\downarrow$$

$$Th(\eta^5\text{-}C_5H_5)_3 + C_3H_8 \qquad \ldots(1.5)$$

1.3.2 The Reductive Elimination Reaction

The reductive elimination reaction is a second means by which organoplatinum complexes may decompose. To illustrate this reaction, we will consider the formation of alkanes, RH, by reductive elimination from alkyl hydrides such as cis-$[PtHR(PPh_3)_2]$.[17] The reaction (equation (1.6)) results in a net decrease in oxidation state from platinum(II) to

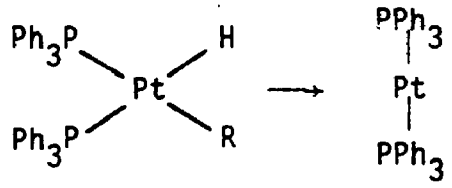

$$+ \ HR \qquad \ldots(1.6)$$

platinum(0). This reaction is facile and elimination of alkane occurs readily at room temperature. The reaction was shown to be intramolecular by deuterium labelling studies. The rate was independent of added phosphine and increased with bulk of the alkyl group as follows, R = Ph > Et > Me > CH_2CH = CH_2.[12] The mechanism proposed for this process is a concerted breaking of the metal-alkyl and metal-hydrogen bonds and formation of the C-H bond in the resulting alkane (Structure 1.1).

Photochemically induced reductive elimination from platinum is also known to occur. The photolysis of $[Br_2PtCH_2CH_2CH_2(NCCH_3)_2]$ leads

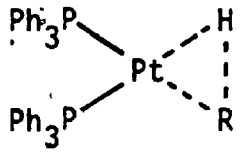

Structure 1.1

primarily to reductive elimination of the alkyl group as cyclopropane (equation (1.7)).[18]

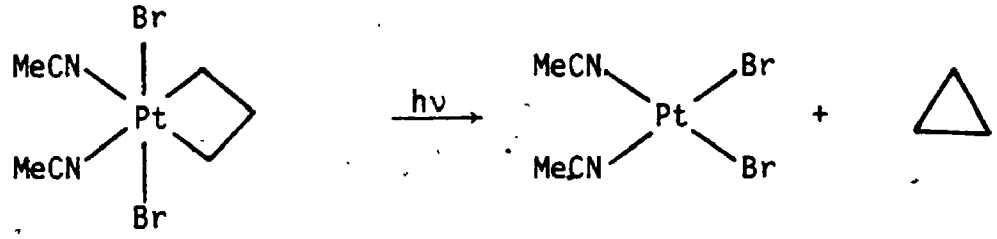

...(1.7)

1.4 The Object of this Thesis

This thesis is primarily concerned with investigation of some basic questions about reactivity and mechanism in organoplatinum chemistry. The two questions are the following:- 1) What are the different features of a photochemically *vs* thermally induced β-elimination, oxidative addition or reductive elimination reaction? 2) Does the inclusion of a second platinum alter the behaviour, from an energetic or mechanistic view, in these types of reactions of organoplatinum complexes?

The first question is of importance from several viewpoints. The field of organometallic photochemistry is, with the exception of metal carbonyls, still in its infancy. It is hoped that the study of organometallic photochemistry may lead to useful synthetic processes which are not available by thermal activation. An insight into the mechanisms

of organometallic photochemistry may also aid in the design of both photocatalysts and solar energy systems.

The second question is of interest as several mechanisms, which are not possible in a mononuclear system, must be considered in binuclear systems. One example of this is shown for the reductive elimination reaction where the transition state of a mononuclear system (structure 1.2) is compared with possible binuclear transition states (structures 1.3 and 1.4).

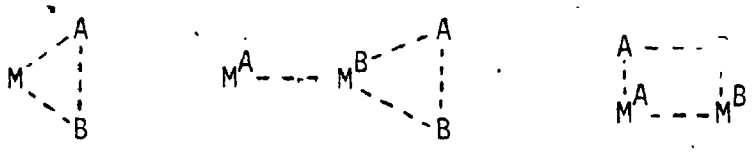

1.2 1.3 1.4

In structure 1.3 the second metal atom (M^A) may stabilise the transition state by electronic interaction with M^B. In the example of structure 1.4 a true binuclear transition state is shown, this mechanism would be impossible without M^A.

The study of bimetallic complexes may identify lower energy pathways, for reactions analogous to those found in mononuclear systems, or entirely new chemical transformations. Very little progress has been made in the elucidation of mechanisms of reaction of binuclear organometallic complexes.

1.5 Binuclear Platinum Chemistry

All the binuclear complexes studied in this work possess the same basic framework of $[Pt_2Cl_2(\mu\text{-dppm})_2]$ (1:5). In this complex the two platinum(I) centers are held together by two bridging dppm ligands. A platinum-platinum bond and two chloride ligands make up the coordination sphere.[19-22]

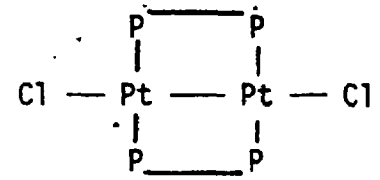

1.5

The $Pt_2(\mu\text{-dppm})_2$ structural frame is quite stable and the complex (1.5) undergoes a variety of reactions in which this unit remains intact. The terminal chloride ligands may be displaced by neutral[23] (equation (1.8)) or anionic[20] (equation (1.9).) ligands.

$$1.5 + 2PPh_3 \rightarrow [Pt_2(PPh_3)_2(\mu\text{-dppm})_2]^{2+} + 2Cl^- \quad \ldots(1.8)$$

$$1.5 + 2Br^- \rightarrow [Pt_2Br_2(\mu\text{-dppm})_2] + 2Cl^- \quad \ldots(1.9)$$

In addition, to the reactions of the terminal chloride ligands, relations involving insertion into the platinum-platinum bond, forming "A-frame" structures, also occur, in which the $Pt_2(\mu\text{-dppm})_2$ framework remains intact. Some examples of this are shown in scheme 1.2.[24]

The reduction of 1.5 by $NaBH_4$ results in the formation of $[Pt_2(\mu\text{-H})H_2(\mu\text{-dppm})_2]^+$ (1.6).[25] This complex, 1.6, contains a bridging

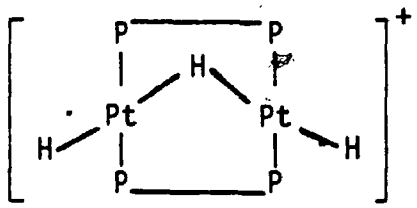

1.6

hydride, which is bound through a three centre two electron bond. An alternate route to the complex 1.6 is by reduction of the monomeric

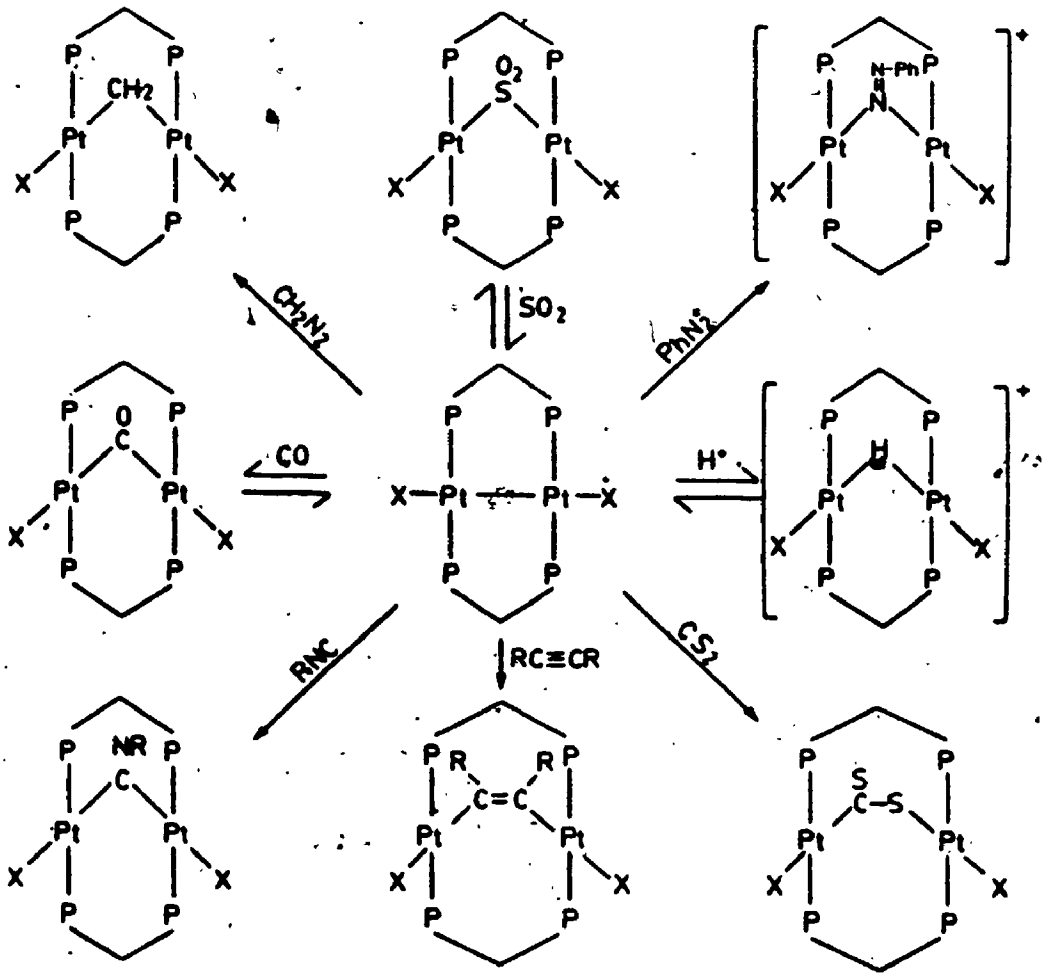

Scheme 1.2

complex $[PtCl_2(dppm)]$, and is the preparation generally used.

The trihydride complex, 1.6, has been shown to undergo reductive elimination of dihydrogen in the presence of two electron donor ligands such as phosphines,[26,27] carbon monoxide[28] and isocyanides[29] according to equation 1.10

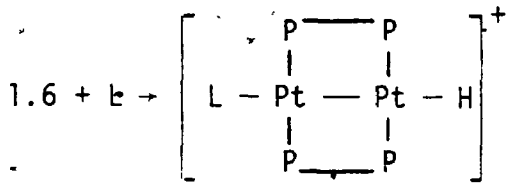

$$1.6 + L \rightarrow [L - Pt(\mu\text{-}dppm)Pt - H]^+ + H_2 \qquad \ldots(1.10)$$

$L = PPh_3$, dppm
$= CO$
$= CNR$

This reaction involves a net two electron reduction in which each platinum(II) is reduced to platinum(I). The A-frame structural unit of 1.6 is general and the corresponding methyl complexes $[Pt_2(\mu\text{-}H)(Me)_{2-n}H_n(\mu\text{-}dppm)_2]^+$ (n = 0 (1.7), n = 1 (1.8)) have been prepared as shown in scheme 1.3.[30,31]

The totally methylated analogue $[Pt_2Me_3(\mu\text{-}dppm)_2]^+$ (1.9) does not have the A-frame structural unit. Its structure, as confirmed by single crystal diffraction,[32] consists of two platinum(II) centres, one with cis and the other with trans phosphorus coordination. A Pt → Pt

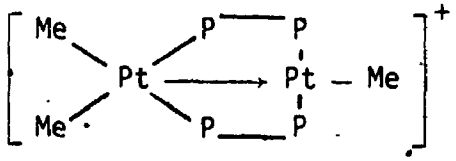

1.9

$[Pt_2Me_3(\mu\text{-dppm})_2]^+ \xrightarrow{NaBH_4}$ 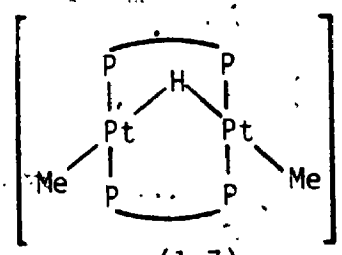

(1.7)

$[Pt_2Cl_2(\mu\text{-}CH_2)(\mu\text{-dppm})_2]^+ \xrightarrow{H^+} [Pt_2Cl(\mu\text{-}Cl)Me(\mu\text{-dppm})_2]^+$

$\downarrow NaBH_4$

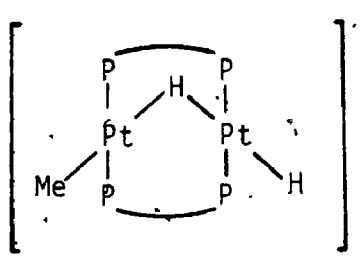

(1.8)

Scheme 1.3

coordinate bond is also present such that the second platinum(II) has square planar geometry. Chapters 2, 3 and 4 describe the study of reductive elimination from these cationic complexes (1.6-1.9) by both thermal and photochemical activation.

The ethyl analogue of 1.9, $[Pt_2Et_3(\mu\text{-dppm})_2]^+$, (1.10), has been shown to β-eliminate according to equation (1.11) and a mechanistic study

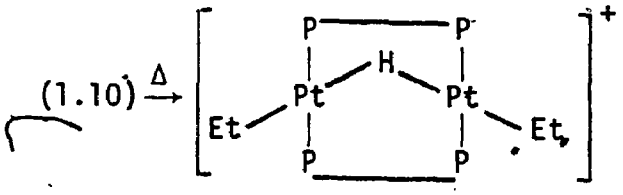

...(1.11)

has been published.[16,33] The ethyl platinum(I) complex $[Pt_2Et(dppm)(\mu\text{-dppm})_2]^+$ (1.11) was recently synthesized by the reaction of $[Pt_2(\mu\text{-dppm})_3]$ with ethyl iodide (equation (1.12)).[34]

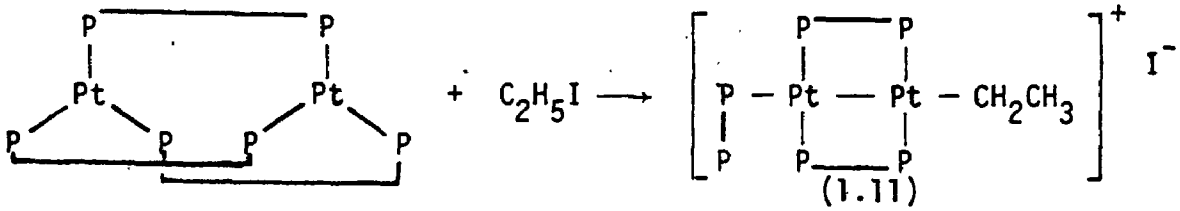

...(1.12)

The mechanism of β-elimination from complex 1.10 and 1.11 by both thermal and photochemical activation form the topic of Chapter 5.

A study of the catalysis of the water gas shift reaction by 1.6 is also included (Chapter 7) in this thesis.

CHAPTER 2

The Mechanism of Ligand Induced Reductive Elimination of Hydrogen from $[Pt_2H_2(\mu\text{-}H)(\mu\text{-}dppm)_2]^+$

2. Introduction

There has been considerable interest in the mechanisms of activation of small molecules by transition metal clusters, with the long-term aims of developing and understanding cluster catalysis and of modelling the chemisorption of small molecules on metal surfaces.[35-37] Oxidative addition or reductive elimination of hydrogen is relevant to many catalytic reactions, and there have been several studies of such reactions with binuclear or polynuclear complexes.[27,35-44] Before considering the mechanisms proposed for reductive elimination from these polynuclear systems it is useful to review what is known about reductive elimination from mononuclear complexes.

From 18-electron complexes, an intramolecular concerted cis-reductive elimination of H_2 has been established in several cases (equations (2.1) and (2.2), L = tertiary phosphine or phosphite).[45,46]

$$[IrH_2(CO)_2L_2]^+ \xrightarrow{-H_2} [Ir(CO)_2L_2]^+ \xrightarrow[fast]{L} [Ir(CO)_2L_3]^+ \qquad \ldots(2.1)$$

$$[CoH_2L_4]^+ \xrightarrow{-H_2} [CoL_4]^+ \xrightarrow[fast]{L} [CoL_5]^+ \qquad \ldots(2.2)$$

A similar mechanism was initially proposed for reductive elimination of H_2 from the 16-electron complexes $[PtH_2L_2]$,[47,48] but more recent studies suggest that an associative mechanism may operate. Thus, the reductive elimination occurs readily in the presence of π-acceptor ligands like CO, but the complexes are otherwise thermally stable.[49,50] Theoretical studies indicate that reductive elimination from $[PtH_2L_2]$ must occur from the cis isomer, but that the activation energy should

be 100-150 kJ mol^{-1}.[51,52] Perhaps coordination of CO lowers this activation energy. In other reductive eliminations from square planar platinum(II) complexes, involving C-C or C-H bond formation, added ligand may retard, accelerate or have no effect on the rates of reduction.[53-55] The situation is complex and not completely understood, and the above mechanistic conclusions for $[PtH_2L_2]$ must be regarded as tentative until more complete studies are reported. The only detailed mechanistic investigation of H_2 elimination from a cluster system was that of Keister et al.[56] These authors studied the elimination of H_2 from a triruthenium cluster, shown in equation (2.3)

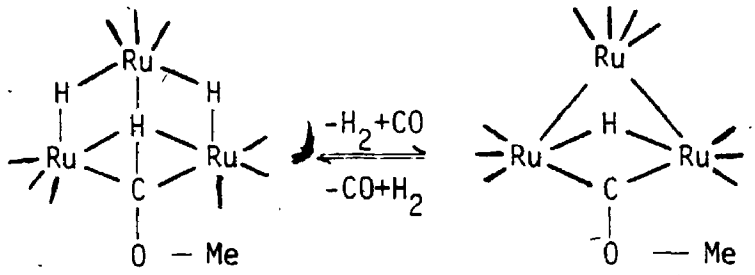

...(2.3)

and found both the activation parameters and isotope effects consistent with a three-center transition state at a single metal site. In contrast to this a true dinuclear mechanism was proposed to account for reductive elimination of hydrogen from $[((n^5\text{-}C_5H_5)FeH(CO))_2(dppe)]$ (equation (2.4)).[44]

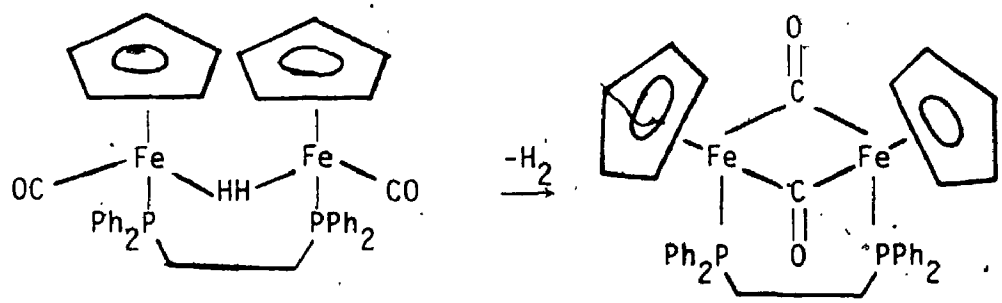

...(2.4)

In this case the authors argued that the rearrangement required for a mononuclear elimination would not occur as the initial complex is both coordinatively and electronically saturated. This observation led to the suggestion that dihydrogen is eliminated in a synchronous manner involving both metal centres. Similar binuclear elimination mechanisms have been proposed by Bitterwolf for dihydrogen elimination involving iron and chromium complexes[57,58] (equations (2.5),(2.6)).

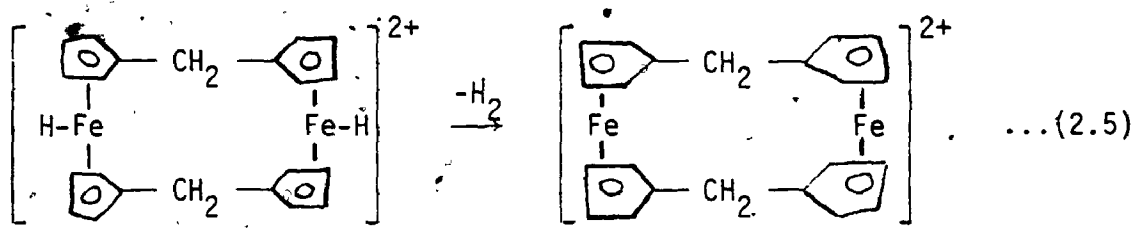

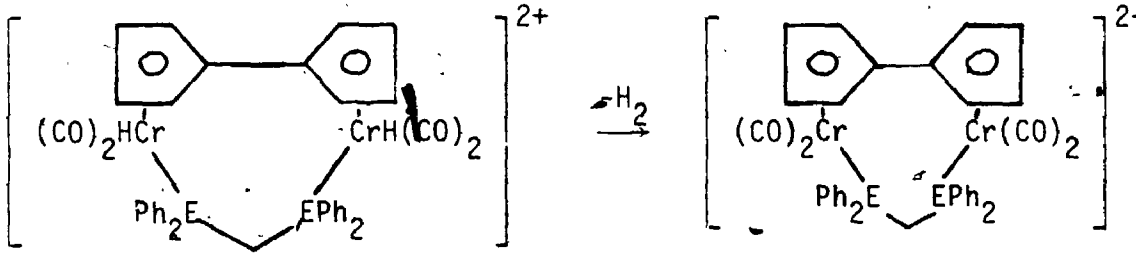

It should be noted that in the latter case (equation (2.6)) the dimeric species is not isolated but fragments to mononuclear complexes. Hence the actual elimination may occur by reaction of the monomers formed.

Although, the binuclear mechanisms proposed are consistent with the observed reactions, it should be noted that mononuclear mechanisms may be proposed to account for the observed reactions.[59] In some cases what was thought initially to be a binuclear reductive elimination reaction was in fact a result of fragmentation and subsequent reaction of the resultant mononuclear compounds. One example of this is

elimination of acetone from $[(\eta^5\text{-}C_5H_5)_2Co_2Me_2(\mu\text{-}CO)_2]$, illustrated in Scheme 2.1.

The reductive elimination of H_2 from the cationic binuclear platinum hydride $[Pt_2H_2(\mu\text{-}H)(\mu\text{-}dppm)_2]^+$, (Ia), dppm = $Ph_2PCH_2PPh_2$, has been shown to be induced by addition of soft donor ligands, L, according to equation (2.7).[27,28]

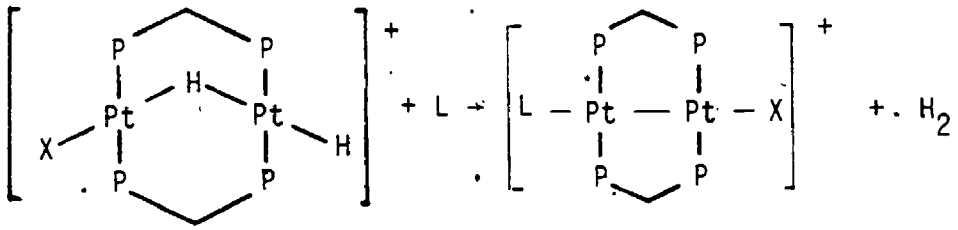

Ia, X = H II, X = H

Ic, X = Me, IIh, X = Me, L = PPh_3 ...(2.7)

P⌒P = dppm

Reactive ligands include tertiary phosphines, isocyanides and carbon monoxide, and the reactions are probably significant in the catalysis of the Water Gas Shift reaction by (Ia).[28] In addition, reactions of alkynes, thiols and diphenylphosphine with (Ia) appear to occur according to equation (2.7) but with subsequent rearrangements.[29,60] The similar complex $[Pt_2HMe(\mu\text{-}H)(\mu\text{-}dppm)_2]^+$ (Ic) undergoes an analogous reaction with H_2 loss on reaction with phosphines (equation (2.7)).[61] It should be noted that loss of CH_4 from (Ic), while not induced by phosphines, may be induced by reaction with an alkyne.[30] In contrast to this the complex $[Pt_2Me_2(\mu\text{-}H)(\mu\text{-}dppm)_2]^+$ (Id) undergoes no reaction upon treatment with phosphine. The reductive elimination of hydrogen from (I) is ideal for study as the reaction is quantitative and no mononuclear species are formed.[27] In addition, the use of two bridging dppm ligands, excludes facile fragmentation to form mononuclear

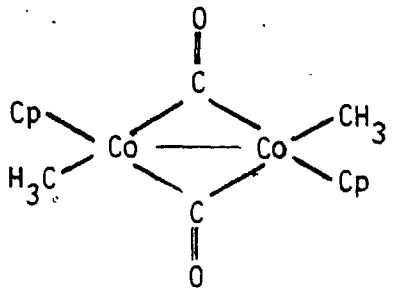

A ⟶ CH_3CCH_3 + $[Co_x(Cp)_y(CO)_z]$ clusters

A ⇌ $2[CpCo(CO)CH_3]$ ⟶

$[CpCo(CO)(CH_3)_2]$ + ["CpCoCO"]

B

B ⟶ CH_3CCH_3 + ["CpCo"]

['CpCoCO"] + ["CpCO"] ⟶ $[Co_x(Cp)_y(CO)_z]$ clusters

Scheme 2.1

intermediates and holds the platinum(II) centers in close proximity, which is expected to enhance the probability of a binuclear reaction mechanism.

2.1 Results

2.1.1 Characterisation of the Products

The reaction of (Ia) according to equation (2.7) has been studied earlier with L = PPh_3, $PMePh_2$, PMe_2Ph and η'-dppm and the products (IIa-d) were characterised.[27] The structure of product (IId) was determined crystallographically and the other products were assigned by their analogous ^{31}P and ^{1}H NMR spectra. These products can all be obtained by the addition of a phosphine to Ia, both in CH_2Cl_2 solution, at room temperature. Upon addition, the pale yellow solution becomes yellow and dihydrogen gas is evolved. The new products L = $PPh_2(2\text{-}MeC_4H_4)$, $PPh_2(4\text{-}MeC_4H_4)$ and $P(4\text{-}ClC_4H_4)_3$ (IIe-g) were all prepared by this route and the products recovered by precipitation with n-pentane. The structure of the complexes(II e-g) were then confirmed by I.R. and ^{1}H NMR spectrum (Table 2.1). The I.R. spectra all show an absorption in the region of 2000 cm^{-1} characteristic of a platinum hydride. The ^{1}H NMR spectra consist of the sum of the spectra due to various isotopomers of (II). The nucleus ^{195}Pt (I = 1/2) is 33.8% abundant whereas the other isotopes have I = 0. From an NMR point of view, we can write the following 4 isotopomers for an unsymmetrical platinum dimer.

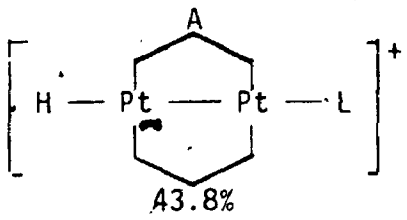

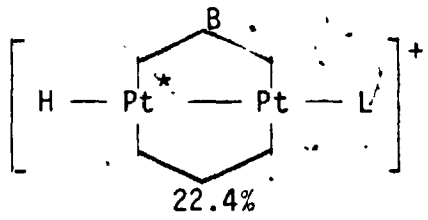

TABLE 2.1

Spectroscopic data for complexes (II)[a]

L	PtH resonance δ(H) ppm	^1J(PtH) Hz	^3J(PH)[b] Hz	^2J(PH)[c] Hz	^3J(PH)[c] Hz	CH_2P resonance δ(H) Hz	^3J(PtH)[d] Hz	ν(PtH)[e] cm^{-1}
PPh_3	-8.97	1005	45	9.5	9.5	4.98	40,72	2006
$P(4\text{-}ClC_6H_4)_3$	-9.27	1008	46	17.5	10.8	5.07	32,70	2020
$PPh_2(4\text{-}MeC_6H_4)$[f]	-8.86	1013	44	9.8	9.8	5.00	35,65	2010
$PPh_2(2\text{-}MeC_6H_4)$[g]	-9.49	1018	46	16	8	5.06	35,72	2025

[a] solvent

[b] trans doublet coupling J(PPtPtH)

[c] couplings to dppm phosphorus

[d] two values due to non-equivalent Pt centers

[e] nujol mull

[f] δ(MeC) 2.32 s

[g] δ(MeC) 2.60 s

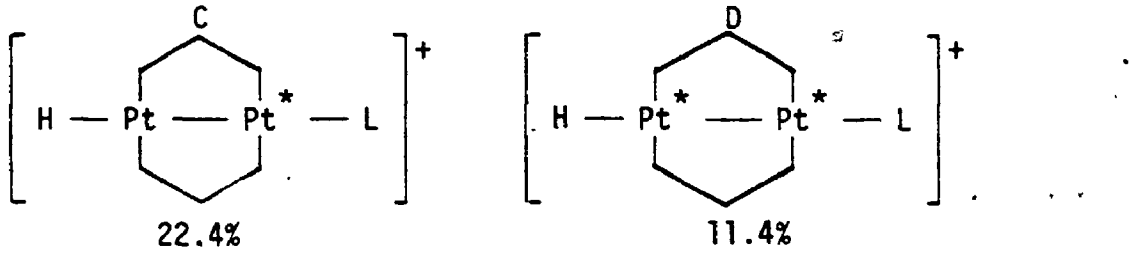

The ^1H spectrum resulting from A is expected to be a singlet of intensity 1. Isotopomers B and C should each give a doublet splitting (B; $^1J(PtH)$; C; $^2J(PtH)$) of intensity 0.5. In the complexes (IIa), and (IIe-g) the coupling $^2J(Pt-H)$ was not observed. However, it is observed in the case of (IIc). In addition to this, the hydrogen phosphorus coupling is also observed. This results in each peak being split into a doublet [trans $^3J(PH)$] of triplets [cis $^2J(PH)$] of triplets [cis $^3J(PH)$].

The reaction of (Ic) with PPh_3 has been established previously and the product (IIh) has been characterised.[30]

2.1.2 Proof of Intramolecular Reaction

In order to determine if the elimination of H_2 was intermolecular or intramolecular, the deuterium substituted complex $[Pt_2(\mu\text{-}D)D_2(\mu\text{-}dppm)_2]^+$, (Ib), was prepared. This complex was prepared by the method generally used for preparation of (Ia) with a few revisions. The $[PtCl_2(dppm)]$ monomer was suspended in MeOD and reduced by the addition of excess $NaBD_4$ as a solid. The product of this reaction was then recovered by filtration. This solid product was then extracted with CH_2Cl_2, and the CH_2Cl_2 extract was added to a methanolic solution of NH_4PF_6. This led to crystallization of (Ib) as the PF_6^- salt.

The IR spectrum (Ib) showed (Pt-D) at 1530 cm^{-1}. Complex (Ia) has ν(Pt-H) at 2113 cm^{-1}. The observed peak at 1530 cm^{-1} is within 2% of the expected value of ~1500 cm^{-1}.

The intramolecular nature of this reaction was then shown by mass spectroscopic analysis of the gas produced from a mixture of Ia and Ib with L. For this study, excess PPh_3 was combined with Ia and Ib (also blanks were done with each individually) and CH_2Cl_2 was distilled into the tube at -78°C. The samples were then warmed to room temperature to ensure reaction and the gas evolved was analyzed by its mass spectrum. The results (Table 2.2) indicate that (Ia) and (Ib), when reacted with L, evolve H_2 and D_2 and an insignificant amount of HD.

2.1.3 The Detection and Characterization of Intermediates

Kinetic studies (vide infra) showed that reaction (2.7) occurs by an associative mechanism involving an intermediate or transition state of stoichiometry [Ia.L], (III), and attempts were made to identify this.

The $^1H\{^{31}P\}$ (Tables 2.3) and $^{31}P\{^1H\}$ NMR spectra of the adduct (IIIa) L = PPh_3, at -90°C gave useful structural data. For these studies a weighed amount of triphenylphosphine was added to a solution of (Ia) of known concentration in CD_2Cl_2 at -78°C, to ensure that no reaction to give (IIa) occurred, and the solution was then inserted into the pre-cooled probe of the NMR spectrometer. Under these conditions, the spectra showed the presence of an equilibrium mixture of (Ia) and (IIIa) as the only platinum-containing species, with the equilibrium favoring (IIIa) as discussed below. In the hydride region of the ^1H NMR spectrum, three resonances of equal intensity due to (IIIa) were observed (Figure 2.1). One of these (δ-9.65) had satellites due to the

TABLE 2.2

Analysis of Isotopic Composition of H_2/D_2 by Mass Spectroscopy

	Mass (g)				Intensity		
Component	Ia	Ib	PPh_3	Mass# 1	2	3	4
	.05	0	.1	0	1	0	0
	0	.05	.1	0	9.5	21	147
	.025	.025	.1	0	123	34	147
	0	0	.1	7	16	0	0

Figure 2.1. Low temperature $^{1}H\{^{31}P\}$ NMR spectra at 100 MHz of (IIIa) in the PtH region. Spectra recorded at (a) -90°C; (b) -80°C; (c) -60°C; (d) -40°C; (e) -20°C. For labelling see Scheme.

coupling $^{1}J(PtH)$535 Hz of intensity one half of the center peak, proving the presence of a bridging hydride.[25] For comparison, (Ia) gives $\delta(\mu\text{-H})$ -5.86, $^{1}J(PtH)$540 Hz.[25] In (IIIa) the two platinum centers must be non-equivalent and it is necessary to assume approximately equal $^{1}J(PtH)$ values. In addition, there were two PtH resonances each with the approximately 1:1:4:1:1 intensity ratio due to coupling to ^{195}Pt characteristic of terminal hydride signals in binuclear platinum complexes.[25] For one of these resonances, the parameters [δ-4.93, $^{1}J(PtH)1140$, $^{2}J(PtH)105$ Hz] resemble those for the terminal hydrides of Ia[δ-6.86, $^{1}J(PtH)1138$, $^{2}J(PtH)103$ Hz], but for the other resonance the couplings were considerably lower [δ-12.38, $^{1}J(PtH)765$, $^{2}J(PtH)95$ Hz].

The $^{31}P\{^{1}H\}$ NMR spectrum (40.5 MHz) of (IIIa) at -80°C contained three resonances with intensity ratios of 2:2:1. The first two appeared as complex multiplets with unresolved fine structure and are assigned to the dppm phosphorus atoms [δ12.24 ppm, $^{1}J(PtP)2720$ and δ-5.00 ppm, $^{1}J(PtP)3125$ Hz], while the peak of intensity of one is assigned to coordinated PPh_3[δ6.0 ppm, $^{1}J(PtP)2350$ Hz]. A peak due to free PPh_3 was also observed (δ-9.8 ppm). $^{31}P\{^{1}H\}$ NMR spectra at 81 MHz were also recorded to confirm these assignments (Figure 2.2).

As the sample was warmed, the two separate peaks due to dppm phosphorus atoms broadened and then coelesced, giving an average chemical shift and $^{1}J(PtP)$ coupling constant [δ4.04 ppm, $^{1}J(PtP)2965$, $^{3}J(P^{A}P^{A''}) + {}^{3}J(P^{A}P^{A'''})75$, $^{3}J(P^{A}P^{A''}) - {}^{3}J(P^{A}P^{A'''})50$ Hz], while the $^{1}J(PtP)$ coupling to the PPh_3 was lost and an average signal due to free and coordinated PPh_3 was seen (Figure 2.2). Similarly in the ^{1}H NMR spectra, the two terminal Pt-H resonances broadened and coalesced as the temperature was raised from -90°C (Table 2.3, Figure 2.1) but the bridging hydride resonance was not significantly changed. These data indicate a fluxional process as shown in equation (2.8).

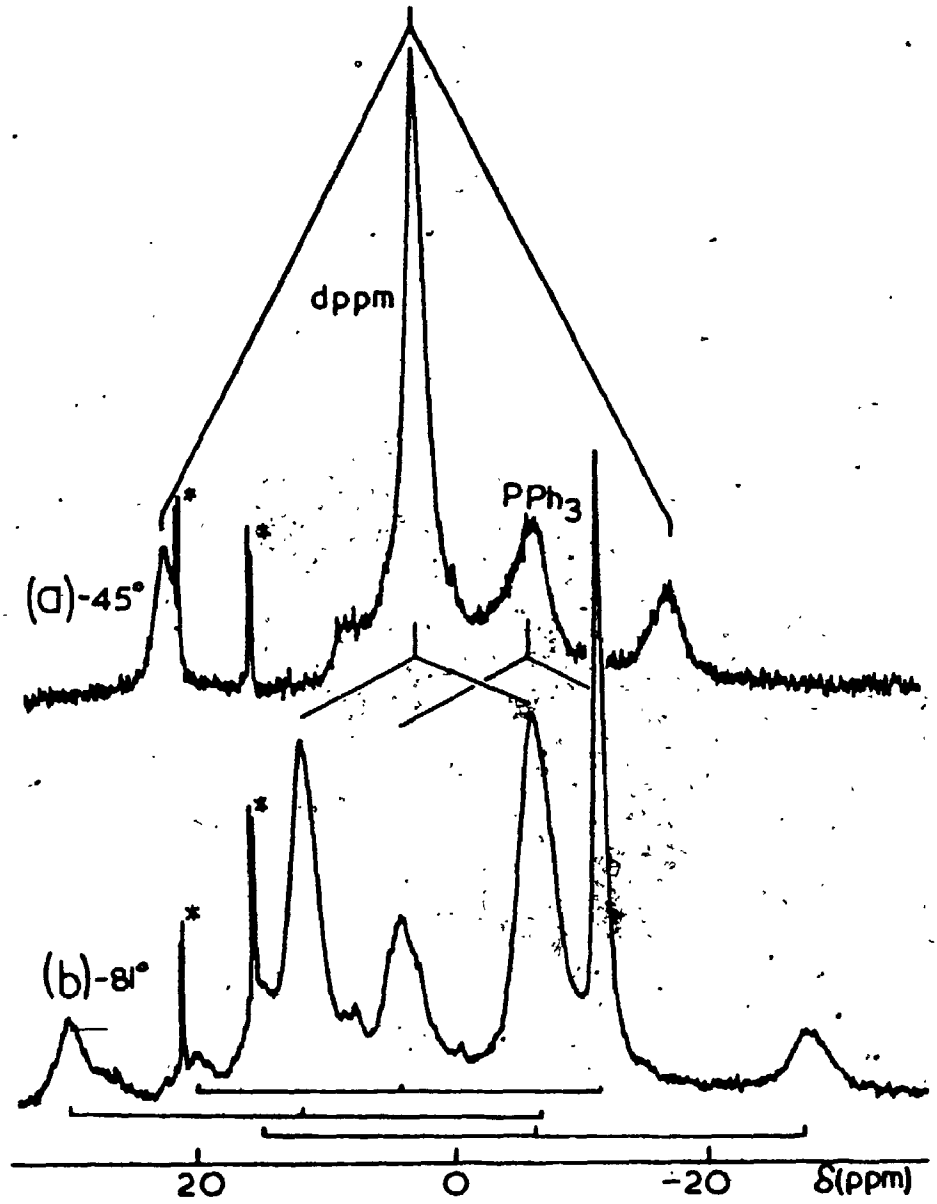

Figure 2.2. ^{31}P $\{^{1}H\}$ NMR spectra (81 MHz) of (IIIa) with excess PPh_3. Spectra recorded at (a) -45°C, the ^{195}Pt satellites of the dppm phosphorus atom signal are indicated above. (b) -81°C in the slow exchange region; corresponding resonances in (a) are indicated above and ^{195}Pt satellites are indicated below. The peaks labelled asterisk are due to an impurity, $[PtH(PPh_3)(dppm)]^+$.

TABLE 2.3

^{1}H NMR Data for Complexes (III)[a]

L	T°C	δ(H^a) ppm	^{1}J(PtH^a) Hz	δ(H^b) ppm	^{1}J(PtH^b) Hz	δ(H^c) ppm	^{1}J(PtH^c) Hz
PPh_3	-90	-4.93[b]	1140	-9.65	535	-12.38[c]	765
	-30	-8.66[d,e]	960	-9.54	535	-8.66[d,e]	960
1-dppm	-90	-5.05	1140	-9.50	540	-12.95	750
	-20	-8.95[d]	945	-9.40	545	-8.95[d]	945
$PPh_2(4\text{-}MeC_6H_4)$	-90	-6.75	[f]	-9.7	[f]	-12.45	770
	-20	-9.6[d,g]	1050	-9.6	530	-9.6[d,g]	1050
$PPh_2(2\text{-}MeC_6H_4)$	-90	[h]		-9.6	520	[h]	
	-20	-8.49[d,i]	[j]	-9.34[i]	[j]	-8.49[d,i]	[j]

[a] See Scheme for labelling, [b] ^{2}J(PtH^a) 105 Hz, [c] ^{2}J(PtH^c) 95 Hz,
[d] average value for exchanging H^a and H^c, [e] ^{2}J(PtH) 100 Hz, [f] not resolved, [g] ^{2}J(PtH) 110 Hz,
[h] very broad, [i] calculated value from δ vs [phosphine], in exchanging system, [j] not calculated.

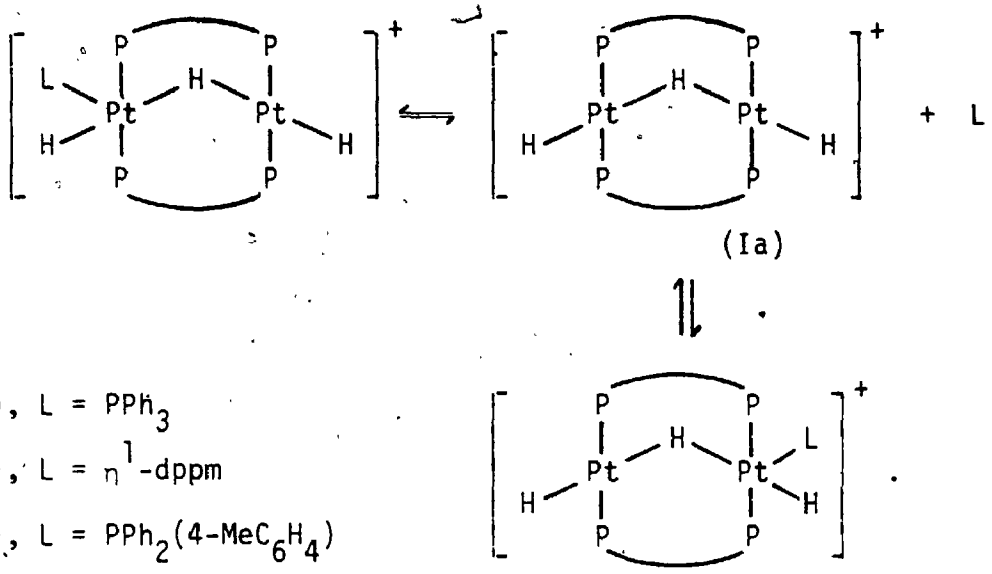

(Ia)

(IIIa), L = PPh_3

(IIIb), L = η^1-dppm

(IIIc), L = $PPh_2(4\text{-}MeC_6H_4)$

(IIId), L = $PPh_2(2\text{-}MeC_6H_4)$

(IIIf), L = $P(4\text{-}Cl_6H_4)_3$

...(2.8)

The rapid reversible addition of PPh_3 to one of the platinum atoms without disruption of the $Pt_2(\mu\text{-}H)$ group is the only mechanism which is consistent with all the data. However, the structure of (IIIa) shown in equation (2.8) is only one of four possible structures varying in the stereochemistry at the five coordinate platinum atom. The NMR data do not distinguish between structures in which this platinum has square pyramidal or trigonal bipyramidal structures and in which attack by PPh_3 occurs exo or endo with respect to the A-frame, but does indicate that the dppm phosphorus atoms remain mutually trans. The structure (IIIa) is considered probable because its formation from (Ia) involves little distortion and because steric effects are expected to favor the exo

addition shown in equation (2.8).[62] It was expected, a priori, that phosphine addition would lead to cleavage of the $Pt_2(\mu\text{-}H)$ group giving a complex, (IV) or (V), Scheme 2.2, with two 16-electron square planar platinum(II) centres but the NMR data is not consistent with either of these structures.

Low temperature $^1H\{^{31}P\}$ NMR spectra for complexes (IIIb)-(IIIf) were also recorded and indicate that the same structure is present in all cases at -90°C (Table 2.3) However, for L = $PPh_2(2\text{-}MeC_6H_4)$ the slow exchange limit was not reached at -90°C and only the $Pt_2(\mu\text{-}H)$ resonance was observed for (IIId), with the terminal hydride resonance being too broad to observe.

For the case of (Ia) with L = PPh_3, a more complete NMR study was carried out to study the kinetics of dissociation of (IIIa) according to equation (2.8). The lifetimes of (IIIa) at different temperatures were determined from the line broadening in the slow exchange region, from the coalescence point and then from the line narrowing in the fast exchange limit as the sample was warmed slowly from -90°C. Independent lifetimes were obtained by study of both the exchanging terminal hydride signals in the $^1H\{^{31}P\}$ NMR spectra and the exchanging dppm phosphorus signals of (IIIa) in the $^{31}P\{^1H\}$ NMR spectra. The data and method of calculation are given in Table 2.4. From these data the activation parameters at 273 K for dissociation of PPh_3 from complex (IIIa) were found to be $\Delta H^{\ddagger}$ 49 ±3 kJ mol^{-1}, $\Delta S^{\ddagger}$ 70 ±13 JK^{-1} mol^{-1} and $\Delta G^{\ddagger}$ 29 ±7 kJ mol^{-1}. The Arrhenius plot is shown in figure 2.3.

Complex Ic underwent a similar reaction upon addition of PPh_3. However in this case two possible products may be formed (equation (2.9)).

TABLE 2.4

Lifetime τ Data for IIIa

	T°C	ln $1/\tau$
^{1}H NMR	-90	4.51[b]
	-80	6.12[b]
	-65	8.1[a]
	-60	9.7[c]
	-40	11.4[c]
^{31}P NMR	-90	.5[b]
	-80	6.38[b]
	-70	7.31[d]
	-65	8.02[a]
	-60	8.65[c]
	-50	10.95[c]

[a] coalescence

[b] lifetime broadening (a limit linewidth was approximated from the linewidth of pure Ia at -90°C)

[c] exchange narrowing

[d] separation of resolved peaks

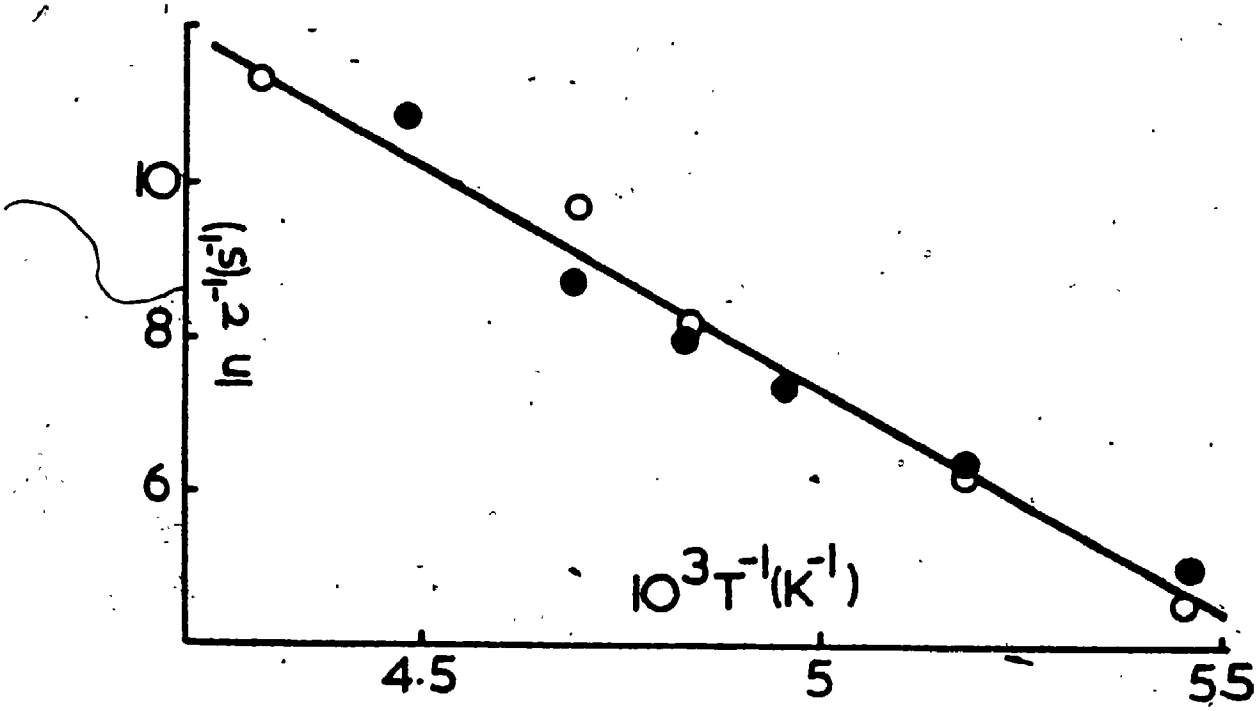

Figure 2.3. Arrhenius plot for dissociation of complex (IIIa) to (Ia) and PPh_3. Open circles indicate data from ^1H NMR and closed circles indicate data from ^{31}P NMR studies.

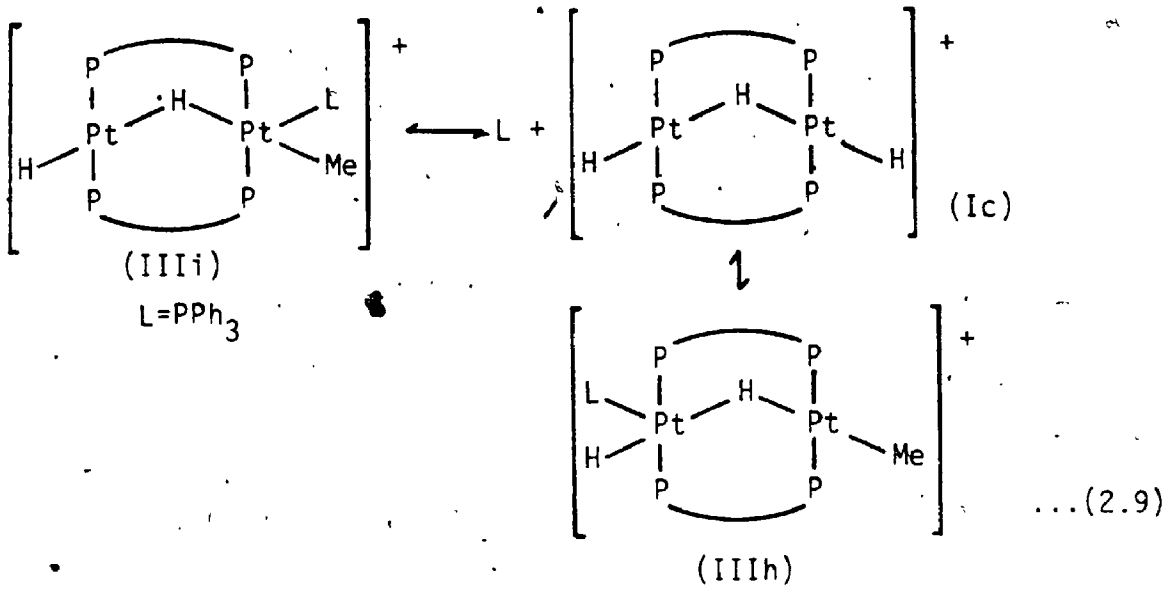

(IIIi)
L=PPh_3

(Ic)

(IIIh)

...(2.9)

The ^1H NMR spectra[64] (Table 2.5) of this complex, (III) at -90°C indicate a terminal hydride at $\delta(H^t)$-11.93 ppm, $^1J(PtH)$ 780 Hz, shifted significantly from a value of $\delta(H^t)$-6.75 ppm, $^1J(PtH)$ 1130 Hz observed for (Ic). As this shift and change in coupling are similar to those observed for the coordination of PPh_3 to (Ia) and as the $^2J(PtH)$ value associated with the methylplatinum group remained 68 Hz, it appears that (IIIh) is formed. Similar data were recorded in the ^{31}P spectra (Table 2.6). In the case of the cation (Id) the ^{31}P NMR spectrum showed no formation of a complex, [Id.PPh_3]. This is consistent with both the lack of reactivity of (Id) towards phosphines and the observed coordination of PPh_3 at the hydride end of (Ic) as in structure (IIIh).

2.1.4 Equilibrium Constants for Intermediate Formation

Equilibrium constants for formation of complexes (III) according to equation (2.8) have been determined at low temperatures by a number of methods. The direct methods will be described here, and a kinetic method will be described later.

TABLE 2.5

^{1}H NMR Data at Varying Temperatures and Equilibrium Constants for Formation of (IIIh)

T°C	$\delta(CH_2P_2)$ ppm	δ(MePt) ppm	K^a L mol^{-1}	$\delta(H^b)$ ppm	K^b L mol^{-1}	$\delta(H^t)$ ppm	K^c L mol^{-1}
-90	5.65, 3.13	-0.05[d]	-	-9.99[e]	-	-11.93[f]	-
-70	5.65, 3.13	-0.03	990	-9.70	830	-11.45	710
-50	4.39	-0.01	227	-9.44	210	-11.02	170
-30	4.47	+0.06	21	-8.77	33	-10.11	34
-20	4.50	+0.06	21	-8.40	16	- 9.54	16
-10	4.56	+0.14	3.2	-8.07	9.1	- 9.04	9.1
30	4.59	+0.19	0.7	-7.00	1.1	- 7.40	1.0
-90[g]	5.54, 3.98	0.21		-6.57		- 6.75	

[a] These values are inaccurate due to the small shift range for δ(Me) and were not used to calculate $\Delta H°$ and $\Delta S°$. [b] Calculated from $\delta(H^b)$. [c] Calculated from $\delta(H^t)$. [d] ^2J(PtMe) 68 Hz. [e] ^1J(PtH) 530 Hz. [f] ^1J(PtH) 780 Hz. [g] Data for $[Pt_2MeH(\mu\text{-}H)(\mu\text{-}dppm)_2]^+$ in absence of PPh_3. Other data with $[Pt]° = [PPh_3]° = 0.154$ M.

TABLE 2.6

$^{31}P\{^1H\}$ NMR Data at Varying Temperatures and Equilibrium Constants for Formation of (IIIh)

T°C	$(P^A)^a$ ppm	K^b $L\,mol^{-1}$	$(P^B)^a$ ppm	K^c $L\,mol^{-1}$
-90[d]	9.88[e]	-	-4.35[f]	
-80	9.47		-4.35	
-60[g]	11.46	112	-1.38	265
-40	12.25	43	1.58	55
-20	13.43	14	4.32	18
0	14.82	5	5.53	14
-	17.1[h]		15.6[h]	

[a] Recorded with $[Pt_2]° = [PPh_3]° = 0.146$ M, [b] calculated from $\delta(P^A)$, [c] calculated from $\delta(P^B)$, [d] $\delta(PPh_3)$ 4.7 ppm, compare to -9.1 ppm for free PPh_3, [e] $^1J(PtP)$ 2880 Hz, [f] $^1J(PtP)$ 3230. This coupling decreased with increasing temperature, [g] fast exchange at this temperature, [h] values in the absence of PPh_3; $^1J(PtP^A)$ 2793; $^1J(PtP^B)$ 2895 Hz.

For the complex with $PPh_2(2\text{-}MeC_6H_4)$ the equilibrium was studied by ^1H NMR spectroscopy at -20°C and 0°C, under conditions where reaction to give (II) did not occur. A fixed concentration of (Ia) was treated with increasing amounts of ligand and the chemical shift of the $Pt_2(\mu\text{-}H)$ signal was measured in each case. In these fast exchange spectra, $\delta(\mu\text{-}H)_{obs} = \rho(Ia)\cdot\delta(Ia) + \rho(IIId)\cdot\delta(IIId)$, where ρ represents the fraction of the complex present and $\delta(Ia)$ and $\delta(IIId)$ are the chemical shifts of the $Pt_2(\mu\text{-}H)$ resonances for the respective complexes. Figure 2.4 shows a graph of $\delta(\mu\text{-}H)_{obs}$ vs. $[PPh_2(2\text{-}MeC_6H_4)]°/[Ia]°$. The equilibrium constant, K, and the unknown shift (IIId) were determined by an iterative procedure[62] to give the best fit shown in Figure 2.4. This gave K = 3.2 L mol^{-1} at 253 K and K = 1.9 L mol^{-1} at 273 K for formation of (IIId). From these data approximate thermodynamic parameters for formation of (IIId) were calculated to be $\Delta H°$ -15 ±1.5 kJ mol^{-1}, $\Delta S°$ -50 ±5 JK^{-1} mol^{-1} and $\Delta G°$ -1.4 ±0.3 kJ mol^{-1} at 273 K. In other cases, this NMR method was not satisfactory because the equilibrium constants were too large to give accurate values of K at the high concentrations needed in this method.

Equilibrium constants for formation of (IIIa), (IIIc) and (IIIf) were determined at 262 K using UV-visible spectrophotometry. At 420 nm the absorbances due to complex (Ia) and free tertiary phosphine ligand are small, so that the absorbance is largely due to complex (III). The absorbance for unit path length is given by $A = \varepsilon(Ia)\cdot[Ia] + \varepsilon(L)\cdot[L] + \varepsilon(III)\cdot[III]$. The only unknown constant is $\varepsilon(III)$, the molar extinction coefficient of the complex (III), and the concentration terms are related to the initial concentrations [Ia]° and [L]° by the unknown equilibrium constant K. Using a fixed concentration of (Ia) and

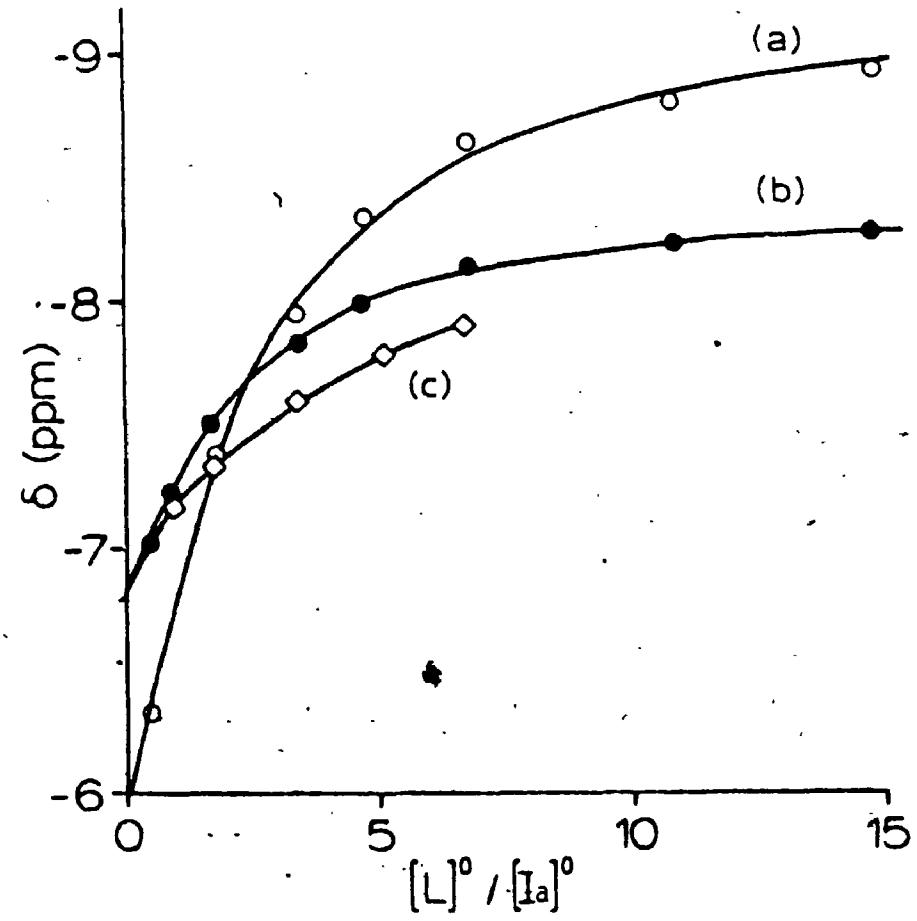

Figure 2.4. Observed points and best fit lines in graph of δ(PtH) vs. [L]°/[Ia]°, where L = $PPh_2(2\text{-}MeC_6H_4)$, in CD_2Cl_2; (a) data for $Pt_2(\mu\text{-}H)$ resonance at -20°C, (b) data for terminal PtH resonance at -20°C, (c) data for terminal PtH resonance at 0°C. Computed shifts for (IIId) are given in Table 2.3, and computed equilibrium constants are in Table 2.7.

varying concentration of added ligand, L, a graph of Absorbance (420 nm) vs. [L]°/[Ia]° was drawn in each case (Figure 2.5). An iterative method[65] was used to give the best fit between observed and calculated absorbance values and the unknown constants K and ε(III) were thus determined. The values obtained are given in Table 2.7.

For L = $P(4\text{-}ClC_6H_4)_3$, the equilibrium constant was determined at 267 K and 259 K by this method, while for L = PPh_3 and $P(4\text{-}ClC_6H_4)_3$ the equilibrium constants were determined at 277 K by a kinetic method to be described later. From these limited data, approximate thermodynamic constants for formation of (IIIa) were calculated as $\Delta H° = -41$ kJ mol^{-1}, $\Delta S°$ -108 ±4 JK^{-1} mol^{-1} at 273 K, and for formation of (IIIf) the corresponding values were $\Delta H°$ -55 ±2 kJ mol^{-1} and $\Delta S°$ -167 ±4 JK^{-1} mol^{-1} at 273 K. These parameters, though approximate, are entirely consistent with the associative nature of the reaction, with the enthalpy term favoring complex formation and the entropy term favoring dissociation of the complex (III).

It is clear that the steric effects due to the ortho methyl substituents in $PPh_2(2\text{-}MeC_6H_4)$ cause the equilibrium constant for formation of (IIId) to be much lower than for (IIIc). We also note that the equilibrium constant for formation of (IIIf) is lower than for (IIIa) or (IIIc), which might be taken to indicate that the weaker donor $P(4\text{-}ClC_6H_4)_3$ gives a weaker PtP bond than PPh_3. However, we note that the entropy term appears to be dominant in determining this order, and a more detailed study involving a wider range of ligands is needed to determine if there is a significant electronic effect on the equilibrium constants for formation of (III).

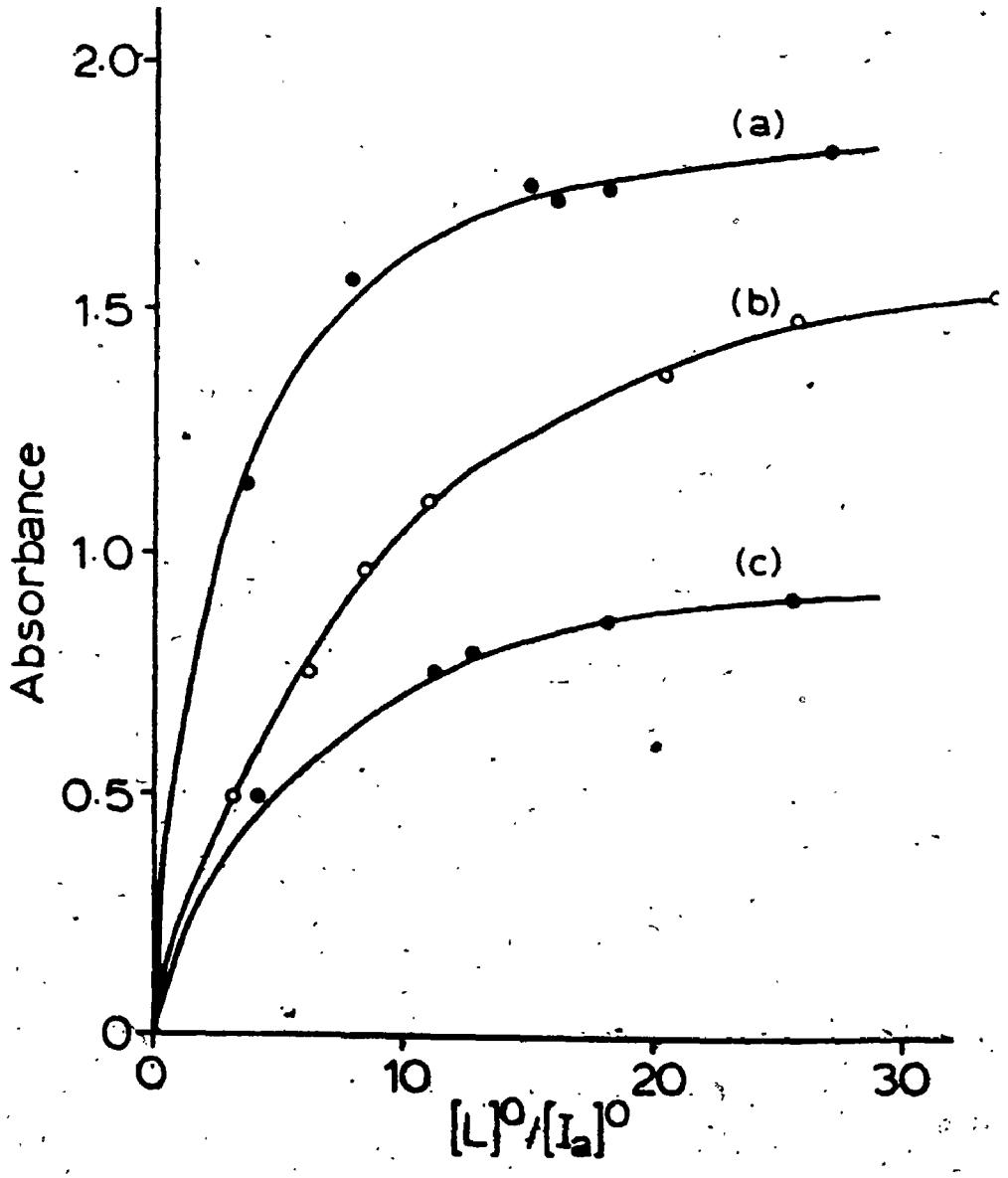

Figure 2.5. Observed points and best fit lines in graph of Absorbance vs $[L]^\circ/[Ia]^\circ$ in CH_2ClCH_2Cl (a) L = PPh_3, $[Ia]^\circ$ 1.124×10^{-3} M at -11°C, (b) L = $P(4\text{-}ClC_6H_4)_3$, $[Ia]^\circ$ 6.25×10^{-4} M, at -14°C, (c) L = PPh_3, $[Ia]^\circ$ 5.792×10^{-4} M, at -11°C. Computed equilibrium constants are in Table 2.7.

TABLE 2.7

Equilibrium Constants for Formation of Complexes (III)

L	T(°C)	Method[a]	K(ℓ mol^{-1})
PPh_3	-11	A	380±8
	4	B	136±4
$P(4\text{-}ClC_6H_4)_3$	-14	A	220±5
	- 6	A	100±2
	4	B	41±2
$PPh_2(4\text{-}MeC_6H_4)$	-11	A	340±7
$PPh_2(2\text{-}MeC_6H_4)$	-20	C	3.2±0.1
	0	C	1.9±0.1

[a] A, from UV-visible absorption data; B, from kinetic data; C, from NMR data. Solvent was CD_2Cl_2.

The equilibrium constants for formation of (IIIh) from (Ic) were also obtained. In the fast exchange region of both the ^{31}P and ^{1}H NMR spectra approximate values of K were calculated by observing the chemical shift of the dppm phosphorus atoms in the ^{31}P NMR spectra (Table 2.6) and the terminal and bridging hydride resonances (^{1}H NMR) (Table 2.5). A graph of ln K vs 1/T is given in Figure 2.6 and analysis of this results in values of ΔH° = -34 ±4 kJ mol^{-1}, ΔS° = -110 ±10 JK^{-1} mol^{-1}, and ΔG°(273 K) = -43 ±.5 JK^{-1} mol^{-1}.

2.1.5 Kinetic Studies of the Reactions

Kinetic studies of reaction (2.7) were carried out using UV-visible spectrophotometry to monitor the reactions. Samples of complex (Ia) in 1,2-dichloroethane solution were allowed to react with a large excess of the tertiary phosphine ligand, L, in a quartz cuvette held in the thermostatted cell compartment of the spectrophotometer. The complexes (II) are yellow while (Ia) is colorless, and so an increase in absorbance in the region 300-360 nm was observed as the reaction occurred (Figure 2.7). For reactions conducted at 298 K or higher the equilibrium concentration of intermediate (III) could be calculated to be 5% or less of the concentration of complex (Ia), and the spectral changes observed are those expected for conversion of (Ia) to (III). Under these conditions, the reactions followed good first order kinetics and graphs of the observed first order rate constants versus ligand concentration were found to give good straight line plots passing through the origin (Figure 2.8): Thus, the reactions follow overall second order kinetics, first order in both platinum complex (Ia) and phosphine ligand, L. Data at 298 K were obtained for L = PPh_3, dppm,

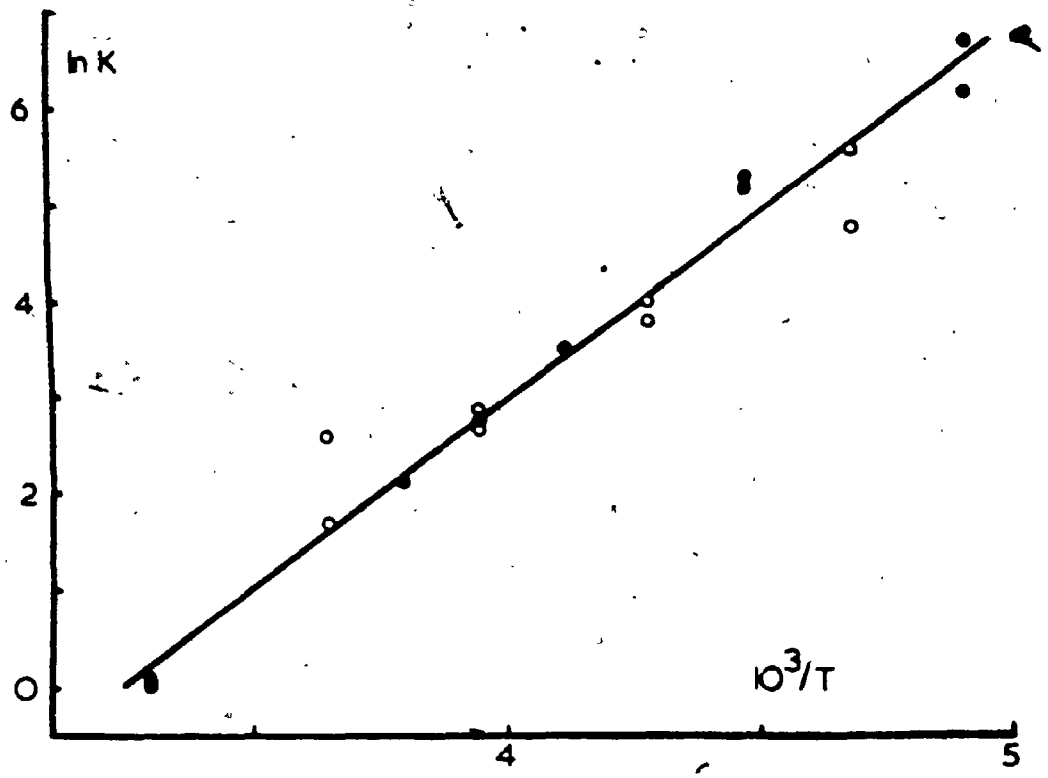

Figure 2.6. lnK plotted against reciprocal absolute temperature for the reaction of equation 2.9; (Ic) ⇌ (IIIh).

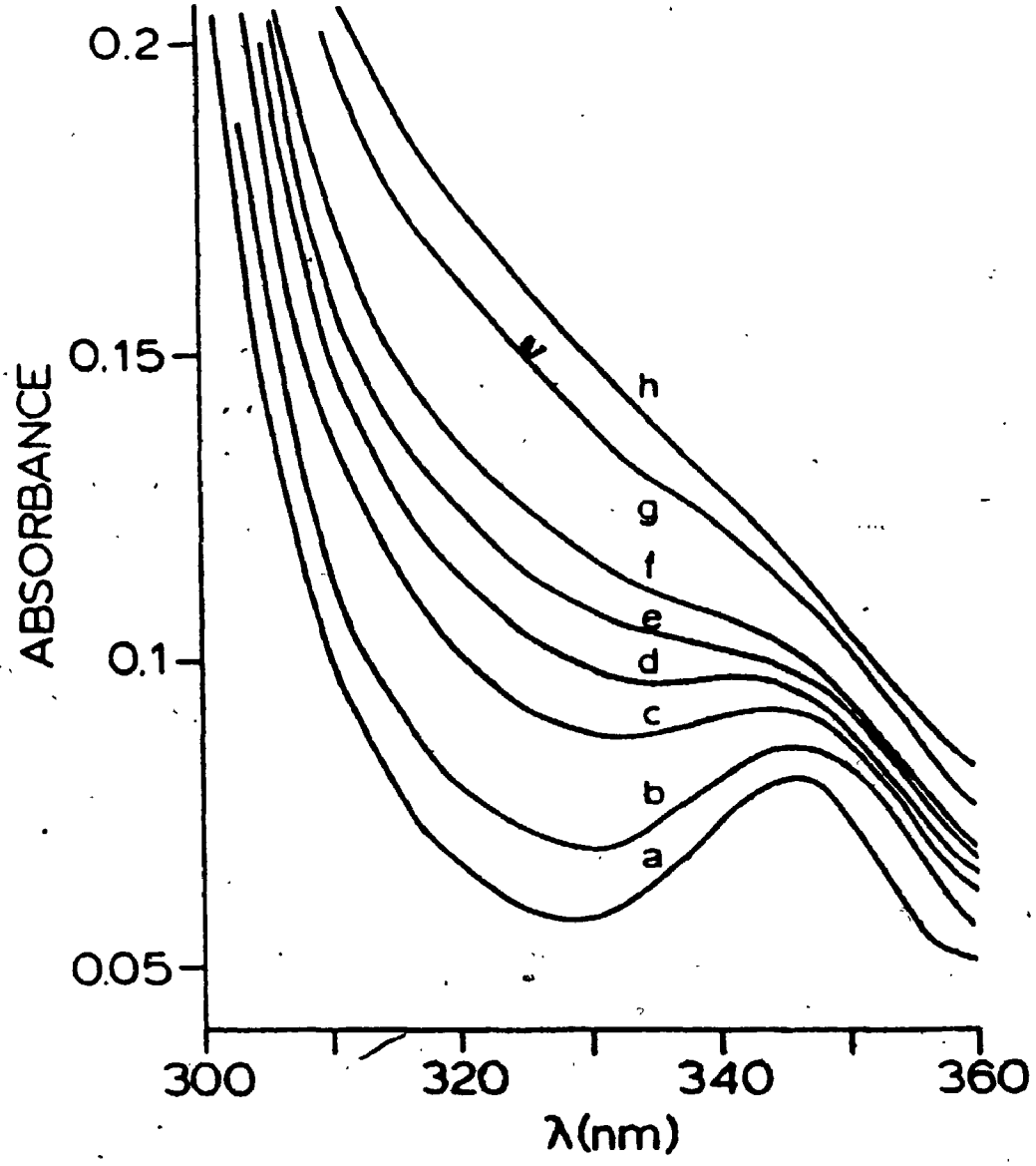

Figure 2.7. Changes in absorption spectrum during reaction of (Ia) with PPh_3 in CH_2ClCH_2Cl. Absorbance increases with time and spectra were recorded at (a) 1 min, (b) 4 min, (c) 8 min, (d) 11 min, (e) 14 min, (f) 18 min, (g) 36 min, (h) 80 min.

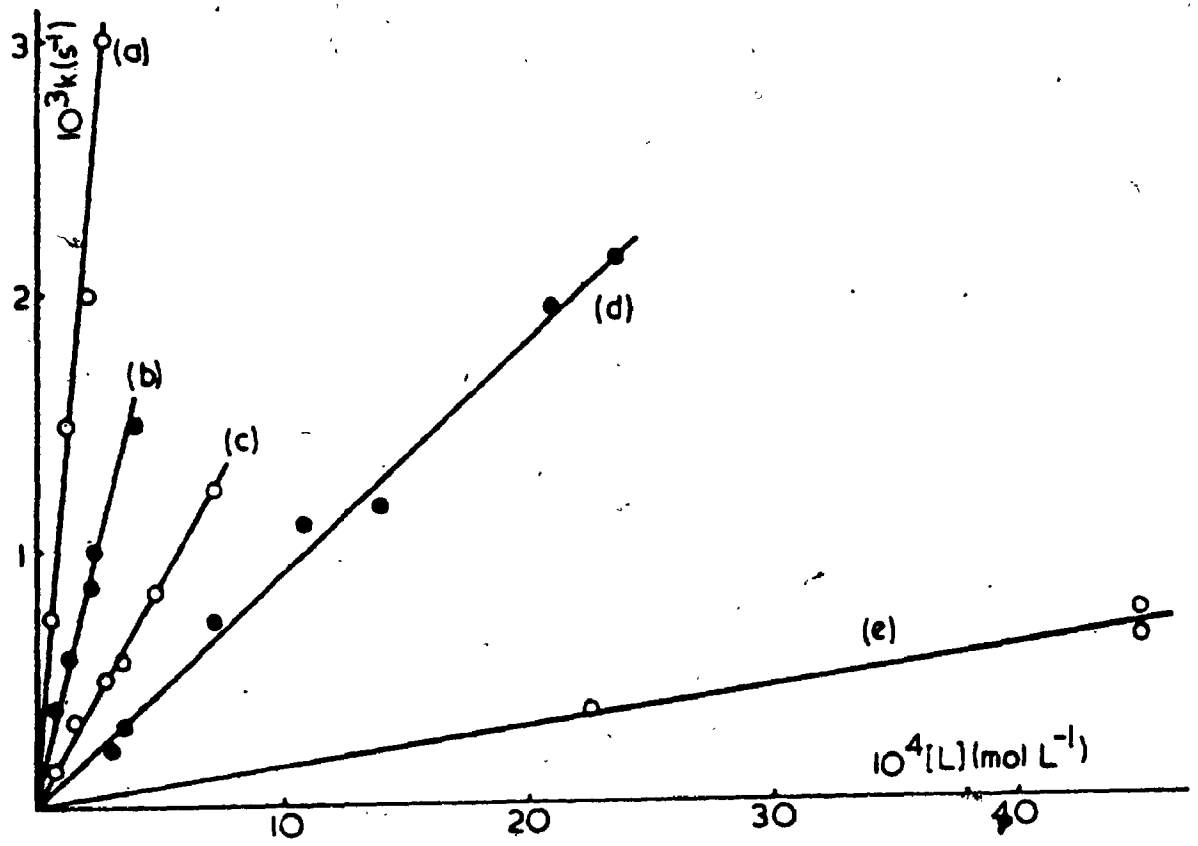

Figure 2.8. Graphs of pseudo first order rate constants for the reaction of equation (3) vs concentration of ligand L at 25°C.

(a) (Ia) with dppm, (b) (Ib) with dppm, (c) (Ia) with PPh_3, (d) (Ia) with $PPh_2(4\text{-}MeC_6H_4)$, (e) (Ia) with $P(4\text{-}ClC_6H_4)_3$.

$PPh_2(4\text{-}MeC_6H_4)$, $PPh_2(2\text{-}MeC_6H_4)$ and $P(4\text{-}ClC_6H_4)_3$. Reliable kinetic data could not be obtained for L = PMe_2Ph or $PMePh_2$. These ligands, when used in excess, appeared to displace dppm from platinum. Qualitative studies, using NMR to monitor reactions, showed that they reacted much faster than PPh_3 with (Ia). The derived second order rate constants for reaction (2.7) are given in Table 2.8. It can be seen that steric effects of the ligand are of prime importance, with the observed second order rate constants falling in the sequence L = PMe_2Ph, $PMePh_2$ > dppm > PPh_3, $PPh_2(4\text{-}MeC_6H_4)$ >> $PPh_2(2\text{-}MeC_6H_4)$. Electronic effects are also significant since the poorer donor $P(4\text{-}ClC_6H_4)_3$ gives a lower rate than PPh_3.

The primary isotope effect on the rate of reaction of PPh_3 or dppm with (Ia) or (Ib) was determined from kinetic studies (Table 2.8). In both cases a significant isotope effect k_H/k_D = 3.5±0.1 was found. For comparison, the related isotope effect for loss of H_2 from $[IrH_2(CO)_2L_2]^+$ is 2.1,[45] for addition of H_2 to $[IrCl(CO)L_2]$ it is 1.22[66] and for loss of CH_4 (or CH_3D) from cis-$[PtH(orD)Me(PPh_3)_2]$ it is 3.3.[54] The result clearly indicates that Pt-H bond cleavage is involved in the transition state and, if the slow step involves reductive elimination, that the transition state is less "product-like" than in reductive elimination from $[IrH_2(CO)_2L_2]^+$.

The data described above support the mechanism shown in equation (2.10)

$$(Ia) + L \underset{}{\overset{K}{\rightleftharpoons}} (III) \xrightarrow{k} (II) + H_2 \qquad \ldots(2.10)$$

There is a rapid pre-equilibrium giving (III), followed by rate determining loss of hydrogen. The kinetics should therefore be described

TABLE 2.8

Observed Second Order Rate Constants ($k_{obs} = kK\ \ell\ mol^{-1}\ s^{-1}$) for the Reaction of Equation (2.7) in 1,2-dichloroethane

L	T°C	$kK(\ell\ mol^{-1}\ s^{-1})$[a]
PPh_3	25	1.6
	35	2.9
	44	5.9
	53	9.9
	60	12.7
PPh_3	25	0.46[b]
$P(4\text{-}ClC_6H_4)_3$	25	0.16
	35	0.26
	44	0.34
	53	0.51
$PPh_2(4\text{-}MeC_6H_4)$	25	0.89
$PPh_2(2\text{-}MeC_6H_4)$	25	3.9×10^{-2}
dppm	25	10.9
dppm	25	3.15[b]

[a] Generally obtained from first order rate constants vs. [L].

[b] value for reaction with $[Pt_2D_2(\mu\text{-}D)(\mu\text{-}dppm)_2][PF_6]$.

by the expression:

$$\frac{d(II)}{dt} = \{kK/(1+K[L])\}\{[II]_\infty - [II]\}[L] \quad ...(2.11)$$

Under the conditions where K[L] is much less than unity, that is when the equilibrium concentration of (III) is small, this will lead to observed second order rate constants given by $k_{obs} = kK$, and most of our kinetic results were obtained in this regime. For the case with $L = PPh_3$, a variable temperature study was carried out and, from the observed second-order rate constants at temperatures from 298-333 K (Table 2.8), the overall activation parameters from the Arrhenius plot (Figure 2.9) were calculated. This gave $\Delta H^{\ddagger}_{obs}$ 51 ±3 kJ mol^{-1}, $\Delta S^{\ddagger}_{obs}$ -63 ±7 JK^{-1} mol^{-1}, $\Delta G^{\ddagger}_{obs}$ 68 ±5 kJ mol^{-1}, calculated at 273 K. Now since the thermodynamic parameters associated with the pre-equilibrium were known, the true activation parameters for the rate determining step, associated with the rate constant k, could be calculated. This gave $\Delta H^{\ddagger}$ 92 ±5 kJ mol^{-1}, $\Delta S^{\ddagger}$ 45 ±10 JK^{-1} mol^{-1} and $\Delta G^{\ddagger}$ 80 ±8 kJ mol^{-1}, calculated at 273 K.

At low temperatures, the rate constant k decreases but the equilibrium constant K increases. Hence conditions can be found where the more general rate expression of equation (2.11) must be used to describe the kinetics. For $L = PPh_3$, this was the case at 277 K and so a kinetic study was made at this temperature. Again good first order plots were obtained under conditions where a large excess of phosphine was used. The presence of significant concentrations of complex (III) is immediately obvious from the UV-visible spectra (Figure 2.10, compare Figure 2.7). Since (IIIa) absorbs more strongly than (IIa) in the region <420 nm, an isosbestic point is seen for runs at high phosphine

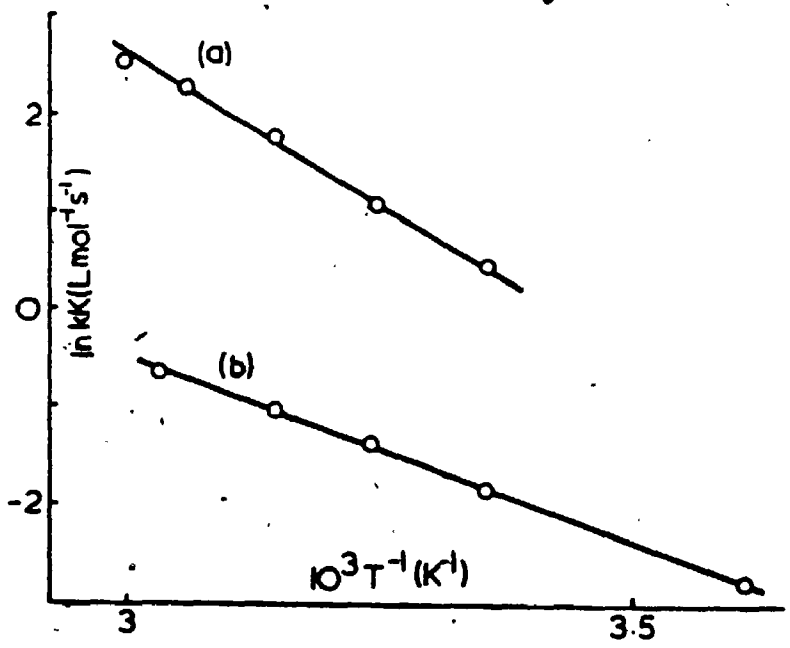

Figure 2.9. Arrhenius plots for the reactions of equation (2.7) with (Ia). (a) L = PPh_3, (b) L = $P(4\text{-}ClC_6H_4)_3$.

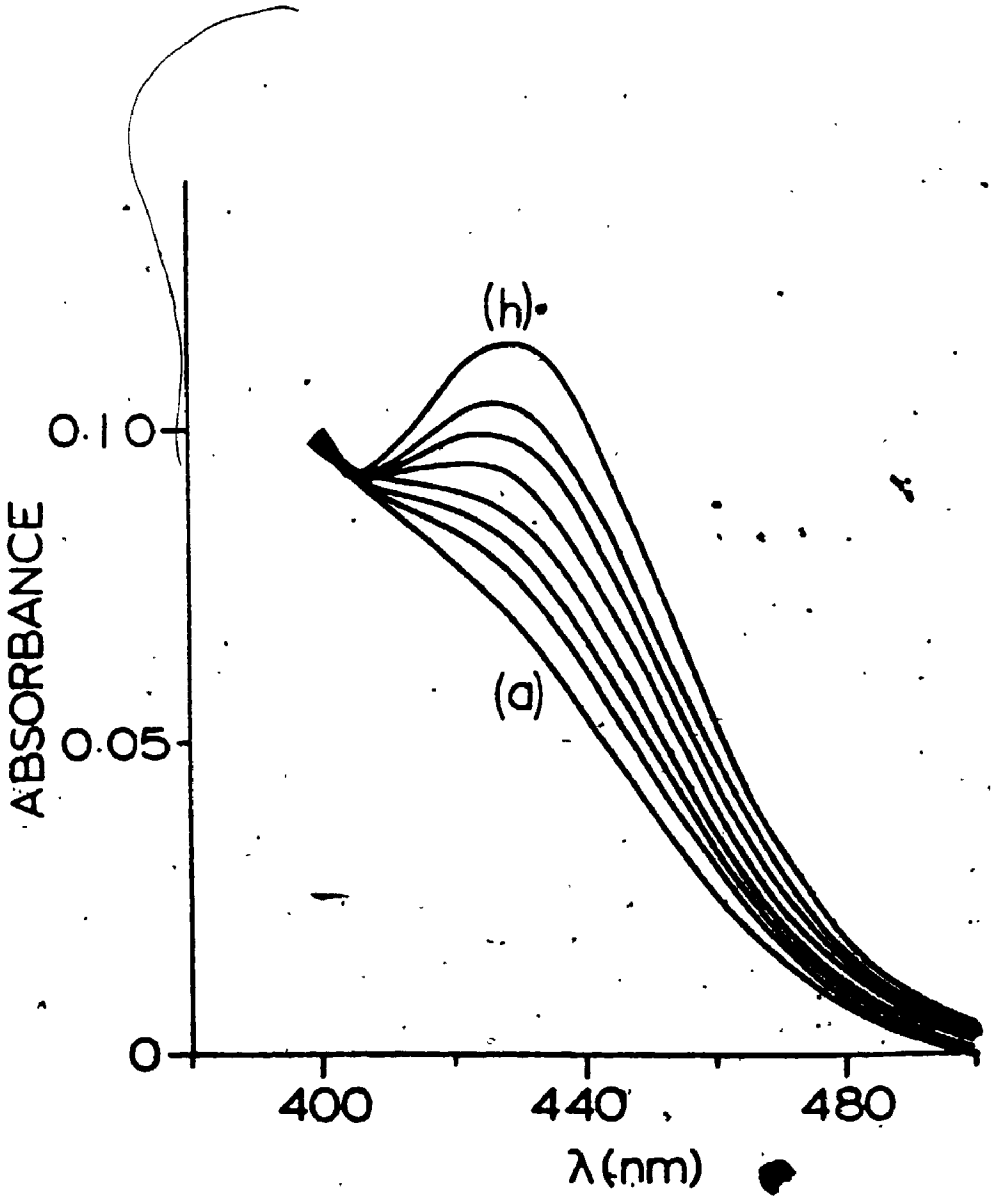

Figure 2.10. Changes in absorption spectrum during reaction of (Ia) with PPh_3 at 4°C. Spectra recorded at (a) 4 min, (b) 14 min, (c) 21 min, (d) 31 min, (e) 46 min, (f) 61 min, (g) 81 min, (h) 134 min.

concentrations. The first order constants in this regime are given by the expression:

$$k_{obs} = kK[L]/ \{1+K[L]\} \qquad ...(2.12)$$

and the observed rate constants are no longer proportional to [L], but rise to a plateau level as [L] is increased. The expression (2.12) can be rearranged to give:[67]

$$1/k_{obs} = 1/kK[L] + 1/k \qquad ...(2.13)$$

Hence a plot of $1/k_{obs}$ vs $1/[L]$ gives a straight line of slope $1/kK$ and intercept $1/k$, from which both k and K can be determined. The plot is shown in Figure 2.11 and analysis gave $K \simeq 135$ L mol^{-1} and $k = 1.1 \times 10^{-3}$ s^{-1}. This value of K at 277 K, together with that measured directly at 262 K, was used to calculate the thermodynamic parameters associated with the pre-equilibrium step when $L = PPh_3$.

A similar variable temperature study of the reaction kinetics of (Ia) with $P(4\text{-}ClC_6H_4)_3$ was carried out over the range 277-326 K, to obtain the activation parameters from the Arrhenius plot (Figure 2.9). In this case the parameters were $\Delta H^{\ddagger}_{obs}$ 30 ±3 kJ mol^{-1}, $\Delta S^{\ddagger}_{obs}$ -150 ±7 JK^{-1} mol^{-1} and $\Delta G^{\ddagger}_{obs}$ 68 ±5 kJ mol^{-1} calculated at 273 K. From the reaction at 277 K, K was also calculated as 41 L mol^{-1}. Again the true activation parameters (at 273 K) associated with the rate constant, k (equation (2.10)), could be calculated and gave $\Delta H^{\ddagger}$ 85 ±5 kJ mol^{-1}, $\Delta S^{\ddagger}$ 17 ±13 JK^{-1} mol^{-1}, $\Delta G^{\ddagger}$ 80 ±9 kJ mol^{-1}.

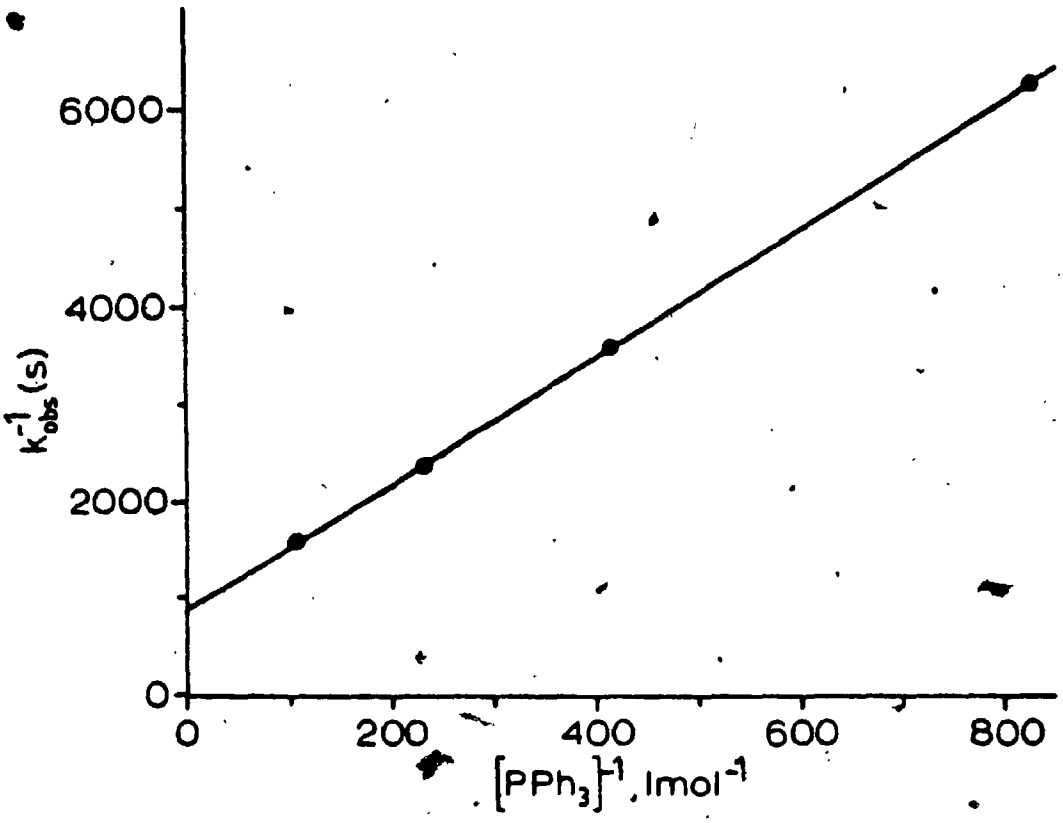

Figure 2.11. Graph of $1/k_{obs}$ vs $1/[L]$ for reaction of PPh_3 with (Ia) at 4°C.

2.2 Discussion

Because this appears to be the first detailed mechanistic study of a reaction involving oxidative addition or reductive elimination of dihydrogen to a binuclear transition metal complex, an attempt has been made to determine the reaction mechanism and also to understand the energetics of the reaction. The energetics of some relevant fluxional processes of complex (Ia) have been studied previously and the free energies of activation of the processes shown in equations (2.14) and (2.15) (at 338 K) have been determined to be 45 kJ mol^{-1} and 68 kJ mol^{-1} respectively.[68]

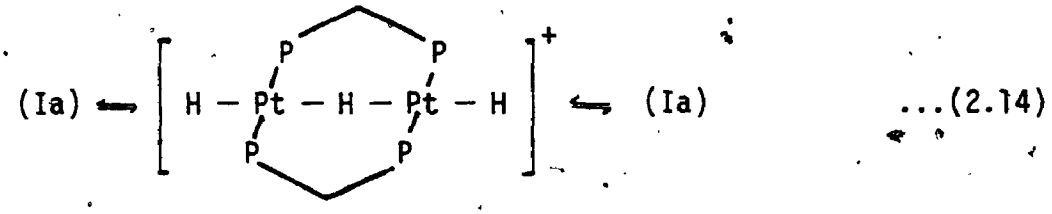

...(2.14)

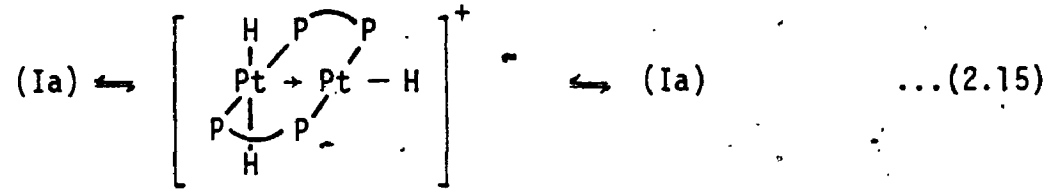

...(2.15)

The first reaction involves inversion of the "A-frame" through an intermediate with a linear Pt(μ-H)Pt group, while the second involves overall bridging for terminal hydride exchange. The reaction of equation (2.15) occurs more rapidly in pyridine solution than in dichloromethane solution but, in the slow exchange limit, the chemical shifts and coupling constants of the hydride ligands of (Ia) are almost identical in the two solvents. Thus hard ligands like pyridine do not appear to form complexes with (Ia) of structure (III) in detectable quantities. The UV-visible and IR spectra of (Ia) in pyridine and dichloromethane are also almost identical, confirming the lack of

complex formation in pyridine. Complex (Ia) has good thermal stability in pyridine and solutions can be heated to 90°C without change.

In contrast, tertiary phosphines form complexes with (Ia) of probable structure (III) and also induce reductive elimination of hydrogen from (Ia). The observation of the rate expression of equation (2.11) for the overall reductive elimination reaction is fully consistent[69] with complex (III) being an intermediate in the reductive elimination reaction, as indicated in equation (2.10), and this conclusion is supported by the observation of a good correlation between the equilibrium constants (K) for formation of (III) and the observed second order rate constants ($k_{obs} = kK$) for reaction (3), for the ligands PPh_3, $PPh_2(4\text{-}MeC_6H_4)$ and $PPh_2(2\text{-}MeC_6H_4)$ (Table 2.9). This correlation also suggests that reductive elimination occurs from the platinum center remote from the coordinated phosphine ligand, L, since the bulky ortho-tolylphosphine would be expected to accelerate reductive elimination relative to the less bulky ligands if hydrogen were lost from the near platinum center.[70]

The problem now is to understand the detailed mechanism of the reductive elimination of H_2 from the intermediate (III) of equation (2.10). Two reasonable mechanisms are shown in Scheme 2.2. Of the complexes shown in Scheme 2.2 (IV), (V) and (VI) have not been detected directly and so a brief justification of their possible roles as intermediates is necessary. It is difficult to envisage reductive elimination of hydrogen from (III) directly since the hydrogen atoms are too far apart for a concerted mechanism to be feasible, and so a rearrangement to complex (IV) or (V) is proposed.

TABLE 2.9

Derived Rate Constants for Hydrogen Elimination

$$[Pt_2H_3]^+ + L \overset{K}{\rightleftharpoons} [Pt_3H_3L]^+ \overset{k}{\Longrightarrow} [Pt_2HL]^+ + H_2$$

Ligand	K(298 K) L mol^{-1}	k_{obs} = kK(298 K) L mol^{-1} s^{-1}	k_{obs}/K k s^{-1}
PPh_3	35	1.6	0.046
PPh_3*	1.0*	0.04*	0.04*
$P(4\text{-}ClC_6H_4)_3$	8.3	0.16	0.019
$PPh_2(2\text{-}MeC_6H_4)$	1.0	.039	0.039

* Data for $[Pt_2MeH(\mu\text{-}H)(\mu\text{-}dppm)_2]^+$

There are good models for complex (IV) in the "face-to-face" complexes such as $[Pt_2(C{\equiv}CR)_4(\mu\text{-dppm})_2]$ and similar complexes,[71,72] but we know of no good models for complex (V).[73] However, if reductive elimination occurs at a single metal center as has been thought probable in some related systems, complex (V) is the most probable intermediate since the mutually cis hydrogen atoms H^a and H^b can be eliminated in a concerted mechanism. Complex (V) could be formed directly from (III) or by isomerization of (IV).[74] Reductive elimination from (V) would give (VI), a platinum(0)-platinum(II) species, which would rearrange to the product (II), probably by hydrogen migration.[75]

An attractive alternative to this mechanism would involve a true binuclear reductive elimination of hydrogen atoms H^b and H^c from complex (IV) to give (II) directly. Such a mechanism has not been favored in the past, perhaps because the simplest mechanism involving a 4-centre transition state (equation (2.16)) is orbitally forbidden.

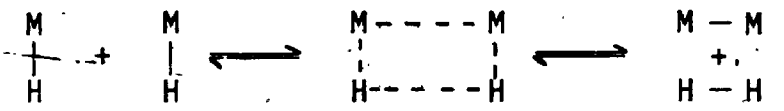

...(2.16)

However, there is evidence for a binuclear mechanism in some cases,[44,58,76] and a more detailed examination of the specific case of complex (IV) indicates that a binuclear reductive elimination may be feasible. In complex (IV), Scheme 2.2, the hydrogen atom H^c is expected to be protonic[77] whereas H^b, being trans to a strong σ-donor, is expected to be much more hydridic. Thus transfer of electron density from the $(Pt\text{-}H^b)$ orbital (HOMO)[78] to the $\sigma^*(Pt\text{-}H^c)$ orbital (LUMO) should occur readily as illustrated in equation (2.17), and H-H

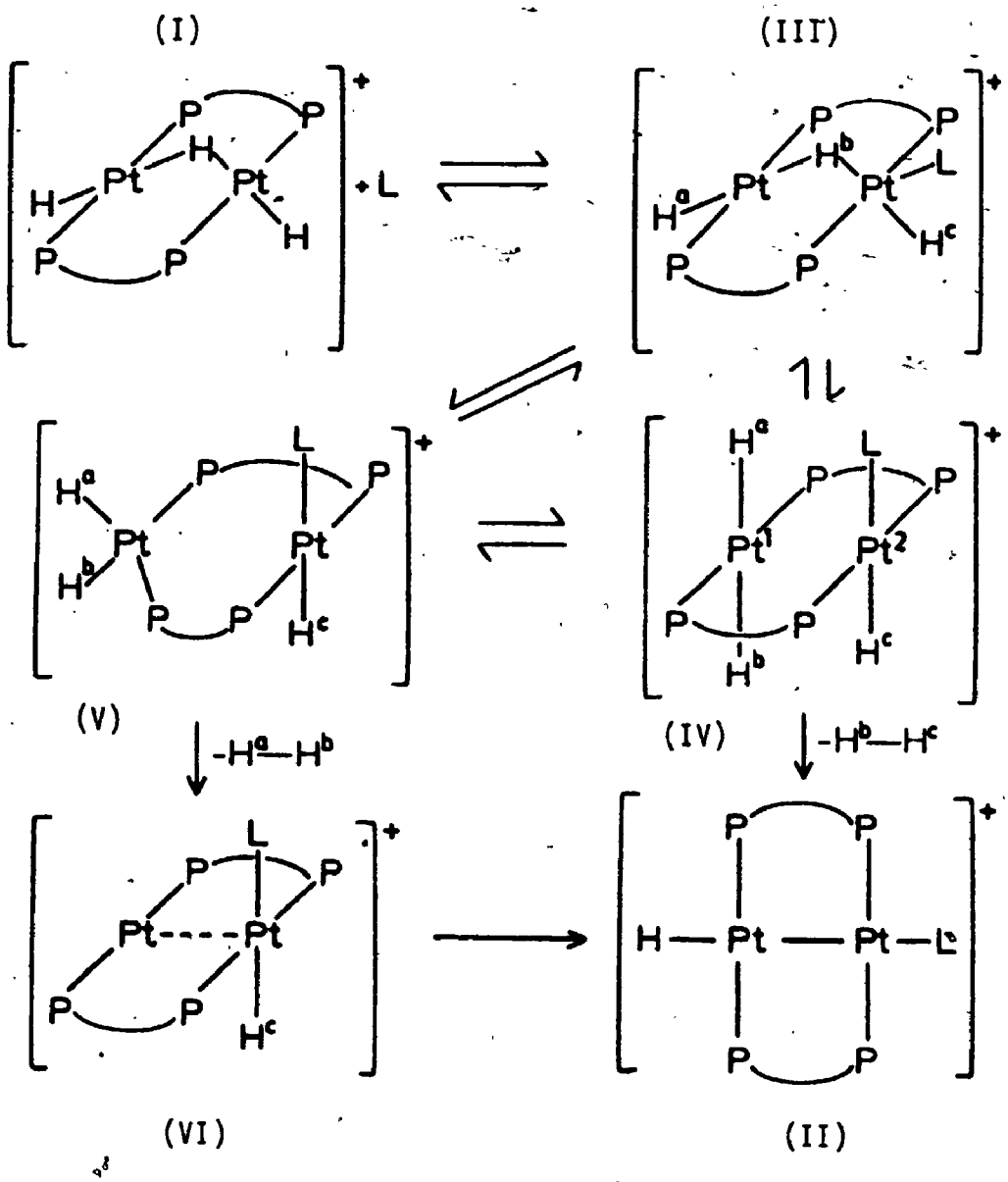

Scheme 2.2

bond formation and Pt-H bond cleavage results naturally.[79]

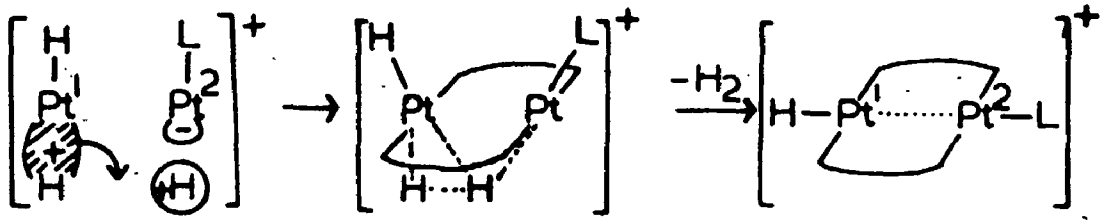

...(2,17)

It is clear that this process does not lead to Pt-Pt bond formation, since the PtPt interaction resulting from equation (2.17) is weakly antibonding in nature, and a $Pt^2(0)$-$Pt^1(II)$ species might be expected. However, as the positive charge on Pt^1 develops it would presumably lead to a $Pt^2 \rightarrow Pt^1$ donor-acceptor bond,[80] using non-bonding d-electron density on Pt^2, and effectively lead to direct formation of the product (II). This mechanism is most attractive when a "hydridic" and "protonic" hydride are eliminated, as in the present case, but is possible in other cases also.[44,82]

Further evidence for a true binuclear reductive elimination reaction comes from consideration of the similarity for the rate of this process in complexes Ia and Ic. The rate constant k at 298° is given in Table 2.9 for Ia with a variety of phosphines and Ic with PPh_3. The similarities between these rates are more easily interpreted if one considers a binuclear elimination.

In the proposed binuclear mechanism the value, k, will represent the rate limiting step in the III → IV → II transformation.

The transformation III → IV scheme is expected to involve hydride inversion in the case of the methyl derivative, and may involve this inversion in the case of the hydride.

Although we have no data on the energy required for this process the inversion of the bridging hydride in (Ia) has a lower activation energy than that for the elimination reaction. The activation energy for inversion of the bridging hydride in (V) is also much lower than that for reductive elimination. This indicates that the inversion process in intermediates of type (III) may be a low energy process. If this is the case, the magnitude of k must be dictated by the ease of elimination from structures of type (IV) (Scheme 2.2). The similarity in values for k is hence reasonable. As each represents reductive elimination from a similar species, this mechanism is also consistent with the isotope effect observed in the reaction of (Ia).

If the reaction occurs through (IV) (Scheme 2.2), then, in the methyl analogue, a rearrangement as shown below in (2.18) would be required.

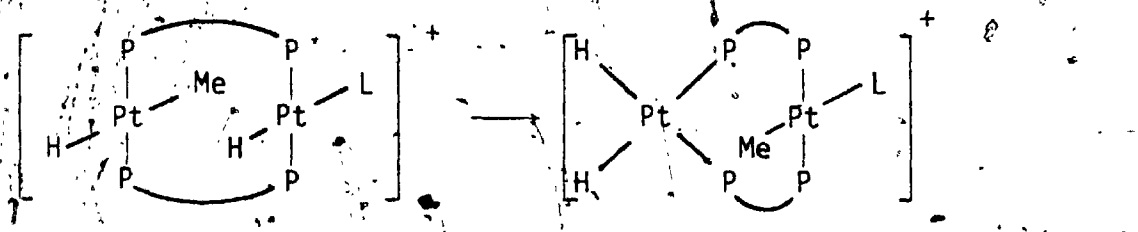

IVh Vh ...(2.18)

Such a rearrangment would presumably occur through intermediates such as (VII) or (VIII), both of which are expected to be high energy intermediates. As such, the rate limiting step would be expected to be the formation of these. If this was the case the observed similarity in

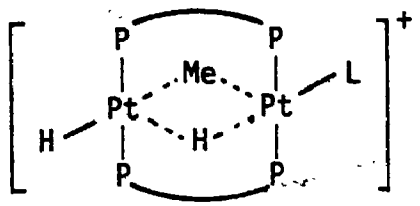

VII

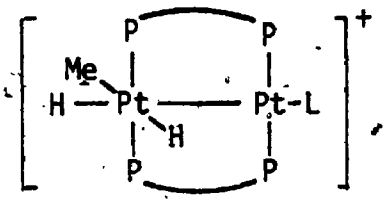

VIII

rate constants k for reductive elimination of hydrogen from (Ia) and (Ic) would be fortuitous.

The reaction coordinate diagram for the reaction of equation (2.10) with L = PPh_3 is shown in Figure 2.12, and a brief discussion of its derivation is given next. The thermodynamic parameters for the pre-equilibrium involving formation of (IIIa), equation (2.8), were determined experimentally, and the activation parameters for dissociation of PPh_3 from (IIIa) were also determined directly. Hence the activation parameters for reaction of PPh_3 with (Ia) to give (IIIa) could be calculated, and this procedure yielded $\Delta H^{\ddagger}$ 8 ±5 kJ mol^{-1}, $\Delta G^{\ddagger}$ 18 ±10 kJ mol^{-1} and $\Delta S^{\ddagger}$ -38 ±17 J K^{-1} mol^{-1} at 273 K. The enthalpy of activation is very small, consistent with the formation of (IIIa) from (Ia) with very little distortion of the bonding framework.

The activation parameters for decomposition of (IIIa) to give (IIa) and H_2 were determined experimentally, but the thermodynamic parameters, $\Delta G°$ and $\Delta H°$, could not be obtained. We have used the values $\Delta H°$ + 30 kJ mol^{-1}, $T\Delta S°$ +40 kJ mol^{-1} and hence $\Delta G°$ -10 kJ mol^{-1}.[83] These values are reasonable but the absolute values are of less significance than the expected result that the reductive elimination of H_2 from (IIIa) is an entropy driven reaction.

Little entropy change is expected for the overall reaction of

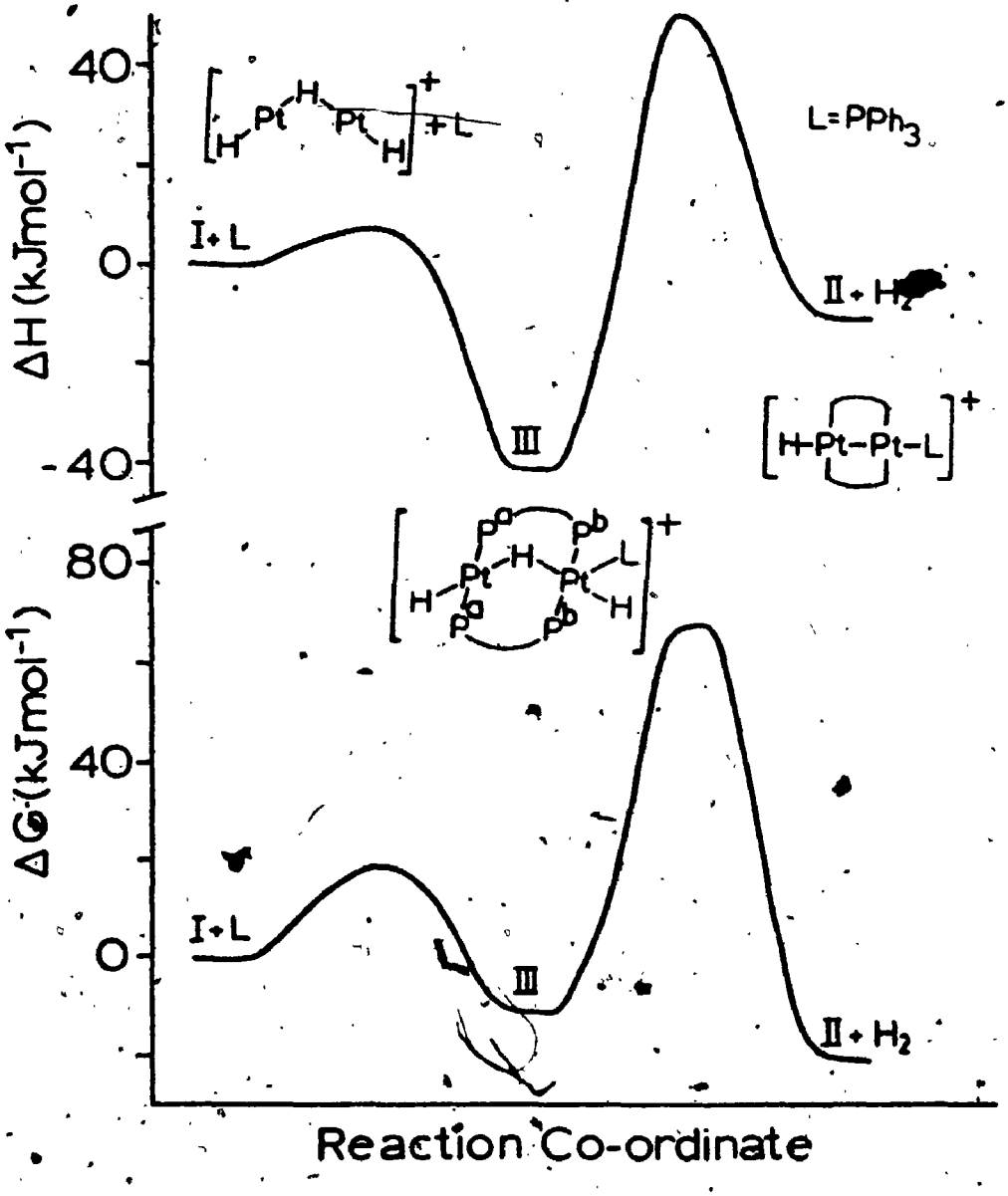

Figure 2.12: Reaction co-ordinate diagram for the reaction of equation (2.10) L = PPh_3.

equation (2.7), and the reactivity of (Ia) with added ligands can be understood in terms of the strength of the Pt-L bond formed. When L = PPh_3, a strong Pt-L bond is formed and hence both intermediate (III) and product (II) are stable with respect to (Ia). The ligand L = CO gives a weaker Pt-L bond and now the forward and back reactions of equation (2.7) occur at very similar rates suggesting that $\Delta G^\circ \sim 0$, and intermediate (III) cannot be detected.[28] When L = MeCN, only the back reaction of equation (2.7) occurs (except with photochemical activation) and again the intermediate (III) cannot be detected.[84] Thus as the Pt-L bond strength decreases in the sequence Pt-P > Pt-CO > Pt-NCMe, the reaction (2.7) changes from being thermodynamically favorable to unfavorable, Figure 2.13, and the remarkable differences between the reactivity of (Ia) with soft ligands like PPh_3 and CO and hard ligands like pyridine and acetonitrile are rationalized.

It is important to determine which is the rate determining step in the reductive elimination reactions. The most compelling evidence comes from the entropy of activation when L = PPh_3. Although the overall apparent entropy of activation for reaction (2.7) is -63 ± 7 JK^{-1} mol^{-1}, when the value of ΔS° of -108 ± 4 JK^{-1} mol^{-1} for the pre-equilibrium step is subtracted, the true value of $\Delta S^\ddagger$ for loss of H_2 from (IIIa) is $+45 \pm 11$ JK^{-1} mol^{-1}. This suggests that the reductive elimination step, which is of course dissociative, is rate determining and the large isotope effect, $k_H/k_D = 3.5$, on the rate is fully consistent with this conclusion.[85]

The enthalpy of activation for the reductive elimination of H_2 from (IIIa) is 92 ± 5 kJ mol^{-1}, very close to the value of 100 kJ mol^{-1} calculated by Noell and Hay for reductive elimination from

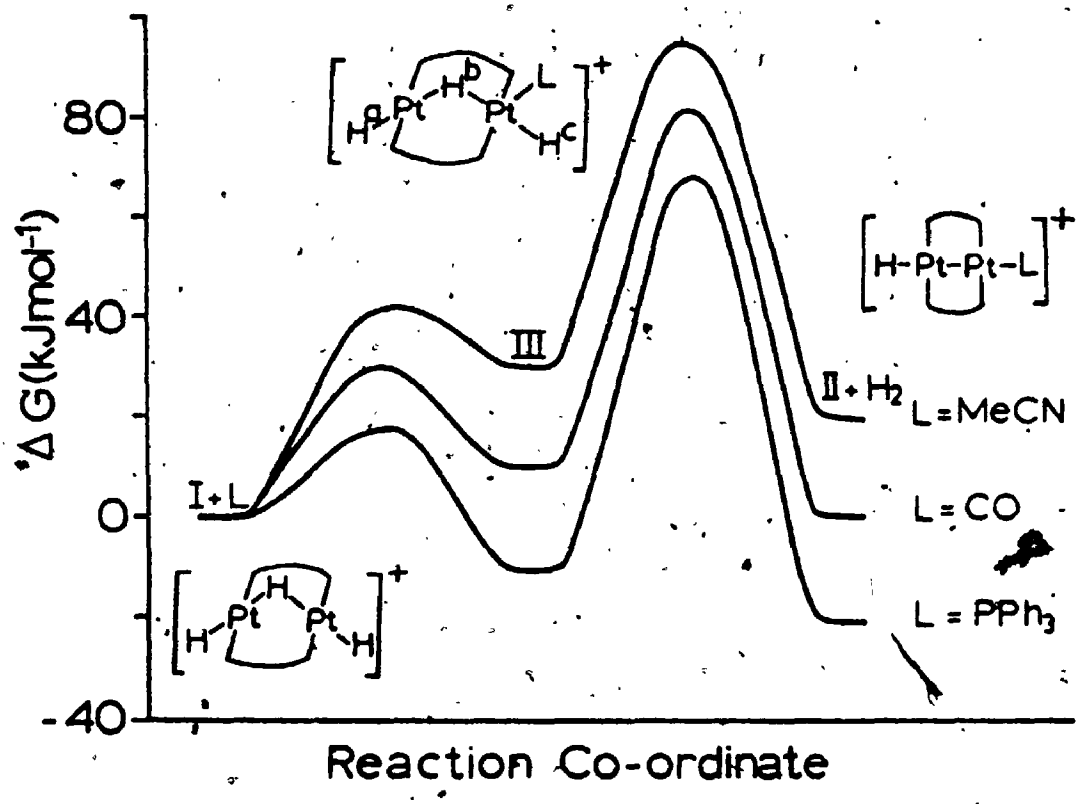

Figure 2.13. Proposed reaction co-ordinate diagrams for the reaction of equation (2.10) for L = PPh_3, CO and MeCN.

cis-$[PtH_2(PMe_3)_2]$. However, the apparent agreement is illusory since a significant component of the observed $\Delta H^{\ddagger}$ must arise from the preliminary rearrangement of (III) to (IV) or (V),[86] Scheme 2.2 , and the true $\Delta H^{\ddagger}$ for the reductive elimination step must be considerably less than 92 ±5 kJ mol^{-1}. It is probable that a Pt-Pt interaction, indicated by the dotted line in intermediate (VI), Scheme, or (VII), equation (2.17) in the binuclear system allows a lower activation energy than in the mononuclear system where the high energy species PtL_2 must be formed. It is likely that cooperative effects of this kind, leading to lower activation energies, may explain differences between mononuclear and polynuclear complexes in their ability to activate small molecules.

2.3 Conclusions

We have shown that reductive elimination of H_2 from $[Pt_2H_2(\mu\text{-}H)(\mu\text{-}dppm)_2]^+$ and $[Pt_2HMe(\mu\text{-}H)(\mu\text{-}dppm)_2]^+$ induced by tertiary phosphine ligands is an intramolecular process and that an intermediate $[Pt_2XH(\mu\text{-}H)L(\mu\text{-}dppm)_2]^+$, with X = H or Me, is involved. The intermediates have been characterized by a number of methods, and the energetics associated with their formation have been studied. The rate determining step involves reductive elimination of hydrogen, but it is thought that prior rearrangement to a second intermediate having no $Pt_2(\mu\text{-}H)$ group is necessary before the reductive elimination can occur. It has not been possible to determine whether the slow step involves reductive elimination at a single platinum center or a true binuclear reductive elimination. However the results obtained for (I) and (Ic) are certainly consistent with the latter. Regardless of the mechanism, it is shown that the activation energy for reductive elimination is less

than that expected for reductive elimination from a mononuclear $[PtH_2L_2]$ complex and hence that cooperative effects in binuclear complexes can lead to enhanced reactivity.

CHAPTER 3

Photochemical Reductive Elimination of Hydrogen From $[Pt_2(\mu\text{-}H)H_2(\mu\text{-}dppm)_2]^+$

3. Introduction

The thermally or photochemically induced reductive elimination of H_2 from mononuclear polyhydrido derivatives of transition metals has been studied in depth.[9,45,46,87,88] The primary reaction, which may be reversible, is often described by the general equation (3.1) and involves a concerted intramolecular reductive elimination.[9,45,46,87-90]

$$[L_nMH_2] \longrightarrow [L_nM] + H_2 \qquad \ldots(3.1)$$

In some cases, for example with $[IrH_2Cl(CO)(PPh_3)_2]$, both thermal and photochemical activation is possible but in other cases, for example with $[IrH_2Cl(PPh_3)_3]$, only photochemical activation is effective.[90] The product $[L_nM]$ is necessarily coordinatively unsaturated and is often highly reactive; it may undergo self-reaction, typically by orthometallation (e.g. when $L_nM = [IrCl(PPh_3)_3]$)[90] or react with solvent (e.g. when $L_nM = [Ir(\eta^5\text{-}C_5Me_5)(PMe_3)]$). This reaction with solvent provides examples of the elusive C-H bond activation in saturated hydrocarbons by transition metal complexes in homogeneous solution (equation (3.2)).[91]

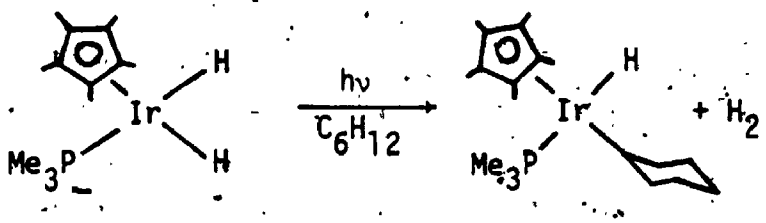

...(3.2)

The species L_nM is expected to be an active catalyst in many cases although this area has not been developed. It may be possible to trap the primary product L_nM with added ligand L but, in the typical case where $[L_nMH_2]$ is an 18-electron complex, L is not involved in the rate-determining reductive elimination step.[9,45,46,87]

In contrast, although there are several examples of thermally induced reductive elimination of H_2 from binuclear and polynuclear transition metal hydrides, very little is known about the mechanism of such reactions.[92] Although almost all mononuclear polyhydrido derivatives of transition metals undergo photochemically induced reductive elimination of H_2,[87,88,93] a few examples of polynuclear transition metal hydrides undergoing such a reaction have been reported.[94] One recent example is the hydrogen elimination from $[[(\eta^5\text{-}C_5H_5)FeH(CO)]_2(dppe)]$ which can be initiated both thermally and photochemically according to equation (2.4).[44] The generality of this reaction is not known, and some polynuclear hydrides do not appear to undergo photochemical reductive elimination. For example $[Re_4H_4(CO)_{12}]$ is emissive in hydrocarbon solutions but is not photochemically decomposed.[95] The photochemical H_2 elimination reaction from dinuclear systems may be important in solar energy conversion schemes. Although no dihydride intermediate has been trapped the production of H_2 is observed under photolysis of aqueous solutions of some binuclear systems.[96,97]

The understanding of the mechanism of photoinduced dihydrogen loss may aid in the development of such transition metal based solar energy conversion systems. As discussed in the previous chapter the cation $[Pt_2H_2(\mu\text{-}H)(\mu\text{-}dppm)_2]^+$, (Ia), undergoes loss of dihydrogen induced by two electron donor ligands such as tertiary phosphines (equation (3.3)).[25-28]

Qualitative experiments indicated that (Ia) was photosensitive, decomposing to yield H_2 in both the solid state or in solution.[25-27,98] Thus the opportunity to investigate the mechanism of photochemically induced reductive elimination from a binuclear polyhydride arose. This complex is a particularly useful one in that the results may be compared not only with photochemical eliminations from mononuclear systems but also with the thermal elimination previously studied.[99]

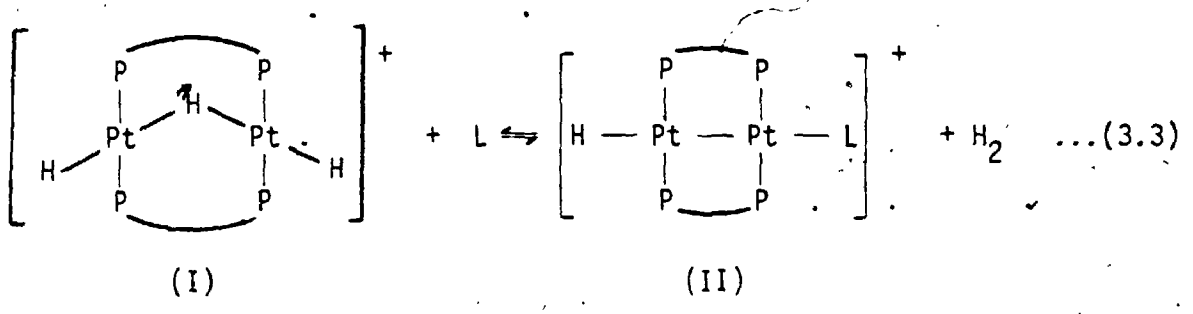

(I) (II) ...(3.3)

3.1 Results

3.1.1 Characterisation of Products

The characterisation of the products of equation (3.3), L = tertiary phosphine, has been described previously.[27,100] The complex (IIa), L = η^1-dppm, was characterised by X-ray crystallography and (IIb), L = PPh_3, by comparison of its spectral properties with those of (IIa). The two new complexes $[Pt_2HL(\mu\text{-dppm})_2][PF_6]$ [(IIc), L = C_5H_5N; (IId), L = MeCN] were prepared by photolysis of (Ia) in pyridine or acetonitrile respectively and were characterised by elemental analysis, and by infrared and NMR spectroscopy. Comparison of spectral data with data for (IIa) and (IIb) was especially useful. Samples for NMR spectroscopy were conveniently prepared by photolysis of degassed solutions of (Ia) in the required solvent in sealed NMR tubes. Thus photolysis of (Ia) in CD_3CN solution led to visible gas evolution, and was accompanied by decay of the hydride resonances, due to (Ia) and growth of a new hydride resonance, due to (IId). This resonance contained 1/4 intensity satellites attributed to coupling to the directly bound Pt atom [^1J(PtH)963Hz] and the far Pt atom [^2J(PtH)76Hz], characteristic of complexes (II) and proving the presence of a terminal hydride in a dimeric molecule. The CH_2 resonance of the dppm ligands gave two distinct couplings ^3J(PtH) of 71 and 52 Hz due to coupling with non-

equivalent ^{195} Pt atoms showing that the dimer was unsymmetrical. The ^{31}P NMR spectrum contained a central [AA'BB'] multiplet with distinctly different couplings $^{1}J(PtP^{A})$ and $^{1}J(PtP^{B})$, again characteristic of complexes of structure (II).[26,27]

The reactions could also be monitored by IR spectroscopy. Thus photolysis of (Ia) in acetonitrile solution contained in a solution IR cell was accompanied by loss of the peak due to (PtH) at 2100 cm^{-1} and growth of a new peak due to the terminal Pt-H stretching vibration of (IId) at 2020 cm^{-1}.

Similar experiments were carried out for the photolysis of (Ia) in pyridine solution and gave similar results. When quantitative monitoring was required, the reactions were followed by UV-visible absorption spectroscopy. Figure 3.1 shows the changes in absorption spectra during photolysis of (Ia) in acetonitrile solution. The photolysis was carried out using 366 nm light from a medium pressure mercury lamp, with the solution contained in a flat-sided pyrex vessel fitted with a sidearm with a 1 mm quartz cuvette. Good isosbestic points were observed at 339 and 371 nm provided that the solution was rigorously deoxygenated before photolysis. If oxygen was present during photolysis, or if oxygen was admitted after photolysis was complete, a further reaction occurred with loss of the isosbestic points, and (IId) could not be isolated from the resulting solutions. The photolysis of (Ia) in pyridine solution was less sensitive to oxygen but good isosbestic points were again observed only for rigorously deoxygenated solutions.

For the syntheses of (IIc) and (IId), the photolysis was carried out at 0°C as above except that a high pressure xenon lamp was used. The solutions were then evaporated under vacuum to give the pure

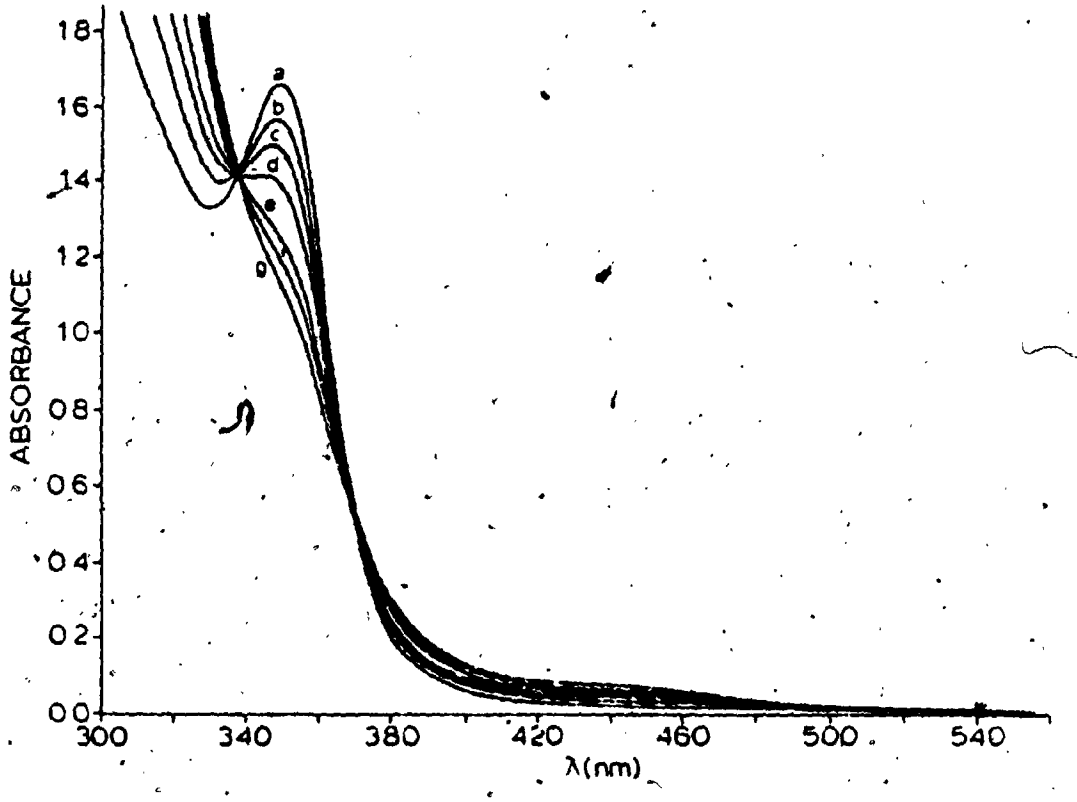

Figure 3.1. Electronic spectral changes accompanying the 366 nm photolysis of (Ia) in CH_3CN. Irradiation times: (a) zero, (b) 3 min, (c) 5 min, (d) 8 min, (e) 13 min, (f) 18 min, (g) 24 min.

products. In another case, photolysis of (Ia) in acetonitrile was carried out to near completion and a sample of the gaseous phase was extracted and analysed by gas chromatography; 1.00 ± 0.08 mol of H_2 was formed for each mol of (Ia) decomposed. Together with the direct characterisation of (IIc) and (IId), this proves that the reaction occurs very cleanly according to the stoichiometry of equation (3.3).

3.1.2 Proof of Intramolecular Reductive Elimination

A sample of $[Pt_2D_2(\mu\text{-}D)(\mu\text{-}dppm)_2][PF_6]$, (Ib), was prepared by reduction of $[PtCl_2(dppm)]$ with $Na[BD_4]$ in MeOD. Earlier studies had shown that the complex could not be prepared from (Ia) and excess D_2O or MeOD with either acid or base catalysis.

A mixture of (Ia) and (Ib), when either treated with triphenylphosphine or irradiated (λ=366 nm) gave very largely H_2 and D_2 with only a small quantity of HD (Table 3.1). Some of this HD arises from ^1H impurities in (Ib) as evidenced by the blank experiment in which (Ib) alone was allowed to react with triphenylphosphine, but the accuracy of the measurements is limited and we cannot exclude the possibility of a minor intermolecular reaction producing HD. The experiment clearly shows that the major part of the reaction involves intramolecular reductive elimination in both the thermal and photochemical cases. In another experiment (Ib) was photolysed in CH_3CN solution in the presence of ~1 mol of H_2. The mass spectrum showed the product to be very largely H_2 and D_2, indicating that the reverse reaction, involving oxidative addition of H_2 to (IId)-d is slow under these conditions. If this reaction were fast, then photolysis of the product would yield HD.

TABLE 3.1

Analysis of isotopic composition of H_2/D_2 by mass spectrometry

Reagents (g)			Solvent	Peak height[a]			
(Ia)	(Ib)	PPh_3		m/e 1	2	3	4
0.05	0	0.1	CH_2Cl_2	0	100	0	0
0	0.05	0.1	CH_2Cl_2	0	6	14	100
0.025	0.025	0.1	CH_2Cl_2	0	84	23	100
0	0.05	b,c	CH_3CN	0	5	16	100
0.025	0.025	b,c	CH_3CN	0	100	8	48
0	0.05	b,d	CH_3CN	0	100	6	40

[a]Background was negligible under the instrument conditions used.

[b]Sample photolysed using 366 nm light.

[c]Photolysis not taken to completion.

[d]Reaction in the presence of H_2 (1 mol).

3.1.3 Quantum Yield Determinations and Sensitization Experiments

Solutions of (Ia) or (Ib) in acetonitrile or pyridine were irradiated with 362±8 nm light from a Jasco Spectroirradiator. The solutions were rigorously degassed prior to irradiation. A typical set of spectra obtained during irradiation of (Ia) in pyridine solution is shown in Figure 3.2. The extent of reaction was determined by monitoring the optical density at 333 nm. The amount of light absorbed by (Ia) (or Ib) was then calculated from the absorption spectra, and correction made for light absorbed by products. Plots of moles reacted vs light absorbed were linear (figure 3.3), yielding the quantum yields from the slopes.

The quantum yields for reaction of (Ia) were .81 (in MeCN) and .57 (in pyridine). The quantum yields for reaction of (Ib) allows calculation of Φ_H/Φ_D as 1.8 for photolysis in MeCN and 1.6 for photolysis in pyridine.

Prolonged photolysis of (IId) in acetonitrile solution led to further changes in the absorption spectrum. However, this reaction was so slow that it did not interfere with the above quantum yield determinations. No serious attempt was made to study this secondary reaction. Admission of air to solutions of (IId) prepared as above led to further spectral changes, with a decrease in absorbance at 450 nm and an increase at 400 nm. However, there were no isosbestic points and we have not succeeded in characterising the products of this subsequent reaction.

The performance of specific quenching experiments to distinguish between singlet and triplet pathways was not possible because of the high extinction coefficients of the complex throughout the ultraviolet

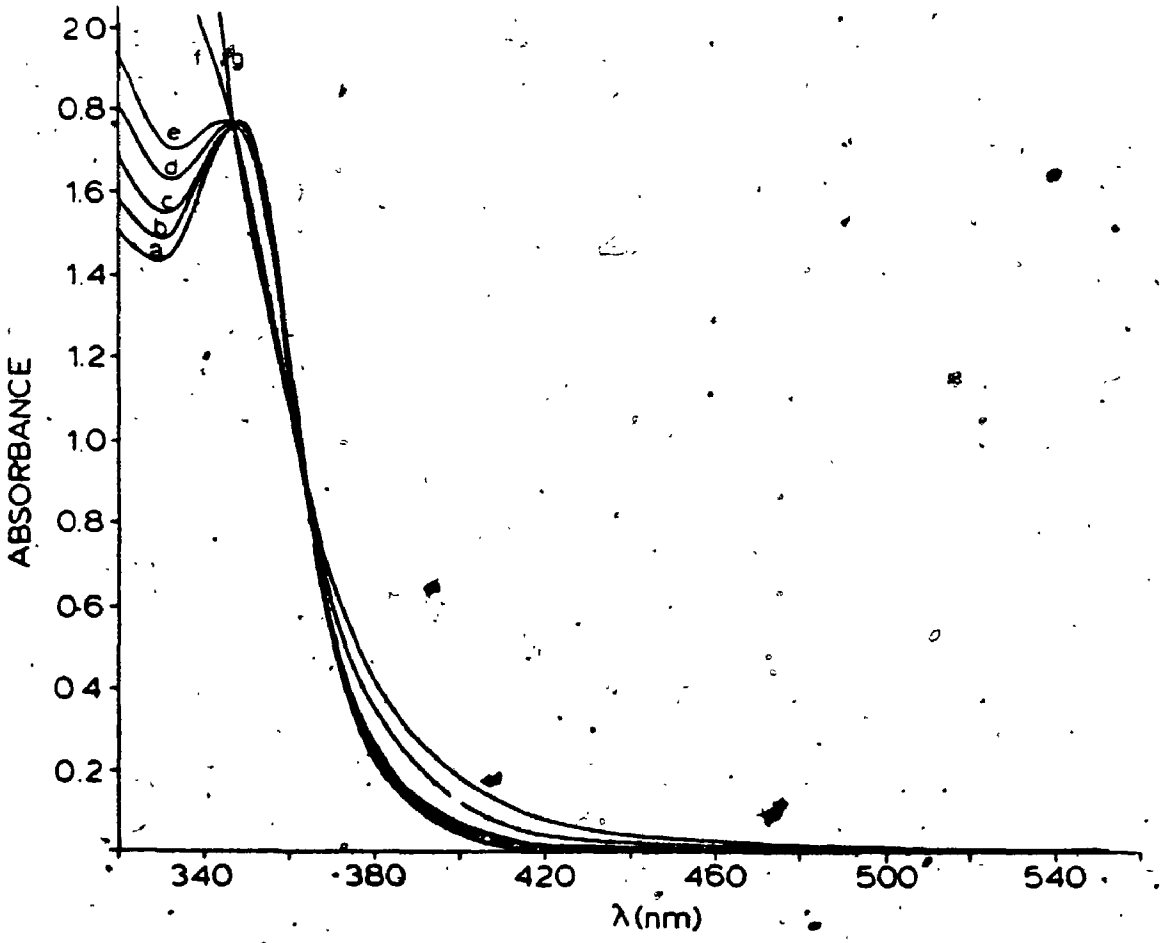

Figure 3.2. Electronic spectral changes accompanying the 362 ± 8 nm photolysis of (Ia) in pyridine. Number of counts of irradiation (a) 0, (b) 1, (c) 2, (d) 4, (e) 6, (f),(g) extended irradiation.

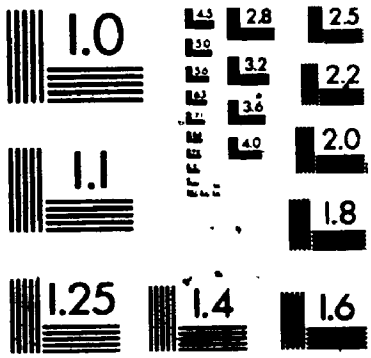
1.0
1.1
1.25
1.4
1.6
1.8
2.0
2.2
2.5
2.8
3.2
3.6
4.0
4.5
5.0
5.6

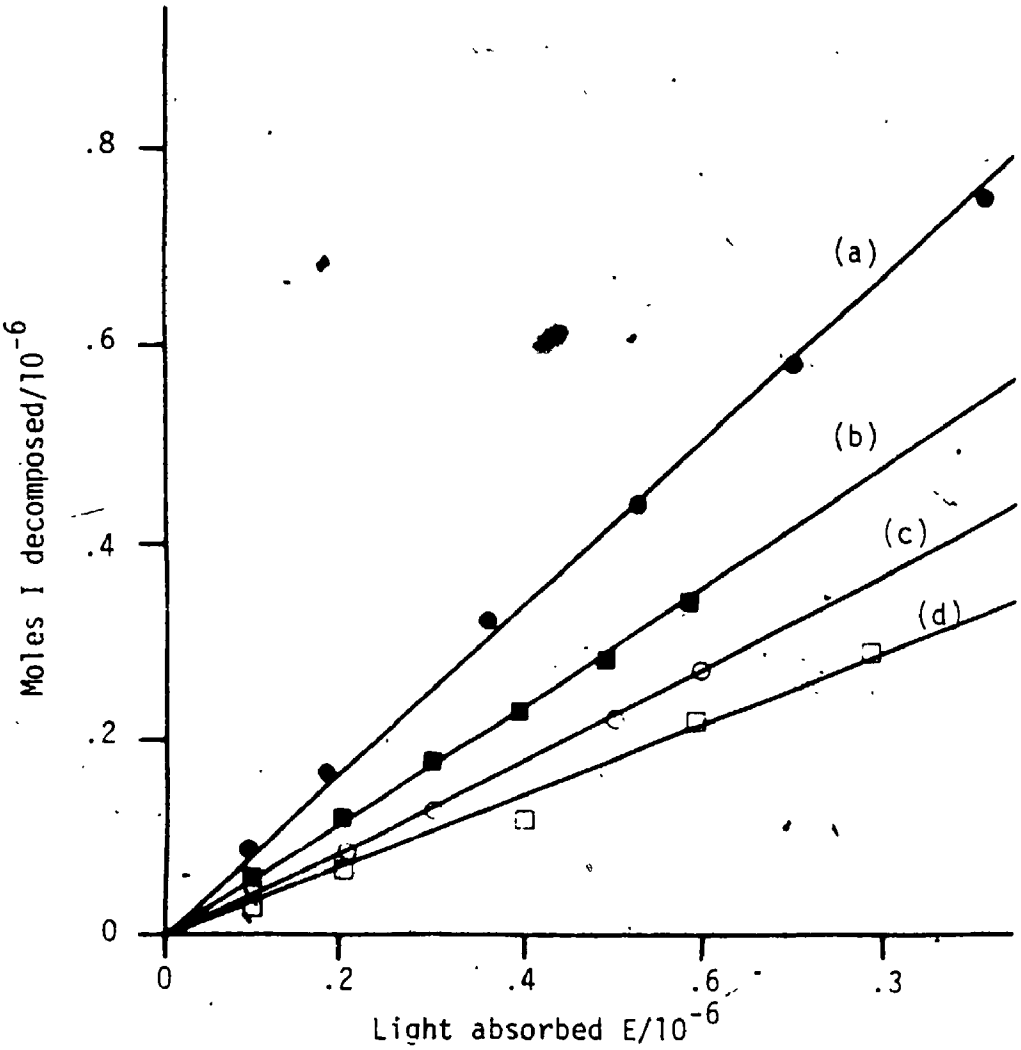

Figure 3.3. Plots of moles decomposed vs Einsteins light absorbed for Ia in MeCN (a) and pyridine (b) and Ib in MeCN (c) and pyridine (d).

region. It was, however, possible to sensitize the reaction in MeCN and monitor its course by means of the terminal Pt-H stretching absorption in the IR spectrum. Concentrations were chosen such that ~90% of the incident light (at 254 nm) was absorbed by the sensitizer, triphenylene (E_S = 83.4 kcal/mole; E_T = 66.5 kcal/mole).[101,102] The spectral distribution of the low pressure Hg lamp used was such that small amounts of light were emitted in the 313 and 366 nm regions. Although the filter solution used removed most of this light, the amount of reaction induced by this light was determined experimentally. This was achieved by determining the rate of reaction when a Pyrex filter was interposed between the sample and the light source. This rate was then subtracted from the rates at which the sensitized and directly induced reactions occurred. A further correction was made for the 10% light absorbed directly by (Ia). The final ratio of rate sensitized/rate direct was, from these rather crude measurements, limited by the degree of conversion possible and by the inaccuracy of the IR measurements. The value found was .57 ± .12 at a concentration of (Ia) of 6.1×10^{-3} mol l^{-1}.

The sensitization experiment alone does not distinguish singlet from triplet energy transfer but, since attempted sensitization by the efficient triplet sensitizer Michler's ketone was negative and since the triplet energies of triphenylene and Michler's ketone (E_T = 62 kcal/mole)[101] are close, we conclude that singlet energy transfer is operative. Assuming the lifetime τ of triphenylene singlet in acetonitrile is essentially the same as in cyclohexane (τ 37 ns)[103], we can approximate the rate of energy transfer by equation (3.4).

$$\text{ratio sensitized/direct} = k_q[Ia]/(k_q[Ia]+\tau^{-1}) \qquad \ldots(3.4)$$

whence k_q, the rate constant for energy transfer is $6(\pm 2) \times 10^9 M^{-1}s^{-1}$. This is somewhat below that of diffusion control ($2.7 \times 10^{10} M^{-1}s^{-1}$ from the modified Debye equation). Allowing for diffusion separation before energy transfer[104] this would be expected to be about $10^{10} M^{-1}s^{-1}$. However, energy transfer to bulky complexes has often been found to be somewhat inefficient even when exothermic[105] and the approximate value we report is not unreasonable. We are therefore led to believe that the reaction takes place from a singlet, not a triplet, state.

3.2 Discussion

According to the calculations of Hoffman and Hoffmann,[63] the LUMO in the cation (Ia) is an orbital of $\underline{b}_2$ symmetry, which is non-bonding between the platinum atoms and the μ-H ligand but is antibonding between the two platinum atoms, while the HOMO is one of a block of 8 closely spaced d-block orbitals (Figure 3.4). The irradiation using 362 nm or 366 nm light is expected to lead to the transition $\underline{d} \rightarrow b_2$ (max 349 cm^{-1} in MeCN). The sensitization experiment indicates that the photochemistry results directly from the primary singlet excited state, and the labelling experiment shows that the reductive elimination of H_2 is an intramolecular reaction. Unfortunately the cation (Ia) is fluxional so that it is not possible to label the bridging or terminal hydride ligands separately and hence to determine unequivocally which two hydride ligands are lost on photolysis.

The simplest interpretation of the above data is that the primary excitation of (Ia) leads to a significant increase in the Pt Pt separation as a result of occupation of the $\underline{b}_2$ molecular orbital.[63]

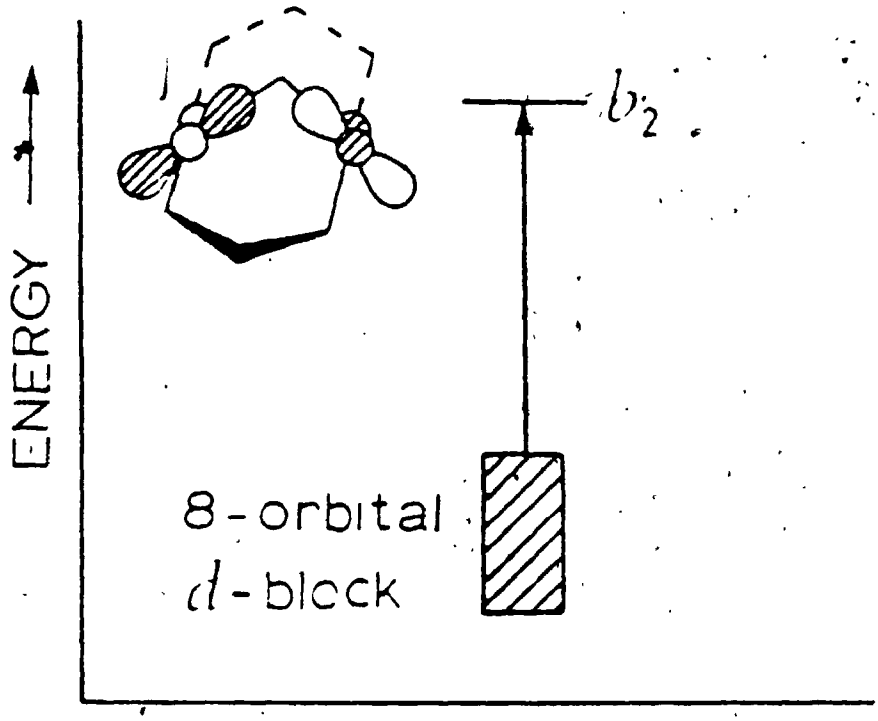

Figure 3.4. Qualitative MO energy level diagram for (Ia), adapted from ref. 63.

This would force the bridging hydride to move with one of the Pt atoms, since a symmetrical μ_2-hydride with a very long Pt-Pt distance would be unfavorable. This deformation may result in a structure such as (III) from which H_2 loss, through a true binuclear mechanism occurs.

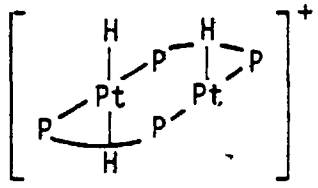

III

It should be noted that objections[92] to this type of reaction discussed in Chapter 2 may not apply in the excited state. An alternate possibility is the rearrangement of (III)→(IV), with a coordinate Pt Pt bond as found in $[Pt_2H_2Cl(\mu\text{-dppm})_2]^+$ (V).[106]

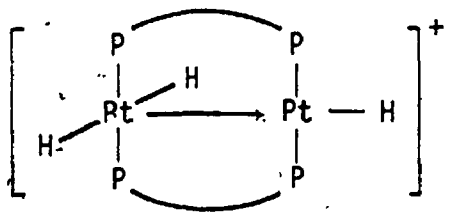

(IV)

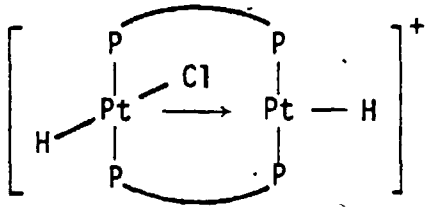

(V)

The isomerization of IV could then occur giving a complex (VI) analogous to that of $[Pt_2Me_3(\mu\text{-dppm})_2]^+$,[32] (VII).

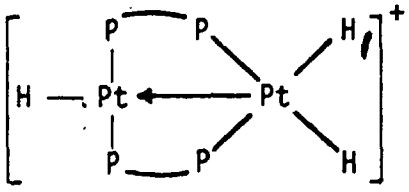

(VI)

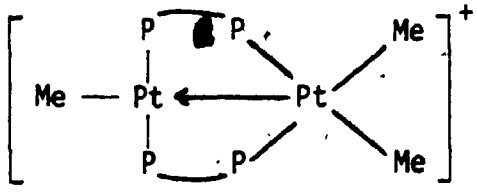

(VII)

This type of cis-trans isomerization is generally thought to occur through dissociation of phosphine, a high energy process. The conversion of (IV) to (VI) would only be expected to occur if (IV) was vibrationally hot, from photolysis, allowing a tetrahedral transition state. Alternatively, (VI) may be formed directly by isomerization of (III) prior to the coordinate bond formation.

A simple mononuclear elimination from (VI) could then occur through a 3 centre transition state as is found in mononuclear systems.

In the case of the thermal reaction the coordination of tertiary phosphine led to formation of an intermediate (VIII) from which loss of H_2

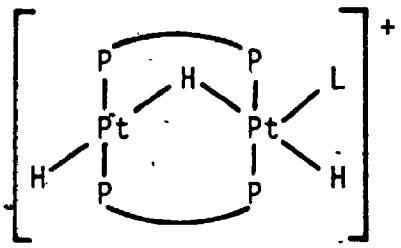

(VIII)

eventually occurred. In the photolysis, there is no evidence for direct participation of pyridine or acetonitrile prior to the reductive elimination step (except possibly to provide a new decay channel). The observations that the quantum yield for photolysis of (Ia) in acetonitrile (0.81) is greater than in pyridine (0.57), whereas pyridine is much the better ligand for platinum, and that photolysis of (Ia) occurs readily in non-donor solvents or in the solid state argue against such solvent participation. Rather, it seems that the donor solvent simply traps the primary product, $[Pt_2H(\mu\text{-dppm})_2]^+$, formed on reductive elimination of H_2. That the donor solvents do not interact strongly with (Ia) in the ground state is shown from the UV, IR and NMR spectra

of solutions of (Ia) which are very similar to those in non-donor solvents.

The observation of a considerably lower isotopic effect on the quantum yields for photolysis of (Ia) vs (Ib), when compared with the corresponding isotopic effects for the thermal reactions induced by triphenylphosphine or dppm, for which $k_H/k_D \sim 3.5$, is of interest since no such comparison appears to have been made previously, even for reactions of mononuclear complexes. The result is, however, difficult to interpret. In the simplest case defined by equation (3.5),

$$(I) \underset{k_d(H,D)}{\overset{}{\rightleftharpoons}} I^* \xrightarrow{k_r(H,D)} \text{product} \qquad \ldots(3.5)$$

it is easily shown that

$$\Phi_H/\Phi_D = k_r(H)/k_r(D).\{k_r(D)+k_d(D)\}/\{k_r(H)+k_d(H)\}$$
$$= \text{isotope effect} \times \tau(H)/\tau(D)$$

Unfortunately, the complexes (I) did not show observable fluoresence (or phosphorescence) so that we have been unable to determine the isotopic effect on the lifetime of the singlet excited state, $\tau(H)/\tau(D)$. Qualitatively, $\tau(H)/\tau(D)$ is expected to be less than unity, but there are insufficient precedents to allow an estimate of how great such an effect might be.[95] Thus the observed magnitudes of Φ_H/Φ_D of 1.6 (L = pyridine) and 1.8 (L = acetonitrile) are considered minimum values for the isotope effects on the rate constants for reductive elimination from the excited states, $k_r(H)/k_r(D)$, and it is not clear whether the isotope effects for these rate constants are significantly

different from the value of k_H/k_D found for the thermal reactions.[104] However the result certainly indicates that partial Pt-H bond cleavage is involved in the transition state for reductive elimination.

This is significant as it suggests that the cis-trans isomerization required for a mononuclear elimination, generally a high energy process, is not involved in the rate determining step. This evidence against the mononuclear elimination is not, however, conclusive as the isomerization of the excited state may occur readily.

3.3 Conclusions

The study described in this chapter is significant since it shows, for the first time, that intramolecular reductive elimination of dihydrogen can occur very efficiently from a binuclear transition metal hydride. It has also been demonstrated that, in the case of (I), the reaction occurs through a singlet state and that there is a significant primary isotope effect on the rate constant for the reductive elimination step.

It has not been possible to determine the intimate mechanism of the reductive elimination step. As discussed, however, a binuclear elimination such as that proposed is consistent with the data.

CHAPTER 4

Photochemistry of Methyl Diplatinum(II) Complexes

4. Introduction

In the previous two chapters loss of H_2 by reductive elimination from the cation $[Pt_2(\mu\text{-}H)H_2(\mu\text{-}dppm)_2]^+$, (I), was described, under both thermal and photochemical conditions. Thermally induced reductive elimination reactions are known not only for H_2 formation but also in cases where C-H and C-C coupling occur. These reactions are significant in catalysis involving formation or activation of alkanes at transition metal centres.[91,108-111]

The photochemical reductive elimination of H_2 from mononuclear complexes is well established, and has now been shown to be operative in binuclear systems. In contrast there have been no detailed studies of photochemical reductive eliminations leading to C-H or C-C bond formation even in mononuclear systems, and there are only a few qualitative reports of such reactions.[18,31,91,112-114]

The only report of photolysis of a metal alkyl hydride, of which I am aware, was reported recently by Bergman and Janowicz.[91] This paper was a description of C-H bond activation by an iridium complex, $[IrH_2(\eta\text{-}C_5Me_5)(PMe_3)]$. Photolysis of this complex causes loss of H_2 followed by oxidative addition of the hydrocarbon solvent. The authors noted that the hydrido (alkyl) metal complexes undergo photoinduced reductive eliminations, but no details of the process were given.

There has been a considerable amount of work done on the photochemistry of complexes of formula $[MR_2L_n]$, R = alkyl, L = ligand. Two major reaction pathways have been established for these complexes.

The first is metal-alkyl bond homolysis. An example of this is the photolysis of cis-$[Pt(C_2H_5)_2(PPh_3)_2]$, which yields ethyl radicals.[12] The second pathway is β-elimination of an alkyl group, such as is thought to occur upon photolysis of $[Th(\eta\text{-}C_5H_5)_3(^iC_3H_7)]$.[16]

Some exceptions to this general pattern of reactivity have been reported. Photolysis of bis-(p-tolyl)zirconocene in benzene forms 4-4'-dimethylbiphenyl in almost quantitative yield, although no mechanistic details were reported.[112] It should be noted that the above organic product is consistent with reductive elimination.

The second exception is the elimination from platinacycles. Platinacyclobutanes under photochemical activation may yield cyclopropane products.[18,113,115,116] It should be noted however that, although the net reaction in these cases is a reductive elimination, a mechanistic investigation indicates the primary photoreaction is at least partly metal-carbon bond homolysis. One case of what appears to be a true reductive elimination is the result of photolysis of the platinacyclopropane $[Pt(C_2H_4)L_2]$ as shown in equation (4.1).[117]

$$L_2Pt\begin{smallmatrix}CH_2\\|\\CH_2\end{smallmatrix} \xrightarrow{h\nu} L_2Pt + C_2H_4 \qquad \ldots(4.1)$$

The study described in this chapter has established the photochemical reductive elimination forming C-H and C-C bonds. The chemical system used was based on the complex ions $[Pt_2H_nMe_{3-n}(\mu\text{-dppm})_2]^+$, n = 0-2. We felt this system was an ideal choice as the trihydride complex (I) was known to eliminate H_2 upon photolysis.

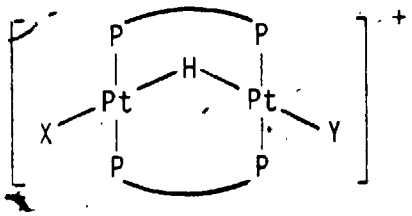

I, X=Y=H

II, X=H, Y=Me

III, X=Y=Me

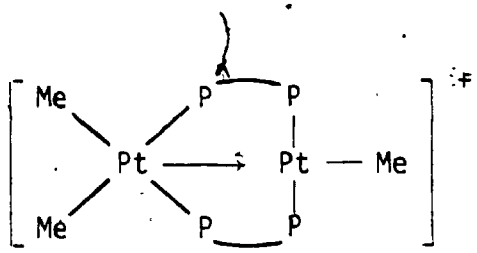

IV

4.1 Results

4.1.1 Photochemistry of the Hydrido bridged "A-Frame" Complexes

As described in the preceeding chapter, photolysis of (I) led to the production of H_2 and the diplatinum(I) complexes (V) (equation (4.2)). Photolysis of (II), $[Pt_2(\mu\text{-}H)HMe(\mu\text{-}dppm)_2]^+$, or (III) $[Pt_2(\mu\text{-}H)Me_2(\mu\text{-}dppm)_2]^+$ was expected to give either hydrido complexes (V) or metny

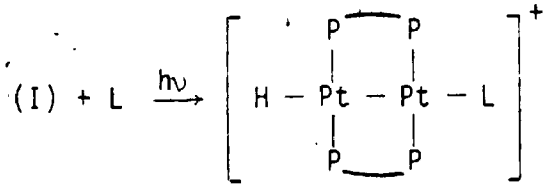

...(4.2)

Va, L = C_5H_5N

Vb, L = MeCN

complexes (VI) (equation (4.3, 4.4)).

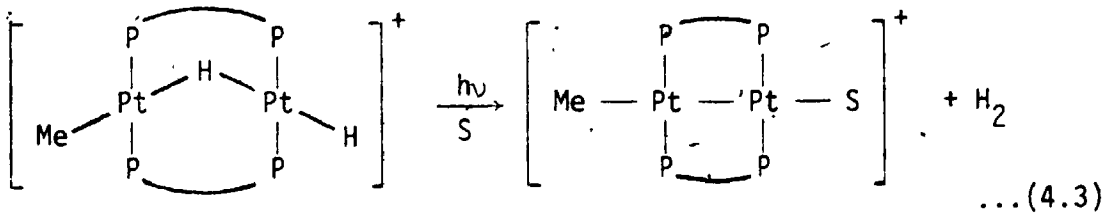

...(4.3)

VIa, S = C_5H_5N; VIb, S = MeCN; VIc, S = Me_2CO

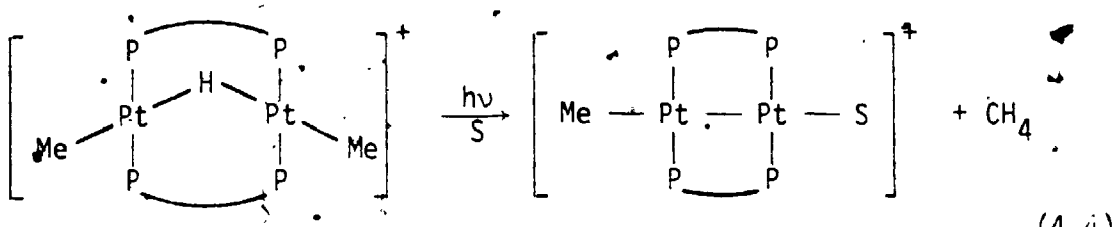

...(4.4)

In each case photolysis of degassed solutions of (II) or (III) led to methylplatinum complexes, (VI), and no hydridoplatinum complexes were observed. In reaction of (II), H_2 was the major gaseous product while traces of methane were also observed. In reaction of (III) the only observed gaseous product was methane.

The new methylplatinum complexes were characterized by their ^1H and ^{31}P NMR spectra (Table 4.1). They are similar to the previously synthesized complexes $[Pt_2MeL(\mu\text{-dppm})_2]^+$, where L = phosphine.

The most stable of these $[Pt_2Me(NC_5H_5)(\mu\text{-dppm})_2][PF_4]$ (VIa) was fully characterised. The ^1H NMR spectrum contains a MePt resonance at 0.53 ppm. The $^2J(PtH)$ value observed was 69 Hz. A further coupling $^3J(PH)$ = 6.5 Hz resulted in a triplet appearance of both the center and satellites. The resonance due to the CH_2 protons of the dppm ligand consisted of a complex multiplet at δ = 5.29 ppm.

The $^{31}P\{^1H\}$ NMR of this complex was also recorded and is characteristic of an asymmetrical diplatinum(I) species. One phosphorus resonance is observed at δ = 8.4 ppm with satellites due to coupling to ^{195}Pt, with $^1J(PtP)$ = 2930 Hz. The second ^{31}P resonance at δ = -4.7 ppm also had platinum satellites with $^1J(PtP)$ = 2850 Hz. From the fine structure of the satellite peaks, the coupling constants due to PP coupling could be determined as $J(PP''')$ = 37 Hz and $J(PP'')$ = 58 Hz. The way in which these spectra are analyzed has been published

previously.[27]

The remaining two platinum(I) species were less stable, and pure samples could not be obtained. They were, however, characterised by their ^1H NMR spectra (Table 4.1), which are very similar to the spectrum of the fully characterised pyridine complex. In addition, the species (VIb) or (IIc) in solution can be converted to the pyridine complex, (VIa), by addition of pyridine. These metathesis reactions were monitored by ^1H NMR spectroscopy. In each case the signal due to the MePt protons of (VIb) or (VIc) disappeared on addition of pyridine, and was replaced by the MePt resonance of (VIa).

Reaction (4.2) involving reductive elimination of H_2 is analogous to reaction (4.1) studied previously, but reaction (4.3) is of a new and significant type and so a labelling experiment was carried out to determine if reductive elimination of methane is an intramolecular or intermolecular process. A mixture of $[Pt_2(\mu\text{-}H)Me_2(\mu\text{-}dppm)_2][PF_6]$ and $[Pt_2(\mu\text{-}D)(CD_3)_2(\mu\text{-}dppm)_2][PF_6]$ gave CH_4 and CD_4, with only traces of CH_3D or CD_3H, on photolysis. It is thus proved that intramolecular reductive elimination occurs. When photolysis was not complete, the yield of CH_4 was greater than that of CD_4. This suggests, as in the photolysis of (I), there is a significant primary isotope effect on the rate of reaction which can be estimated as $\Phi_H/\Phi_D = 1.5$.

Quantum yields for photolysis of (II) or (III) in pyridine or acetonitrile were determined by irradiation of rigorously degassed solutions in quartz cuvettes with 362±7 nm light from a Jasco Spectroirradiator, previously calibrated using ferrioxalate actinometry. Typical sets of UV-visible absorption spectra obtained during irradiation of (II) and (III) are shown in Figures 4.1 and 4.2. For photolysis of

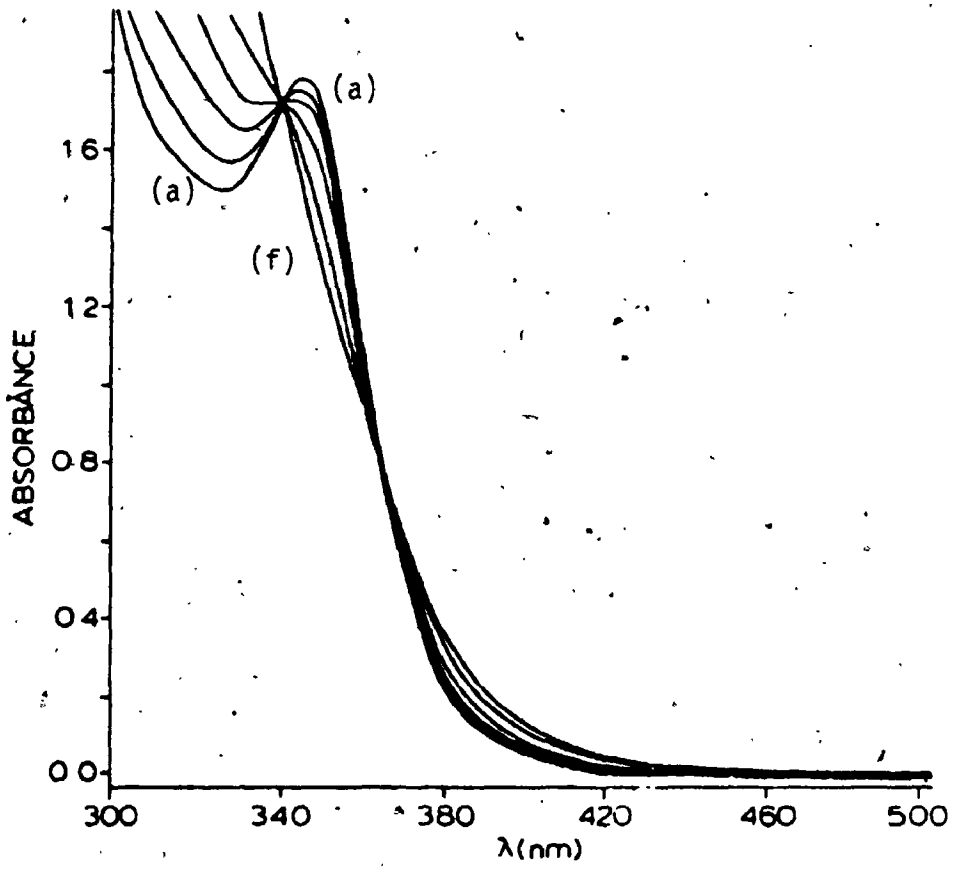

Figure 4.1. Changes in the UV-visible absorption spectrum on irradiation of $[Pt_2H(\mu\text{-}H)Me(\mu\text{-}dppm)_2]^+$ in MeCN, with the following numbers of Einsteins of incident light (362±7 nm): (a) 0, (b) 4.0×10^{-7}, (c) 8.0×10^{-7}, (d) 14.4×10^{-7}, (e) 26.4×10^{-7}, (f) extended irradiation.

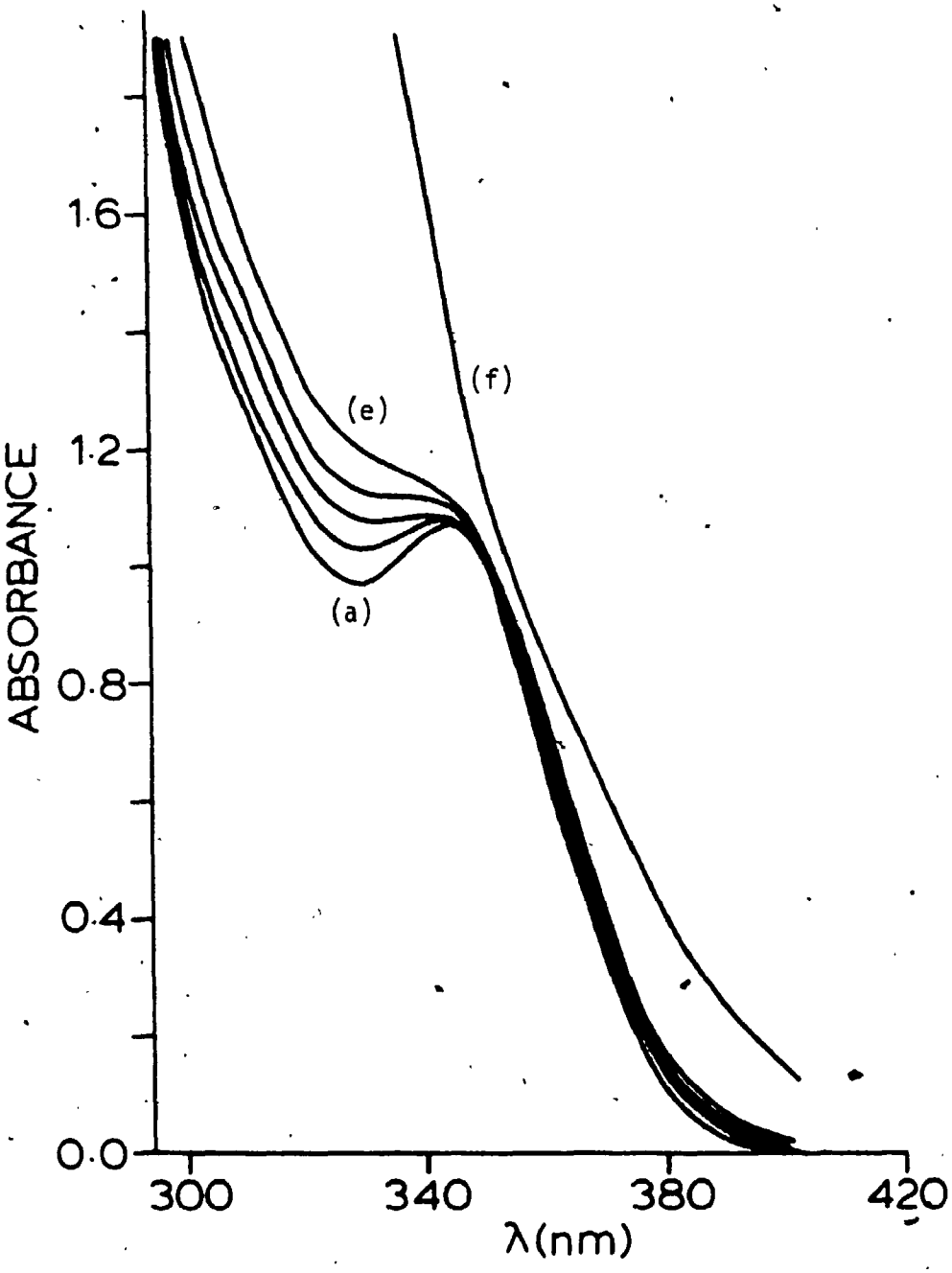

Figure 4.2. Changes in the UV-visible absorption spectrum on irradiation of $[Pt_2(\mu\text{-}H)Me_2(\mu\text{-}dppm)_2]^+$ in MeCN, with the following numbers of Einsteins of incident light (362±7 nm): (a) 0, (b) 3.6×10^{-7}, (c) 6.0×10^{-7}, (d) 8.4×10^{-7}, (e) 11.2×10^{-7}, (f) extended irradiation.

TABLE 4.1

NMR Data for the Complexes $[Pt_2MeL(\mu\text{-dppm})_2]^+$

^1H NMR DATA

L	$\delta(CH_3)$	$^2J(PtH)$	$^3J(PH)$
pyridine	.53 ppm	69 Hz	6.5 Hz
$NCCH_3$	.15 ppm	62 Hz	6 Hz
$OC(CH_3)_2$	.29 ppm	70 Hz	7.5 Hz

$^{31}P\{^1H\}$ NMR DATA

L	δP^A	$J(PtP)$	δP^B	$J(PtP)$	$^2J(P^AP^B)$	$^2J(P^AP^{B'})$
pyridine	8.4 ppm	2930 Hz	-4.67 ppm	2850 Hz	37.5 Hz	57.5 Hz

(II) good isosbestic points were observed (Figure 4.1) but for photolysis of (III) there were no crossover points in the UV-visible spectra (Figure 4.2). In each case, the extent of reaction was determined by monitoring the optical density at suitable points, and good linear plots of quanta observed by (II) or (III) vs. extent of conversion were then obtained. From these data, the quantum yields were determined and values are given in the Table 4.2.

It can be seen from Table 4.2 that the quantum yields for photolysis of (I)-(III) are all high, with Φ for (I) > (II) ≃ (III), and the quantum yields are in all cases slightly higher in acetonitrile than in pyridine.

4.1.2 Photochemistry of the Trimethyldiplatinum(II) Complex, $[Pt_2Me_3(\mu\text{-dppm})_2]^+$

Photolysis of complex $[Pt_2Me_3(\mu\text{-dppm})_2]^+$, (IV) in pyridine gave no gas evolution, and monitoring by ^1H and $^{31}P\{^1H\}$ NMR indicated that the products were mononuclear complexes as shown in equation (4.8)

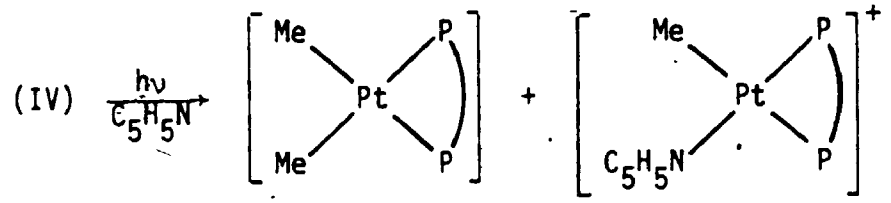

...(4.8)

(VII)

These complexes could not be separated, but were positively identified by the ^1H and $^{31}P\{^1H\}$ NMR spectra. $[PtMe_2(dppm)]$ is a known complex and was characterised by comparison of the NMR parameters with those for an authentic sample.[118,119] A sample containing the cation

TABLE 4.2

Quantum Yields (362 nm) for Photolysis of Diplatinum Complexes

Complex	Quantum Yield[a] Py	MeCN
$[Pt_2H_2(\mu\text{-}H)(\mu\text{-}dppm)_2][PF_6]$[b]	0.57	0.31
$[Pt_2H(\mu\text{-}H)Me(\mu\text{-}dppm)_2][SbF_6]$	0.21	0.37
$[Pt_2(\mu\text{-}H)Me_2(\mu\text{-}dppm)_2][PF_6]$	0.30	0.34
$[Pt_2Me_3(\mu\text{-}dppm)_2][PF_6]$[c]	0.6	0.1

[a] In all cases, these are quantum yields for decomposition of reagent.

[b] Geoffroy et.al. quote a quantum yield of .62 using 366 nm light.

[c] Quantum yield equals 0.6 in C_6H_6 and 0.3 in acetone.

$[PtMe(C_5H_5N)(dppm)]^+$, (VII), was prepared independently by reaction of [PtClMe(dppm)] with one mol equivalent of silver nitrate followed by excess pyridine.

The central part of the $^{31}P\{^1H\}$ NMR spectrum of (VII) in pyridine-d_5 is analyzed as an [AX] spin system, and appears as a pair of doublets centred about δ = -26.6 ppm and δ = -42.3 ppm with the coupling $^2J(pp)$ = 38 Hz. Each doublet has satellites due to coupling with ^{195}Pt (I = 1/2). This coupling $^1J(PtP)$ = 3388 Hz for the resonance at δ = 42.3 ppm and $^1J(PtP)$= 1270 Hz for the resonance at δ = -26.6 ppm. The resonance at -42.3 ppm is assigned as due to the phosphorus trans to pyridine and the resonance centred about -26.6 ppm due to phosphorus trans to methyl. The coupling $^1J(PtP)$ is similar to that found for the phosphorus atom trans to methyl in [PtClMe(dppm)] where $^1J(PtP)$ = 1248 Hz. The $^1H\{^{31}P\}$ NMR spectrum of this complex consists of a 1:4:1 triplet at 1.02 ppm, due to the methylplatinum group with $^2J(PtH)$ = 61 Hz. Selective ^{31}P decoupling experiments were also carried out. When the ^{31}P atom at -42.3 ppm was decoupled, a doublet coupling $^3J(PH)$ was observed and found to equal 8 Hz. In the spectrum with no ^{31}P decoupling a second doublet splitting with $^3J(PH)$ = 3 Hz is observed.

Extended photolysis of the above mixture did lead to some ethane formation and an uncharacterized symmetrical diplatinum complex was also formed. The quantum yield of the primary photochemical reaction of equation (4.5) was high (Table 4.2), but the second photolysis was very inefficient and has not been studied in detail.

Photolysis of (IV) in acetonitrile occurred cleanly in the initial stages to give ethane and complex (VIb), identified by its ^1H and $^{31}P\{^1H\}$ NMR and UV-visible absorption spectra. However, the

quantum yield was low (Table 4.2) and, as a result, further photolysis of product (IVb) became competitive in the later stages and the isosbestic points were lost. This reaction gave the first indication of a photochemical reductive elimination with C-C bond formation, and so the photolysis was studied in several other solvents.

Efficient reductive elimination of ethane occurred on photolysis of (IV) in benzene, acetone or dichloromethane as solvents. In benzene, the product of photolysis was very insoluble and precipitated during photolysis so that an accurate quantum yield could not be obtained.[120] In acetone, the primary products were C_2H_6 and complex (VIc) and the stoichiometry was clean until the late stages, when photolysis of (VIc) became a problem. In this reaction 1.0±0.1 mol of ethane was formed for each mol of (IV) decomposed and the quantum yield (362±7 nm) was 1.2±0.3. The large uncertainty in the quantum yield arose due to problems with the secondary photolysis of (VIc). The quantum yield is within experimental error of 1.0, and is an order of magnitude greater than that in acetonitrile solvent.

In dichloromethane solution, the stoichiometry of reaction was different and only 0.5 mol of C_2H_6 was formed for each mol of (IV) decomposed (equation (4.6)).

$$2[Pt_2Me_3(\mu\text{-dppm})_2]^+ \xrightarrow[CH_2Cl_2]{h\nu} 2[Pt_2Me_2(\mu\text{-Cl})(\mu\text{-dppm})_2]^+ + C_2H_6 \qquad \ldots(4.6)$$
(VIII)

The product (VIII) has been characterised previously[29] and was isolated in quantitative yield. That the reaction occurred cleanly is shown by the isosbestic point in the U.V. spectra for the reaction

(Figure 4.3). It is clear that a chlorine atom abstraction from solvent dichloromethane occurs during this reaction. The quantum yield for disappearance of (IV) was 2.0±0.1 (Figure 4.4).

Because this clean photochemical C-C coupling reaction has no precedents, attempts were made to determine if the elimination is an intramolecular process. Photolysis of an equimolar amount of $[Pt_2Me_3(\mu\text{-dppm})_2][PF_6]$ and $[Pt_2(CD_3)_3(\mu\text{-dppm})_2][PF_6]$ in CH_2Cl_2 or acetone gave a product ratio C_2D_6:CH_3CD_3 of 1:0.4 and 1:1.0 respectively (C_2H_6 yields could not be determined accurately due to high background at m/e 30, under the conditions used, with analysis by mass spectrometry). An intramolecular reaction should give C_2D_6:CH_3CD_3 = 1:0, while an intermolecular coupling reaction should give a ratio of 1:2. The experiment thus proves that at least 50% of the reaction occurs by intramolecular coupling in acetone and at least 80% in dichloromethane.

An effort was made to determine which two methyl groups in 4 were eliminated. However, an attempt to synthesize the unsymmetrical labelled complex ion $[(CD_3)_2Pt(\mu\text{-dppm})_2PtCH_3]^+$ by reaction of $[Pt(CD_3)_2(dppm)]$ with [PtClMe(dppm)] gave a sample of (IV) in which complete scrambling of CD_3 and CH_3 groups had occurred, as determined by ^1H NMR spectroscopy. Thus it was not possible to solve this important problem. We suspect that the alkyl for alkyl exchange reactions which lead to this scrambling, and which have also been observed in other diplatinum complexes,[121] may also account for the apparent intermolecular component of the reductive elimination reaction noted above.

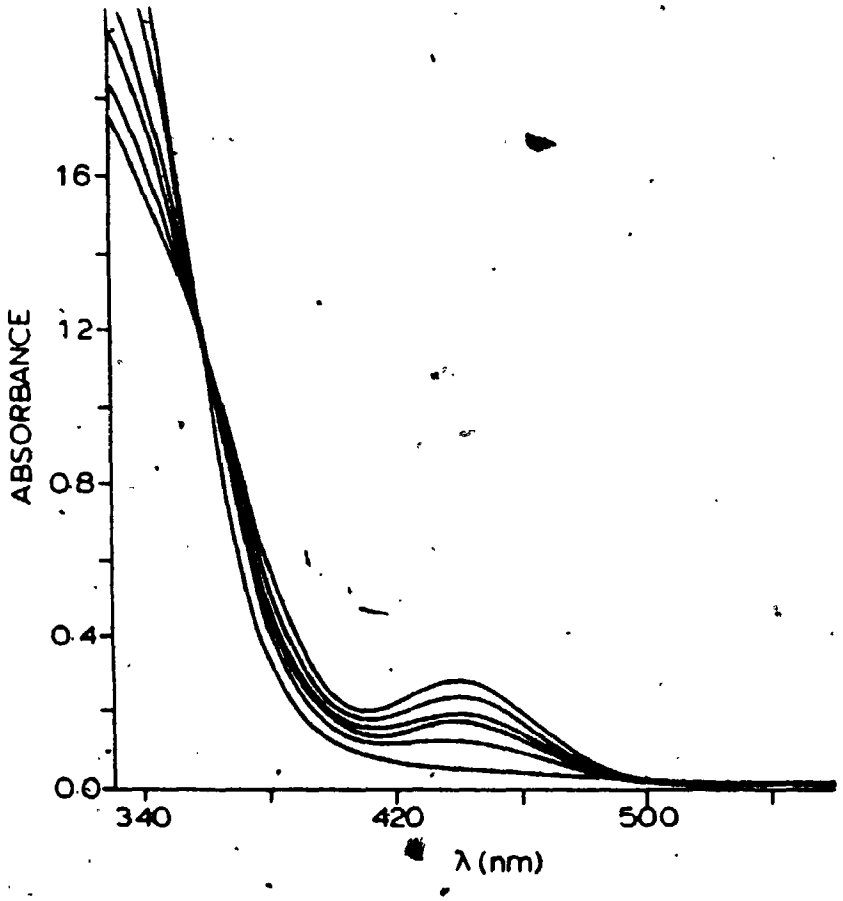

Figure 4.3. Changes in absorption on photolysis of $[Pt_2Me_3(\mu\text{-dppm})_2][PF_6]$ in CH_2Cl_2. Absorbance at 450 nm decreases on photolysis.

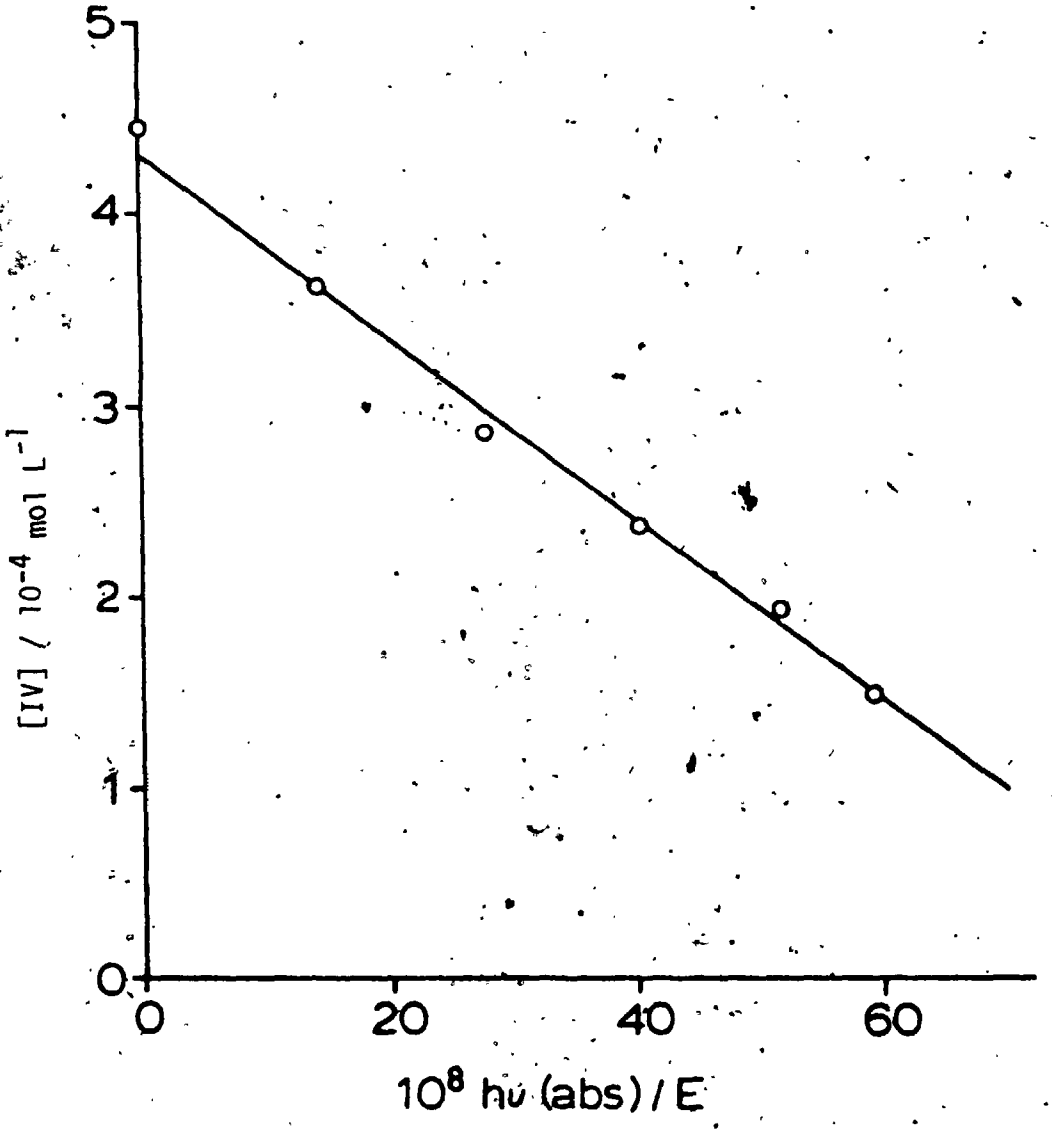

Figure 4.4. Plot of concentration of $[Pt_2Me_3(\mu\text{-dppm})_2]^+$, (IV), vs light absorbed , showing that the quantum yield is independent of concentration of (IV).

4.2 Discussion

The photolysis of the family of complex cations, (I)-(III) in each case leads to an overall binuclear reductive elimination in which the formal oxidation state of each platinum centre decreases from +II to +I. The reactions are very selective. Thus complex (II) gives hydrogen rather than CH_4 and complex (III) gives CH_4 rather than C_2H_6, and so it can be concluded that bond formation is favoured in the sequence H-H > CH_3-H > CH_3-CH_3 in these complexes. However, it should be noted that, in (I)-(III), hydride occupies the bridging position and, since it is possible that the reactions always involve loss of the bridging ligand, only for (II) is there positive evidence that H-H bond formation is preferred rather than CH_3-H bond formation. The same selectivity is observed in thermal reductive eliminations induced by tertiary phosphine ligands, but hexafluorobut-2-yne induces selective reductive elimination of methane from (II).[30] In the thermal reactions, the rates of reaction follow the sequence (I) > (II) > (III), but there are only small differences in the rates of the photochemical reactions (Table 4.2). In particular, the quantum yields for photolysis of (II) (which gives H_2) and (III) (which gives CH_4) are very similar.

It has been proved that the reductive eliminations from (II) and (III) are intramolecular, but the detailed mechanisms of reaction cannot be determined unequivocally. For photolysis of (I) a mechanism involving reductive elimination of H_2 from a single metal centre was proposed initially, but a subsequent study of the thermal reductive elimination suggested a true binuclear reductive elimination in which hydride ligands coupled across two platinum centres (Chapter 2). The

results from the present study can be interpreted in terms of either mechanism (see Chapter 3 for related discussions of mechanisms in binuclear and cluster complexes), but the primary photochemical step in all cases is probably the cleavage of the $Pt_2(\mu\text{-}H)$ linkage by excitation of an electron to a $\sigma^*(PtPt)$ orbital.[63]

The photochemically induced reductive elimination of ethane from (IV) appears to be a unique reaction. Photolysis of alkyl transition metal complexes usually gives homolysis of the M-C bond to give alkyl radicals,[122] though β-elimination, isomerization, loss of other ligands with no reaction of the M-R bond and other reactions can also occur.[18,87,123,125] Photolysis of mononuclear alkyl platinum(II) or alkylplatinum(IV) complexes leads primarily to formation of alkyl radicals,[126,127] though net reductive elimination may be observed with platina(IV)cycloalkanes.[18,115,116]

We have shown that the reductive elimination of ethane is at least partially intramolecular by a labelling experiment, and we believe that this reaction is almost entirely intramolecular. In order to give the observed quantum yields (Table 4.2) for an intermolecular elimination, the lifetime of the excited state would need to exceed 10^{-5} s to allow complete quenching by a second molecule of (IV) assuming $k_q \sim 10^{10}$ s^{-1} and ~99% efficiency of quenching) at the concentrations used. Few lifetimes of organometallic excited states have been measured but most such lifetimes are $<10^{-6}$ s at 298 K.[129-132] In addition, an intermolecular process should give a concentration-dependent quantum yield which was not observed (Figure 4.4). There are two properties of (IV) which might lead to its unique reactivity. Firstly, the primary photochemical process almost certainly will involve cleavage of the Pt-Pt bond by

excitation of an electron to the σ^*(PtPt) orbital, and this excited state is not possible with mononuclear complexes. However, it is not obvious why this excited state should cause reductive elimination from the dimethylplatinum centre.[128] The result of the cleavage would generate a species such as (IX) (Scheme 4.1). A mononuclear elimination, (IX) → (X), would be expected to be less favourable than direct elimination of ethane from (IV), where the electron withdrawing effect of Pt^B would enhance the formation of a platinum(0) product.[17] Alternatively, since (IV) is binuclear, new mechanisms, such as a true binuclear elimination (IX) → (XI) to (X) become possible.

Finally in CH_2Cl_2 the resultant species, (X), must accept a methyl group from a second molecule of (IV) and abstract a Cl radical from dichloromethane to give the observed products, (VII). Since the observed quantum yield is 2.0, the true quantum yield for the reductive elimination is 1.0.

Finally, a comment is needed on the solvent dependence of the quantum yields and reaction products. The good donor pyridine can presumably coordinate to the monomethylplatinum centre of (IX) after photochemical cleavage of the PtPt bond, and cleavage of the dimer to mononuclear fragments (equation (4.4)) follows. In the poor donor solvents such as benzene and acetone, the excited state gives intramolecular loss of C_2H_6 with a quantum yield of 1. The lower quantum yield in acetonitrile may be explained if this is a good enough ligand for platinum to coordinate reversibly and hence deactivate the excited state but not good enough to cause breakdown to mononuclear fragments.

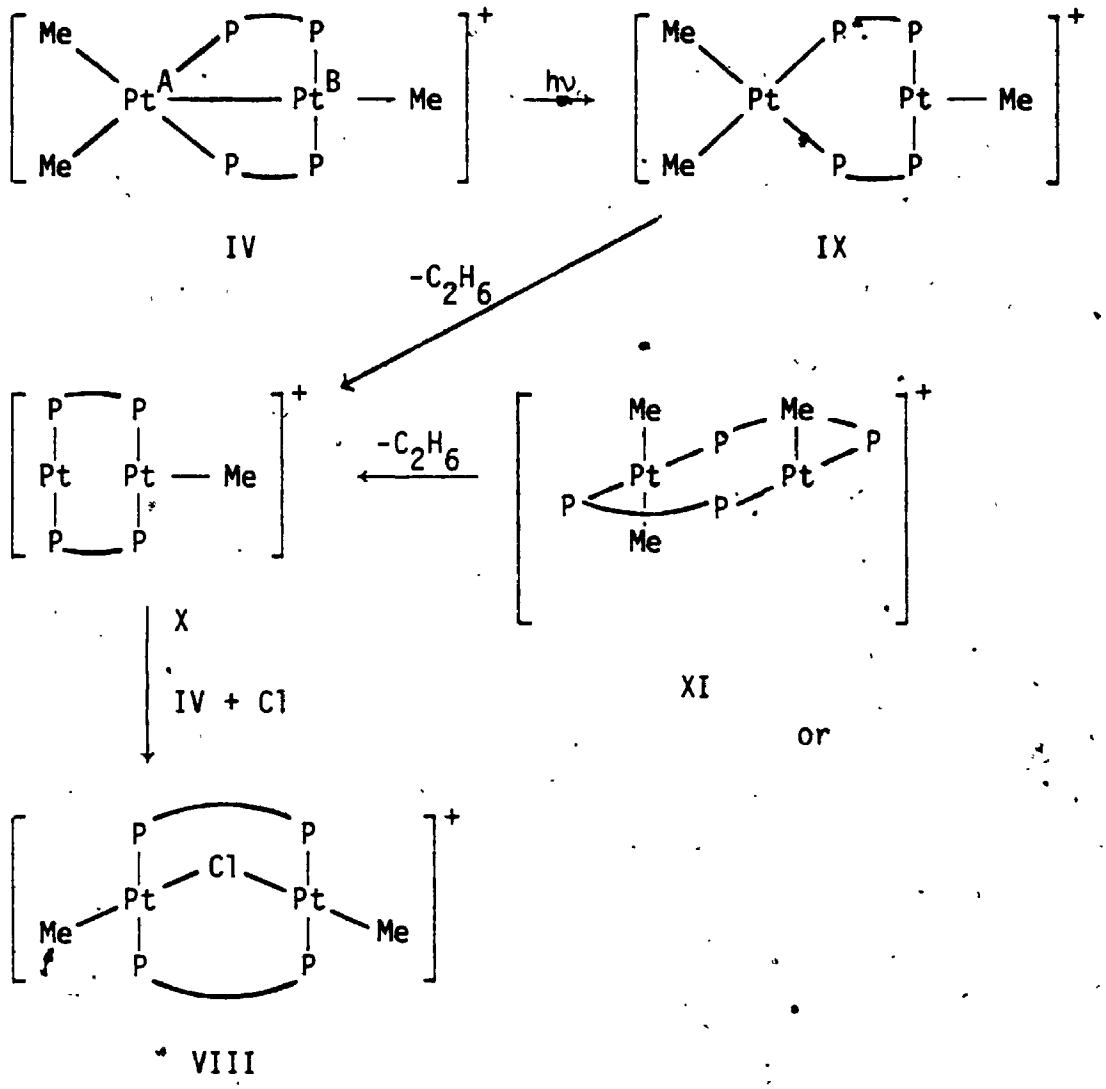
Me
P
P
A
Pt
Pt
B
Me
Me
P
P
+
hν
Me
P
P
Pt
Pt
Me
Me
P
P
+
IV
IX
-C2H6
P
P
Pt
Pt
Me
P
P
+
-C2H6
Me
Me
P
P
Pt
Pt
P
P
Me
+
X
IV + Cl
XI
or
P
P
Cl
Pt
Pt
Me
Me
P
P
+
VIII

Scheme 4.1

4.3 Conclusions

We have established that concerted reductive elimination forming C-H and C-C bonds may be photochemically activated. The selective elimination of hydrogen rather than methane from (II) indicates that the ease of elimination is $H_2 > CH_4$.

CHAPTER 5

β-Elimination from Binuclear Ethyl Platinum Complexes

5. Introduction

In previous chapters, reductive elimination reactions involving binuclear methyl(hydrido)diplatinum complexes were studied under both photochemical and thermal activation. In this chapter, a study of the thermal and photochemical β-elimination reaction from a binuclear system is described. The β-elimination reaction (equation (5.1)), unlike reductive elimination, does not involve change in oxidation state at the metal.

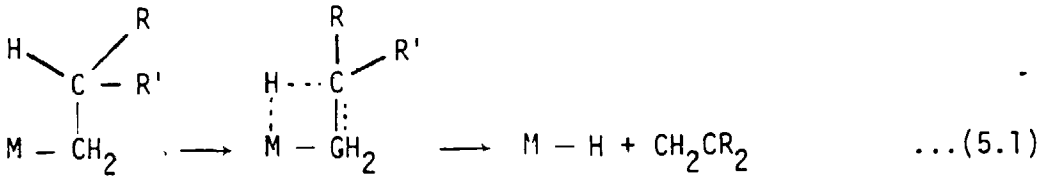

...(5.1)

In mononuclear systems, the mechanism of the thermally induced reaction generally involves rate limiting creation of a vacant coordination site followed by fast irreversible β-elimination. Hence, in $[PtEt_2L_2]$ decomposition occurs through rate limiting dissociation of a phosphine ligand, L, followed by fast irreversible β-elimination of ethylene.[133] The resultant hydrido ethyl complex is unstable and reductively eliminates ethane (equation (5.2)).

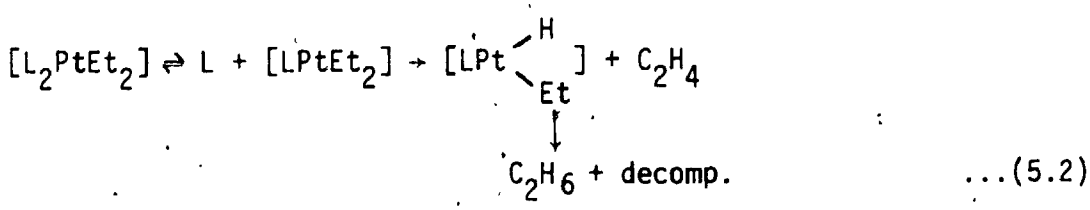

...(5.2)

This mechanism is impeded by addition of free phosphines and

recent evidence suggests that, under some conditions, an alternate mechanism, in which elimination occurs from the four coordinate starting complex, may be operative. In any case, it was shown that, with sufficient free phosphine added to the system, the β-elimination step occurred prior to the rate limiting step.[134]

The β-elimination reaction has also been observed in binuclear systems. One example of this involves the complex $[Mo_2Et_2(NMe_2)_4]$ which β-eliminates upon addition of carbon dioxide to the system.[135] This is followed by loss, presumably through reductive elimination, of ethane. Deuterium labelling experiments, (equation (5.3)), showed that the reaction was intramolecular and that the β-elimination occurred after the rate limiting step.[136,137]

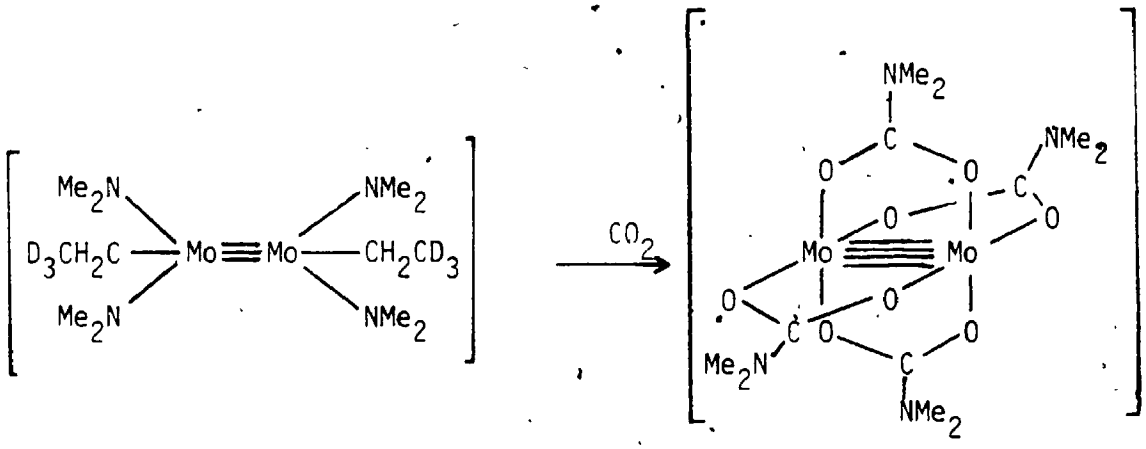

...(5.3)

Photochemically induced β-elimination has also been observed. One recent example of this involves $[(\eta\text{-}C_5H_5)W(CO)_3(CH_2CH_2C_6H_5)]$ which upon irradiation at 77 K loses CO and forms a stable hydrido(olefin)

complex (equation (5.4)).[138,139] The product complex, $[(\eta\text{-}C_5H_5)W(CO)_2(H)(CH_2{=}CHC_6H_5)]$, isomerizes at room temperature to yield $[(\eta\text{-}C_5H_5)W(CO)_2(\eta^3\text{-}CH(CH_3)(C_6H_5))]$, the product observed for room temperature photolysis.[140]

$$(\eta\text{-}C_5H_5)W(CO)_3(CH_2CH_2C_6H_5) \xrightarrow[77K]{h\nu}$$

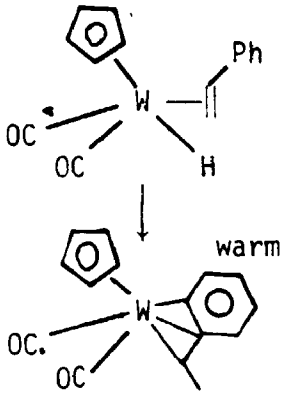

...(5.4)

The thermally induced β-elimination reaction from a binuclear platinum(II) complex has been studied previously.[121] The complex cation $[Pt_2Et_3(dppm)_2]^+$, (I), was found to undergo β-elimination of ethylene (equation 5.5). Although the authors were able to show that

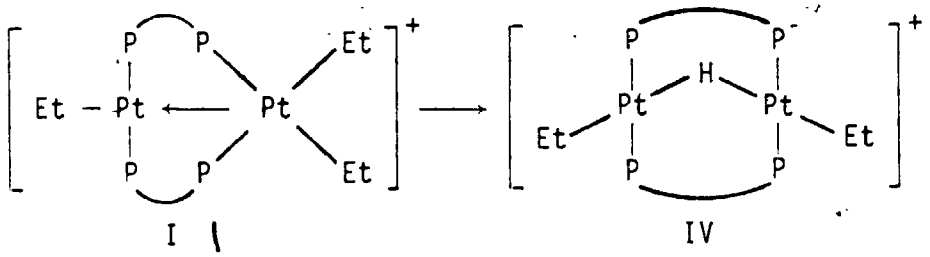

...(5.5)

the rate determining step in the reaction was not the β-elimination, they were unable to determine if the rate limiting step occurred before or after the β-elimination.

In this chapter, the photochemically induced β-elimination reaction from (I) is examined. A study of both the thermal and photochemical reactions of the diplatinum(I) cation, $[Pt_2Et(dppm)(\mu\text{-}dppm)_2]^+$,

(II), is also described. This allows a comparison of the reactivity pattern for β-elimination in a diplatinum(II) complex, (I), with a Pt → Pt coordinate bond, and in a diplatinum (I) complex, (II), with a covalent Pt-Pt bond.

5.1 Results

5.1.1 Photochemistry of $[Pt_2Et_3(\mu\text{-dppm})_2]^+$

The complex $[Pt_2Et_3(\mu\text{-dppm})_2]^+$, (I), was known to be photosensitive yielding approximately equal amounts ethane and ethylene upon broadband photolysis.[121] These observed gaseous products are consistent with an initial β-elimination followed by ethylene loss and reductive elimination of ethane from the resultant complex, (equation (5.6)). The second step of this sequence, reductive elimination of

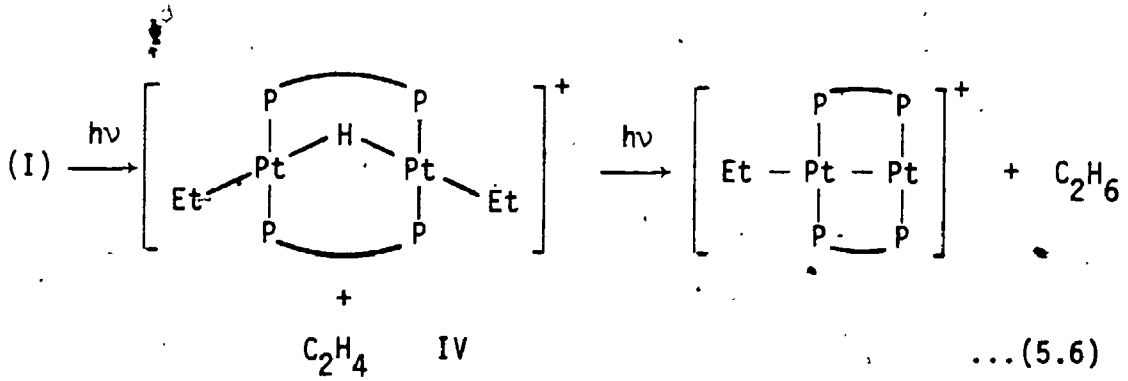

...(5.6)

ethane, is analogous to loss of methane observed in photolysis of $[Pt_2(\mu\text{-H})Me_2(\mu\text{-dppm})_2]^+$ (Chapter 4).

In order to determine if this mechanism is reasonable, a sample of (I) was photolyzed with the filtered ($\lambda \triangleright 420$ nm band pass) output of a medium pressure mercury lamp. Analysis of the ^{31}P NMR spectrum of the photolysis products indicated that, after 10 minutes, 44% conversion to $[Pt_2(\mu\text{-H})Et_2(\mu\text{-dppm})_2]^+$, (IV),[121] had occurred, and a small amount (~1%) of a new complex was also observed. Gas analysis by G.C.

indicated the presence of both ethylene (75±10%) and ethane (25±10%) but no butane. In order to establish that the unidentified complex was a result of decomposition of (IV), and not formed in competition with it, the sample was photolyzed further (after removing the gaseous products). The product mixture after one hour was found to contain none of complex (I), but 55% (IV) and 45% of the unidentified complex. The gaseous products were now much richer in ethane (C_2H_6:C_2H_4 = 50:50), indicating that the basic reaction sequence outlined in equation (5.6) is probably correct. Although we cannot rule out a small amount of a competing process, in which ethane is formed directly from (I), it has been established that the major reaction sequence is (I) → (IV) + ethylene followed by ethane loss from (IV). Degassing the samples was found to have no effect on the reaction, showing that oxygen does not quench the reaction or react with intermediates.

We have attempted to measure quantum yields for photolysis of (I). However, the minor products formed are coloured red, and hence it was not possible to monitor decay of (I) by monitoring changes in the UV-visible absorption spectra in the visible region. Qualitatively, it can be said that photolysis is efficient (we estimate $\Phi > 0.5$) and the compound (I) is certainly much more photosensitive than (II), which can be stored as a solid in the light for weeks without significant decomposition.

5.1.2 Thermolysis of $[Pt_2Et(dppm)(\mu\text{-}dppm)_2]^+$, (II)

Solutions of (I) in degassed acetonitrile are decolourised upon heating and a gas is evolved. In degassed acetonitrile exhaustive thermolysis followed by G.C. analysis of the gaseous products

identified both ethylene and ethane in a 2:1 ratio. The expected product of β-elimination is $[Pt_2H(dppm)_3]^+$, (III) was not a component of the product mixture, as confirmed by the ^{31}P NMR spectrum of the products (see Experimental).

In order to determine if the reaction did proceed through (III), a sample of (III) was decomposed and the resultant mixture found by ^{31}P NMR spectroscopy to contain the same species observed in decomposition of (II). The initial reaction is then probably given by equation (5.5).

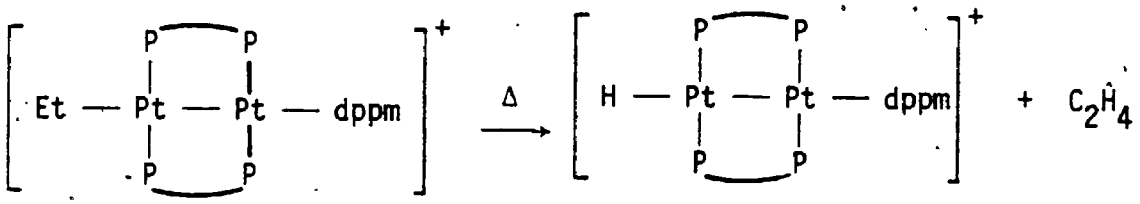

(II) (III) ...(5.5)

A sample of $[Pt_2(CH_2CD_3)(dppm)(\mu\text{-}dppm)_2]^+$, (IIb), was dissolved in acetonitrile and thermolyzed in a 5 mm NMR tube and the reaction was followed at 100°C. The decay of the CH_2 signal, in the ^1H NMR spectrum, due to the ethyl group was observed. During the course of the reaction, no scrambling of the deuterium label, which would be expected to give rise to $PtCD_2CH_2D$ groups and hence to a peak in the ^1H NMR spectrum due to the terminal methyl group, was observed. This indicates that the rate limiting step does not occur after β-elimination.

The rate of the reaction was studied by monitoring the decay of the peak centred at 466 nm in the visible absorption spectra (figure 5.1). In the early stages of the reaction, an isosbestic point was present (λ = 443 nm). Plots of log concentration of (II) vs. time were

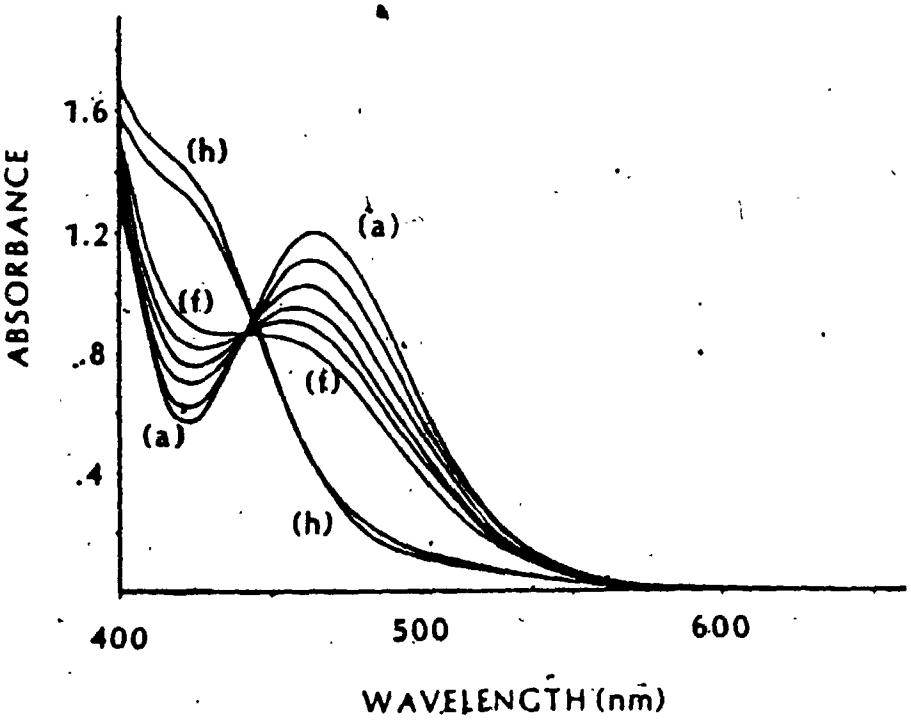

Figure 5.1. Visible spectra recorded during the decomposition of II at 100°C. Absorbance at 466 nm decreases with time and spectra (a → h) were recorded at 0, 123, 213, 314, 416, 510, 1970 and 3160 min.

found to be linear (figure 5.2) (correlation coeff. > .99). For data collected prior to loss of the isosbestic point (approximately one half-life) the slope of this line gives the first order rate constant, k, for the rate law (equation (5.6)).

$$-\frac{d(II)}{dt} = k[II] \qquad \ldots(5.6)$$

The rate constants (Table 5.1) were measured under a variety of conditions and the results may be summarized as follows. Oxygen enhances the rate of decomposition of (II) and, in the presence of O_2, the reaction rate is independent of solvent coordinating ability. In degassed solutions, the rate of the reaction has an insignificant primary isotope effect, $k_H/k_D = 1.1 \pm .2$. The rate of the reaction is also insensitive to addition of dppm or (IIIb).

5.1.3 Photochemistry of $[Pt_2Et(dppm)(\mu\text{-}dppm)_2]^+$, (II)

Photolysis of oxygen free samples of $[Pt_2Et(dppm)(\mu\text{-}dppm)_2]^+$, (II), leads to decolourization of the sample. This is a result of loss of absorption at 466 nm (figure 5.3) and provides a convenient means by which the reaction may be followed. A mixture of gases is produced during the course of the reaction. A gas chromatographic analysis of the gas indicated production of both ethylene (.8 mol per mol (II) decomposed) and ethane (.2 mol per mol (II) decomposed). The expected platinum product, (III), is also produced and may be identified by a terminal ν(Pt-H) absorption at 2010 cm^{-1} in the I.R. spectrum. The reaction does not occur cleanly, however, and the maximum yield of (III) obtained was 65%. In order to confirm that the stoichiometry of equation (5.5) is followed, the following experiments were carried out

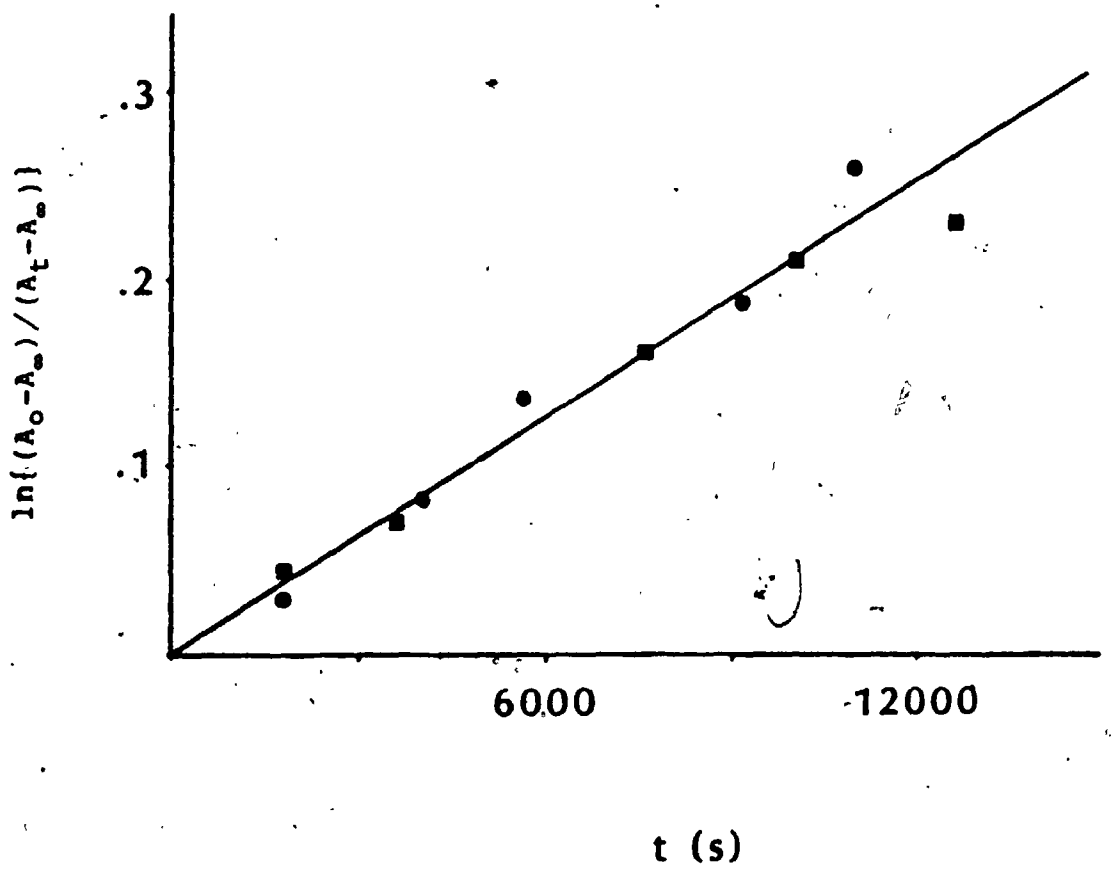

Figure 5.2. First order plot for decomposition of (II) (dots) and (IIb) (squares) in acetonitrile at 100°C.

TABLE 5.1

First Order Rate Constants, k, for

Decomposition of $[Pt_2R(dppm)_3]^+$

R	Solvent	Temperature °C	dppm grm/5 mL	k $s^{-1}/10^5$
CH_2CH_3	MeCN	64		8.5±.3
	DMSO	64		7±.3
	DMSO	78		27±2
H	MeCN	64		38±2
CH_2CH_3	MeCN	100		2.2±.3[a]
CH_2CD_3	MeCN	100		2.0±.3[a]
CH_2CD_3	MeCN	100	.009	1.7±.3[a]
CH_2CD_3	MeCN	100	.006	2.5±.3[a]
CH_2CD_3	MeCN	100	.015	2.0±.3[a]
CH_2CD_3	MeCN	100	.022	1.7±.3[a]
CH_2CD_3	MeCN	100		1.7±.3[a,b]

[a] samples were degassed

[b] measured in the presence of equimolar $[Pt_2D(dppm)_3]^+$

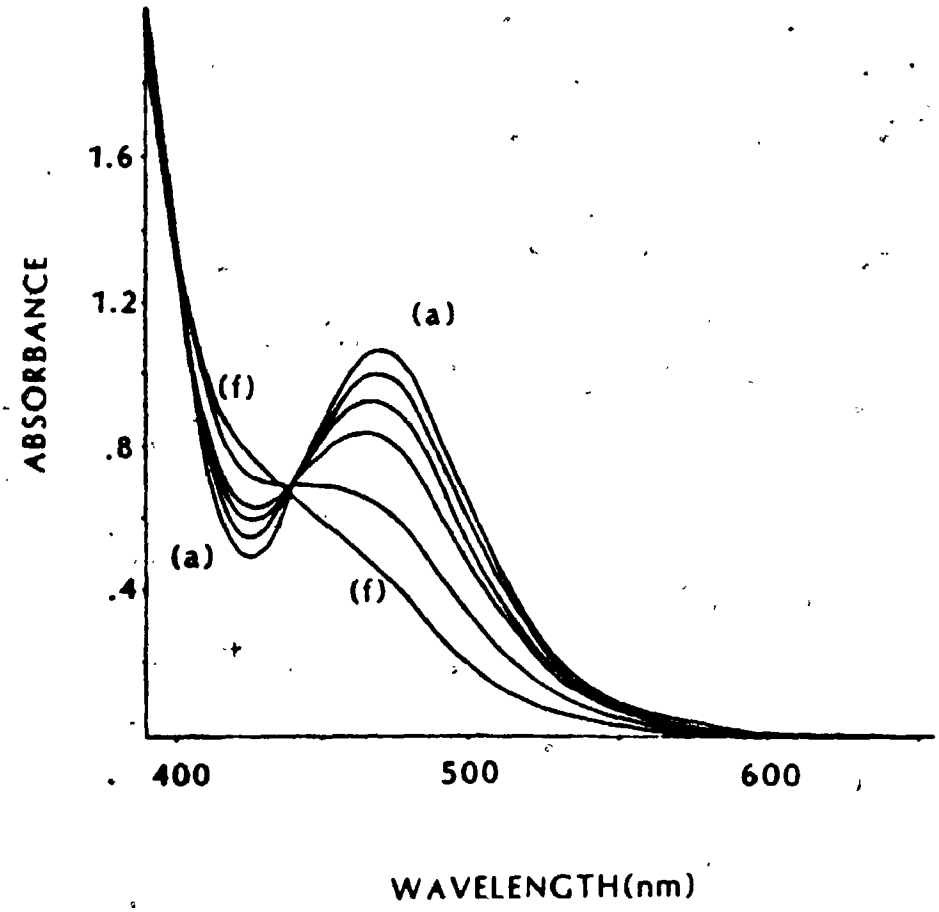

Figure 5.3. Visible spectral changes associated with photolysis of (II) in acetone. Photolysis was conducted with a xenon lamp using wavelengths longer than 500 nm, spectra were recorded at (a → f) 0, 11, 25, 40, 70, 110 min. photolysis times.

Firstly, the sample was irradiated at shorter wavelength and this gave rise to a lower yield of (III). Secondly, a sample was prepared in which a mixture of (II) and (III) was photolyzed. Analysis of gas products indicated an increase in the ethane to ethylene ratio from .30±.05 to .50±.05. These results are consistent with a clean β-elimination according to equation (5.5), followed by a secondary reaction involving (II) and (III), in which ethane is produced.

The β-elimination was observed to occur irreversibly as partial photolysis of $[Pt_2CH_2CD_3(\mu\text{-dppm})_2(dppm)]^+$, (IIb), did not result in any scrambling of the deuterium label in unreacted starting material, as determined by ^1H NMR spectroscopy. Quantum yields were measured for photolysis using 500 nm light for decomposition of (II) and (IIb) in acetonitrile. The quantum yields were found to be low, (for II, $\Phi = 5.3 \times 10^{-4} \pm .5 \times 10^{-4}$; for IIb, $\Phi = 5.2 \times 10^{-4} \pm .5 \times 10^{-4}$) and showed no isotope effect within the accuracy of the measurements (figure 5.4). The addition of free dppm was found to have a small effect (Φ for (II) with dppm added = $5.5 \times 10^{-4} \pm .5 \times 10^{-4}$). However, given the limited accuracy of the experiment, this is probably not significant. The measured quantum yields for decomposition were found to increase slightly for photolyses with shorter wavelength light (λ = 473 nm; $\Phi = 6.5 \times 10^{-4} \pm 1 \times 10^{-5}$). However, this could be due to the increased rate of photolysis of (III) in the reaction mixture, when the incident light is absorbed more strongly by (III).

In an experiment, analogous to that done for the thermal elimination from (II), a sample of (IIb) was photolyzed in an NMR tube. In the ^1H NMR spectrum no scrambling of the label (giving rise to $PtCD_2CH_2D$ and its associated methyl signal) was observed. This indicates

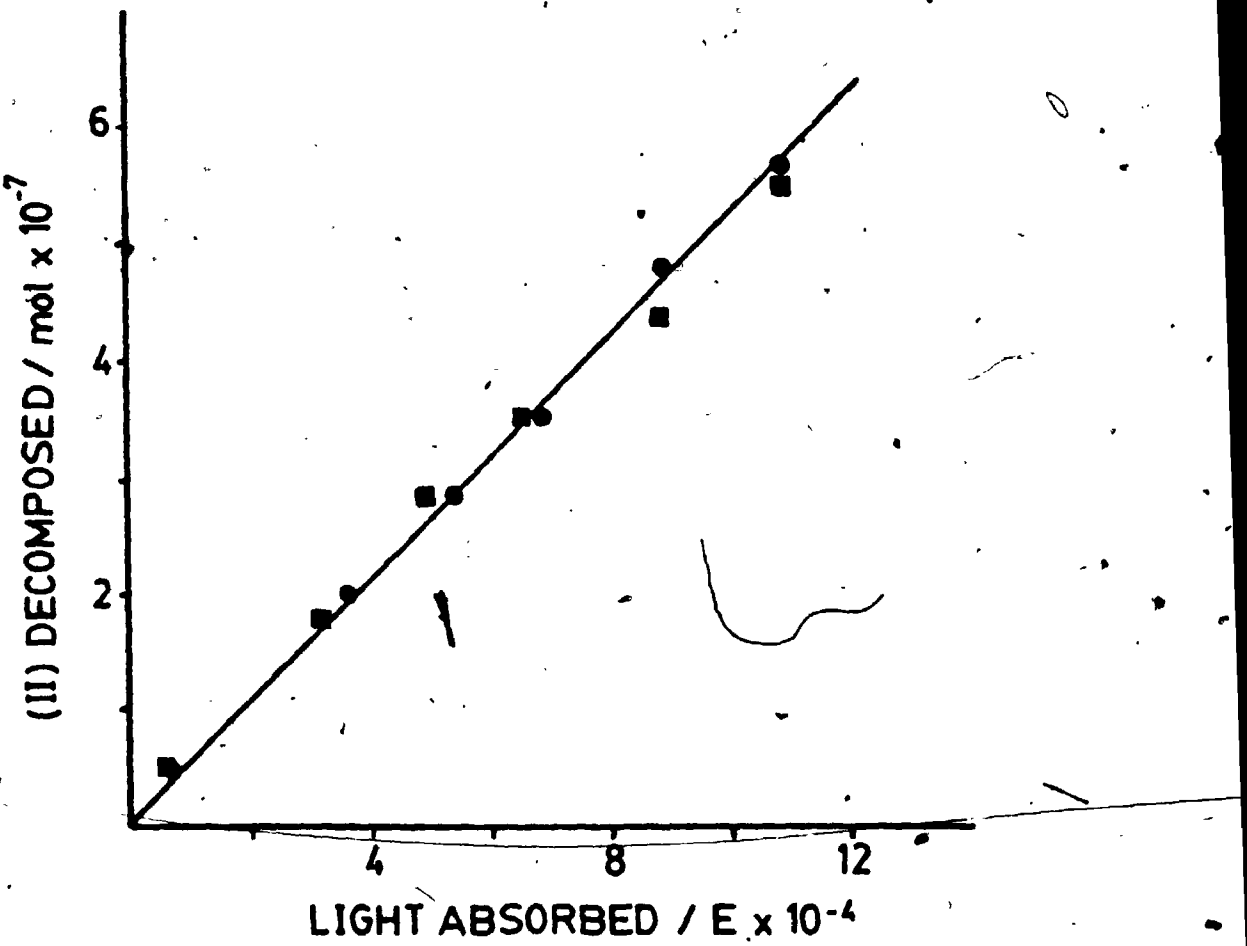

Figure 5.4. Plot of Moles (II) (squares) and (IIb) (circles) decomposed vs light absorbed.

that the β-elimination step is not reversible.

5.2 Discussion

The complex (I), when irradiated, β-eliminated and loses ethylene to form (IV) in high chemical yield. As discussed in Chapter 4, which describes the photolysis of the analogous methyl complex, $[PtMe_3(\mu\text{-dppm})_2]^+$, the primary photoprocess, arising from $d \rightarrow \sigma^*(PtPt)$ excitation, is expected to involve breaking the metal-metal coordinate bond.

Two possible mechanisms for the reaction are shown in Scheme 5.1. Heterolytic cleavage of the coordinate bond leads to the complex with structure (V). The proposed intermediate, (V), then undergoes an isomerization at the unsaturated platinum center, to give an intermediate of structure (VI). This isomerization is required to produce a geometry in which β-hydride elimination may occur. The isomerization of unsaturated platinum(II) centers has been proposed previously to be a low energy process.[133] With a vacant coordination site cis to the ethyl group on the unsaturated platinum center, β-elimination may occur in a process analogous to that in monomeric systems,[133] producing (VII). An alternate possibility is a binuclear β-elimination forming (VIII). The product complex (IV) is then formed following loss of ethylene and isomerization.

In the thermally activated β-elimination reaction of (I) studied previously,[121] the overall rate constant was found to show no significant deuterium isotope effect. If the thermal reaction of (I) occurs by an initial cleavage of the metal-metal bond, then this must be the rate limiting step. If the following isomerizations required high

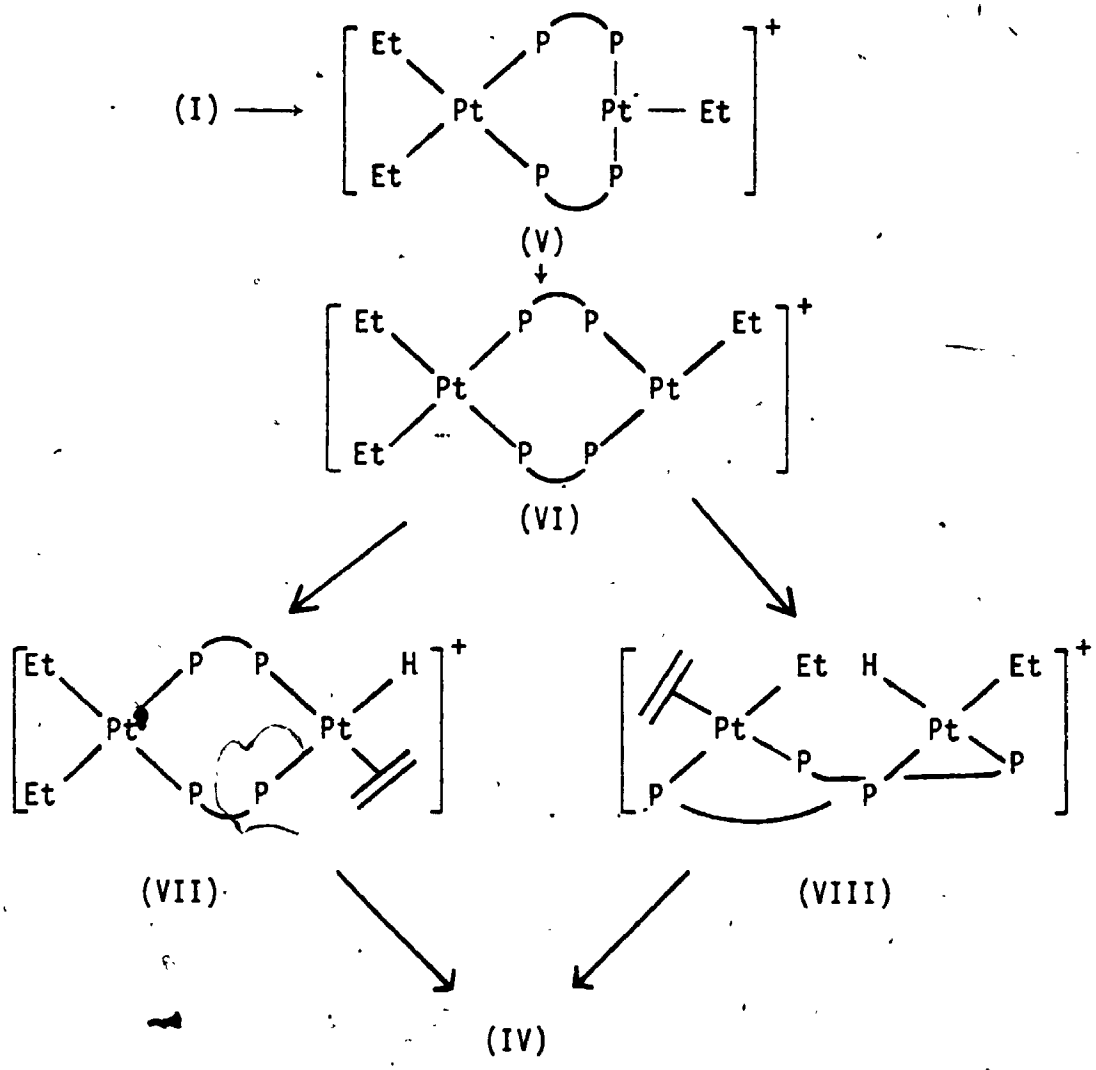

Scheme 5.1

activation energy the buildup of an intermediate would be expected in the photochemical reaction, and this was not observed.

The primary photoprocess in reaction of (II) is presumably metal-metal bond cleavage. The bonding in (II) can be understood in terms of combination of two T-shaped, d^9, 15 valence electron fragments to form an occupied σ_b ($2a_1$) orbital and an empty σ^* ($2b_2$) orbital.[63,141] Excitation is then expected to produce a $\sigma_b \rightarrow \sigma^*$ excited state resulting in cleavage of the metal-metal bond.

Many metal-metal bonded systems are known to cleave on photolysis. However, these typically involve 18-electron metals and cleave to generate a 17-electron radical species.[87] In the only study of an electronically similar system, involving 16-electron d^9 metal centers, photolysis of $[MM'(CNCH_3)_6][PF_6]_2$ (M = M' = Pt,Pd; M = Pt, M' = Pd) led to homolytic cleavage of the metal-metal bond resulting in 15-electron radical centers.[141]

The mechanism leading to β-elimination may once again be considered in terms of a binuclear and a mononuclear system. The transformation (IV) to (X) in Scheme 5.2 is the result of hydrogen atom abstraction by the remote platinum. An alternate mechanism is through structure (XI). In this case the β-elimination may occur from a radical center; this type of reactivity has been observed previously in a thorium complex.[123]

Another possibility is disproportionation to a platinum(0) and a platinum(II) centre. If this occurred, a binuclear β-elimination, as in (IX), would be improbable as the three coordinate platinum(0) would not be expected to adopt the t-shaped geometry. The transformation through (XI), however, appears reasonable in that it is consistent with observed

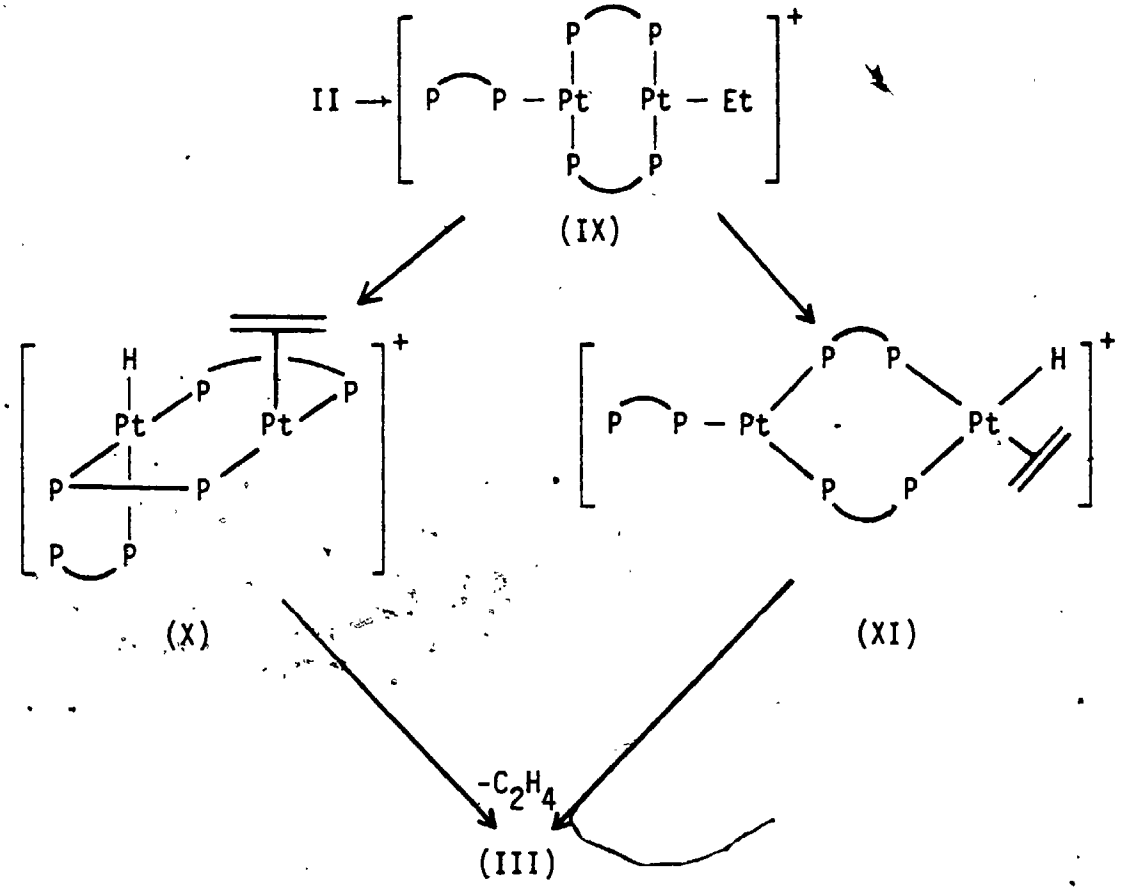

Scheme 5.2

β-elimination reactions in mononuclear platinum(II) systems.[133]

The mechanism of the thermal reaction is consistent with thermolysis resulting in metal-metal bond cleavage and the β-elimination reaction may occur in the same manner as the photochemical reaction.

It should be noted that, if the thermolysis of both (I) and (II) do proceed through rate limiting platinum-platinum bond cleavage, the greater reactivity of (I) reflects the ease of cleavage of the coordinate verses the covalent bond.

5.3 Conclusions

The β-elimination reactions of (I) and (II) can both be initiated photochemically, leading to the production of the stable platinum hydride species (IV) and (III). In each case the primary photoprocess is thought to involve metal-metal bond cleavage. The corresponding thermal reactions are also consistent with initial metal-metal bond cleavage.

Unfortunately, in this and previous studies of binuclear β-elimination reactions, it was not possible to conclude if a true binuclear mechanism is operative.

The last conclusion we can draw is that photochemical β-elimination from (I) is a lower energy pathway of decomposition than the reductive elimination which was observed in the photochemistry of $[Pt_2Me_3(\mu\text{-dppm})_2]^+$. This is somewhat surprising in view of the high efficiency of the reductive elimination of ethane (Φ = 1.0) from $[Pt_2Me_3(\mu\text{-dppm})_2]^+$, but is consistent with previous studies which have shown that β-elimination from coordinatively unsaturated platinum(II) centres is very rapid.[12,133]

CHAPTER 6

The Mechanism of a Photochemically Induced Oxidative Addition Reaction to Platinum(II)

6. Introduction

The oxidative addition reaction of an alkyl halide to a transition metal center is of considerable synthetic utility.[6] The overall reaction involves the oxidation of a metal complex accompanied by an increase in coordination number (equation (6.1)). The types of

$$L_mM^n + RX \rightarrow L_mM^{n+2}(R)(X) \qquad \ldots(6.1)$$

mechanisms identified for this reaction can be divided into two classes. In the first class, a concerted two-equivalent transformation occurs while, in the second class, a series of one equivalent transformations, involving paramagnetic interactions, occurs.[9]

The concerted process may occur through a two or three center transition state represented by structures A and B respectively.

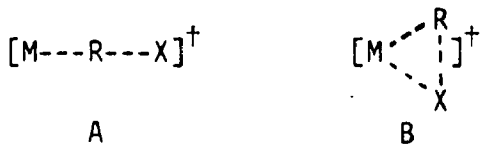

A B

The two-centre transition state, an S_N2 displacement, must result in stereochemical inversion at the carbon center. The rate of this reaction is expected to increase with leaving group ability of the halide (RI > RBr > RCl) and decrease with increasing steric bulk of the

alkyl groups.[9] One example where this mechanism has been established is in the oxidative addition of optically active α-phenethylbromide to $[Pd(PPh_3)_4]$ (equation (6.2)), where inversion of configuration was found to occur with high (95%) enantiomeric excess.[142]

$$[Pd(PPh_3)_3] + PhCH(CH_3)Br \longrightarrow \left[PhCH(CH_3) - Pd(PPh_3) - Br \right] + PPh_3 \quad \ldots(6.2)$$

The three center transition state (Structure B) is expected to result in retention of stereochemistry at the carbon center. Mechanisms involving this type of transition state have not yet been established for alkyl halide addition. It has, however, been shown to occur in the addition of carbon-carbon bonds, as illustrated by the retention of configuration in equation (6.3) for a cyclopropane derivative,[143] and hence must be considered possible for alkyl halide addition.

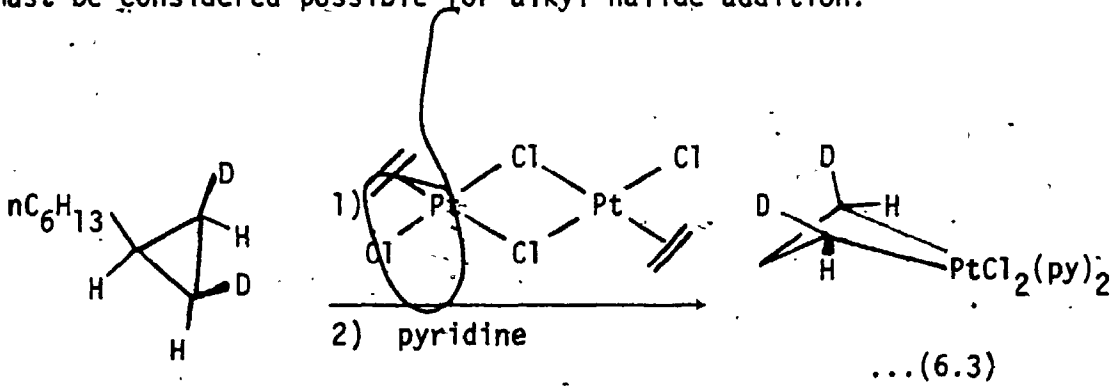

...(6.3)

The second type of mechanism involves two one electron oxidation steps. This may be the result of direct halogen atom abstraction in an inner sphere mechanism (equation (6.4)) or an initial electron transfer from the metal complex to the alkyl halide in an outer sphere mechanism followed by abstraction of the anionic halogen (equation (6.5)).[9]

$$L_nM + RX \rightarrow L_nMX^{\cdot} + R^{\cdot} \qquad \ldots(6.4)$$

$$L_nM + RX \rightarrow [L_nM]^{+}[RX]^{-} \rightarrow L_nMX^{\cdot} + R^{\cdot} \qquad \ldots(6.5)$$

The formed radicals may react in a non-chain or chain mechanism.

In the oxidative addition of methyl iodide to $[Pt(PPh_3)_3]$ a non-chain mechanism is believed to be operative (equation 6.6)).

$$[Pt(PPh_3)_3] + CH_3I \rightarrow [CH_3]^{\cdot} + [PtI(PPh_3)_3]^{\cdot}$$
$$\downarrow$$
$$[PtCH_3I(PPh_3)_2] + PPh_3 \qquad \ldots(6.6)$$

The presence of a radical mechanism was shown by ESR spectroscopy, by which technique, radicals were detected by the use of a spin trap.[144] The observation that no inhibition occurred when free radical scavengers were added[145] indicated the non-chain nature of the reaction.

In contrast to this, chain mechanisms have been proposed for the oxidative addition of a variety of species to $[Pt(PEt_3)_3]$. One example, the addition of n-butyl bromide produces not only the platinum(II) product expected, trans-$[PtBuBr(PEt_3)_2]$ (Bu = n-butyl), but also some trans-$[PtHBr(PEt_3)_2]$ and trans-$[PtBr_2(PEt_3)_2]$.[146] The formation of trans-$[PtBr_2(PEt_3)_2]$ is proposed to result from an initiation sequence generating free n-butyl radicals as in equation (6.7). The presence of free butyl radicals was indicated by the

$$[Pt(PEt_3)_3] + 2BuBr \rightarrow [PtBr_2(PEt_3)_2] + PEt_3 + 2Bu^{\cdot} \qquad \ldots(6.7)$$

formation of butane and butene by radical disproportionation as in equation (6.8). The formation of the oxidative addition product was

$$2[CH_3CH_2CH_2]^{\cdot} \rightarrow CH_3(CH_2)_2CH_3 + CH_3CH_2CHCH_2 \qquad ...(6.8)$$

proposed to occur through the chain sequence in equation (6.9). It

$$[Pt(PEt_3)_3] + Bu^{\cdot} \rightarrow [PtBu(PEt_3)_2]^{\cdot} + PEt_3$$

$$[PtBu(PEt_3)_3]^{\cdot} + BuBr \rightarrow [PtBuBr(PEt_3)_2] + Bu^{\cdot} \qquad ...(6.9)$$

should be noted that the formation of the remaining platinum product trans- $[PtHBr(PEt_3)_2]$, is consistent with β-elimination from the coordinately unsaturated $[PtBu(PEt_3)_2]^{\cdot}$, followed by halogen abstraction as in equation (6.10).

$$[PtBu(PEt_3)]^{\cdot} \rightarrow [PtH(PEt_3)_2]^{\cdot} + CH_3CH_2CHCH_2$$

$$[PtH(PEt_3)_2]^{\cdot} + BuBr \rightarrow [PtHBr(PEt_3)_2] + Bu^{\cdot} \qquad ...(6.10)$$

Further evidence comes from the observation that the reaction is inhibited by the addition of free radical scavengers.[146]

The reaction of isopropyl iodide (^{i}PrI) with $[PtMe_2(phen)]$ (I) giving trans oxidative addition (equation (6.11), N-N: 1,10-phenantholine) forming the platinum(IV) product (II) was investigated recently.[147]

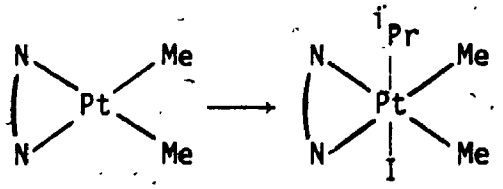

(I) (II) ...(6.11)

It was shown that this was a radical process, and both O_2 and olefins could be trapped by intermediate isopropyl radicals forming the

insertion products (III) and (IV).[148]

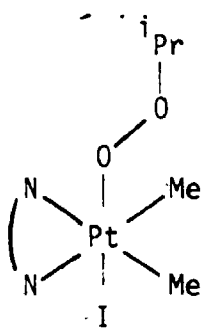

(III)

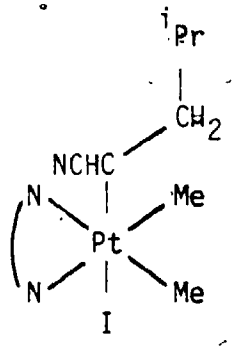

(IV)

During the course of this study,[147] it was observed that the reaction was accelerated by light. Herein we report the study of the mechanism of this reaction under photochemical activation.

6.1. Results

6.1.1 Emission Studies

The complex (I) gave no detectable emission at room temperature. However, in an ether glass at 77 K, emission is observed. The total emission shown in figure 6.1(d) is a result of excitation at 300 nm. The inset as figure 6.1(e) is the observed emission resulting from excitation at 400 nm. The observation of two emitting states in complexes with similar ligands is not unusual, however the sensitivity of fluorescence is such that one must consider the possibility of an impurity being responsible for one or both of the emissions. The evidence against this is as follows.

1) The results are reproduceable for different preparations of (I).

2) The excitation spectra of the different emissions (figure 6.1 (c) for emission 450 nm, figure 6.1(b) for emission at 530 nm) are identical in peak position for the region λ 250 nm → 360 nm, after

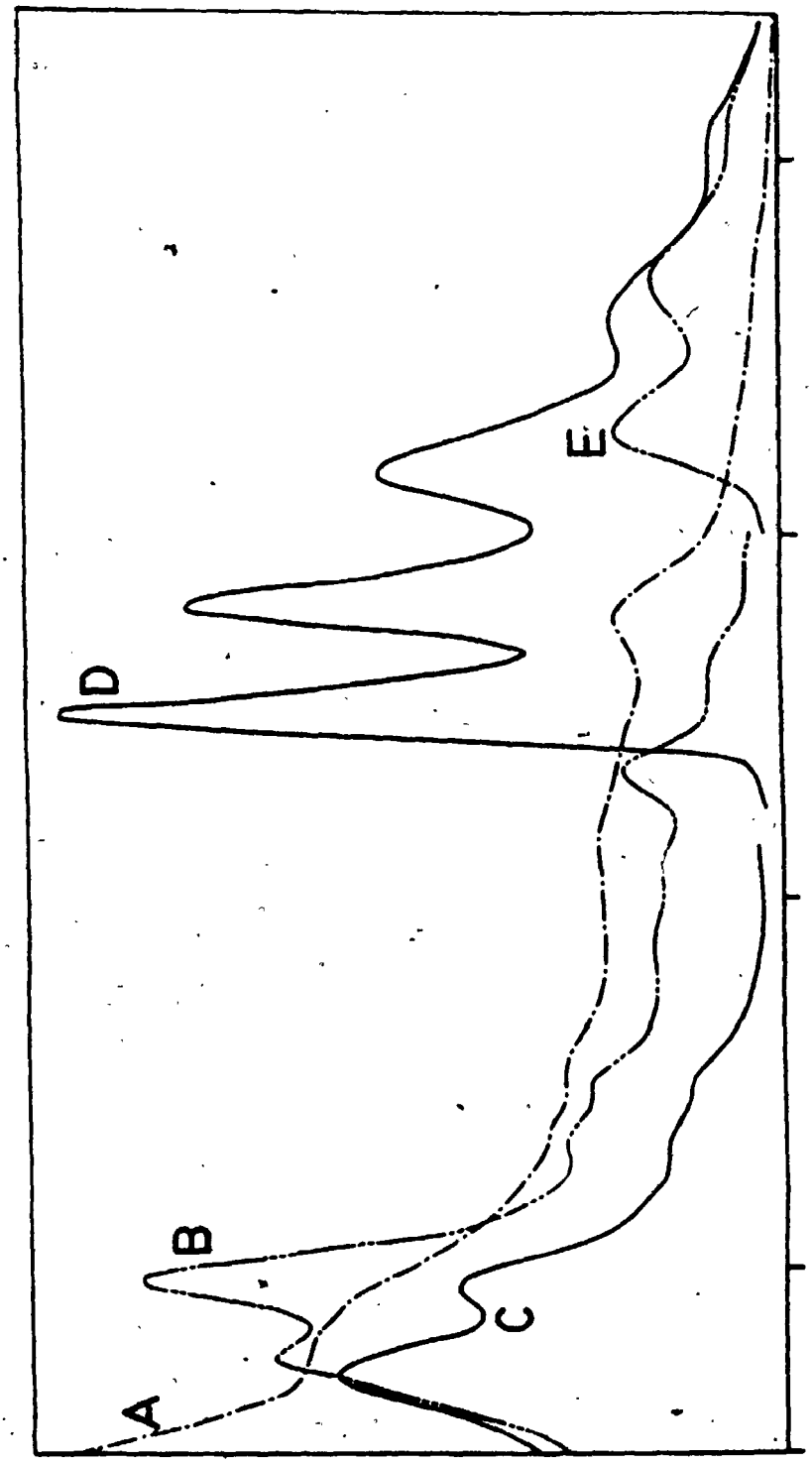

Figure 6.1. Spectral properties of [$PtMe_2$(phen)], showing the absorption spectrum, A; the excitation spectrum of the emission at 530 nm, B; the excitation spectrum of the emission at 450 nm, C; the emission spectrum due to the excitation at 300 nm, D; and the emission spectrum due to excitation at 450 nm, E; all at 77 K.

which point the higher energy emission is not observed.

3) The ratio of emission yield at λ_{ex} = 350 nm to λ_{ex} = 435 nm is identical for the emission at 570 nm and 615 nm. This would not be expected to be the case if the similarity in high energy excitation spectra was due solely to the tail of the emission at 450 nm.

4) The excitation spectra (figure 6.1(b)(c)) are in qualitative agreement with the absorption spectra, figure 6.1(a). The energies of absorption and emission are summarized in Table 6.1.

6.1.2 Characterization

Although the reaction was found to follow the stoichiometry of equation (6.11) in diffuse daylight, we wished to confirm this under conditions which were clearly photochemical. For this experiment, a solution containing [$PtMe_2$(Phen)], (I), and isopropyl iodide in acetone was degassed and sealed in a pyrex container with an attached optical cell. Irradiation with the filtered light (pass λ > 420 nm) from a medium pressure Hg lamp led to decolourization. This decay of the absorption in the electronic spectrum of (I), due to a metal to ligand charge transfer band,[149] provided a convenient means to follow the extent of reaction. A typical spectral change is shown in figure 6.2. The reaction was complete after a five minute irradiation time. The solution was then evaporated leaving a solid residue. This was dissolved in acetone-d_6 and the ^{1}H NMR spectrum was obtained. The product was found to be pure (II).

A second experiment was carried out as above except that a free radical inhibitor, 4-methoxyphenol, was added to the solution prior to degassing. In this case the light output from the mercury lamp was not intense enough to promote reaction on a convenient time scale and hence

TABLE 6.1

Absorption and Emission Assignments for

$[PtMe_2(phen)]$ and 1,10-phenanthroline

	Absorption (kk)	Assignment	Emission (kk)	Assignment
$[PtMe_2(phen)]$	42.	$IL^a(\pi-\pi^*)$		
	35.	$IL^a(\pi-\pi^*)$	22.2	$IL^a\ ^3(\pi-\pi^*)$
			20.7	
			19.2	
	28.6	$MLCT^b(d-\pi^*)$		
	21.0	$MLCT^b(d-\pi^*)$	18.9	$MLCT\ ^3(d-\pi^*)$
			17.6	
			16.3	
1,10-phenanthroline	37.7	$(\pi-\pi^*)$		
	29.6	$(\pi-\pi^*)$	27.4	$^1(\pi-\pi^*)$
			26.3	
			25.0	
			21.8	$^3(\pi-\pi^*)$
			20.5	
			19.2	

[a] IL = Intraligand band

[b] MLCT = Metal to ligand charge transfer band

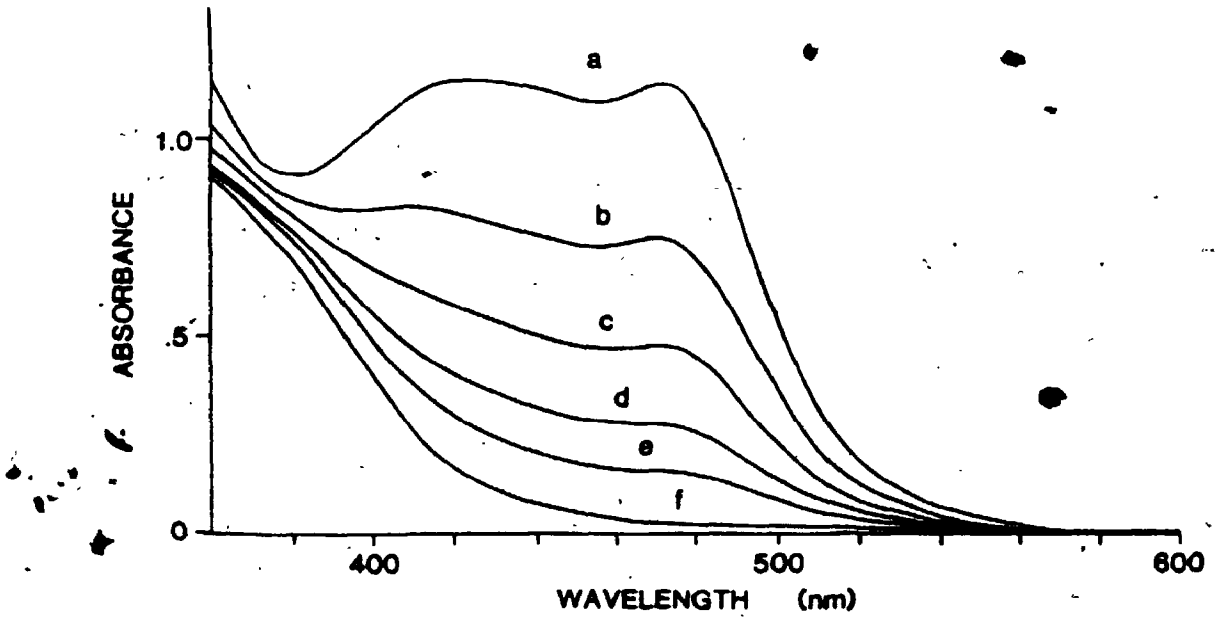

Figure 6.2. Electronic spectral changes accompanying the 473 nm photolysis of (I) and isopropyl iodide in acetone, with the following number of counts of irradiation: a) 0; b) 1; c) 2; d) 3; e) 4; f) extended irradiation.

a 150 W high pressure xenon lamp was used. After five minutes under these conditions, the reaction was near completion and the products were identified by the ^1H NMR spectra after working up as above. In this case an approximately 1:1 mixture of (II) and $[PtMe_2I_2(phen)]$, (V) , was formed. This increased formation of (V) indicates that it is formed in the initiation step.

6.1.3 Trapping of Intermediates

Solutions of (I) and ^iPrI in benzene were irradiated in the cavity of an E.S.R. spectrometer. Under these conditions, no signal was observed in either fluid or frozen (77 K) solutions. On the addition of DMPO to fluid solutions, two signals were observed. The first signal (g = 2.0069) was a doublet of triplets due to coupling with the β hydrogen, a_β^H = 21.8 G, and nitrogen, a_N = 14.3 G. The parameters are in the range expected for simple alkyl radical trapping (equation (6.12)).

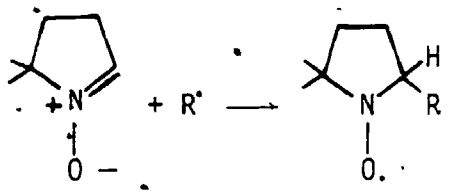

...(6.12)

For example the literature value for the n-butyl adduct is a_N = 14.24, a_β^H = 20.41.[150]

A second signal was also observed (g = 2.0063, a_N = 14.5 G, width = 1.6 G). This was presumably the result of a reaction with O_2, as the signal was not observed in deoxygenated samples.

As no literature value was available for the isopropyl adduct of DMPO, it was prepared independently by decomposition of $Hg(^iPr)_2$.

The complex $Hg(^iPr)_2$ was prepared and identified by its ^1H NMR spectrum.[151] Dialkyl mercury complexes are known to lose alkyl

radicals on thermolysis or irradiation by U.V. light.[152] A mixture of $Hg(^{i}Pr)_2$ and DMPO in benzene was found to produce ESR signals identical to those above upon thermolysis.

6.1.4 Quantum Yields

The Effect of Concentration of Reactants and of Light Intensity on the Quantum Yields

Rigorously degassed acetone solutions containing (I) and isopropyl iodide were flame sealed in quartz cuvettes. Irradiation at 473 nm was carried out with a standardized light source and the concentration of (I) was monitored by the decrease in optical density at 473 nm. Both the concentration of (I) and the light absorbed by (I) were then calculated. The slope of a graph of moles of (I) reacted vs Einsteins of light absorbed by (I) gives the quantum yield. Plots are shown in Figure 6.3 for a variety of isopropyl iodide concentrations. In each case an excess of isopropyl iodide was used, such that its concentration remained constant throughout the experiment. In each case, a plot of moles (I) reacted vs Einsteins light absorbed was linear over the course of the reaction.

This indicates that the quantum yield was unaffected by the concentration of (I) as the reactions were generally followed for at least seventy-five percent reaction.

As can be seen in Figure 6.3, the concentration of isopropyl iodide did have an effect on the quantum yield. This variation was studied over the concentration range from 2×10^{-3} mol L^{-1} to 8×10^{-3} mol L^{-1} and a first order relationship between isopropyl iodide concentration and quantum yield for reaction of (I) was found, Figure 6.4 (data in Table 6.2). It should be noted that, in each case,

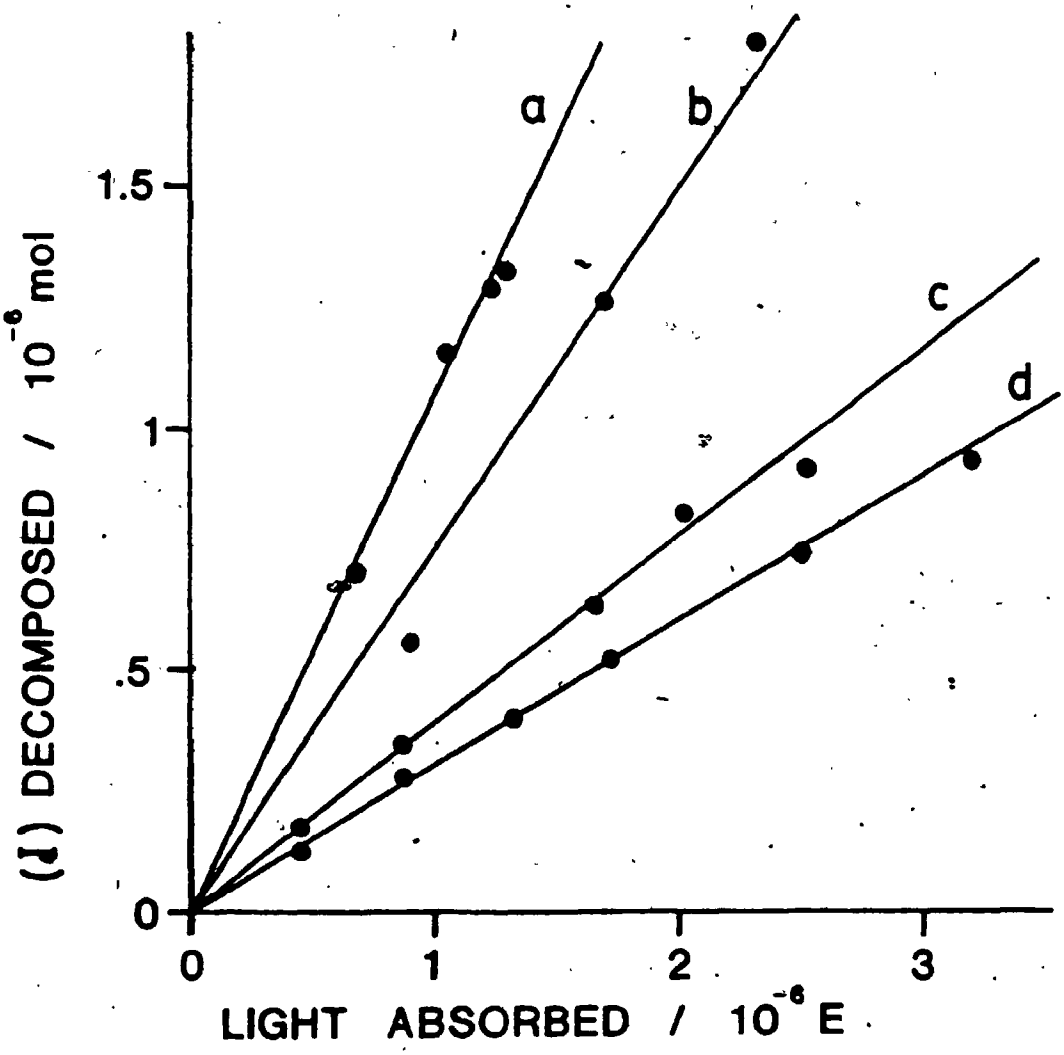

Figure 6.3. Plot of moles (I) decomposed vs light absorbed in the presence of the following isopropyl iodide concentrations: a) 8.33×10^{-3} mol L^{-1}; b) 5.83×10^{-3} mol L^{-1}; c) 3.27×10^{-3} mol L^{-1}; d) 2.38×10^{-3} mol L^{-1}.

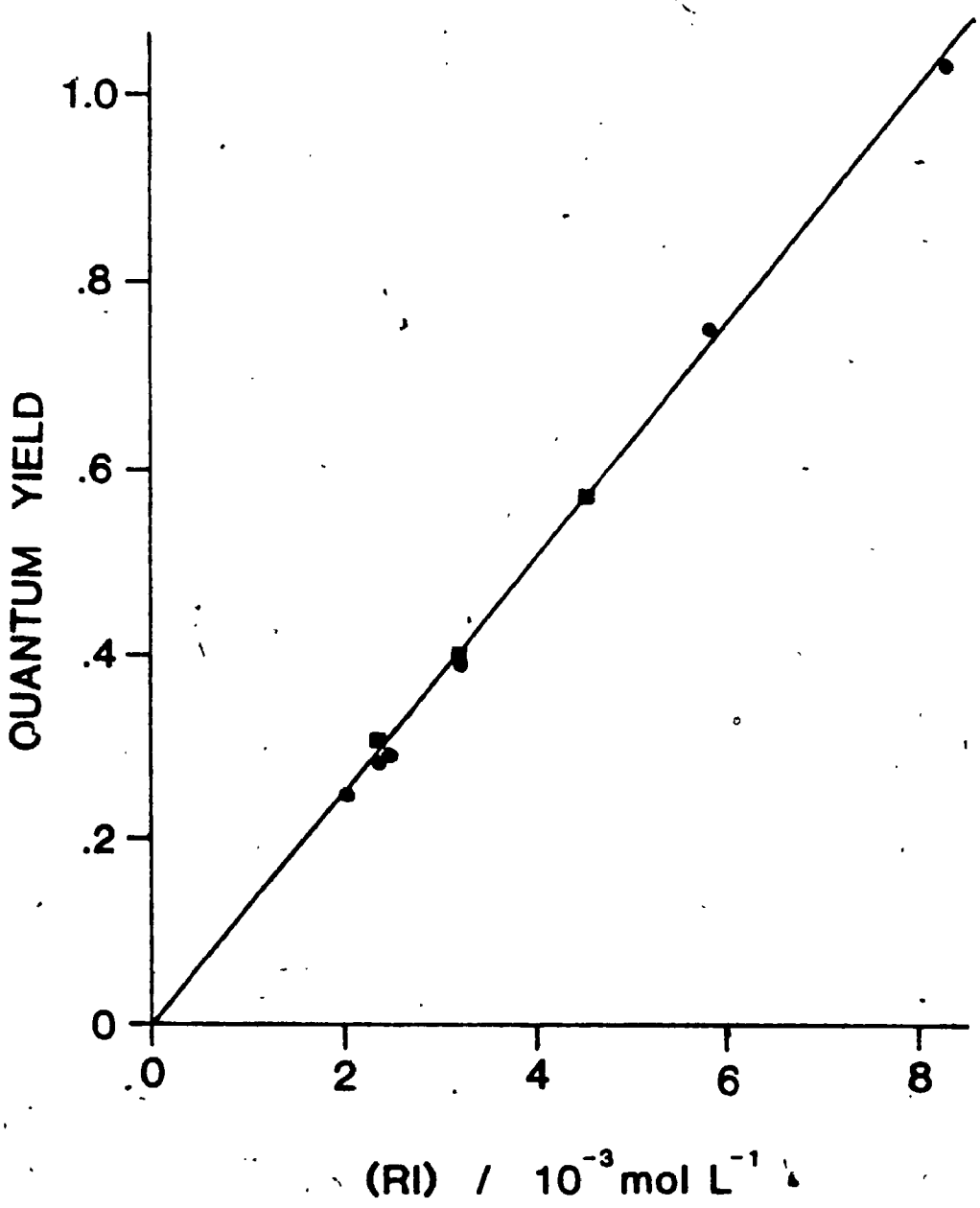

Figure 6.4. Plot of quantum yield for reaction of (I) with isopropyl iodide vs isopropyl iodide concentration; the incident light intensity is, 1.0×10^{-6} E $count^{-1}$, circles and 0.5×10^{-6} E $count^{-1}$, squares.

TABLE 6.2

Quantum Yields for Reaction of (I) with Isopropyl Iodide in Acetone

$[^{i}PrI]$ mol $L^{-1} \times 10^{3}$	Φ	Light Intensity E/count $\times 10^{6}$
2.01	.25	1.0
2.38	.285	1.0
2.5	.29	1.0
3.27	.39	1.0
5.83	.75	1.0
8.33	1.07	1.0
2.38	.31	.5
2.27	.40	.5
4.55	.57	.5

the reaction was also monitored in the dark in order to confirm that no contribution due to a thermal process was occurring over the time period of the quantum yield measurements.

In each quantum yield measurement, the absorbed light varied with the concentration of (I). The linear graphs of moles (I) reacted vs Einsteins light absorbed hence indicate that there is no dependence of the quantum yield on light intensity. In order to confirm that this observed lack of dependence on concentration of (I) and light intensity was not an artifact arising from a dependence on both concentration of (I) and light intensity having opposing effects, experiments were done in which a 50% neutral density filter was interposed between the light source and the sample. As can be seen in Figure 6.4 (data in Table 6.2) this experiment confirmed that no dependence between the quantum yield, for reaction of (I) with isopropyl iodide, and either the concentration of (I) or the light intensity existed.

The Effect of Oxygen on the Quantum Yield

One experiment was carried out without degassing the reaction mixture of (I) and isopropyl iodide. Stock solutions of (I) and isopropyl iodide in acetone (O_2 concentration 2.4×10^{-3} mol L^{-1}) were mixed and added to a cuvette. In this case a plot of moles (I) reacted vs light absorbed was not linear, but had an increasing slope (figure 6.5). The initial quantum yield was 1×10^{-3} with an isopropyl iodide concentration of 8.33×10^{-3} mol L^{-1}. The quantum yield increased greatly over the course of the reaction to a maximum observed value of 3×10^{-2}.

It is interesting to note that the rate of the reaction of (I) with isopropyl iodide was independent of oxygen concentration under thermal

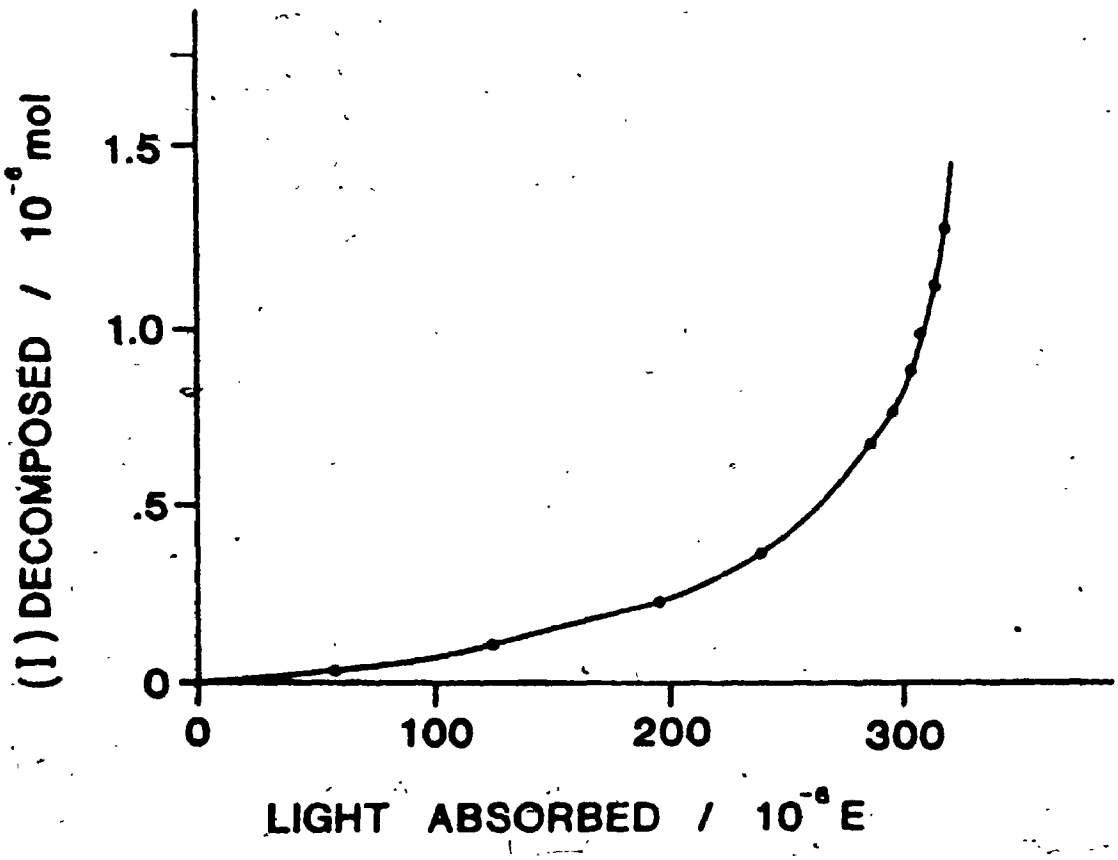

Figure 6.5. A plot of moles [$PtMe_2$(phen)] decomposed vs light absorbed in the presence of oxygen and isopropyl iodide.

activation.

The Effect of Solvent

The quantum yield for decomposition of (I) was measured in benzene and acetonitrile, in order to determine the effect on the quantum yield of changing the solvent polarity at constant concentration of isopropyl iodide. In acetone, the quantum yield is .68 at $[^{i}PrI] = 5.6 \times 10^{-3}$ mol L^{-1} (interpolated value). In benzene, a quantum yield of .24 was observed, whereas, in acetonitrile, the quantum yield was 1.8×10^{-3} at $[^{i}PrI] = 5.6 \times 10^{-3}$ mol L^{-1}. In acetonitrile, this value was not constant and was found to increase during the course of the reaction. An attempt was made to measure the quantum yield in the presence of p-benzoquinone but a thermal reaction occurred.

The Effect of Free Radical Inhibitors

The effect of free radical traps on the quantum yield for decomposition of (I) was measured, using degassed solutions. For this study, three inhibitors were used: 4-methoxyphenol, p-benzoquinone and hydroquinone. All three were found to have a retarding effect on the quantum yield (Table 6.3). A plot of moles (I) reacted vs light absorbed is shown in Figure 6.6 for two different concentrations of p-benzoquinone, showing longer retardation at higher p-benzoquinone concentrations. For hydroquinone, although an inhibition was noted, the spectral changes indicated the formation of colored products. Hence this data is of a qualitative nature only.

For p-methoxyphenol the data were not reproducible as the inhibition of the reaction varied greatly with extent of reaction. Hence a small variation in extent of reaction caused a large error in

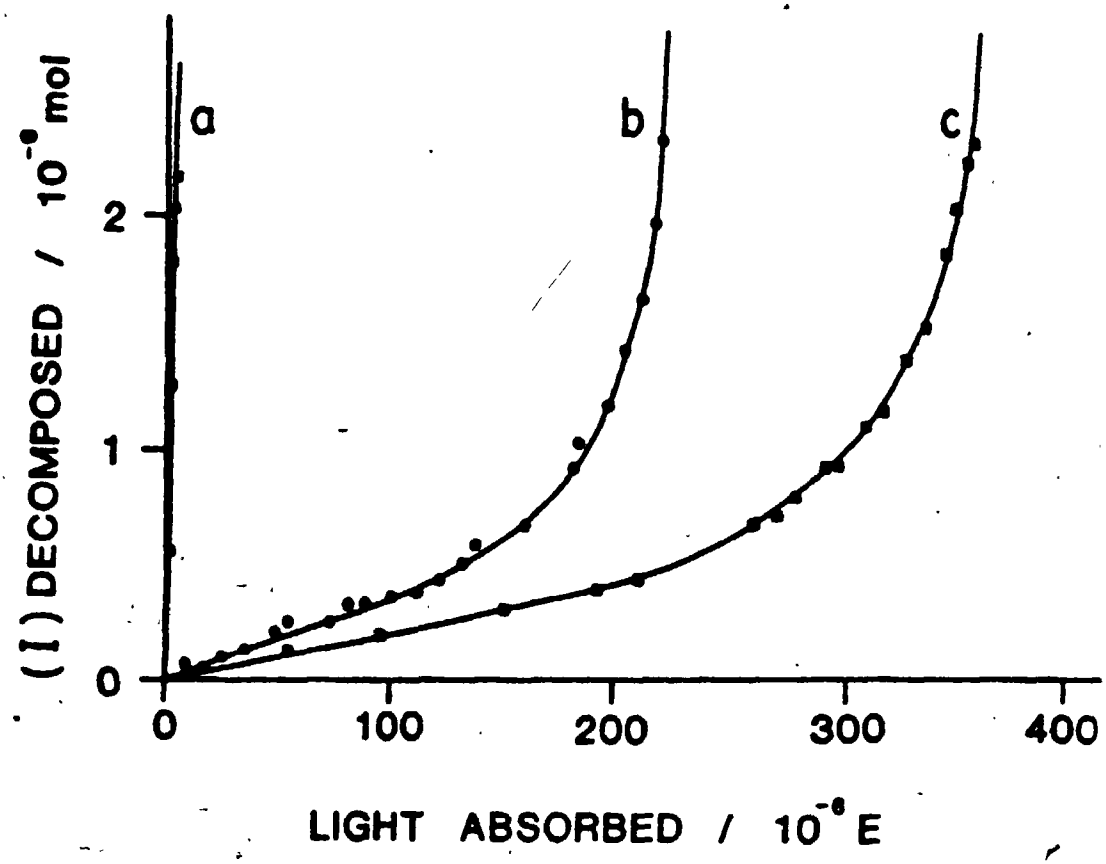

Figure 6.6. A plot of moles (I) decomposed vs light absorbed in an acetone solution containing isopropyl iodide and the following concentrations of the free radical inhibitor benzoquinone; a) 0.0 mol L^{-1}, b) 8.8×10^{-5} mol L^{-1}; c) 1.9×10^{-4} mol L^{-1}.

determining the initial quantum yields (Table 6.3).

The data for the inhibitor p-benzoquinone was reproducible, although significant changes in Φ also occurred over the course of the reaction. In addition, complications occurred with high concentrations of p-benzoquinone ($>10^{-3}$ M) with formation of coloured by-products.

Triplet Sensitization

The reaction was sensitized by the addition of benzophenone. In this experiment, an acetone solution containing (I), isopropyl iodide and benzophenone was degassed and the extent of reaction followed by monitoring changes in the absorption spectrum in the usual way. The source of light used was such that 80% of the light (λ = 362 nm) was absorbed by the sensitizer. Under these conditions, 20% of the light was absorbed directly by (I). Energy transfer to (I) from benzophenone, at the concentration used, was assumed to occur with 100% efficiency from the triplet state (E_T = 417 nm, τ_T = 12 μ sec; Φ_{ISC} = 1),[101] with no transfer from the singlet state. Under these conditions, the quantum yield for the reaction from the sensitized triplet state [= moles (I) reacted/moles triplet state of (I) produced] was found to be .16 ± .08. The large error in quantum yield is due to a portion of the reaction occurring by direct absorption by (I) under the conditions used. A correction for direct absorption was made, but this cannot be done with great accuracy.

The quantum yield for reaction by direct absorption of 473 nm light by (I) under identical concentration conditions ([^{i}PrI] = 1.3×10^{-3} mol L^{-1}) is 0.16. Hence, the quantum yield for intersystem crossing from the initially excited singlet state to the reactive triplet state is 1.0 ± .3.

TABLE 6.3

The Effect of Inhibitors on Quantum Yield for Reaction of (I) with Isopropyl Iodide

	Inhibitor mol L^{-1}	isopropyliodide mol L^{-1}	Φ Initial
benzoquinone			
	$.88\times10^{-4}$	6.2×10^{-3}	.0024
	1.8×10^{-4}	6.2×10^{-3}	.0015
	1.9×10^{-4}	5.6×10^{-3}	.0010
	2.2×10^{-4}	6.2×10^{-3}	.00066
	9.5×10^{-4}	5.6×10^{-3}	.00030
	76×10^{-4}	6.2×10^{-3}	.006
4-methoxyphenol			
	$.65\times10^{-4}$	6.2×10^{-3}	.072
	1.3×10^{-4}	6.2×10^{-3}	.049
	2.6×10^{-4}	6.2×10^{-3}	.043
	7.0×10^{-4}	7.7×10^{-3}	.005
	7.25×10^{-4}	6.0×10^{-3}	.0015
	42×10^{-4}	6.2×10^{-3}	.00043
hydroquinone			
	4.4×10^{-3}	5.8×10^{-3}	.0045

Triplet Quenching

The qualitative result of sensitization suggested that the reaction occurred through the triplet state. In order to verify this, the reaction was quenched by pyrene, (Q), (E_T = 595 nm, E_S = 372 nm)[101] In these experiments the complex was irradiated at 473 nm. Hence no singlet quenching could occur. The introduction of a triplet quencher provides an extra mechanism for decay of the excited triplet state. Hence an increase in quencher concentration causes a decrease in reaction quantum yield. The data are presented as a Stern-Volmer plot of quantum yield in the absence of quencher, Φ, divided by quantum yield in the presence of quencher, $\Phi(Q)$, vs the concentration of quencher used, [Q], in figure 6.7.

The significance of this straight line plot will be discussed after a kinetic scheme is developed.

6.2 Discussion

6.2.1 The Electronic Structure of [$PtMe_2$(phen)]

The absorption spectrum of [$PtMe_2$(phen)], (I), has been studied previously. Four distinct bands were assigned.[149] Two high energy bands, in the regions 36,100 cm^{-1} (band 1) and 33,300 cm^{-1} (band 2), were assigned to ligand localized π-π^* transitions. The band positions are similar to the absorptions of free 1,10-phenanthroline and were not dependent on solvent polarity, consistent with the π-π^* assignment. The two energies of the additional bands at 28,600 cm^{-1} (band 3) and 20,900 cm^{-1} (band 4) in acetone solvent were solvent dependent and hence were assigned as d-π^* metal to ligand charge transfer bands.

Before considering the emission from complex (I), it is useful to review the phosphorescent emission from the free 1,10-phenanthroline

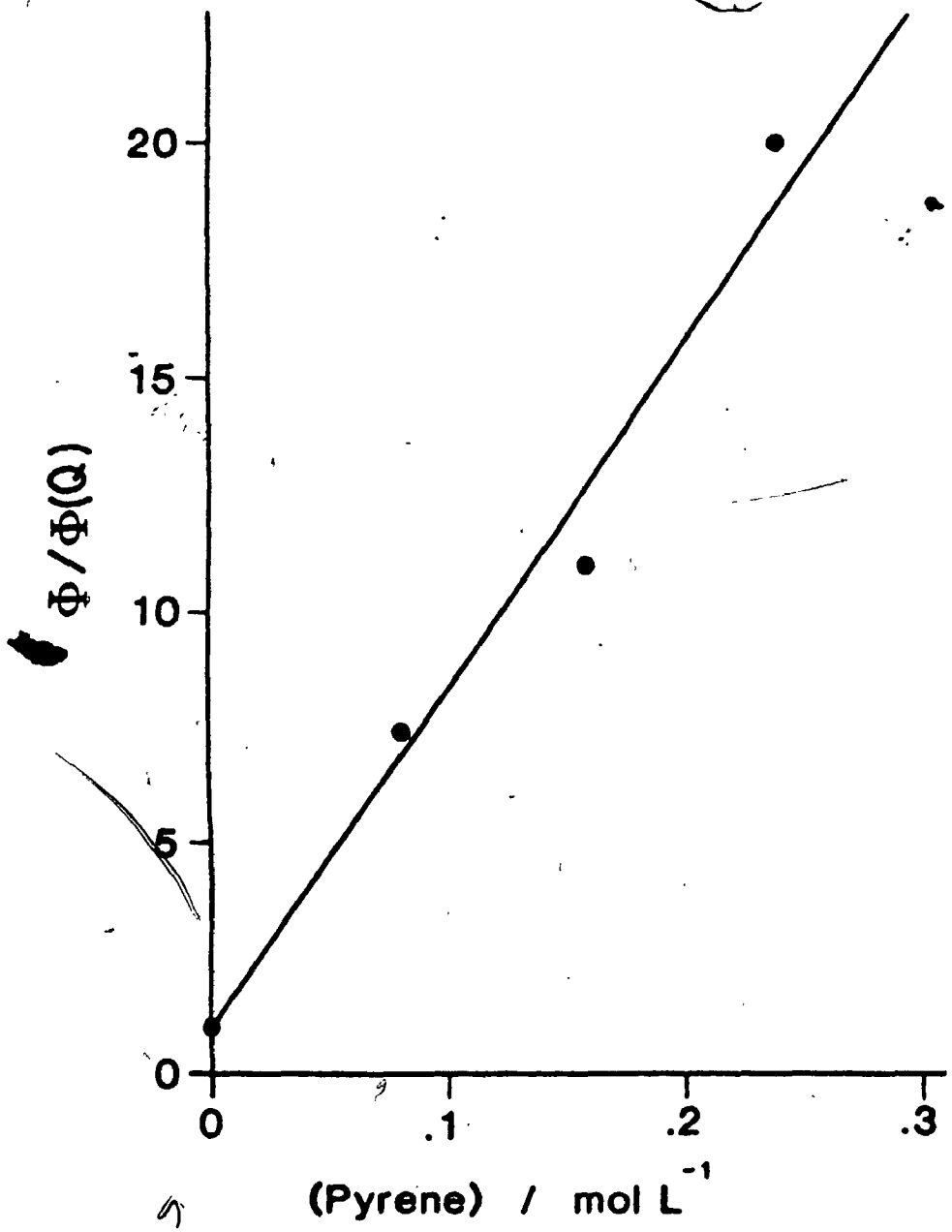

Figure 6.7. A Stern-Volmer plot of quantum yield in the absence of quencher, Φ, over quantum yield in the presence of quencher, Φ(Q), vs the concentration of the quencher, pyrene.

ligand (Table 6.1). The emission is observed in the region 21,800 cm^{-1} with resolved vibrational progression (20,500 cm^{-1} and 19,200 cm^{-1}). The emission has been assigned to a $^3(\pi-\pi^*)$ phosphorescence.[153]

The emission spectrum of (I) consists of two separate structured emissions, (Figure 6.1, Table 6.1). The high energy emission at 22,300 cm^{-1} is similar to the emission of the free ligand, in both energy and vibrational structure. Since coordination of the ligand is expected to cause only slight perturbation of the $^3(\pi-\pi^*)$ transition, compared to the free ligand, the high energy emission from (I) is assigned as a ligand localised $(\pi-\pi^*)$ transition. A similar assignment has been made in a variety of systems[154] such as a fac-$[LRe(CO)_3(phen)]^+$[155] (L = py, PhCN, CH_3CN) and $[Rh(phen)_3]Cl_3$[153]. It should be noted that, in these complexes, only a slight (less than ~1,000 cm^{-1})[156] shift in emission from the free ligand is observed. The possibility of emission due to an impurity in the sample of free 1,10-phenanthraline is ruled out, since the emission can be induced by excitation in a region where the free ligand does not absorb (λ = 350 nm). The lower energy emission at 19,000 cm^{-1} also has vibrational structure. The energy of this band is shifted significantly (28,000 cm^{-1}) from the emission for free 1,10-phenanthroline. A slight overlap with the MLCT absorption band 4 is observed. This low energy emission is assigned as the inverse of the metal to ligand charge transfer absorption $(d \rightarrow \pi^*)$. Previous examples of structured metal to ligand charge transfer emissions have been observed in complexes of d^6 metal ions. Examples include cis-$[IrCl_2(phen)_2]Cl$ and $[Ru(phen)_3]I_2$, in which the emissions were shifted 1,100 cm^{-1} and 4,600 cm^{-1} respectively to low

energy from the free ligand, and were also assigned as a charge transfer emission.[157,158] It should be noted that the state from which the low energy emission from (I) is observed is probably a triplet and the small shift from the absorption band is explained by the large spin-orbit coupling due to platinum. In some metal complexes such as $[IrCl_2(phen)_2]Cl$ the spin-orbitally enhanced MLCT singlet-triplet absorption is observed to be superimposed upon the MLCT singlet-singlet absorption.[153] Similar spin-orbit coupling would be expected in (I) and hence the small shift between the lowest energy absorption and emission bands of (I) is not incompatible with a triplet ($d-\pi^*$) emission. The observation of emission from both ligand localized and MLCT states is not unique. Similar phenomena have been observed for a variety of metal ligand combinations. Previous examples include fac-$[XRe(CO)_3(3\text{-benzoylpyridine})_2]$ (X = Cl, Br, I), in which the intraligand transition is $n-\pi^*$,[159] and fac-$[(CH_3CN)Re(CO)_3(phen)]^+$, in which the intraligand transition is $\pi-\pi^*$.[155]

The excitation spectra (figure6.1c) indicate that the ligand localized $^3(\pi-\pi^*)$ state of (I) is not accessible from the low energy MLCT absorption band, 4. In our study of the photochemistry of (I), irradiations were carried out at 473 nm and hence the chemistry is the result of the lower energy $^3(d \rightarrow \pi^*)$ MLCT excited state.

The reaction induced by MLCT excitation of (I) in the presence of ^{i}PrI is oxidative addition of ^{i}PrI forming $[PtMe_2{}^i PrI(phen)]$ according to equation (6.11). The free radical chain nature of the mechanism is demonstrated by the reduced quantum yields in the presence of free radical inhibitors. The nature of the initiation, propagation and termination steps will now be considered.

6.2.2 Initiation

It is clear that, under the conditions used, the reaction of (I) with ^{i}PrI is photochemically initiated. The ability to quench the reaction with the triplet quencher pyrene or sensitize the reaction with the triplet sensitizer benzophenone are all consistent with the predominantely triplet MLCT, $^{3}(d \rightarrow \pi^*)$, being the reactive state. The high value (1.0±.3) of the quantum yield for intersystem crossing from the $^{1}(d \rightarrow \pi^*)$ to the $^{3}(d \rightarrow \pi^*)$ state is consistent with the large spin-orbit coupling of the platinum atom and the $^{1}(d \rightarrow \pi^*)$ and $^{3}(d \rightarrow \pi^*)$ states are probably not pure. Hence the spin selection rules do not apply.[154]

In the presence of the free radical inhibitor 4-methoxyphenol the reaction occurred much less efficiently and produced $[PtI_2Me_2(phen)]$, (V) as in equation (6.13).

$$[PtMe_2(phen)] + 2\,{}^{i}PrI \xrightarrow[\text{4-methoxyphenol}]{h\nu} [PtI_2Me_2(phen)] + 2\,{}^{i}Pr\cdot \qquad \ldots(6.13)$$

The overall initiation sequence, which we propose (scheme 6.1) to explain the formation of (V), is analogous to the initiation observed for the oxidative addition of BuBr to $[Pt(PEt_3)_3]$ (equation 6.7), although in this case the reaction is photochemically activated.

Irradiation of (I) produces a triplet excited state with unit efficiency. This excited platinum complex, (VI), (Scheme 6.1) may then decay to the ground state with a rate constant k_d or react in a bimolecular fashion with isopropyliodide producing (VII) and free isopropyl radicals. The intimate nature of this reaction is not known. However, it may proceed either by direct halogen abstraction from isopropyliodide by the electron deficient platinum(III) centre of (VI)

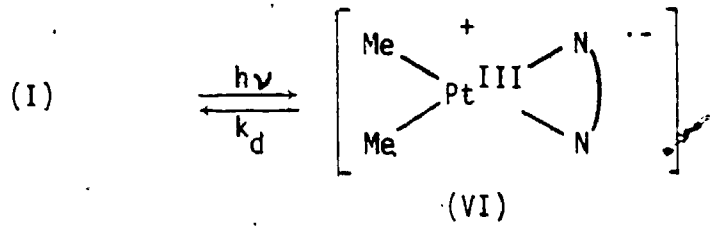

(VI)

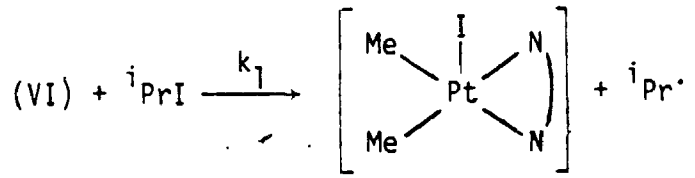

(VII)

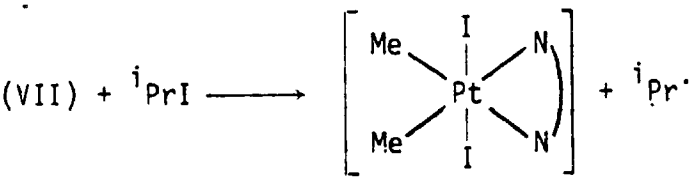

(V)

Initiation Sequence

Scheme 6.1

as in equation (6.14) or via an initial electron transfer from the electron rich phenanthroline ligand of (VI) to isopropyl iodide followed by net iodide transfer as shown in equation (6.15).

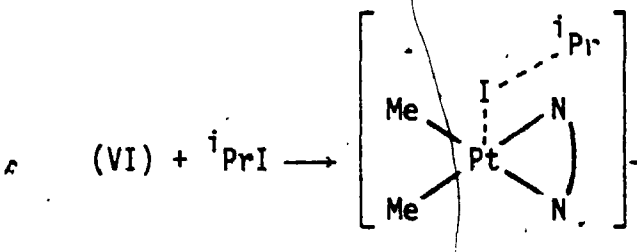

...(6.14)

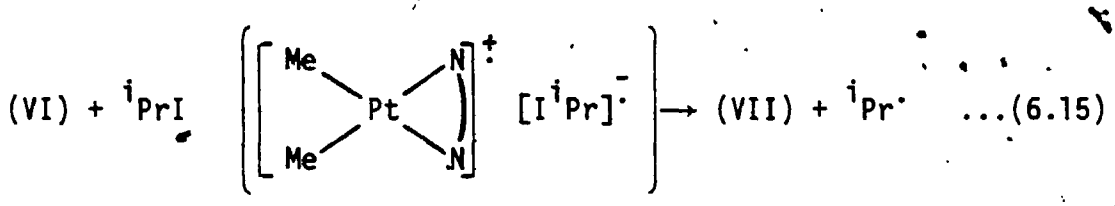

...(6.15)

The final step, abstraction of a second iodide by the platinum(III) centre of (VII) (Scheme 6.1), is expected to be fast due to the instability of the paramagnetic platinum(III).

6.2.3 Propagation

The initiation sequence was found to produce two moles of isopropyl radicals. The trapping of only isopropyl radicals by DMPO, as observed by E.S.R. spectroscopy, implicate the isopropyl radical as the radical chain carrier. In order to produce the observed reaction product, (II), the sequence of equation (6.16) and (6.17) is proposed.

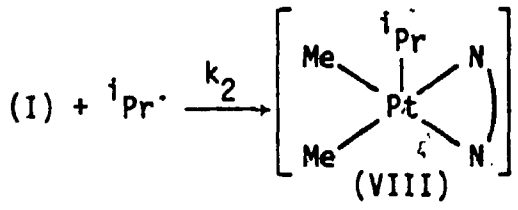

...(6.16)

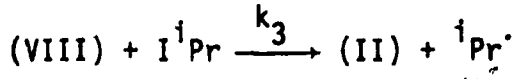

...(6.17)

A similar sequence of events is believed to be operative in the oxidative addition of BuBr to $Pt(PEt_3)_3$[146] (equation (6.9)).

6.2.4 Termination

The addition of a free radical scavenger was found to reduce the observed quantum yield by as much as a factor of 2×10^3 (Table 6.3). This observation indicates a minimum chain length of 1000 (a quantitative estimate of the chain length will be presented later). The products derived from the termination step will represent less than .05% of the total reaction products when (I) is photolyzed in the presence of ^{i}PrI. Because of the small amount of termination products formed, direct chemical identification of the termination products is not possible. One may, however, utilizing the above scheme for initiation and propagation, investigate the nature of the termination reaction by a kinetic means.

If we assume a termination sequence involving a bimolecular collision between free isopropyl radicals and an unknown species, (X), leading to non-radical products, equation (6.18), the rate of this termination is given by equation (6.19). We can now develop an

$$^{i}Pr\cdot + X \rightarrow \text{non radical product} \qquad \ldots(6.18)$$

$$-\frac{d[^{i}Pr\cdot]}{dt} = k_4[^{i}Pr\cdot][X] \qquad \ldots(6.19)$$

expression for the observed quantum yield, Φ, for reaction of (I) using the sequence described by Scheme 6.1 and equations (6.14 and 6.15). Assuming steady state concentrations for the excited platinum complex, (VI), and all radicals, (VII, VIII and the isopropyl radical)

the quantum yield for reaction of (I) is described by equation (2.20).

$$\Phi = \frac{k_1[^iPrI]}{k_d+k_1[^iPrI]} \left(1 + \frac{2k_2}{k_4} \frac{[I]}{[X]}\right) \quad \ldots(6.20)$$

The development of this equation is given in Appendix 6.I. The chain length is given by $\frac{k_2}{k_4}$ and is greater than 1000. Hence, at a constant isopropyl iodide concentration, the quantum yield is expected to be directly proportional to the concentration of (I). As we can see from Figure 6.3 the quantum yield is independent of the concentration of (I). In order to remove this dependence of the concentration of (I) in equation (6.20), we propose that the termination is a result of a bimolecular collision between isopropyl radicals and (I), equation (6.21).

$$^iPr\cdot + (I) \xrightarrow{k_2} \text{non-radical products} \quad \ldots(6.21)$$

The expression for the quantum yield using the termination step (6.21), developed in Appendix 6.I is given by equation (6.22).

$$\Phi = \frac{k_1[^iPrI]}{k_d+k_1[^iPrI]} \left(3 + \frac{2k_2}{k_4}\right) \quad \ldots(6.22)$$

In this expression Φ is independent of the concentration of (I) as was observed experimentally.

The termination step may be the result of hydrogen abstraction by isopropyl radical from either the methyl or the 1,10-phenanthroline ligand of (I). An alternate possibility is nucleophilic attack by isopropyl radical on the coordinated 1,10-phenanthroline,[160] reminiscent of the well known addition of alkyl radicals to aromatic

π-systems.[161] Whatever the intimate details of the process, the resultant platinum complex is removed from the propagation sequence.

It should be noted that, in the case of isopropyl radical attack at the platinum metal of (I) giving rise to (VIII), followed by decay of (VIII) to non-radical products at a rate equal to k_6[VIII], the quantum yield is given by equation (6.23) (developed in Appendix 6.II).

$$\Phi = \frac{k_1[^iPrI]}{k_d+k_1[^iPrI]} \left[3 + \frac{2k_3}{k_6}[^iPrI]\right] \qquad ...(6.23)$$

From the long chain length, (1000), and high observed quantum yields (>.21 at $[^iPr] = 2 \times 10^{-3}$ molar) we can calculate that the efficiency of the initiation must be less than 10^{-3}. This indicates that the rate of decay to ground state for the excited platinum species (VI) is much faster than the rate of iodide abstraction from isopropyl iodide and hence $k_d >> k_1[RI]$. Given this, equation (6.22) results in a linear dependence between Φ and the concentration of isopropyl iodide and equation (6.23) gives a squared dependence between Φ and the concentration of isopropyl iodide. The dependence is clearly linear, as shown in figure 6.4, and hence the termination reaction of isopropyl radicals with (I) must occur at either the methyl or 1,10-phenanthroline ligands.

The entire reaction sequence of initiation propagation and termination is summarized in Scheme 6.2.

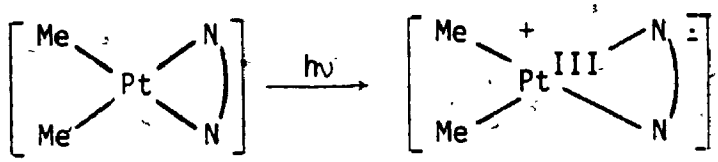

(I) (VI)

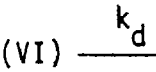

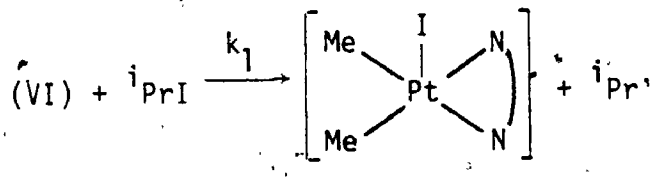

(VII)

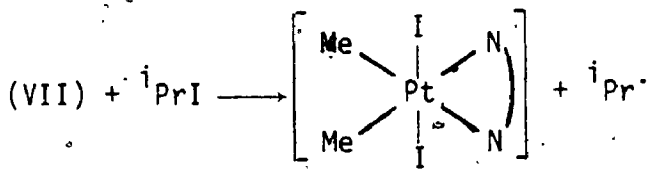

(V)

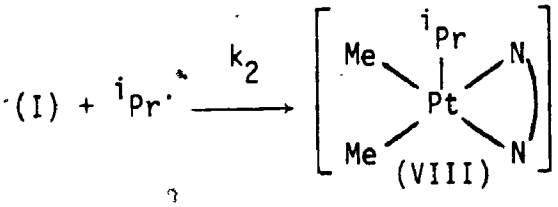

(VIII)

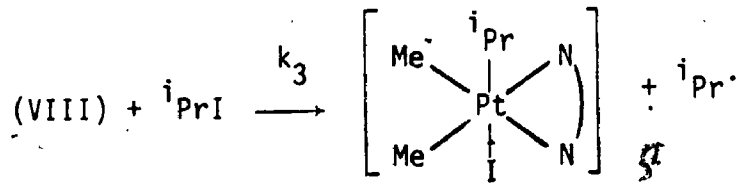

(II)

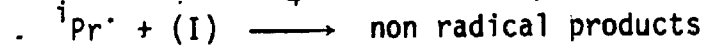

Scheme 6.2

6.2.5 Rate Constants

If we introduce a triplet quencher, Q, into the reaction mixture of (I) and isopropyl iodide we provide a new decay channel for the excited platinum complex (VI) as shown in equation (6.24). This was

$$(VI) + Q \longrightarrow (I) + {}^3Q^* \qquad \ldots(6.24)$$

done by the addition of pyrene (Q). The triplet energy of pyrene, (E_T = 595 nm), is lower than the triplet energy of (I) and hence we can assume the rate of quenching is diffusion controlled. The rate constant, k_{diff}, for the process is therefore expected to be 3×10^{10} s^{-1} in acetone.[101]

The quantum yield in the absence of quencher, Φ, is given by equation (6.22). Including the new decay channel for (VI), equation (6.24), gives rise to a new expression for the quantum yield in the presence of quencher, $\Phi(Q)$, as shown in equation (6.25). A Stern-

$$\Phi(Q) = \frac{k_1[{}^iPrI]}{k_d + k_1[{}^iPr] + k_{diff}[Q]} \left(3 + \frac{2k_2}{k_4}\right) \qquad \ldots(6.25)$$

Volmer plot of $\Phi/\Phi(Q)$ against concentration of pyrene, [Q] (figure 6.7) will have a slope of $k_{diff}/(k_d + k_1[{}^iPrI])$. Since $k_1[{}^iPrI] << k_d$, the observed slope, 74±9, allows calculation of the rate constant, k_d, to be 4.1 (±0.5) $\times 10^8$ s^{-1}. The lifetime, τ, of the reactive triplet state, (VI), is given by $(k_d)^{-1}$ or 2.5 (±.3) $\times 10^{-9}$ s. This lifetime is much shorter than triplet lifetimes observed in typical organic compounds.[101] For example, pyrene has a triplet lifetime of greater than 10^{-4} at room temperature.[101] The shorter lifetime of (VI) is due to a breakdown in the selection rules, governing triplet-singlet

transitions, caused by the large spin-orbit coupling of the platinum metal centre. Such short lifetimes for lowest energy triplet states are common when a second or third row transition metal is present. For comparison the solution lifetime of emission from a ^{3}MLCT excited state of cis-$[Ir(phen)_2Cl_2]Cl$ is 3.8×10^{-8} sec at room temperature.[153]

We will now consider the effect of adding a free radical inhibitor, (IN), to the reaction, scheme 6.2. Assuming that the inhibitor traps only isopropyl radicals, as shown in equation (6.26), we can now develop

$$^{i}Pr^{\cdot} + IN \xrightarrow[k_5]{} {}^{i}PrIN \qquad \ldots(6.26)$$

(see Appendix 6.I) an expression for the ratio of the quantum yield in the presence of inhibitor, $\Phi(IN)$, compared to the quantum yield in the absence of inhibitor, Φ, as shown in equation (6.27).

$$\frac{\Phi(IN)}{\Phi} = \frac{k_4}{2k_2} + \frac{k_4[Pt]}{k_5[IN]} \qquad \ldots(6.27)$$

As can be seen from equation (6.27) a plot of $\Phi(IN)/\Phi$ vs $[Pt]/[IN]$ is expected to be linear. Such a plot is shown, in Figure 6.8, using the inhibitor para-benzoquinone. From equation (6.27) we can see that the slope of this plot, $6\pm1 \times 10^{-4}$, corresponds to k_4/k_5 and that the intercept, $3\pm1 \times 10^{-4}$, corresponds to $k_4/2k_2$.

It should be noted that the average chain length is given by the ratio of the rate of propagation, $k_2[I][^{i}Pr^{\cdot}]$, to the rate of termination, $k_4[I][^{i}Pr^{\cdot}]$, or k_2/k_4. Hence one half the inverse of the intercept of Figure 6.8 gives the chain length as 1700 (±700).

It should be noted that, in the interpretation of the triplet quenching data, it was implicitly assumed that pyrene, the quencher

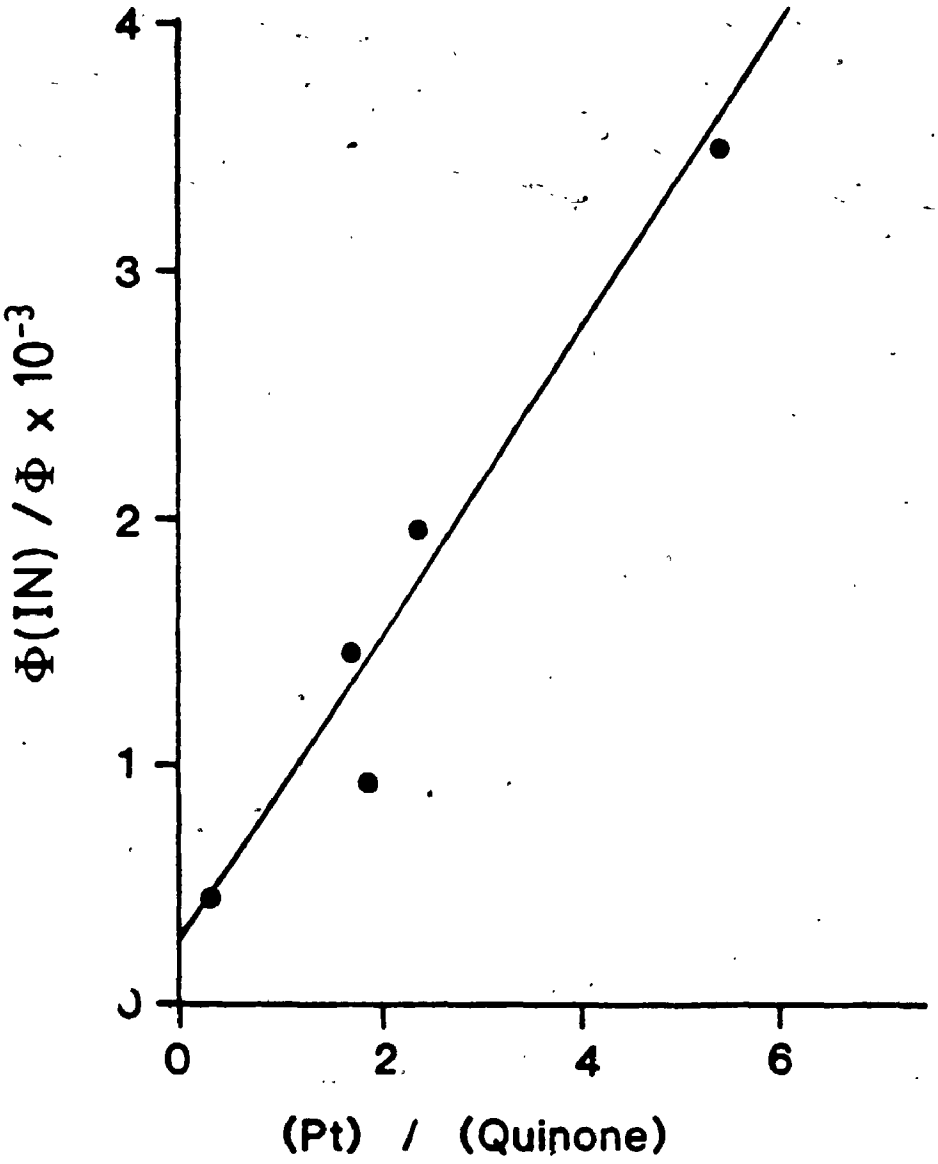

Figure 6.8. A plot of quantum yield in the presence of inhibitor, $\Phi(IN)$, over quantum yield in the absence of inhibitor, Φ, vs concentration of $[PtMe_2(phen)]$ over concentration of the free radical inhibitor, benzoquinone.

used, did not act as a free radical inhibitor. We can see from equation (6.27) that if inhibition was occurring the quantum yield would vary as a function of concentration of (I). No such dependence was observed and hence our assumption that pyrene acts only as a triplet quencher, and not as a free radical inhibitor, is valid.

The last relationship required is for the quantum yield, Φ, in the absence of both quencher and inhibitor, equation (6.22). It should be noted that k_d, $4.1(\pm.5) \times 10^8$ s^{-1} is much larger than $k_1[^iPrI]$, as indicated by the observed linearity of a plot of Φ^{-1} vs concentration of isopropyl iodide, figure 6.3. The slope of this graph, 123±5, corresponds to the quantity $k_1(3+2k_2/k_4)/k_d$. Using the value for k_d obtained from triplet quenching experiments and the value of $2k_2/k_4$ obtained from free radical inhibition experiments, we can arrive at a value of $1.5(\pm.7) \times 10^7$ L mol^{-1} s^{-1} for k_1. The original assumption, that k_d is greater than $k_1[^iPrI]$ can now be tested. The maximum concentration of isopropyl iodide used was less than 10^{-2} mol L^{-1}. Hence $k_1[^iPrI]$ has a maximum value of less than 2.2×10^5 s^{-1}, much less than $4.1(\pm.5) \times 10^8$ s^{-1} observed for k_d.

Although we now have absolute values for k_1 and k_d, the remaining rate constants k_2, k_4 and k_5 can only be obtained as relative values. In order to determine absolute values for k_2 and k_4 we must assume a value for k_5, the rate constant for isopropyl radical attack at <u>para</u>-benzoquinone. The only estimate of a rate constant for free radical attack on <u>para</u>-benzoquinone, $2.0(\pm1) \times 10^7$ L mol^{-1} s^{-1}, was for attack by the 5-hexenyl radical at 69°C.[162,163] Assuming a temperature dependence such that the rate at 25°C is 1.0×10^7 L mol^{-1} s^{-1}, as was observed for a variety of systems involving attack by the 5-hexenyl

radical on other molecules,[163] we can now calculate k_2 and k_4. It is found that $k_2 = 1.0(\pm.2) \times 10^7$ L mol^{-1} s^{-1} and $k_4 = 6(\pm3) \times 10^3$ L mol^{-1} s^{-1}. It should be noted that the errors given for the values k_2 and k_4, above, assume the value of k_5, 1.0×10^7 L mol^{-1} s^{-1} has no associated error. The actual error on the values of k_2 and k_4 are presumably much larger and hence the values given should be regarded as approximate.

It is comforting to note the results of a study carried out previously which gave a very similar value for k_2. In this study, acrylonitrile was added to a reaction mixture of (I) and isopropyl iodide.[147] Under these conditions, formation of the product, (II), as in equation (6.16-6.17), occurs in competition with formation of the insertion product, (IV) by the steps outlined in equations (6.28, 6.29 and 6.30). By analyzing the ratio of products (II) to (IV), the relative

$$^{i}Pr\cdot + CH_2{=}CH(CN) \xrightarrow{k_6} (^{i}Pr\text{-}CH_2CH(CN))\cdot \qquad \ldots(6.28)$$

$$(^{i}PrCH_2CH(CN))\cdot + (I) \longrightarrow$$

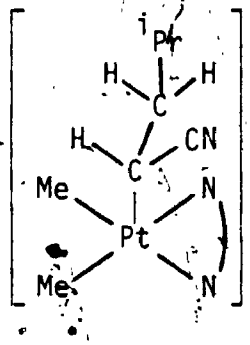

(IX) $\qquad \ldots(6.29)$

$$(IX) + {}^{i}PrI \longrightarrow (IV) + {}^{i}Pr\cdot \qquad \ldots(6.30)$$

value of k_2 to k_6 was found to be 20(±10). If we use as the value for k_6, 5.3×10^5 L mol s^{-1}, which is the measured rate constant for 5-hexenyl radical attack on acrylonitrile at 25°C, we arrive at a value

of $1(\pm.5) \times 10^7$ L mol^{-1} sec^{-1} for k_2.[113]

The agreement between these two values of k_2, measured by completely different methods, is further evidence for the validity of the proposed mechanism (Scheme 6.2).

6.3. Conclusions

We have shown that the photochemical initiation of reaction between isopropyl iodide and [$PtMe_2$(phen)] occurs from a state with considerable triplet character, and have established the free radical chain nature of the photo initiated oxidative addition. The mechanisms of the initiation, propagation and termination steps of the chain reaction have been elucidated and, for the first time, approximate rate constants for several of the elementary steps have been determined.

APPENDIX 6.I

Analyzing the Kinetics in Terms of Scheme 6.2, Equation 6.24 and 6.26

$$-\frac{d[I]}{dt} = I_{abs} - k_d[VI] + k_2[{}^iPr^\cdot][I] + k_4[{}^iPr^\cdot][I] - k_{diff}[Q][I]$$

$$-\frac{d[VI]}{dt} = I_{abs} - k_d[VI] - k_1[VI][{}^iPrI] - k_{diff}[Q][VI]$$

$$\frac{d[{}^iPr^\cdot]}{dt} = 2k_1[{}^iPr^\cdot][VI] - k_4[{}^iPr^\cdot][I] - k_5[{}^iPr^\cdot][IN] - k_2[{}^iPr^\cdot][I] + k_3[VIII][{}^iPrI]$$

$$\frac{d[VIII]}{dt} = k_2[{}^iPr^\cdot][I] - k_3[VIII][{}^iPrI]$$

Assume steady state concentrations for [VI], [VIII] and $[{}^iPr^\cdot]$.

$$[VI] = \frac{I_{abs}}{k_d + k_1[{}^iPrI] + k_{diff}[Q]} \qquad [VIII] = \frac{k_2}{k_3}\frac{[{}^iPr^\cdot][I]}{[{}^iPrI]}$$

$$[{}^iPr^\cdot] = \frac{2k_1[{}^iPrI][VI]}{k_4[I] + k_5[IN]}$$

$$-\frac{d[I]}{dt} = Iabs - \frac{k_d I_{abs}}{k_d + k_1[{}^iPrI] + k_{diff}[Q]} + \frac{(k_2 + k_4)2k_1[{}^iPr]I_{abs}[Pt]}{(k_4[I] + k_5[IN])(k_d + k_1[{}^iPrI] + k_{diff}[Q]}$$

$$\frac{k_{diff}[Q]I_{abs}}{k_d + k_1[{}^iPrI] + k_{diff}[Q]}$$

$$\Phi = \frac{k_1[{}^{i}PrI] + \frac{(k_2+k_4)(2k_1[{}^{i}PrI][I])}{k_4[I]+k_5[IN]}}{k_d+k_1[{}^{i}PrI]+k_{diff}[Q]} \qquad \ldots(6.I)$$

6.22

In the absence of quencher, Q, and inhibitor, IN, equation 6.I simplifies to equation 6.22.

$$\Phi = \frac{k_1[{}^{i}PrI]}{k_d+k_1[{}^{i}PrI]} \left(3 + \frac{2k_2}{k_4}\right) \qquad \ldots(6.22)$$

6.20

Equation 6.20 is developed by removing [Q] and [IN] and k_4 and replacing $k_5[IN]$ by $k_4[X]$ in 6.I. The result is equation 6.20

$$\Phi = \frac{k_1[{}^{i}PrI]}{k_d+k_1[{}^{i}PrI]} \left(1 + \frac{2k_2[I]}{k_4[X]}\right) \qquad \ldots(6.20)$$

6.25

Removing $k_5[IN]$, from equation 6.I results in equation 6.25

$$\phi(Q) = \frac{k_1[{}^{i}PrI]}{k_d+k_1[RI]+k_{diff}[Q]} \left(3 + \frac{2k_2}{k_4}\right) \qquad \ldots(6.25)$$

6.27

The result of removing $k_{diff}[Q]$ terms from 6.I is divided by equation 6.22 giving

$$\frac{\phi(IN)}{\Phi} = \frac{1 + \frac{(k_2+k_4)2[I]}{k_4[I]+k_5[IN]}}{3 + \frac{2k_2}{k_4}}$$

But, $\frac{k_2}{k_4}$, the chain length, is much greater than 3 and $k_2 >> k_4$. Also $k_5[IN] >> k_4[Pt]$ under the conditions used. Hence, we can further simplify to equation 6.27

$$\frac{\Phi(IN)}{\Phi} = \frac{k_4}{2k_2} + \frac{k_4}{k_5}\frac{[I]}{[IN]} \qquad \ldots(6.27)$$

APPENDIX 6.II

Development of Equation 6.23 Utilizing Scheme 6.1 and Equations 6.16 and 6.17 Also adding the Following

$$VIII \xrightarrow{k_6} \text{Non Radical Products}$$

The following differential equations apply.

$$-\frac{d[I]}{dt} = Iabs - k_d[VI] + k_2[{}^{i}Pr^{\cdot}][I]$$

$$-\frac{d[VI]}{dt} = Iabs - k_d[VI] - k_1[VI][{}^{i}PrI]$$

$$-\frac{d[{}^{i}Pr^{\cdot}]}{dt} = 2k_1[{}^{i}PrI][VI] - k_2[{}^{i}Pr^{\cdot}][I] + k_3[VIII][{}^{i}PrI]$$

$$\frac{d[VIII]}{dt} = k_2[{}^{i}Pr][I] - k_3[VIII][{}^{i}PrI] - k_6[VIII]$$

Assume steady state concentration for [VI], [$^{i}Pr^{\cdot}$] and [VIII]

$$[VI] = \frac{Iabs}{k_d + k_1[{}^{i}PrI]} \qquad [{}^{i}Pr^{\cdot}] = \frac{2k_1[{}^{i}PrI][VI]}{k_4[I]}$$

$$[VIII] = \frac{k_2[{}^{i}Pr^{\cdot}][I]}{k_3[{}^{i}PrI] + k_6[VIII]}$$

$$\phi = \frac{k_1[{}^{i}PrI]}{k_d + k_1[{}^{i}PrI]} \left(3 + \frac{2k_3[{}^{i}PrI]}{k_6}\right) \qquad \ldots(6.23)$$

CHAPTER 7

Catalysis of the Water Gas Shift Reaction by $[Pt_2H_2[\mu\text{-}H](\mu\text{-}dppm)_2]^+$

7.0 Introduction

The water gas shift reaction (equation (7.1)) has been important industrially for over 40 years.[164] Heterogeneous catalysts for

$$H_2O + CO \rightleftharpoons H_2 + CO_2 \qquad \ldots(7.1)$$

equation (7.1) require high temperatures. For example, Fe_3O_4 based systems operate at temperatures exceeding 350°C.[165] The development of a catalyst system which operates at lower temperatures is desirable as the equilibrium constant, K, for equation (7.1) increases with decreasing temperatures (for example, $K = 1.5 \times 10^3$ at 127°C, K = 127 at 327°C).[166] To date, several homogeneous catalysts have been found which operate at lower temperature than the heterogeneous catalysts.[167-171]

The complex cation $[Pt_2H_2(\mu\text{-}H)(\mu\text{-}dppm)_2]^+$, (I) was known to reversibly add CO, displacing dihydrogen (equation (7.2)).

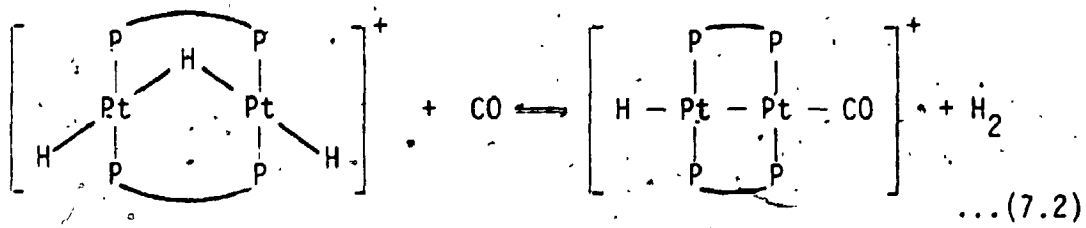

$$\ldots(7.2)$$

(II)

Known reactions of platinum carbonyl complexes (equation (7.3)[172] and (7.4)[170]) can be combined, with equation (7.2), to provide all the steps necessary for a possible catalytic scheme (Scheme 7.1).

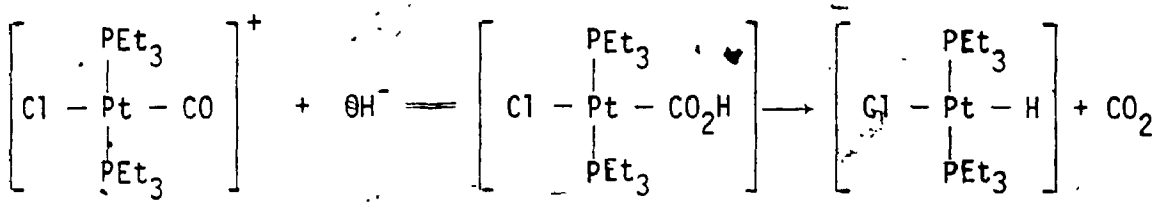

... (7.3)

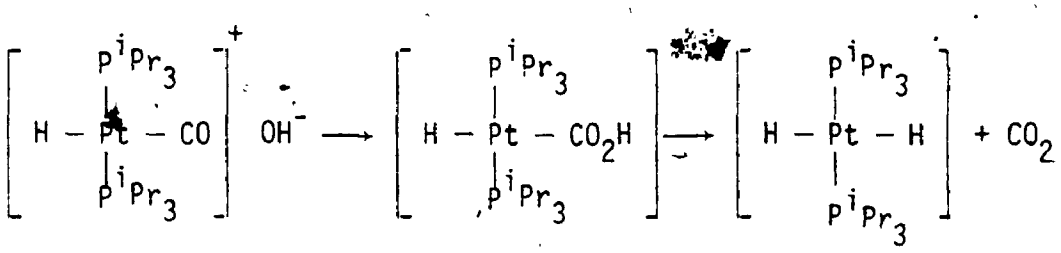

...(7.4)

With these facts in mind, we undertook a study of the catalysis of equation (7.1) by complex (I).

7.1 Results

7.1.1 Kinetics of the Catalysis

The complex $[Pt_2(\mu\text{-}H)H_2(\mu\text{-}dppm)_2]^+$, (I), was found to catalyze the water gas shift reaction (equation (7.1)). Typical reactions were carried out at 100°C in a Parr pressure reactor purged with CO using a water methanol solvent (1:2 Vol/Vol). The extent of reaction was determined by gas chromatographic analysis of the vapour phase. Both carbon dioxide(monitored by a Porapac Q column) and dihydrogen (monitored by a molecular sieve type 5A column) were found to be produced in equimolar amounts. For an initial pressure of CO equal to 110 psi, the rate of formation of carbon dioxide (or dihydrogen) was found to be first order with respect to initial concentration of (I) and the turnover rate was 3.0±.2 mol H_2 (or CO_2) mol $(I)^{-1}$ h^{-1}

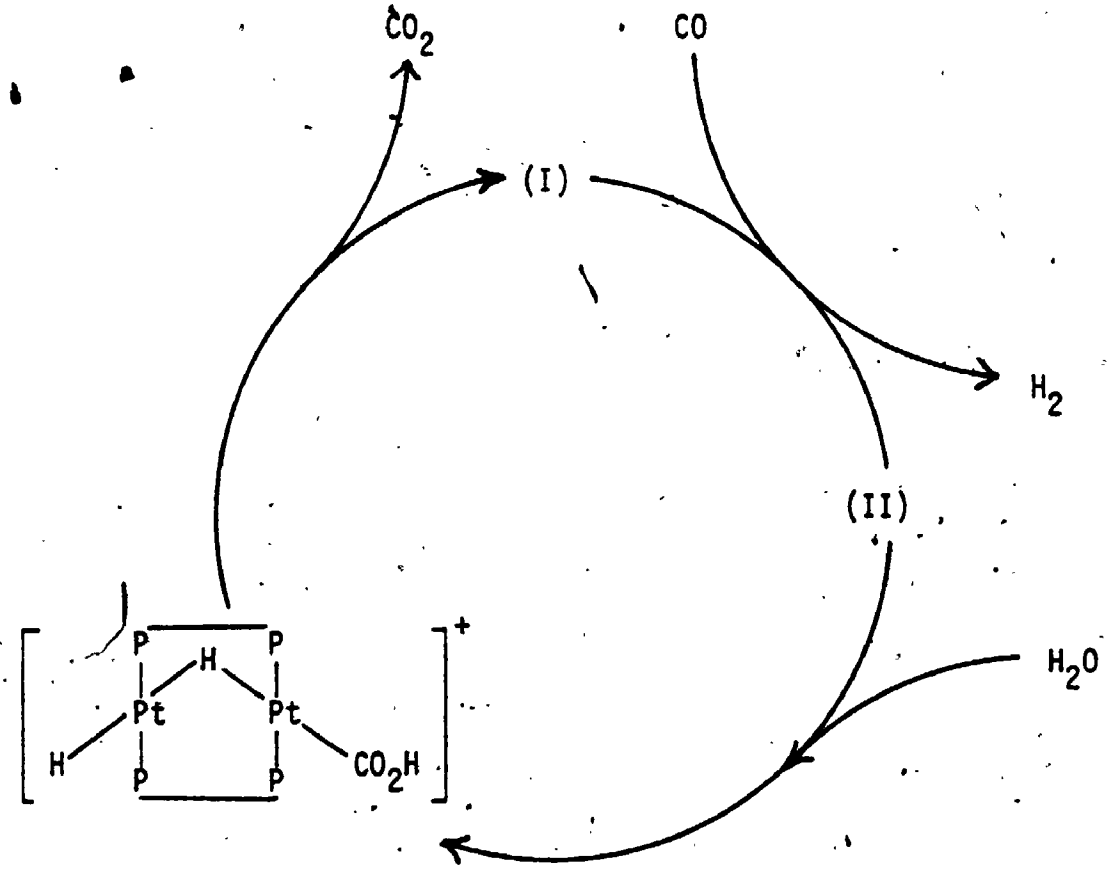

Scheme 7.1

(figure 7.1 and table 7.1). The dependence on carbon monoxide pressure was more complicated and the rate of the reaction was found to increase dramatically at pressures less than one atmosphere (figure 7.2). The addition of NaOH or LiCl had no effect initially on the rate of the reaction (Table 7.1). However in the presence of NaOH, decomposition of the catalyst occurred after approximately three hours.

7.1.2 Complexes Present in the Catalytic Solution

The material recovered from the catalytic solution at high pressure consists of a mixture of complexes. The first of these complexes, $[Pt_4(\mu\text{-}CO)_2(\mu\text{-}dppm)_3(\eta'\text{-}Ph_2PCH_2POPh_2)]$, (III), was obtained from a catalytic mixture in which dioxygen was not rigorously excluded. The complex (III) was obtained as red crystals by slow evaporation of the catalytic mixture and the structure (figure 7.3) was solved by single crystal X-ray diffraction.[173] It was found that formation of this complex was not observed if oxygen was rigorously excluded from the reaction vessel. The second major species (IV) crystalizes from the catalytic mixture as yellow needles. It has a characteristic I.R. absorption due to the presence of bridging carbonyls ($\nu(CO) = 1750\ cm^{-1}$). The ^{31}P NMR spectrum of this complex is well resolved (figure 7.4) and independent of temperature. The ^{195}Pt satellites appear to be too complex for a simple dimeric species (compare figure 7.4 (a), which shows satellites due to (IV), with figure 7.4 (b) which shows the corresponding satellites due to $[Pt_2Cl_2(\mu\text{-}dppm)_2]$[21]). The complex appears to be symmetrical as indicated by the ^{31}P NMR resonances being symmetrical about $\delta = -14.6$ ppm. The ^{195}Pt NMR spectrum was also obtained (figure 7.5) and the main triplet is indicative of a structure

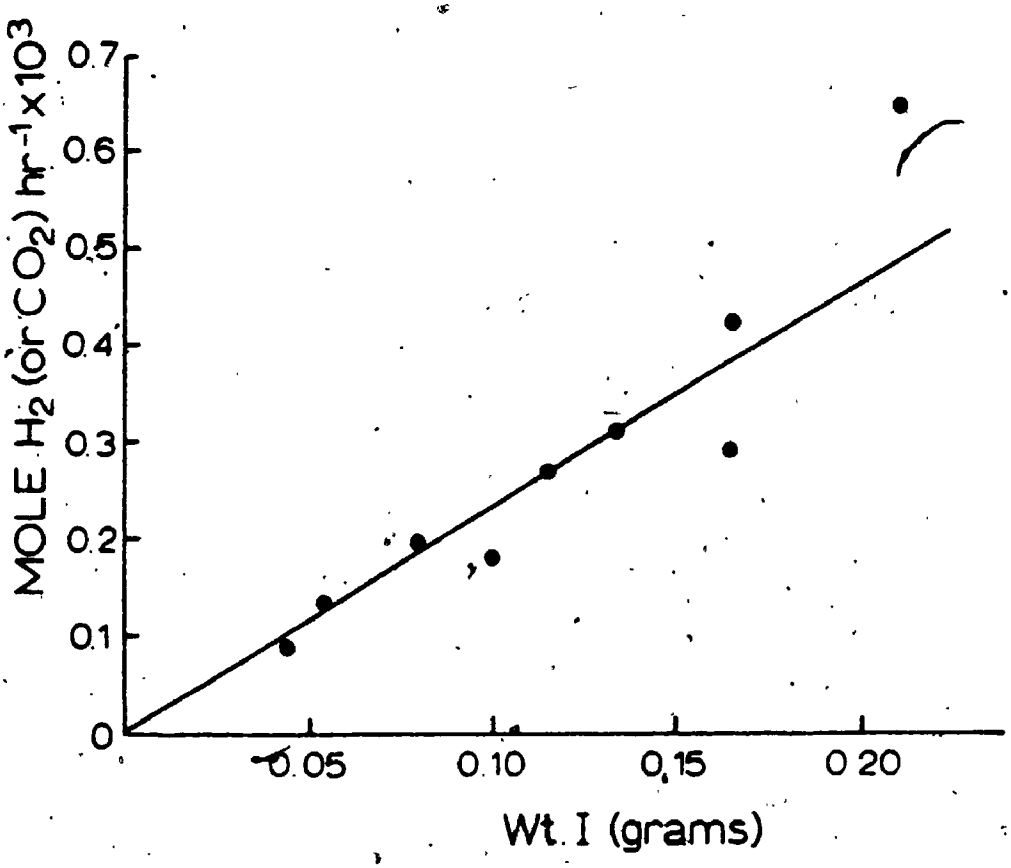

Figure 7.1. Dependence on rate of the water gas shift reaction on the weight of the catalyst precursor (as the PF_6^- salt) at an initial pressure of CO of 7.5 atm.

TABLE 7.1

Water Gas Shift Reaction Data

Init. P_{CO} atm.	Rate $CO_2(H_2)$ mol. prod./mol. cat. hr.	wt. cat. grams
6.9	3.4 (3.5)	.0328
5.5	4.3	.0292
4.1	2.6	.0287
2.7	4.1	.0280
7.5	4	.2108
.195	11	.0300
.13	25.2	.0300
.52	8.1	.0304
.28	5.35	.0300
.69	8.96	.0300
.68	7.4	.0262
.45	9.0	.0346
.15	20	.0325
7.5	2.6	.0444
1.0	6.0	.0549
7.5	2.5	.1585
7.5	2.8	.1342
7.5	3	.1163
5.5	3.5 (3.5)	.0521
7.5	3.2	.0796
7.5	3.3	.1662
7.5	(3.2)	.0540
7.5	2.3	.1013
7.5	2.8	.0589+.0061 grm LiCl
7.5	(2.8)	.0549+.8 grm NaOH

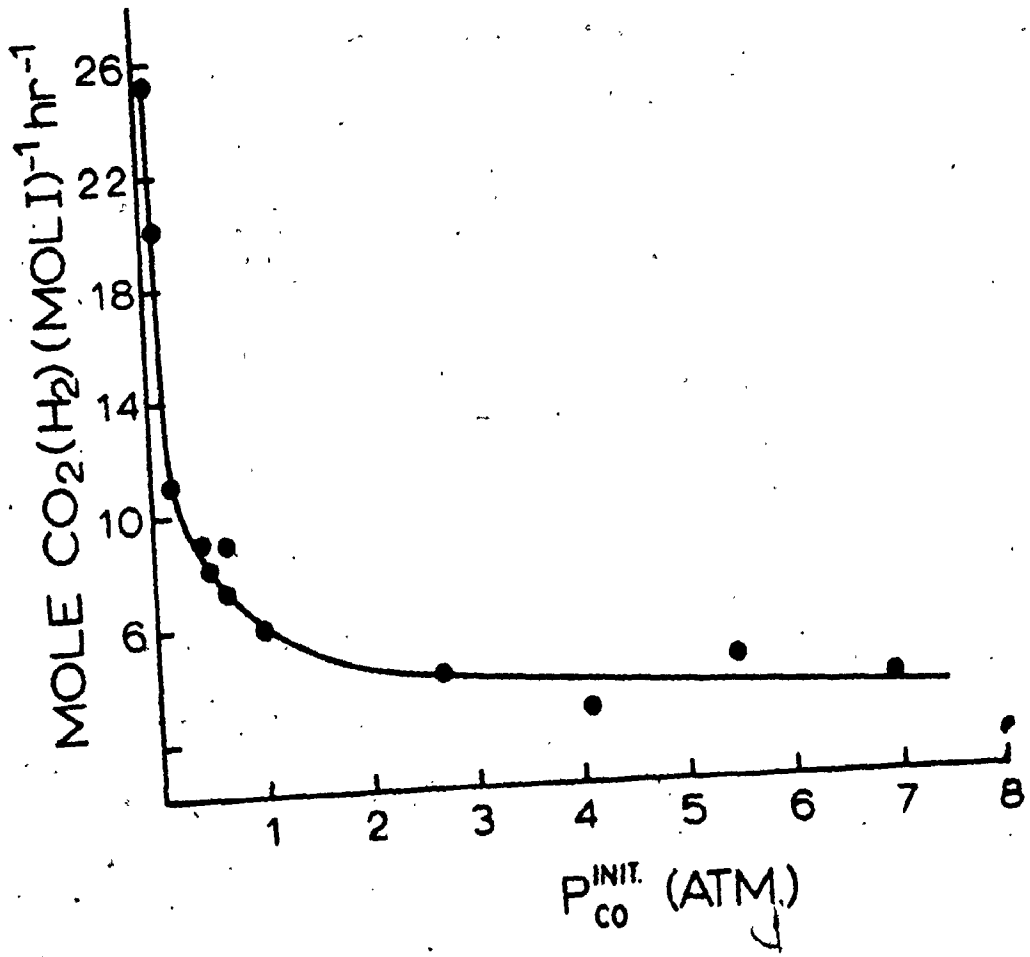

Figure 7.2. Dependence of turnover rate on the pressure of carbon monoxide. In each case the catalyst precursor, (I) as the PF_6^- salt, (0.03 g), was dissolved in solvent mixture.

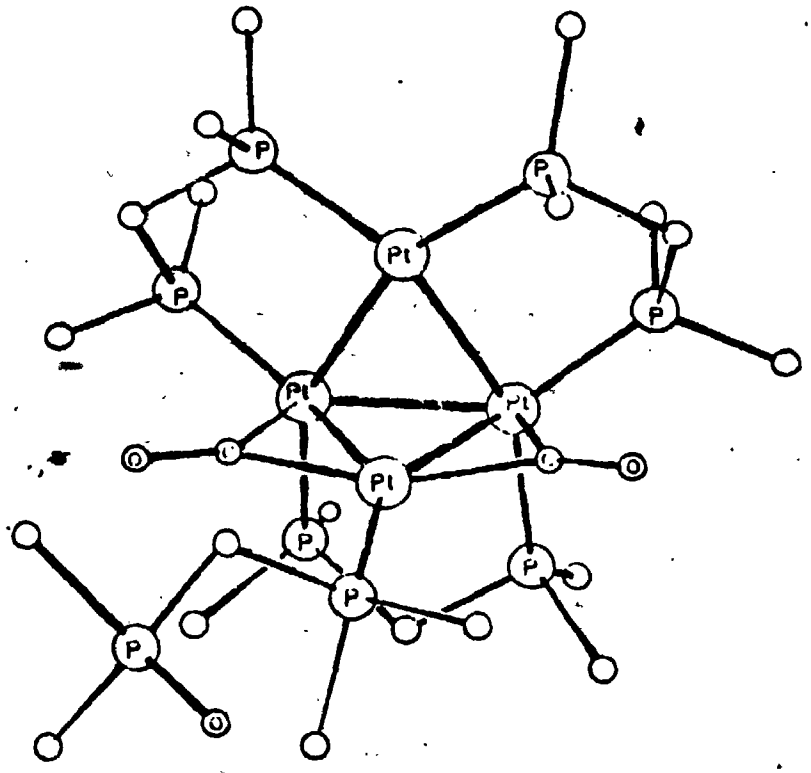

Figure 7.3. Molecular structure of $[Pt_4(\mu\text{-}CO)_2(\mu\text{-}Ph_2PCH_2PPh_2)_3(Ph_2PCH_2POPh_2)]$. Hydrogens and five carbon atoms of each phenyl group are omitted for clarity.

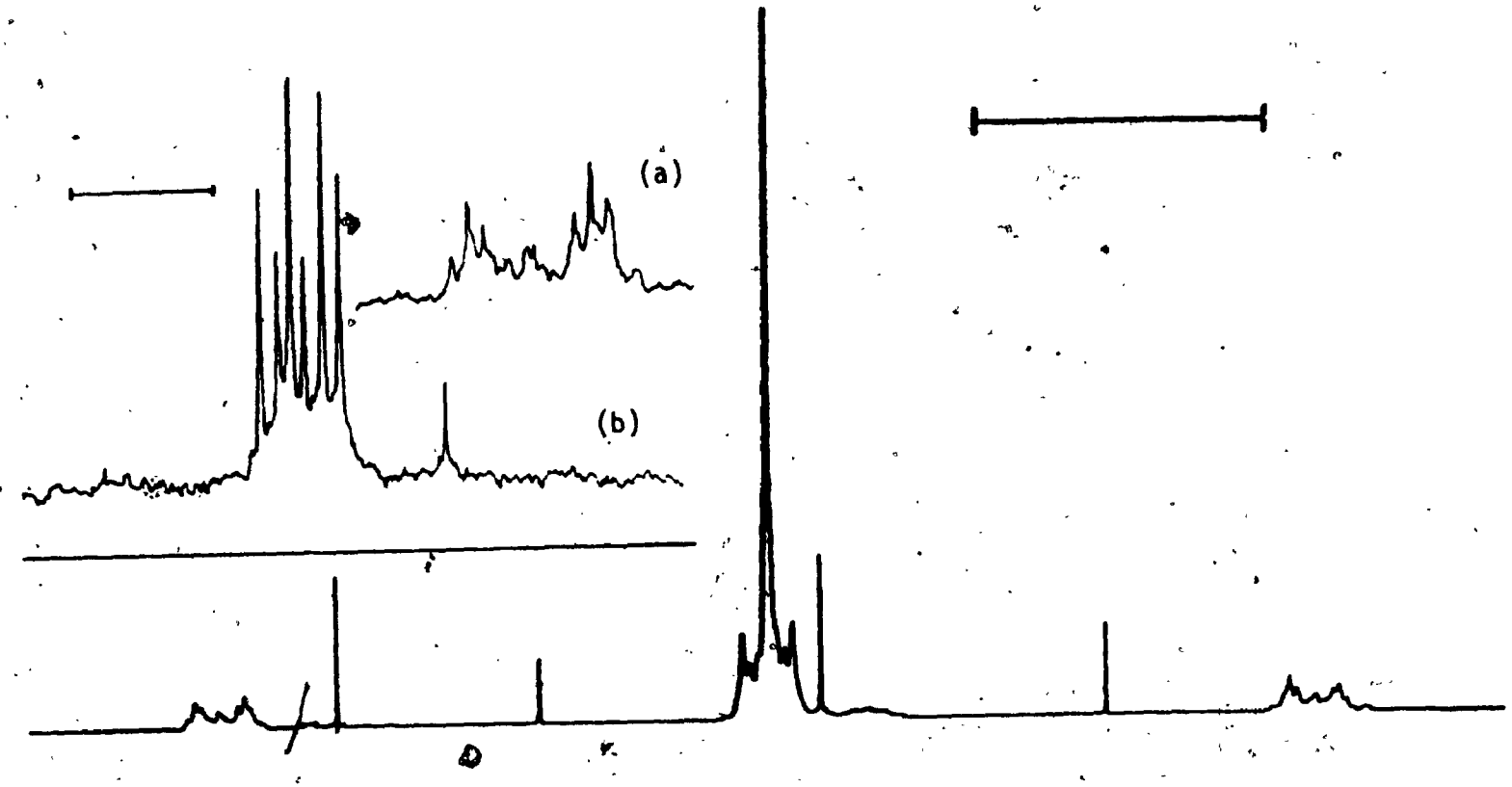

Figure 7.4. The ^{31}P NMR spectrum (81 MHz) of (IV), the field strength increases from left to right and the bar represents 1000 Hz. Inset are the low-field satellites of (IV) (a) and $[Pt_2Cl_2(\mu\text{-dppm})_2]$ (b) on an expanded scale in which the bar represents 200 Hz.

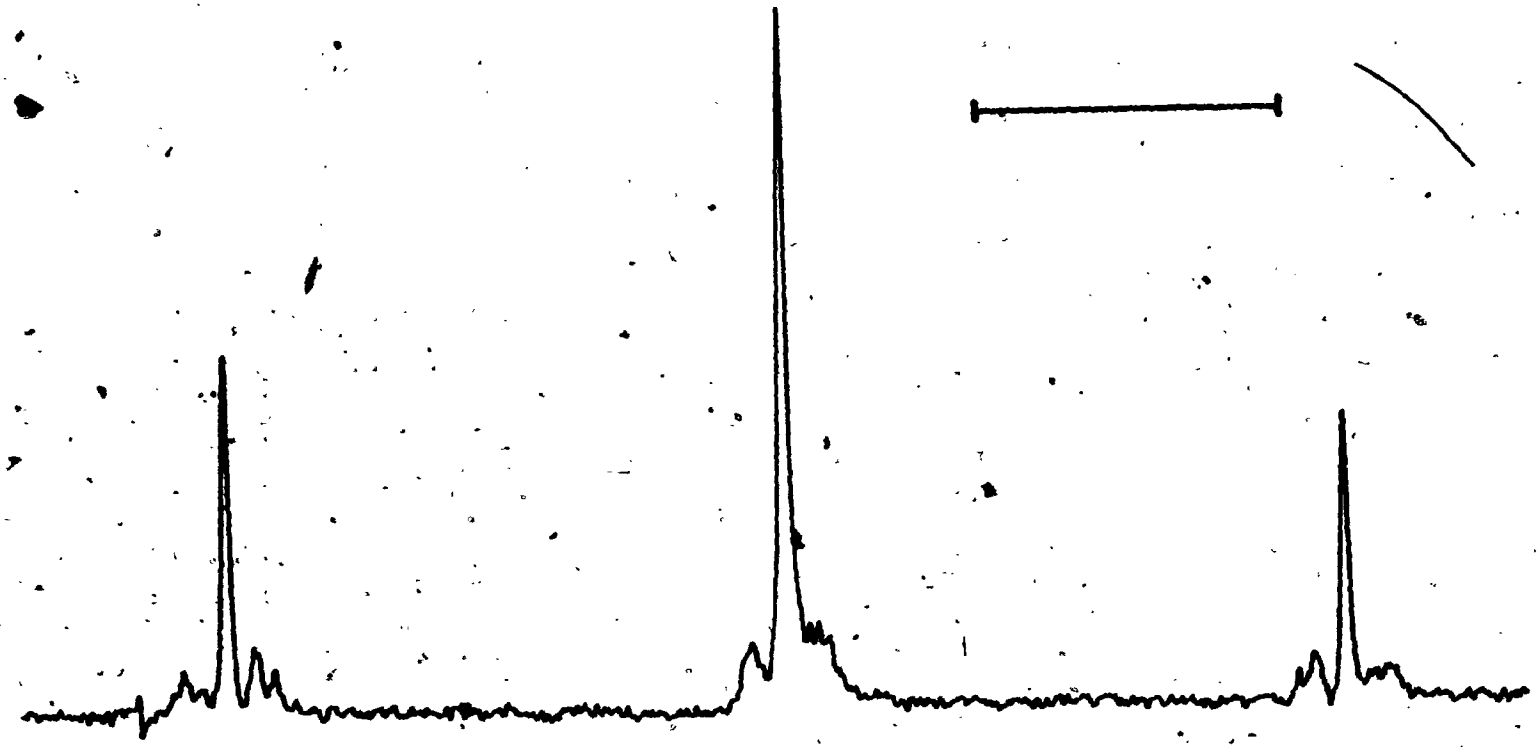

Figure 7.5. Platinum-195 NMR spectrum (43 MHz) of complex (IV). Field strength increases from left to right and the bar represents 2000 Hz.

in which two phosphorus atoms are directly bonded to each platinum centre. The ^{195}Pt NMR spectrum is also consistent with a symmetrical species.

The $^{1}H\{^{31}P\}$ NMR spectrum of (IV) contains peaks due to both the phenyl rings and the CH_2 groups of the dppm ligands. The resonances due to the CH_2 groups form an AB pattern, indicating inequivalence at the two protons of each CH_2P_2 unit.

Summarizing, in complex (IV) the phosphorus atoms are all chemically equivalent, the platinum atoms are all equivalent, and the protons on the methylene unit of the dppm ligands are inequivalent. In some reaction mixtures, minor products were present as shown by additional I.R. absorptions due to terminal CO groups at $\nu(CO)$ = 2020, 2030, 2060 cm^{-1} and due to bridging CO groups at $\nu(CO)$ = 1800 cm^{-1}. These products were not reproducibly formed and appear to be the result of impurities.

The catalytic mixture was investigated <u>in situ</u> by sealing a sample of (I) under CO in an NMR tube. The mixture was heated to 100°C for 24 hours and the ^{31}P NMR spectrum was then obtained, at 60°C. The NMR spectrum was found to contain primarily peaks due to (IV) and also a new species (V) [$\delta(P)$ = -5.9 ppm, $^{1}J(Pt^{P})$ = 2060 Hz].

7.2 <u>Discussion</u>

The complex, $[Pt_2H_2(\mu\text{-}H)(\mu\text{-dppm})_2]^+$, (I), in a water-methanol solvent mixture does lead to the catalysis of the water gas shift reaction. It appears, however that (I) is not an active catalyst but a catalyst precurser. The evidence for this is as follows: a linear relationship exists between the initial concentration of (I) and the

rate of CO_2 production, yet no (I) is observed in the catalytic mixture. In experiments done in the presence of oxygen, the catalyst became less active over a period of time and catalysis occurred in the absence of oxygen. Hence (III) is not the catalyst. The probable catalyst is either (IV) or a species in equilibrium with it.

The complex, (III), formed when the reaction is carried out in the presence of oxygen, was found to be $[Pt_4(\mu\text{-}CO)_2(\mu\text{-}Ph_2PCH_2PPh_2)_3(Ph_2PCH_2POPh_2)]$ (figure 7.3) by a single crystal X-ray diffraction study. The formation of (III) can be understood in terms of equation (7.5).

$$2(II) + \frac{1}{2}O_2 \longrightarrow (III) + 2H^+ \qquad \ldots(7.5)$$

The formation of a Pt_4 cluster (figure 7.3), may be a result of a kinetic effect, resulting from dimerization of the initial binuclear complex, (I). This is suggested as most platinum(0) clusters are trinuclear[174,176] although other tetranuclear clusters are known.[177]

A definitive chemical formulation for complex (IV) must await the results of a single crystal X-ray diffraction study. We can establish that the complex (IV) is not a binuclear system as the ^{31}P NMR spectrum is far too complex to be fitted to a $Pt_2(\mu\text{-dppm})_2$ system. Both a trinuclear and tetranuclear cluster are possible.

One possible trinuclear structure is (V).

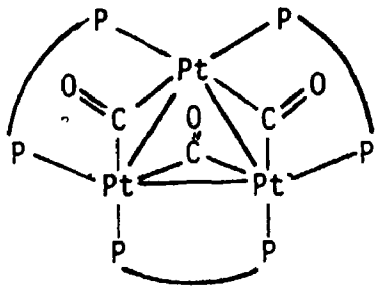

(V)

This cluster has 48 valence electrons, and including metal-metal bonds, results in each platinum attaining an 18-electron configuration.

We will now consider possible tetranuclear formulations for (IV).

Tetranuclear clusters of platinum are known and may have a butterfly, tetrahedral or square type framework.[180,182] The butterfly structure is immediately ruled out as it results in two distinct types of platinum environment and at least two different ^{31}P environments illustrated by structure (VI). This is inconsistent with the ^{195}Pt and ^{31}P NMR spectra.

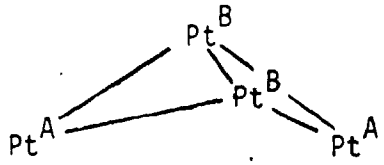

(VI)

A tetrahedral structure with two phosphorus donors per platinum, as predicted by the triplet ^{195}Pt NMR spectrum, is shown as structure (VII).

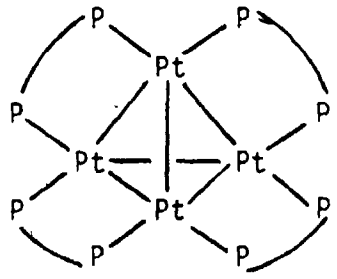

(VII)

In order for (VII) to be consistent with the IR and ^1H NMR spectrum, which predict a single type of bridging CO and inequivalent protons on the methylene of the dppm ligand, bridging CO groups must be included across each platinum-platinum bond which is bridged by dppm ligands. Such bridging is not possible, however, due to geometric considerations.

A square arrangement of platinum atoms, such as (VIII) is consistent with the observed spectral parameters.

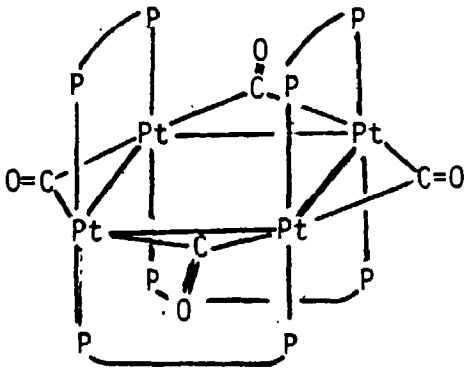

(VIII)

Once again we have a 64 valence electron cluster with four bridging CO groups. Including the four platinum-platinum bonds result in an 18 electron configuration for each platinum centre.

The mechanism of the catalysis has not been determined. However, the reaction occurs more slowly at high concentrations of CO, and is first order in catalyst concentration. One possible reason for CO inhibition is that a coordinative unsaturated intermediate may be trapped by CO, forming an inactive species. A plot of the rate of reaction vs reciprocal CO pressure (figure 7.6) is approximately linear and extrapolates to a rate of 3 moles CO_2 (or H_2) produced per mole (I)

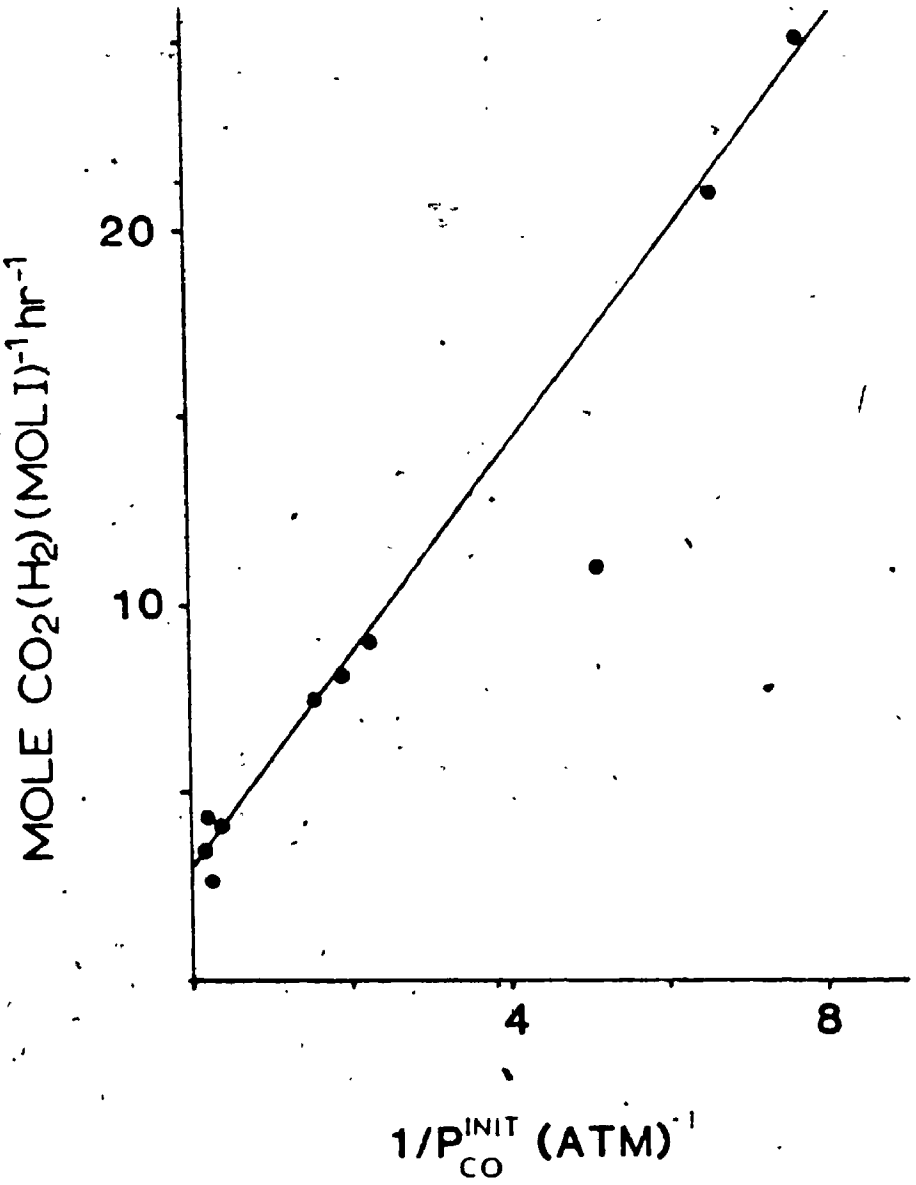

Figure 7.6. A plot of turnover rate vs reciprocal CO pressure.

per hour at infinite CO pressure.

The result suggests that there are two active catalysts, one operative only at low pressures of carbon monoxide.

Such a system is represented in Scheme 7.2. If k_4 and k_5 are large, such that the rate determining steps are represented by step two and three, Scheme 7.2, then the rate of the catalysis is given by equation (7.6).

$$\text{rate} = k_2[A] + k_3K\frac{[A]}{[CO]} \qquad \ldots(7.6)$$

We can define α as a stoichiometric factor relating (I) to (A) according to equation (7.7), in which only the platinum atoms are

$$I \rightarrow \alpha A \qquad \ldots(7.7)$$

accounted for, i.e. if (A) is a trinuclear species then α is 2/3. Assuming the equilibrium concentration of species other than (A) in the catalytic mixture are low the product $\alpha[I]$ may be substituted for [A] in equation (7.6). The result, equation (7.8), then has the functional dependence on rate on CO pressure observed in Figure 7.6.

$$\frac{\text{rate}}{[I]} = \alpha k_2 + \alpha\frac{Kk_3}{[CO]} \qquad \ldots(7.8)$$

The ^{31}P spectrum of the catalytic mixture is consistent with the species (IV) being identified with (A). A detailed discussion of the mechanism of the catalysis must await a structure determination of (IV), but it seems that loss of CO from (IV) must generate a more reactive catalyst.

$$A \underset{\longleftarrow}{\xrightarrow{K}} B + CO \qquad \text{STEP 1}$$

$$A \xrightarrow[H_2O]{k_2} C + CO_2 + H_2 \qquad \text{STEP 2}$$

$$A \xrightarrow[H_2O]{k_2} C' + CO_2 + H_2 \qquad \text{STEP 3}$$

$$C + CO \xrightarrow{k_4} A$$

$$C' + CO \xrightarrow{k_5} B$$

Scheme 7.2

7.3 Conclusions

The water gas shift reaction is indeed catalysed when (I) is added, albeit probably not by the mechanism initially proposed (Scheme 7.1). The formation of the unusual cluster, (III), indicates that dimerization of a binuclear complex may occur.

Despite our present lack of knowledge about the mechanism of the catalysis, it should be noted that the catalytic activity of the system under these mild conditions is very high. At 100°C and 0.13 atmospheres carbon monoxide, the turnover rate, 12.6 mol H_2 (mol Pt)$^{-1}$ h^{-1}, is much higher than observed for other homogeneous catalysts. For comparison, the highest turnover rate for the series of carbonyls, $[Fe(CO)_5]$ and $M(CO)_6$ (M = Cr, Mo, and W) at similar temperatures was for $[W(CO)_6]$, which at 110°C and p(CO) = 7.7 atm, catalyzed at a rate of 0.5 mol H_2 per mol $W(CO)_6$ per hour.[169] (It should be noted that at 95°C no catalysis was observed.)

$[Pt(PEt_3)_3]$ at 100°C and 20 atm CO gives a rate of 0.5 moles H_2 per mole $[Pt(PEt_3)_3]$ per hour.[184] A $[Rh(CO)_2I_2]^-$ system gives a turnover rate of 1 mole H_2 per mole Rh per hour at 1 atm CO and 100°C.[185]

CHAPTER 8

Experimental Details

8. General Experimental

NMR spectra were recorded using a Varian XL-100 or XL-200 spectrometer. Chemical shifts are reported relative to T.M.S. (^{1}H NMR) or external $PO(OMe)_3$ (^{31}P NMR). Infrared spectra were recorded using a Beckmann 4250 spectrophotometer. U.V.-visible spectra were recorded using a Cary 118 spectrophotometer. Mass spectra were obtained on a Varian Mat 311A spectrometer. Gas analysis was carried out on a Varian Model 1420 gas chromatograph with 6' x 1/8" column packed with either molecular sieve 5A (H_2) or Porapak Q (CO_2 and hydrocarbons). E.S.R. spectra were recorded with a Varian E-12 E.P.R. spectrometer.

Elemental analyses were carried out by Guelph Chemical Laboratories Ltd.

Unless otherwise specified, degassing was done by three freeze-pump-thaw cycles, pumping each time to a residual pressure of 5×10^{-5} torr at 77 K.

8.1 Calibration of the Light Source for Quantum Yield Determinations

The light source used was a Jasco CRM-FA Spectroirradiator. This system is equipped with a counter monitoring the energy output at a reference wavelength. Assuming a constant spectral distribution for the light source, one may calibrate the light output at a given wavelength relative to the counter once and the quantum yields are then measured relative to the counter. In practice, the spectral distribution of the light source was found to be constant for greater than 600 hours

of operation. In order to ensure consistency, the counter was standardized approximately every 200 hours of operation, or every six months (elapsed time) whichever was less, and whenever the light source, or power supply was serviced.

The method of calibration was that of Parker and Hatchard using the potassium ferrioxalate system.[186] The photochemical reduction of the iron salt, $K_3[Fe(C_2O_4)_3]$ in sulfuric acid occurs readily at 362 nm with a quantum yield of 1.21 for Fe^{2+} formation. A 6.00×10^{-3} M solution of $K_3[Fe(C_2O_4)_3]$ was prepared in 0.1 N aqueous H_2SO_4. A sample (3.0 mL) of this solution was then irradiated for 5 counts in a 1 cm cuvette. Under these conditions, greater than 99% of the light is absorbed by the $K_3[Fe(C_2O_4)_3]$. An aliquot (1.0 mL) of this solution was mixed with a 1,10-phenanthroline solution (1.0 mL) (0.1% by weight) and a buffer solution (0:50 M) (prepared from 600 mL 1 N NaO_2CCH_3 and 360 mL H_2SO_4 diluted to 1 L). This solution was diluted to 25.0 mL and allowed to stand for one hour. During this time an iron(II) complex of 1,10-phenanthroline, $[Fe(phen)_3]^{2+}$, is formed.

The optical density at 510 nm is then used to determine the number of moles of $K_3[Fe(C_2O_4)_3]$ decomposed. The experiment was repeated using 0, 10, 15, and 20 counts and the observed absorbance values are given in Table 8.1.

A plot of absorbance of the final solution vs counts of irradiation gave a slope of 0.0220 (correlation coefficient .9996).

The light output is then calculated by converting to moles iron(II) complex formed per count irradiation then dividing by the quantum yield to give light output in units of Einsteins per mole. In this case, the slope (.0220) is multiplied by a correction factor to take into account

TABLE 8.1

Actinometry Results

Exposure Counts	Abs at 510	$Abs_c - Abs_{blank}$
0	.003	0
5	.1039	.1009
10	.2266	.2236
15	.3307	.3277
20	.4400	.4370

dilution (0.075) and divided by the molar extinction coefficient of the iron(II) complex (1.11×10^4 L mol^{-1} cm^{-1}) and by the actual quantum yield (1.21) to give a light output of 1.23×10^{-7} E $count^{-1}$.

8.2 Experimental for Chapter 2

The complex $[Pt_2H_2(\mu\text{-}H)(\mu\text{-}dppm)_2][PF_6]$ was prepared by the literature method.[25]

8.2.1 Preparation of $[Pt_2D_2(\mu\text{-}D)(\mu\text{-}dppm)_2][PF_6]$

This was prepared by a modification of the method used for $[Pt_2H_2(\mu\text{-}H)(\mu\text{-}dppm)_2][PF_6]$. Solid $Na[BD_4]$(0.5g) was added slowly (2h) in small portions (0.01 g) to a stirred suspension of $[PtCl_2(dppm)]$(1.0g) in MeOD (20 mL) in a flask flushed with N_2, and the resulting mixture was stirred for 1 h. The mixture was filtered, the solid was extracted with CH_2Cl_2 (10 mL) and the filtered solution was added to a solution of $NH_4[PF_6]$(0.36 g) in CH_3OD (20 mL). The volume was reduced to 15 mL using a rotary evaporator and the white crystals of $[Pt_2D_2(\mu\text{-}D)(\mu\text{-}dppm)_2][PF_6]$ which formed were filtered, washed with n-pentane, and dried under vacuum. IR(nujol): ν(PtD) 1537 cm^{-1}; ν(PtH) absent; c.f. for (Ia), ν(PtH) 2100 cm^{-1}.

UV-visible spectrum of $[Pt_2H_2(\mu\text{-}H)(\mu\text{-}dppm)_2][PF_6]$: λmax 348 nm, ε 4.90×10^3 l mol^{-1} cm^{-1} (pyridine solution); λmax 349 nm, ε 4.09×10^3 l mol^{-1} cm^{-1} (MeCN solution). NMR data for (Ia) in CD_3CN: δ(PtH)-6.9 ppm, ^1J(PtH) 1152 Hz, ^2J(PtH) 112 Hz; $\delta(Pt_2\mu\text{-}H)$-5.85 ppm, ^1J(PtH) 546 Hz; $\delta(^{31}P)$ 17.9 ppm, ^1J(PtP) 2755 Hz, ^2J(PtP) 6 Hz, ^2J(PP) 64 Hz, ^3J(PP) 17 Hz. NMR data for $[Pt_2H_2(\mu\text{-}H)(\mu\text{-}dppm)_2][PF_6]$ in C_5D_5N(0°C): δ(PtH)-6.7 ppm, ^1J(PtH) 1146 Hz; $\delta(Pt_2\mu\text{-}H)$ 5.9 ppm, ^1J(PtH) 545 Hz; $\delta(^{31}P)$ 17.3 ppm, ^1J(PtP) 2760 Hz, ^2J(PtP) 20 Hz,

$^2J(PtP)$ 20 Hz, $^2J(PP)$ 59 Hz, $^3J(PP)$ 19 Hz.

8.2.2 Preparation of New Complexes, $[Pt_2HL(\mu\text{-dppm})_2]^+$

Complex $[Pt_2H_2(\mu\text{-H})(\mu\text{-dppm})_2][PF_6]$ (.10 g, 7.65×10^{-5} moles) was dissolved in CH_2Cl_2 (3 mL). The ligand (7.65×10^{-5} mole) was dissolved in CH_2Cl_2 (2 mL) and added dropwise to the platinum containing solution. Solutions turned yellow and gas was produced. After reaction was complete [20 min., L = $PPh_2(4\text{-}MeC_6H_4)$; 1h., L = $P(4\text{-}ClC_6H_4)_3$; 72 h., L = $PPh_2(2\text{-}MeC_6H_4)$], the product was precipitated by addition of n-pentane. The solid samples were then dried under high vacuum. Anal. Calcd. for $[Pt_2H\{PPh_2(4\text{-}MeC_6H_4)\}dppm)_2][PF_6]$: C, 52.4; H, 3.9. Found: C, 52.3; H, 4.0. Calcd. for $[Pt_2H\{PPh_2(2\text{-}MeC_6H_4)\}(dppm)_2][PF_6]$: C, 48.9; H, 3.6. Found: C, 48.9; H, 3.6.

8.2.3 Studies of Reaction Rates

The solvent in these studies, CH_2ClCH_2Cl, was purified by distillation from K_2CO_3. It is essential that the solvent be dry and acid-free.

In a typical reaction $[Pt_2H_3(dppm)_2][PF_6]$ (.0097 g) was dissolved in CH_2ClCH_2Cl (.1L) and $PPh_2(4\text{-}MeC_6H_4)$ (.0500 g) was dissolved in CH_2ClCH_2Cl (25 mL). 2.0 mL of the platinum containing solution was added to a clean dry 5.0 mL volumetric flask. 0.25 ml phosphine solution was added to this and then CH_2ClCH_2Cl was added to a final volume of 5.0 ml. This was taken as time zero. The flask was shaken vigorously for ~40 sec. then 2.5 mls of the solution was transferred to a quartz optical cell and put in the thermostatted (25°C) compartment of a Cary 119 spectrophotometer.

The optical density of the region from 320 → 400 nm was recorded as

a function of time. A plot of $\ln(A_\infty - A_t)$ vs. t was made and found to be linear giving a first order rate constant of 2.39×10^{-4} s^{-1}.

The volume of ligand solution added was varied to allow determination of first order rate constants as a function of [L]. For the series [L] = (3.623×10^{-4}, 7.246×10^{-4}, 10.87×10^{-4}, 14.49×10^{-4}, 21.24×10^{-4} and 23.7×10^{-4} the following first order rate constants were observed. $k = 3.2 \times 10^{-4}$, 7.5×10^{-4}, 11.4×10^{-4}, 11.6×10^{-4}, 19.4×10^{-4} and 21.2×10^{-4} s^{-1} respectively. A plot of k vs. [L] was found to be linear giving rise to the second order rate constant 0.89 ℓ mol^{-1} s^{-1}.

The above procedure was repeated at 25°C for L = PPh_3. Again the reaction was first order in both complex $[Pt_2(\mu\text{-}H)H_2(\mu\text{-dppm})_2]^+$ and L giving a second order rate constant of 1.6 ℓ mol^{-1} s^{-1}. This was repeated with $[Pt_2(\mu\text{-}D)D_2(dppm)_2]^+$ and a rate constant of .455 ℓ mol^{-1} s^{-1} was found.

Single experiments were conducted at T = 35, 44, 53, and 60°C and the rate law assumed to be second order giving k = 2.9, 5.89, 9.86 and 12.73 ℓ mol^{-1} s^{-1} respectively.

8.2.4 Equilibrium Constant Determination by UV-visible Spectroscopy

In a typical experiment complex $[Pt_2(\mu\text{-}H)H_2(\mu\text{-dppm})_2]^+$ (0.0774 g) was dissolved in CH_2ClCH_2Cl (50 mL). 2.5 mL of this solution was transferred to a UV cell and cooled to ~-70°C. A solid sample of $PPh_2(4\text{-}MeC_6H_4)$ (0.0158 g) was then added to this and the spectrum between 400 and 600 nm was recorded on the warmed (-11°C) sample. This procedure was repeated using different weights of ligand. Cooling was achieved by circulating a cooled ethylene glycol-water mixture through the cell compartment. The absorbance at 420 nm was then used in order

to calculate the equilibrium constant.

This procedure was repeated at -11°C for two different concentrations of $[Pt_2(\mu\text{-}H)H_2(\mu\text{-}dppm)_2]^+$ with L = PPh_3, and was also performed at -6°C and -14°C for L = $P(4\text{-}ClC_6H_4)_3$. An attempt was made to determine the equilibrium constant for L = dppm at -11°C by this method, but this was unsuccessful due to reaction to give $[Pt_2H(dppm)(\mu\text{-}dppm)_2]^+$.

The extinction coefficients of $[Pt_2H_3L(\mu\text{-}dppm)_2]^+$ and the K_{eq} values were then solved from the following relationship:

$A = \varepsilon_I[Pt_2H_3(dppm)_2]^+ + \varepsilon_{III}[Pt_2H_3L(\mu\text{-}dppm)_2]^+ + \varepsilon_L[L]$ where

$K = [Pt_2H_3L(\mu\text{-}dppm)_2]^+/[Pt_2H_3(dppm)_2]^+[L]$ and $[Pt_2H_3(dppm)_2]^+{}^\circ$ and $[L]^\circ$ are known.

A best fit to the observed graph of Absorbance vs. $[L]^\circ/[Pt_2H_3(dppm)_2]^+{}^\circ$ was found using a standard computer program.[65]

8.2.5 Equilibrium Constant Determination by NMR Spectroscopy

In an NMR tube, complex $[Pt_2H_3(dppm)_2]^+$ (0.1189 g) was dissolved in CD_2Cl_2 (0.5 mL) and a small amount of TMS was added. The spectrum was obtained at -20°C for the region δ1 to -10 ppm. The sample was then removed from the probe and cooled to -78°C. Solid $PPh_2(2\text{-}MeC_6H_4)$ (.0119 g) was added to this sample. The sample was then shaken for 30 s, returned to the probe at -20°C and allowed to equilibrate and the NMR spectrum was recorded. The sample was removed, cooled to -78°C an additional amount of ligand (.0108 g) was added, and the NMR spectrum was recorded. This was repeated several more times. The shift of the $Pt_2(\mu\text{-}H)$ proton was then used to calculate K from a non-linear regressive fit of the observed shift vs. $[L]^\circ/[Pt_2H_3(dppm)_2]^+{}^\circ$ curve.[65] The value thus obtained was 3.2 $\ell\ mol^{-1}$. This procedure was repeated at 0°C to

to give K = 1.9 ℓ mol^{-1}. In the case of $[Pt_2H(\mu\text{-}H)Me(\mu\text{-}dppm)_2]^+$ with PPh_3 a slightly different procedure was used.

Triphenylphosphine (0.077 mmol) was added to a solution of $[Pt_2H(\mu\text{-}H)Me(\mu\text{-}dppm)_2][SbF_6]$ (0.077 mmol) in CD_2Cl_2 (0.50 mL) in an NMR tube cooled to -78°C. After dissolution of the PPh_3 at -78°C, the tube was added to the probe (precooled to -90°C) of a Varian XL100 NMR spectrometer. The ^1H NMR spectrum was recorded and further spectra were recorded at higher temperatures, until reaction to give H_2 and methyldiplatinum(I) complex was significant. The variable temperature $^{31}P\{^1H\}$ NMR spectra were obtained in a similar way but using a Varian XL200 NMR spectrometer.

A similar experiment was carried out using PPh_3 (1.5×10^{-4} mol) and $[Pt_2(\mu\text{-}H)Me_2(\mu\text{-}dppm)_2][PF_6]$ (0.66×10^{-4} mol) in CD_2Cl_2 (1.3 mL). ^1H and $^{31}P\{^1H\}$ NMR spectra from -90°C - 0°C showed only signals due to the reagents, with no evidence for complex formation.

8.2.6 Kinetics of dissociation of PPh_3 from complex $[Pt_2H_3(PPh_3)(\mu\text{-}dppm)_2]^+$

A sample of complex $[Pt_2H_3(\mu\text{-}dppm)_2]^+$ in CD_2Cl_2 (0.18 M) in an NMR tube was cooled to -90°C in the probe of the NMR spectrometer, and the spectrum was recorded. PPh_3 was added as a solid to give a 0.20 M solution. The cold tube was shaken to give a homogeneous solution, being careful to keep it cold, and was returned to the NMR probe at -90°C. The spectrum was recorded and further spectra were obtained at 10°C intervals as the probe was slowly warmed. Lifetimes were calculated from the spectra at each temperature. A similar experiment was carried out using ^{31}P NMR spectroscopy.

8.3 Experimental for Chapter 3

8.3.1 Preparation of $[Pt_2H(py)(\mu\text{-dppm})_2][PF_6]$

A solution of $[Pt_2H_2(\mu\text{-H})(\mu\text{-dppm})_2][PF_6]$ (0.2 g) in pyridine (2 mL) contained in a Pyrex tube (10 mL) was deoxygenated by bubbling pure N_2 for 45 min. The sample was photolysed, using a 150 W xenon lamp placed 25 cm from the sample, for 40 min. at 0°C. Water and Corning 0-52 filters were used to remove IR and wavelengths shorter than 360 nm respectively. The yellow solution obtained was added to petroleum ether (b.p. 30-60°C, 5 mL), when the product precipitated as a yellow oily solid. The solvents were decanted off and the product was dried under vacuum, giving a yellow solid. IR(nujol or pyridine solution): ν(PtH) 2000 cm^{-1}. NMR(C_5D_5N): δ(PtH)-7.66 ppm, ^1J(PtH) 938 Hz, ^2J(PtH) 66 Hz, ^2J(PH) 16 Hz, ^3J(PH) 5 Hz; $\delta(CH_2P_2)$ 5.4 (m) ppm; $\delta(^{31}P)$ 17.2 ppm, ^1J(PtP) 3480 Hz and 7.7 ppm, ^1J(PtP) 2890 Hz, $^2J(P^AP^B)$ 59 Hz, $^4J(P^AP^{B'})$ 31 Hz. Anal: Calc. for $C_{55}H_{50}F_6NP_5Pt_2$; C, 47.7; H, 3.6; N, 1.0. Found: C, 47.8; H, 3.6; N, 1.3%.

8.3.2 Preparation of $[Pt_2H(MeCN)(\mu\text{-dppm})_2][PF_6]$

A solution of $[Pt_2H_2(\mu\text{-H})(\mu\text{-dppm})_2][PF_6]$ (0.11 g) in MeCN (15 mL) contained in a Pyrex flask (25 mL capacity) was deoxygenated by 3 freeze-pump-thaw cycles. The irradiation was effected using a focussed beam from a 150 W xenon lamp 25 cm from the sample, filtered as in the previous experiment. When reaction was complete (~20 min. irradiation), the solution was cooled to 0°C and the solvent was removed under high vacuum, leaving the product as an orange solid in analytically pure form. IR(nujol): ν(PtH) 2030 cm^{-1}; MeCN solution,

ν(PtH) 2020 cm^{-1}, NMR(CD_3CN): δ(PtH)-9.0 ppm, ^1J(PtH) 963 Hz, ^2J(PtH) 76 Hz, ^2J(PH) 15 Hz, ^3J(PH) 5 Hz; $\delta(CH_2P_2)$ 4.5 ppm, $^2J(Pt^AH)$ 71 Hz, $^2J(Pt^BH)$ 52 Hz, J(PH) 9 Hz; $\delta(^{31}P)$ 15.6 ppm, ^1J(PtP) 3522 Hz and 6.4 ppm, ^1J(PtP) 2840 Hz. Anal. Calc. for $C_{52}H_{48}F_6NP_5Pt_2$: C, 46.4; H, 3.6; N, 1.0. Found: C, 46.3; H, 3.6; N, 1.1%.

8.3.3 Studies of hydrogen evolution

A solution of $[Pt_2H_2(\mu\text{-}H)(\mu\text{-}dppm)_2][PF_6]$ (0.065 g, 4.9×10^{-5} mol) in MeCN(25 mL) was deoxygenated by bubbling N_2 for 45 min. The reaction vessel was a flat-sided Pyrex flask, fitted with a side-arm with a 1 mm quartz cuvette attached to allow monitoring of the course of the reaction by UV-visible spectroscopy. The solution was irradiated using a 400 W mercury lamp placed 15 cm from the sample, and using H_2O and Corning 0-52 filters. The photolysis was monitored by UV-visible spectroscopy. The reaction was stopped before completion and, from the optical density change at 333 nm, it was calculated that 3.7×10^{-5} mol of $[Pt_2H_2(\mu\text{-}H)(\mu\text{-}dppm)_2]^+$ had reacted. A sample of the gas phase (1.0 mL) was taken through a septum using a gas syringe and the H_2 determined by GC (after a preliminary calibration was made). The total H_2 formed was $3.7 \pm 0.3 \times 10^{-5}$ mol.

For isotope analyses, a sample [0.05 g of $[Pt_2H_2(\mu\text{-}H)(\mu\text{-}dppm)_2][PF_6]$, $[Pt_2D_2(\mu\text{-}D)(\mu\text{-}dppm)_2][PF_6]$ or a mixture] was placed in a small reaction vessel (~10 mL) fitted with a stopcock, and the solvent CH_3CN (2 mL) was condensed into the vessel at 77 K under vacuum. The solution was warmed to room temperature and photolysed as above. The vessel was then attached to the gas inlet system of the mass spectrometer, the solution was cooled to 77 K and the gas phase was admitted to the mass

spectrometer.

8.3.4 Quantum Yield Determinations

Irradiations were carried out using the 362 nm band of the Jasco CRM-FA Spectroirradiator.

In a typical experiment, a solution of $[Pt_2H_2(\mu\text{-}H)(\mu\text{-}dppm)_2][PF_6]$ in MeCN (5 mL, 4.16×10^{-4} M) was degassed by 3 freeze-pump-thaw cycles, pumping each time to a residual pressure of 5×10^{-5} torr at 77 K. The solution was then flame-sealed in a 1 cm quartz cuvette. The reaction was monitored by the change in optical density of the solution at 333 nm, since the greatest changes were observed at this wavelength. As a result, the experiments were not carried out in the usual way since less than 90% of the incident light at 362 nm was absorbed (figure 3.1). After each irradiation the concentration of both $[Pt_2H_2(\mu\text{-}H)(\mu\text{-}dppm)_2]^+$ and $[Pt_2H(NCMe)(\mu\text{-}dppm)_2]^+$ were calculated from the absorbance at 333 nm. The average concentrations over the irradiation period and hence the % light absorbed by each species were then calculated. Linear plots of $[Pt_2H_2(\mu\text{-}H)(\mu\text{-}dppm)_2]^+$ vs quanta absorbed by $[Pt_2H_2(\mu\text{-}H)(\mu\text{-}dppm)_2]^+$ were obtained (correlation coefficients > 0.99), and the quantum yields were calculated from the slopes of these lines (figure 3.3). The quantum yields determined were .81($[Pt_2H_2(\mu\text{-}H)(\mu\text{-}dppm)_2]^+$ in MeCN), .45($[Pt_2D_2(\mu\text{-}D)(\mu\text{-}dppm)_2]^+$ in MeCN), .57($[Pt_2H_2(\mu\text{-}H)(\mu\text{-}dppm)_2]^+$ in pyridine), .35($Pt_2D_2(\mu\text{-}D)(\mu\text{-}dppm)_2]^+$ in pyridine).

8.3.5 Singlet Sensitization

In a typical experiment, a solution of $[Pt_2H_2(\mu\text{-}H)(\mu\text{-}dppm)_2]^+$ in MeCN (5 mL, 6.16×10^{-3} M) was added to triphenylene (0.0153 g). The IR spectrum of the resulting solution was recorded (NaCl plates, 1 mm

pathlength) from 2200-2000 cm^{-1}. The sample contained in the IR cell was then irradiated using light from a Model UVS-11 Mineralight Lamp (λ=254 nm) placed 5 cm from the sample. A 1 cm quartz cuvette containing aqueous KI(9.8×10^{-5} M)-I_2(3.1×10^{-5} M) was used as a filter. After 5 min. of irradiation, the IR spectrum (2200-2000 cm^{-1}) was recorded, and the above process was repeated 3 times. The extent of reaction was monitored from the changes in absorbance at 2098 cm^{-1}, corresponding to the maximum absorbance due to ν(PtH) of $[Pt_2H_2(\mu\text{-}H)(\mu\text{-}dppm)_2]^+$. From this a plot of moles per liter $[Pt_2H_2(\mu\text{-}H)(\mu\text{-}dppm)_2]^+$ was reacted vs irradiation time was made. The plot was linear (correlation coefficient .994) and the slope was 1.49×10^{-3} mol L^{-1} sec^{-1}. This was repeated three times to give an average value of $1.47 \pm .11 \times 10^{-3}$ mol L^{-1} sec^{-1}.

The experiment was also performed with no triphenylene present, and the average of four trials gave a value of $1.94 \pm .25 \times 10^{-3}$ mol L^{-1} sec^{-1}. This experiment was repeated using a pyrex filter between the light source and sample. A slope of $4.5 \pm .5 \times 10^{-5}$ mol L^{-1} sec^{-1} (average of two trials) was obtained.

The data without the pyrex filter is corrected for reaction occuring by non 254 nm light by subtracting the value ($4.5 \pm .5 \times 10^{-4}$ mol L^{-1} sec^{-1}) found with the pyrex filter present. The rate of the sensitized reaction was also corrected for reaction due to light absorbed directly. This led to a rate sensitized of 8.5×10^{-4} mol L^{-1} sec^{-1} and rate direct of 14.9×10^{-4} mol L^{-1} sec^{-1}.

The ratio, rate sensitized/rate direct is used according to equation (3.4) to give a value of k_q of $6(\pm 2) \times 10^9$ M^{-1} s^{-1}.

8.3.6 Triplet Sensitization

Michler's ketone (0.040 g) was added to a solution of $[Pt_2H_2(\mu\text{-}H)(\mu\text{-}dppm)_2]^+$ in MeCN (5 mL, 1.61×10^{-3} M). The solution was then irradiated and the reaction monitored as for the singlet sensitized reaction. No change in absorbance at 2098 cm^{-1} was detected on prolonged irradiation of the solution containing the ketone.

8.4 Experimental for Chapter 4

8.4.1 Preparation of $[Pt(CD_3)_2(dppm)]$

A solution of CD_3Li (24 mL, 1.7 M), freshly prepared from Li and CD_3I in ether, was added dropwise to a suspension of $[PtCl_2(dppm)]$ (1.52 g) in ether (30 mL) cooled to 0°C. The solution was allowed to warm to room temperature. After 1 h, the mixture was hydrolysed with cold saturated aqueous NH_4Cl solution (5 mL). The layers were separated, and the aqueous layer was further extracted with CH_2Cl_2. The organic extracts were dried over $MgSO_4$ and evaporated to yield the product (0.62 g).

8.4.2 Preparation of $[Pt_2(CD_3)_3(\mu\text{-}dppm)_2][PF_6]$

A mixture of $[Pt(CD_3)_2(dppm)]$ (0.19 g) and $[PtCl_2(dppm)]$ (0.066 g) in methanol (15 mL) was heated under reflux for 1 h. $[NH_4][PF_6]$ (0.12 g) was then added, heating was continued for 5 min., the solution was cooled and water was added dropwise to precipitate the product as a yellow solid. This was purified by precipitation from CH_2Cl_2 solution by slow addition of hexane. NMR(CD_2Cl_2): $\delta(P^A)$ 27.13, $^1J(Pt^AP^A)$ 1459 Hz and $\delta(P^B)$ 23.66, $^1J(Pt^BP^B)$ 3009Hz. The proton NMR spectrum showed no signals due to methylplatinum groups.

8.4.3 Preparation of $[Pt_2(\mu\text{-}D)(CD_3)_2(\mu\text{-}dppm)_2][PF_6]$

This was prepared by the literature method[31] for the synthesis of $[Pt_2(\mu\text{-}H)(CH_3)_2(\mu\text{-}dppm)_2][PF_6]$; but using $[Pt_2(CD_3)_3(\mu\text{-}dppm)_2][PF_6]$ (0.09 g), $NH_4[PF_6]$ (0.06 g) in CH_3OD (10 mL) with $Na[BD_4]$ (0.1 g) in CH_3OD (3 mL). The yield was 0.06 g (70%). NMR(CD_2Cl_2): δ(P) 13.5 ppm, ^1J(PtP) 2884 Hz; ^2J(PtP) 24 Hz, ^2J(PP) 51 Hz and ^3J(PP) 15 Hz.

8.4.4 Preparation of $[Pt_2Me(py)(\mu\text{-}dppm)_2][SbF_6]$

A solution of $[Pt_2H(\mu\text{-}H)Me(\mu\text{-}dppm)_2][SbF_6]$ (0.05 g) in dry pyridine (20 mL) was deoxygenated by passing nitrogen through the solution for 45 min. The reaction vessel was a flat-sided Pyrex flask, with a sidearm fitted with a 1 mm quartz cuvette to allow monitoring of the reaction by UV-visible absorption spectroscopy. The solution was irradiated for 2 h., using a medium pressure Hg lamp 12 cm from the sample and using a water filter, after which no further change in absorption spectrum occurred. A sample of the gas phase was analysed by GC, and showed hydrogen and a trace of methane to be present. The solvent was then removed under high vacuum to give the product as a yellow solid in quantitative yield. Anal. Calc. for $C_{56}H_{52}NF_6P_4Pt_2Sb$: C, 45.2; H, 3.5. Found: C, 44.7; H, 3.[illegible]%. NMR(CD_2Cl_2): $\delta(PtCH_3)$ 0.53 ppm, ^2J(PtH) 72.5 Hz, ^3J(PH) 11 Hz and $\delta(CH_2P_2)$ 5.29 ppm. $\delta(P^A)$ 8.4 ppm, $^1J(PtP^A)$ 2930 Hz and $\delta(P^B)$-4.7 ppm, $^1J(PtP^B)$ 2850 Hz, $^2J(P^AP^B)$ 37.5 Hz, $^3J(P^AP^{B'})$ 57.5 Hz.

This same product was formed by the similar photolysis of $[Pt_2(\mu\text{-}H)Me_2(\mu\text{-}dppm)_2][SbF_6]$ (0.03 g) in pyridine (5 mL), but in the case the only gaseous product was CH_4. The product was identified by the ^1H and $^{31}P\{^1H\}$ NMR spectra.

8.4.5 Preparation of $[Pt_2Me(Me_2CO)(\mu\text{-dppm})_2][PF_6]$

A solution of $[Pt_2Me_3(\mu\text{-dppm})_2][PF_6]$ (0.05 g, 3.9×10^{-5} mol) in dry acetone (5 mL), in an apparatus with a sidearm fitted with a 1 mm quartz cuvette, was degassed by several freeze-pump-thaw cycles and then photolysed using a 150 W xenon lamp with water and Corning 0-52 filters. The reaction was monitored by UV-visible spectroscopy, and when complete the gaseous phase was analysed by G.C. Ethane ($4.0 \pm 0.2 \times 10^{-5}$ mol) was the only gas formed.

The product was isolated as a yellow solid by evaporation of the solvent under high vacuum, and was identified by the ^1H NMR spectrum in $(CD_3)_2CO$. $\delta(PtCH_3)$ 0.29 ppm, $^2J(PtH)$ 70 Hz, $^3J(PH)$ 7.5 Hz.

The complex could be converted to $[Pt_2Me(C_5H_5N)(\mu\text{-dppm})_2][PF_6]$ by adding pyridine (.5 mL) to an NMR sample of $[Pt_2Me(Me_2CO)(\mu\text{-dppm})_2][PF_6]$.

$[Pt_2Me(Me_2CO)(\mu\text{-dppm})_2]^+$ as the SbF_6^- salt, was also prepared by similar photolysis of a degassed solution of $[Pt_2H(\mu\text{-H})Me(\mu\text{-dppm})_2][SbF_6]$ (0.10 g) in $(CD_3)_2CO$ (0.7 mL) and was identified as above. The acetone complex decomposed over a period of several hours to an unidentified product. NMR$(CD_3)_2CO$: $\delta(PtCH_3)$ 0.24 ppm, $^2J(PtH)$ 82 Hz, $^3J(PH)$ 7 Hz.

8.4.6 Preparation of $[Pt_2Me(CD_3CN)(\mu\text{-dppm})_2][SbF_6]$

This was obtained and identified by photolysis of $[Pt_2H(\mu\text{-H})Me(\mu\text{-dppm})_2][SbF_6]$ in CD_3CN as described above. This complex was stable in CD_3CN solution in the absence of oxygen, but decomposed on evaporation of the solvent. The same product was formed by similar photolysis of $[Pt_2(\mu\text{-H})Me_2(\mu\text{-dppm})_2][SbF_6]$ or, as the PF_6^- salt, by photolysis of $[Pt_2Me_3(\mu\text{-dppm})_2][PF_6]$. NMR$(CD_3CN)$: $\delta(PtCH_3)$ 0.80 ppm, $^2J(PtH)$ 60 Hz, $^3J(PH)$ 6.5 Hz.

8.4.7 Photolysis of $[Pt_2Me_3(\mu\text{-dppm})_2][PF_6]$ in CD_2Cl_2

$[Pt_2Me_3(\mu\text{-dppm})_2][PF_6]$ (.0843 g) was dissolved in CD_2Cl_2 (1 mL) in a 5 mm NMR tube. The solution was then degassed, flame sealed and then irradiated using a 150 W xenon lamp source filtered through Corning 0-52 and H_2O filters. Photolysis was continued for 30 min. The ^1H and $^{31}P\{^1H\}$ NMR spectra showed the product to be $[Pt_2Me_2(\mu\text{-Cl})(\mu\text{-dppm})_2][PF_6]$.[119]

The NMR tube was then opened and the gas product analysed by G.C. The gases C_2H_6, CH_4, and C_2H_4 were observed in a ratio of 1:0.08:0.02. NMR(CD_2Cl_2): $\delta(PtC\underline{H}_3)$ 0.51 ppm, $^3J(PH)$ 6.6 Hz, $^2J(PtH)$ 88 Hz and $\delta(C\underline{H}_2P_2)$ 4.09 ppm. $\delta(P)$ 11.5 ppm, $^1J(PtP)$ 3030 Hz, $^2J(PtP)$ 37 Hz, J(PP) 30 Hz.

8.4.8 Preparation of $[PtMe(C_5H_5N)(dppm)][NO_3]$

A solution of $AgNO_3$ (0.060 g) in methanol (12 mL) was added dropwise to a solution of [PtClMe(dppm)] (0.20 g) in CH_2Cl_2 (50 mL). The mixture was then filtered to remove AgCl and pyridine (0.5 mL) was added. After 10 min. the solvent was evaporated under vacuum to give the product. NMR(C_5D_5N): $\delta(P^A)$ -26.6 ppm, $^1J(PtP^A)$ 3388 Hz, $^2J(P^AP^B)$ 38 Hz, and $\delta(P^B)$ -42.3 ppm. $^1J(PtP^B)$ 1270 Hz, $^2J(P^AP^B)$ 38 Hz. $\delta(PtC\underline{H}_3)$ 1.02 ppm, $^3J(P^BH)$ 8 Hz, $^3J(P^AH)$ 3 Hz, $^2J(PtH)$ 61 Hz.

The assignments were confirmed by selective decoupling of P^A and observing loss of $^3J(P^AH)$ coupling.

When the photolysis of $[Pt_2Me_3(\mu\text{-dppm})_2][PF_6]$ was carried out in C_5D_5N with monitoring by ^1H and $^{31}P\{^1H\}$ NMR, an equimolar mixture of $[PtMe_2(dppm)]$, and $[PtMe(C_5D_5N)(dppm)]^+$ was formed. The parameters for the latter complex were identical with those of the sample prepared above.

8.4.9 Quantum Yield Determinations

Irradiations were performed using the 362 nm band of the Jasco CRM-FA Spectroirradiator.

In a typical experiment, a solution of $[Pt_2Me_3(\mu\text{-dppm})_2][PF_6]$ in CH_2Cl_2 (4.0 mL 4.45×10^{-4} M). The solution was then flame sealed in a 1 cm quartz cuvette. The reaction was monitored by following the change in optical density at 440 nm. The data were then analysed by calculating the concentration of $[Pt_2Me_3(\mu\text{-dppm})_2]^+$ after each irradiation. From this an average concentration over each irradiation interval, and hence the percent light absorbed, was calculated. Linear plots of $[Pt_2Me_3(\mu\text{-dppm})_2]^+$ concentration vs. quanta of light absorbed by $[Pt_2Me_3(\mu\text{-dppm})_2]^+$ were obtained (correlation coeff. > 0.99) (figure 4.4). The quantum yield was then calculated from the slope of this line.

The quantum yield measurement in benzene was complicated by precipitation of a white microcrystalline material after ~40% reaction at which state an isosbestic point at 360 nm was lost. The final absorption was estimated and the quantum yield calculated as 0.6. The error due to this estimation is difficult to assess. Quantum yield are given in Table 4.2.

8.4.10 Proof of intramolecular reaction

A mixture of $[Pt_2(\mu\text{-D})(CD_3)_2(\mu\text{-dppm})_2][PF_6]$ (0.025 g) and $[Pt_2(\mu\text{-H})(CH_3)_2(\mu\text{-dppm})_2][PF_6]$ (0.025 g) in pyridine (5 mL) was degassed and photolysed to partial conversion. The gaseous products were analysed using a Varian MAT 311A mass spectrometer. For comparison, photolysis of the pure labelled materials were also carried out and the gases analysed in the same way. The above system gave $CD_4:CD_3H:CH_3D:CH_4$ = 1:0.04:0.02:1.6.

Experiments using $[Pt_2(CD_3)_3(\mu\text{-dppm})_2][PF_6]$ and $[Pt_2(CH_3)_3(\mu\text{-dppm})_2][PF_6]$ were carried out in a similar way.

8.5 Experiment for Chapter 5

Samples of $[Pt_2(CH_2CH_3)(dppm)_3][PF_6]$ and $[Pt_2(CH_2CD_3)(dppm)_3][PF_6]$ were obtained from Dr. M.P. Brown,[34] and $[Pt_2(CH_2CH_3)_3(dppm)_2][PF_6]$ was prepared by Dr. K.A. Azam.[121]

8.5.1 Photolysis of $[Pt_2Et_3(\mu\text{-dppm})_2]^+$

A sample of $[Pt_2Et_3(\mu\text{-dppm})_2][PF_6]$ (.05 g) was dissolved in CD_2Cl_2 (1 g) in a 5 mm NMR tube. This sample was then irradiated with the filtered output from a medium pressure Hg lamp. The sample was placed 12 cm from the lamp and both a water and $\lambda > 420$ nm filter were interposed between the lamp and sample. Following 10 min. of irradiation, a sample of the gas above the liquid was analysed by G.C. (poropak Q column) and found to contain 75%±10% C_2H_4 and 25%±10% C_2H_6. The ^{31}P NMR spectrum of the solution was obtained and found to contain peaks due to the starting material (≈55%), $[Pt_2(\mu\text{-H})Et_2(\mu\text{-dppm})_2]^+$ (≈44%) and an unidentified compound (≈1%).

The gas was then removed by a stream of N_2 and the procedure was repeated, this time photolyzing the solution for 1 h. The results obtained for gas analysis were now 50% C_2H_4 and 50% C_2H_6. The ^{31}P NMR spectrum indicated that no starting material remained and the products were $[Pt_2(\mu\text{-H})Et_2(\mu\text{-dppm})_2]^+$ (≈55%) and the unidentified compound (45%).

The experiment was repeated under degassed conditions to yield, after 40 min irradiation, 25% $[Pt_2Et_3(\mu\text{-dppm})_2]^+$, 64% $[Pt_2(\mu\text{-H})Et_2(\mu\text{-dppm})_2]^+$ and 11.0% of the new complex. The gas analysis indicated

C_2H_4 (75%) and C_2H_6 (25%).

The ^{31}P NMR spectra of both $[Pt_2Et_3(\mu\text{-dppm})_2]^+$ and $[Pt_2(\mu\text{-H})Et_2(\mu\text{-dppm})_2]^+$ have been reported previously.[121] The unknown complex had the following NMR parameters: $\delta(^{31}P)$ = 11.8 ppm, $^1J(PtP)$ = 3320 Hz.

8.5.2 Thermolysis of Degassed Solutions of $[Pt_2Et(dppm)_3]$

A sample of $[Pt_2Et(dppm)_3][PF_6]$ (.0071 g) was dissolved in acetonitrile (5.0 mL), degassed and flame sealed into a quartz faced cuvette. The visible absorption spectrum was recorded. The sample was then placed in a steam bath at 100°C. Periodically the sample was removed, cooled to room temperature, and the absorption spectrum recorded. In the early stages (approximately one half-life), an isosbestic point was evident at 442 nm (figure 5.1). First order analysis of the data, figure 5.2, indicated a rate constant of $2.2\pm.3 \times 10^{-5}$ s^{-1} for decomposition of $[Pt_2Et(dppm)_3]^+$.

Identical experiments were conducted with $[Pt_2(CH_2CD_3)(dppm)_3][PF_6]$. In the case of $[Pt_2(CH_2CD_3)(dppm)_3][PF_6]$, additional experiments were carried out in the presence of dppm and $[Pt_2D(dppm)_3][PF_6]$. When these additives were used they were mixed with $[Pt_2(CH_2CD_3)(dppm)_3]$ prior to dissolution. The obtained first order rate constants are given in Table 5.1.

Thermolysis was also conducted and monitored by NMR spectroscopy. In this case a sample of $[Pt_2(CH_2CD_3)(dppm)_3][PF_6]$ (0.0813 g) in d^3-acetonitrile (0.8 mL) was degassed and flame sealed in a 5 mm NMR tube. The sample was then heated to 100°C in a steam bath. The ^1H NMR spectrum was run periodically and the loss of intensity of the resonance due to

the ~~Pt~~-CH_2 protons was observed (δ = .53 ppm, $^2J(PtH)$ = 58 Hz, $^3J(PP)$ = 7.5 Hz). Throughout the reaction, no resonance due to the methyl group ($PtCH_2\underline{CH}_3$) (δ = 1.97 ppm) was observed.

At completion of the reaction, the ^{31}P NMR spectrum was obtained and found to contain resonances due to an unknown species which gave an $[A_2B_2]$ multiplet, with ^{195}Pt satellites. The product had the following spectral parameters; $\delta(P^A)$ = 2 ppm, $^1J(PtP^A)$ = 3120 Hz; $\delta(P^A)$ = 5.5 ppm, $^1J(PtP^B)$ = 3050 Hz.

The tube was then opened and the gas phase was analysed by G.C. and found to contain ethylene and ethane in a 2 to 1 ratio.

Thermolysis of an identically prepared sample of $[Pt_2H(dppm)_3][PF_6]$ gave rise to identical platinum-containing products as determined by the $^{31}P\{^1H\}$ NMR spectrum. However no gas was produced.

8.5.3 Thermolysis of Non-degassed Solutions of $[Pt_2Et(dppm)_3][PF_6]$

A sample of $[Pt_2Et(dppm)_3][PF_6]$ (.0241 g) was dissolved in DMSO (25 mL) [purified by recrystallization]. This solution was kept at a constant temperature of 78°C by placing it in a cold finger above refluxing ethanol. Aliquots were withdrawn at different times and the visible absorption spectra were obtained. Initially an isosbestic point was present at λ = 432 nm, however this was lost after about 2 half lives. The rate constant for the reaction was found, by a first order analysis, to be $2.7\pm.2 \times 10^{-4}$ s^{-1}.

Similar experiments were conducted at 64°C, using a methanol reflux, in both acetonitrile and DMSO solvents. The first order rate constants are given in Table 5.1. Following reaction the solutions were evaporated and an infrared spectrum was obtained on the residue. No

absorption due to a platinum hydride was observed in the region of 2000 cm^{-1}.

8.5.4 Photolysis of $[Pt_2Et(dppm)(\mu\text{-}dppm)_2]^+$

A sample of $[Pt_2Et(dppm)_3][PF_6]$ (.097 g) in acetone (10 mL) was degassed and flame sealed into a pyrex vessel with a 1 mm pathlength quartz optical cell attached.

The sample was irradiated with a 150 W xenon lamp placed 25 cm from the sample. The output of the lamp was filtered by placing a filter (Corning 3-73, pass $\lambda > 410$ nm) between lamp and sample. The sample was removed periodically and the visible absorption spectrum was obtained. After five hours, no further change in the absorption was observed. The sample was then opened and the solvent was removed under vacuum. The product (.08 g) was then dissolved in CH_2Cl_2 and the I.R. spectrum was obtained. An absorption at $\nu(PtH) = 2010$ cm^{-1} was identified as due to $[Pt_2H(dppm)_3]^+$ by comparison with the I.R. spectrum of an authentic sample of $[Pt_2H(dppm)_3]^+$. By measuring the intensity of the absorption at 2010 cm^{-1}, the product mixture was found to contain 25% by weight $[Pt_2H(dppm)_3][PF_6]$.

The experiment was then repeated with a new filter, such that only $\lambda > 510$ nm was passed to the sample (Corning 3-70). In this case the final product was found to contain 65% $[Pt_2H(dppm)_3][PF_6]$ by weight.

In a similar experiment, a sample of $[Pt_2Et(dppm)_3][PF_6]$ (.019 g) in acetone (2 mL) was degassed and photolyzed (using the Corning 3-70 filter). The reaction was monitored by observing changes in the visible absorption spectrum. At 66% reaction, the reaction was stopped. The gas was analyzed and found to contain 0.82 moles of ethylene and 0.22 moles

of ethane per mole $[Pt_2Et(dppm)_3][PF_6]$ decomposed; a ratio of ethane to ethylene of .3. This experiment was repeated with a mixture of $[Pt_2Et(dppm)_3][PF_6]$ (.011 g) and $[Pt_2H(dppm)_3][PF_6]$ (.010 g). The ratio of ethane to ethylene produced was found to be 0.50. A sample of $[Pt_2CH_2CD_3(dppm)_3][PF_6]$ was degassed and flame sealed in a 5 mm NMR tube. The sample was irradiated as above and the ^1H NMR spectrum was obtained periodically. The signal due to the Pt-CH_2 group was observed to decrease. During the course of the reaction no signal due to $PtCH_2CH_3$ was observed.

8.5.5 Quantum Yield Determinations

The quantum yields for decomposition of $[Pt_2CH_2CH_3(dppm)_3]^+$ and $[Pt_2CH_2CD_3(dppm)_3]$ in acetonitrile were determined.

In a typical experiment $[Pt_2CH_2CH_3(dppm)_3][PF_6]$ (.0207 g) was dissolved in acetonitrile (10.0 mL). A portion of this solution (4.0 mL) was then degassed and flame sealed into a 1.0 cm path length quartz cuvette.

The sample was then irradiated with the Jasco CRM-FA spectro-irradiator. The intensity of the band used (500±4 nm) had been calibrated relative to the 362 nm band using a thermopile. The light flux of the 362 nm band had been calibrated using the chemical actinometer potassium ferrioxalate as described in section 8.1. The extent of reaction and hence the concentration of $[Pt_2(CH_2CH_3)(dppm)_3]^+$ was monitored by measuring the optical density at 466 nm.

The light absorbed was then calculated as described in Chapter 3. Plots of moles $[Pt_2(CH_2CH_3)(dppm)_3]^+$ decomposed vs moles light absorbed were linear, giving a slope equal to the quantum yield $5.3\pm.5 \times 10^{-4}$. The quantum yield for decomposition of $[Pt_2(CH_2CD_3)(dppm)_3]^+$ under

identical conditions was found to be $5.2\pm.5 \times 10^{-4}$. The difference is not significant as illustrated by a plot of moles $[Pt_2(CH_2CH_3)(dppm)_3]^+$ and moles $[Pt_2(CH_2CD_3)(dppm)_3]^+$ against light absorbed shown in Figure 5.4.

The quantum yield for decomposition of $[Pt_2(CH_2CH_3)(dppm)_3]^+$ in 0.066 molar dppm was found to be $5.5\pm.5 \times 10^{-4}$.

In a similar manner, quantum yields for decomposition of $[Pt_2(CH_2CH_3)(dppm)_3]^+$ and $[Pt_2(CH_2CD_3)(dppm)_3]^+$ were measured using 473±4 nm light and found to be $6.4\pm.5 \times 10^{-3}$ and $6.6\pm.5 \times 10^{-3}$ respectively.

8.6 Experimental for Chapter 6

$[PtMe_2(phen)]$ was obtained by a previously published procedure[187] and identified by its ^1H NMR spectrum. NMR(CD_2Cl_2): $\delta(PtC\underline{H}_3)$ 1.14 ppm, $^2J(PtH)$ 86 Hz, δ(phen H) 7.52-9.28 ppm.

$Hg(^iPr)_2$ was obtained by a known procedure and identified by its ^1H NMR spectrum.[151] NMR(C_6D_6): $\delta(C\underline{H}(CH_3)_2)$ -0.75 ppm and $\delta(CH(C\underline{H}_3)_2)$ -0.5 ppm, $^3J(HgH)$ 120 Hz, $^3J(HH)$ 7 Hz (shifts relative to ext. TMS).

Spectroscopic grade acetone and "gold label" acetonitrile were used without further purification.

8.6.1 Preparation of $[PtIMe_2{}^iPr(phen)]$

A solution of $[Pt\ Me_2(phen)]$ (5×10^{-3} mol L^{-1}) and isopropyl iodide (5.2×10^{-3} mol L^{-3}) was degassed in acetone. The sample was irradiated with the light output from a medium pressure mercury lamp, filtered through both H_2O and a C-370 filter. The sample was placed

15 cm from the light source. The reaction was monitored by following the decrease in optical density at 473 nm. At the end of the reaction (≈5 min), the vessel was opened and the solvent was evaporated using a rotary evaporator. The ^{1}H NMR spectrum was then obtained on the product and found to be identical with the spectrum of an authentic sample.[188]

NMR(CD_2Cl_2): $\delta(PtC\underline{H}_3)$ 1.58 ppm, $^2J(PtH)$ 72 Hz; $\delta(C\underline{H}Me_2)$ 1.81 ppm, $^3J(HH)$ 6.5 Hz and $\delta(CH(C\underline{H}_3)_2)$ .16 ppm, $^3J(HH)$ 6.5 Hz, $^3J(PtH)$ 65 Hz.

A similar experiment was carried out in which p-methoxyphenol (2.4×10^{-2} mol L^{-1}) was added prior to degassing the solution. In this case, the output from the Hg lamp used previously was insufficient to induce reaction and hence a 150 W high pressure xenon lamp was used. Again, the output was filtered through H_2O and a Corning 0-52 filter. The product mixture, as identified by the ^{1}H NMR spectrum, consisted of an approximately 1:1 mixture of [$PtIMe_2{}^iPr$(phen)] and [PtI_2Me_2(phen)], identified by its ^{1}H NMR spectrum.[188]

NMR(CD_2Cl_2): $\delta(PtC\underline{H}_3)$ 2.53 ppm, $^2J(PtH)$ 74 Hz and δ(phen) 8.0-9.25 ppm.

8.6.2 ESR Spectra

A degassed solution of [$PtMe_2$(phen)] and isopropyl iodide in benzene was irradiated in the cavity of the ESR spectrometer; no signal was observed. The experiment was repeated with DMPO (.1 mL) added and an intense ESR signal was observed. When irradiation was halted, the signal decayed slowly and reappeared on further irradiation (g 2.0063, peak width = 1.6 g, hyperfine splitting: a_β^H = 21.8 g, a_N = 14.3 g). An identical signal was obtained upon warming a solution of $Hg(^iPr)_2$ and DMPO in benzene.

8.6.3 Quantum Yield Determinations

The 473 nm band of the Jasco CRM-FA spectroirradiator was used, calibrated as described in section 8.5.5.

In a typical experiment stock solutions of [$PtMe_2$(phen)] and isopropyl iodide in acetone were prepared. Aliquots of these were mixed and 5.0 mL of the resultant solution (concentration of [$PtMe_2$(phen)] = 6.6×10^{-4} M; concentration of isopropyl iodide = 5.83×10^{-3} M) degassed. A plot of moles [$PtMe_2$(phen)] reacted vs light absorbed was made. This was found to be linear (figure 6.3), and the quantum yield was obtained from the slope.

This experiment was repeated with a variety of isopropyl iodide concentrations and the quantum yields are reported in Table 6.2.

Quantum yields were also determined in the presence of the free radical scavengers, benzoquinone and 4-methoxyphenol. In a typical experiment a solution (4.0 mL) containing [$PtMe_2$(phen)] (6.54×10^{-4} mol L^{-1}), isopropyl iodide (6.2×10^{-3} mol L^{-1}) and benzoquinone (2.2×10^{-4} mol L^{-1}) was degassed and flame sealed into a quartz cuvette. The solution was then irradiated, and the extent of reaction was determined by monitoring the optical density at 473 nm. A plot of moles [$PtMe_2$(phen)] reacted vs Einsteins light absorbed was then constructed (figure 6.6). The quantum yield was calculated from the initial slope of this line and found to be 6.6×10^{-4}. The quantum yields are reported in Table 6.3 for a variety of concentrations of both benzoquinone and 4-methoxyphenol.

Triplet quenching experiments were also undertaken using the known triplet quencher pyrene.[101] In a typical experiment a solution (5 mL) of [$PtMe_2$(phen)] (1.37×10^{-4} mol L^{-1}), isopropyl iodide

(1.30×10^{-3} mol L^{-1}) and pyrene (8.0×10^{-2} mol L^{-1}) was degassed and flame sealed in a quartz cuvette. The solution was then irradiated at 473 nm and the extent of reaction was determined by the optical density at 473 nm. For this experiment, the light source was not calibrated and hence plots of moles [$PtMe_2$(phen)] reached vs. counts irradiation was made. A blank experiment was done, with no pyrene present, and analyzed in the same manner. The slope of the plot for the blank experiment divided by the slope in the presence of pyrene gave rise to a ratio, $\Phi/\Phi(Q)$ of 7.2. This experiment was repeated with different pyrene concentrations of 0.159 mol L^{-1} and 0.239 mol L^{-1} to yield ratios $\Phi/\Phi(Q)$ of 11 and 20, respectively.

The reaction was also triplet sensitized using benzophenone.[101] In this experiment, a solution of [$PtMe_2$(phen)] (1.37×10^{-4} mol L^{-1}), isopropyl iodide (1.30×10^{-3} mol L^{-1}) and benzophenone (0.02 mol L^{-1}) was degassed and flame sealed. The irradiation was then carried out using the 362 nm band of the light source. The observed quantum yield, calculated in the usual way was found to be 0.68. The quantum yield was then measured under identical conditions in the absence of benzophenone and found to be 2.6. Under the concentration conditions used, 20% of the light was absorbed directly by [$PtMe_2$(phen)]. Hence, correcting for this, the quantum yield for reaction from the sensitized triplet state is 0.15.

8.7 Experimental for Chapter 7

8.7.1 Catalysis of the Water Gas Shift Reaction

In a typical reaction [$Pt_2(\mu\text{-}H)H_2(dppm)_2$][$PF_6$] (.1515 g) was introduced into a Parr pressure reactor (300 mL) with MeOH (50 mL) and

distilled H_2O (25 mL). The vessel was then flushed with N_2 for 30 min. and charged with CO to a pressure of 125 p.s.i. The mixture was then heated to 100°C±1°C (after a stabilization period of 15 min.). Aliquots of gas were removed through a gas sampling system connected directly to a gas injector on the gas chromatograph. The gas was then analyzed for H_2 (using a 6' Molecular Sieve 5A column) or CO_2 (using a 6' Porapak Q column) and peak heights compared with standard curves, and CO_2 was corrected for its solubility in the mixture.[189]

Plots of moles CO_2 (or H_2) produced vs. time were linear. The slope of this plot divided by the number of moles $[Pt_2(\mu\text{-}H)H_2(dppm)_2][PF_6]$ gives the turnover rate. The data is presented in Table 7.1.

8.7.2 Preparation of the Red Cluster $[Pt_4(\mu\text{-}CO)_2(\mu\text{-}dppm)_3(\eta'\text{-}Ph_2PCH_2POPh_2)]$

$[Pt_2(\mu\text{-}H)H_2(dppm)_2][BPh_4]$ (.2067 g), H_2O (10 mL) and MeOH (50 mL) were introduced into the autoclave. Dinitrogen was bubbled through the solution for 1/2 hour. A pressure of CO (150 p.s.i.) was then introduced into the vessel and it was heated to 100°C for 30 hrs. The pressure was then released and the solution allowed to evaporate for 60 h. The solvent was then decanted leaving red crystals. m.p. 220-230 dec. Anal. calcd. for $C_{102}H_{88}O_3P_8Pt_4$: C, 52.3; H, 3.76. Found: C, 46.82; H, 3.58.

8.7.3 Preparation of the Yellow Clusters

$[Pt_2(\mu\text{-}H)H_2(dppm)_2][PF_6]$ (.2050 grams) was introduced into the autoclave with H_2O (10 mL) and methanol (50 mL). The reactor was then purged with N_2 for 30 min. and charged with CO (160 p.s.i.). The reactor was then heated to 100°C for 32 hours. The pressure was then released from the reactor and the red-yellow solution filtered into a

round bottom flask. N_2 was bubbled through this solution for 14 hours. The liquid layer was then decanted leaving yellow needles which were dried under high vacuum. Yield: 0.185 g, m.p. 234°C dec with evolution of a gas. Anal. calcd. for $C_{108}H_{88}O_4P_8Pt_4$: C, 51.4; H, 3.62. Found: C, 46.82; H, 3.58.

8.7.4 In Situ Study of the Catalytic Mixture by NMR

$[Pt_2(\mu\text{-}H)H_2(dppm)_2][PF_6]$ (.0526 g) was introduced into a 10 mm NMR tube with H_2O (.3 mL) and MeOH (1.4 mL). The tube was then sealed under CO (.51 atmospheres) and heated to 100°C for 3.5 h. The ^{31}P NMR was then run at 60°C for 3 h and the tube was then heated to 100°C for an additional 18.5 h. The ^{31}P NMR was then obtained at 60°C over a time period of 4 hours. The tube was then opened and an IR spectrum of the solid was recorded. The liquid layer was then evaporated and an IR spectrum of the remaining solid was obtained.

References

1. D. McDonald and L.B. Hunt, "A History of Platinum and its Allied Metals", Johnson Matthey, London, 1982.
2. J.C. Marriott, J.A. Salthouse, M.J. Ware and J.M. Freeman, J. Chem. Soc. Chem. Comm., 595 (1970).
3. V.G. Albano, P.L. Bellan and V. Scatturn, J. Chem. Soc. Chem. Comm., 507 (1966).
4. S. Otsuka, T. Yoshida, M. Matsumoto and K. Nakatsu, J. Am. Chem. Soc., 98, 5850 (1976).
5. J.R. Boehm and A.L. Balch, J. Organomet. Chem., 112, C20 (1976).
6. F.R. Hartley,"The Chemistry of Platinum and Palladium", Applied Science, London, 1973.
7. J.D. Schagen, A.R. Overbeek and H. Schenk, Inorg. Chem., 17, 1938 (1978).
8. U. Belluco, "Organometallic and Coordination Chemistry of Platinum", Academic Press, London, 1974.
9. J.K. Kochi, "Organometallic Mechanisms and Catalysis", Academic Press, London, 1978.
10. J. Chatt and B.L. Shaw, J. Chem. Soc., 5075 (1962).
11. G.M. Whitesides, E.J. Panek and E.R. Stedronsky, J. Am. Chem. Soc., 94, 232 (1972).
12. F.R. Hartley, "Comprehensive Organometallic Chemistry", G. Wilkinson, F.G.A. Stone, and E.W. Abel Eds., Pergamon Press, Toronto, Chapter 39, 1982.
13. J. Chatt and B.L. Shaw, J. Chem. Soc., 705 (1959).
14. J. Chatt and B.L. Shaw, J. Chem. Soc., 4020 (1959).
15. R.J. Kazauskas and M.S. Wrighton, Organometallics, 1, 602 (1982).

16. D.G. Kalina, T.J. Marks and W.A. Wachter, J. Am. Chem. Soc., 99, 3877 (1977).

17. G. Abis, A. Sen and J. Halpern, J. Am. Chem. Soc., 100, 2915 (1978).

18. C.L. Duncan, R.J. Puddephatt and C.F.H. Tipper, J. Organomet. Chem., 186, 419 (1980).

19. H. Schmidbaur, J.R. Mandl, A. Frank and G. Huttner, Chem. Ber., 109, 466 (1976).

20. M.P. Brown, R.J. Puddephatt and M. Rashidi, Inorg. Chim. Acta , 19, L33 (1976).

21. M.P. Brown, R.J. Puddephatt, M. Rashidi and K.R. Seddon, J. Chem. Soc. Dalton, 951 (1977).

22. M.P. Brown, R.J. Puddephatt, M. Rashidi, Lj. Manojlović-Muir, K.W. Muir, T. Solomon and K.R. Seddon, Inorg. Chim. Acta , L33 (1977).

23. M.P. Brown, S.J. Franklin, R.J. Puddephatt, M.A. Thomson and K.R. Seddon, J. Organomet. Chem., 178, 281 (1979).

24. R.J. Puddephatt, Chem. Soc. Rev., 12, 99 (1983).

25. M.P. Brown, R.J. Puddephatt, M. Rashidi and K.R. Seddon, J. Chem. Soc. Dalton, 516 (1978).

26. M.P. Brown, J.R. Fisher, Lj. Manojlović-Muir, K.W. Muir, R.J. Puddephatt, M.A. Thomson and K.R. Seddon, J. Chem. Soc. Chem. Comm., 931 (1979).

27. M.P. Brown, J.R. Fisher, R.H. Hill, R.J. Puddephatt and K.R. Seddon, Inorg. Chem., 20, 3516 (1981).

28. M.P. Brown, J.R. Fisher, A.J. Mills, R.J. Puddephatt and M.A. Thomsdn, Inorg. Chim. Acta, 44, L271 (1980).

29. R.J. Puddephatt, "Catalytic Aspects of Metal Phosphine Complexes", Advances in Chemistry Series, 196, E.C. Alyea and D.W. Meek, Eds., Am. Chem. Soc., 1982.

30. K.A. Azam and R.J. Puddephatt, Organometallics, 2, 1396 (1983).

31. M.P. Brown, S.J. Cooper, A.A. Frew, Lj. Manojlović-Muir, K.W. Muir, R.J. Puddephatt and M.A. Thomson, J. Chem. Soc. Dalton, 299 (1982).

32. M.P. Brown, S.J. Cooper, A.A. Frew, Lj. Manojlović-Muir, K.W. Muir, R.J. Puddephatt, K.R. Seddon and M.A. Thomson, Inorg. Chem., 20, 1500 (1981).

33. K.A. Azam, M.P. Brown, S.J. Cooper and R.J. Puddephatt, Organometallics, 1, 1183 (1982).

34. Prepared by the method used for Synthesis of $[Pt_2Me(dppm)_3]^+$.[61] K.A. Azam, M.P. Brown, R.H. Hill, R.J. Puddephatt, and A. Yavari, Manuscript in preparation.

35. E.L. Muetterties and J. Stein, Chem. Rev., 79, 479 (1979).

36. A.J. Deeming, "Transition Metal Clusters", B.F.G. Johnson, Ed., Wiley, New York, Pg.391, (1980).

37. M.H. Chisholm, Ed., "Reactivity of Metal-Metal Bonds", Am. Chem. Soc. Symposium Series, 155, 327 (1981).

38. S.A.R. Knox, J.W. Koepke, M.A. Andrews, and H.D. Kaesz, J. Am. Chem. Soc., 97, 3942 (1975); Y. Doi, K. Koshizuka and T. Keii, Inorg. Chem., 21, 2732 (1982).

39. A.P. Sattelburger, R.B. Wilson Jr. and J.C. Huffman, J. Am. Chem. Soc., 102, 7113 (1980).

40. J.J. Bonnet, A. Thorez, A. Maisonnat, J. Galy and R. Poilblanc, J. Am. Chem. Soc., 101, 5940 (1979).

41. C.P. Kubiak, C. Woodcock and R. Eisenberg, Inorg. Chem., 21, 2119 (1982).

42. T.H. Tulip, T. Yamagata, T. Yoshida, R.D. Wilson, J.A. Ibers and S. Otsuka, Inorg. Chem., 18, 2239 (1979); T. Yoshida, T. Yamagata, T.H. Tulip, J.A. Ibers and S. Otsuka, J. Am. Chem. Soc. 100, 2063 (1978).

43. J.R. Norton, Acc. Chem. Res., 12, 139 (1979).

44. S.G. Davies, J. Hibberd, S.J. Simpson and O. Watts, J. Organomet. Chem., 241, C31 (1983).

45. M.J. Church, M.J. Mays, R.N.F. Simpson and F.P. Stefanini, J. Chem. Soc. A, 2909 (1970); M.J. Mays, R.N.F. Simpson and F.P. Stefanini, J. Chem. Soc. A, 3000 (1970).

46. E.L. Muetterties and P.L. Watson, J. Am. Chem. Soc., 98, 4665 (1976).

47. T. Yoshida, Y. Ueda and S. Otsuka, J. Am. Chem. Soc., 100, 3941 (1978).

48. H.C. Clark, A.B. Goel and C.S. Wong, Inorg. Chim. Acta , 34, 159 (1979).

49. G.K. Anderson, H.C. Clark and J.A. Davis, Organometallics, 1, 550 (1982).

50. R.S. Paonessa and W.C. Trogler, J. Am. Chem. Soc., 104, 1138 (1982).

51. K. Kitaura, S. Obara and K. Morokuma, J. Am. Chem. Soc., 103, 2891 (1981).

52. J.O. Noell and P.J. Hay, J. Am. Chem. Soc., 104, 4578 (1982).

53. R. DiCosimo and G.M. Whitesides, J. Am. Chem. Soc., 104, 3601 (1982).

54. L. Abis, A. Sen and J. Halpern, J. Am. Chem. Soc., 100, 2915 (1978).

55. P.S. Braterman, R.J. Cross and G.B. Young, J. Chem. Soc. Dalton, 1306 (1976).

56. L.M. Bavaro, P. Montangero and J.B. Keister, J. Am. Chem. Soc., 105, 2977 (1983).

57. T.E. Bitterwolf and A.C. Ling, J. Organomet. Chem., 57, C15 (1973).

58. T.E. Bitterwolf, J. Organomet. Chem., 252, 305 (1983).

59. J. Halpern, Inorg. Chim. Acta , 62, 31 (1982); R.G. Bergman, Accts. Chem. Res., 13, 113 (1980).

60. R.J. Puddephatt and M.A. Thomson, Inorg. Chem., 21, 725 (1982).

61. K.A. Azam, R.J. Puddephatt, M.P. Brown and A. Yavari, J. Organomet. Chem., 234, C31 (1982).

62. Theoretical studies indicate that either exo or endo (often termed attack at the pocket position of the A-frame) attack is possible, and examples of both are known, see ref. 63 and references therein.

63. D.M. Hoffman and R.Hoffmann, Inorg. Chem., 20, 3543 (1981).

64. The ^{1}H N M R Spectra of the Complex Cation (IV) were recorded by K.A. Azam.

65. B.L. Shapiro and M.D. Johnston Jr., J. Am. Chem. Soc., 94, 8185 (1972).

66. P.B. Chock and J. Halpern, J. Am. Chem. Soc., 88, 3511 (1966).

67. F. Basolo and R.G. Pearson, "Mechanisms of Inorganic Reactions", 2nd ed., Wiley, New York, 1967.

68. R.J. Puddephatt, K.A. Azam, R.H. Hill, M.P. Brown, C.D. Nelson, R.P. Moulding, K.R. Seddon and M.C. Grossel, J. Am. Chem. Soc., 105, 5642 (1983).

69. The kinetic expression (equation 2.11) does not constitute a proof of the proposed mechanism, since a similar expression would be obtained if the mechanism were described by the equation:-

$$(III) \overset{K}{\rightleftharpoons} (Ia) + L \overset{k}{\longrightarrow} (II) + H_2$$

70. The accelerating effect of bulky ligands on reductive elimination in mononuclear complexes is well-established. See for example J.U. Mondal and D.M. Blake, Co-ord. Chem. Rev., 47, 205 (1982).

71. A.L. Balch, "Homogeneous Catalysis with Metal Phosphine Complexes", L. Pignolet Ed., Plenum, New York, in press.

72. R.J. Puddephatt, M.A. Thomson, J. Organomet. Chem., 238, 231 (1982).

73. The Closest Model is $[Pt_2Me_3(\mu\text{-dppm})_2]^+$ shown in Chapter 1 as Structure (1.9).

74. It has been shown that cis-trans isomerization occurs readily in mononuclear complexes $[PtH_2L_2]$,[50] and reductive elimination of the mutually trans H^a and H^b in complex (IV), Scheme, is unlikely.[50-52]

75. Hydride migration in binuclear platinum complexes by terminal $\rightleftharpoons$ bridging hydride transformations is well-known.[25,42,68]

76. K.P.C. Vollhart and T.W. Wejdman, J. Am. Chem. Soc., 105, 1676 (1983).

77. Complexes such as $[HPt(PPh_3)_3]^+$ are deprotonated readily to give $[Pt(PPh_3)_3]$.[8]

78. We recognise that the H.O.M.O. may actually be a non-bonding d-orbital on Pt, but this will be the highest σ-M.O.

79. R.G. Pearson, "Symmetry Rules for Chemical Reactions", Wiley, New York, 1976.

80. Metal-metal donor-acceptor bonds are now common in this area of chemistry.[32,81]

81. D.M. McEwan, P.G. Pringle and B.L. Shaw, J. Chem. Soc. Chem. Comm., 859 (1982).

82. Note that a mechanism involving loss of H^+ from (IV) followed by formal recombination with H^- is ruled out by the proof that the reductive elimination is intramolecular.

83. Noell and Hay calculated $\Delta H°$ +30 kJ mol^{-1} for reductive elimination of H_2 from cis-$[PtH_2(PMe_3)_2]$.[52] If we assume that $\Delta H°$ for the reaction (III) → (V) balances that for the rearrangement of (VI) − (II), then the reaction (III) → (II) + H_2 will also have $\Delta H° \sim$+30 kJ mol^{-1}. Note that $T\Delta S$ +40 kJ mol^{-1} is a typical value for a dissociative reaction and that (IIIa) → (Ia) + PPh_3 gives $T\Delta S$ +42 kJ mol^{-1}.

84. H.C. Foley, R.H. Morris, T.S. Targos and G.L. Geoffroy, J. Am. Chem. Soc., 103, 7337 (1981).

85. If the bridge splitting reaction (III) → (V) were rate determining, a significant isotope effect might also be observed but a smaller value for $\Delta S^{\ddagger}$ would be expected.

86. Note for example that H^a and H^b in complex (V) are equivalent, yet no exchange between terminal and bridging hydride in (IIIa) is seen up to 253 K. Hence $\Delta G^{\ddagger}$ for (III) → (V) must be greater than 50 kJ mol^{-1} and it is probable that (V) is significantly higher in energy than (III).

87. G.L. Geoffroy and M.S. Wrighton, "Organometallic Photochemistry", Academic, New York, 1979.

88. G.L. Geoffroy, Prog. Inorg. Chem., 27, 123 (1980).

89. L. Vaska and M.F. Werneke, Trans. N.Y. Acad. Sci., 33, 70 (1971).

90. G.L. Geoffroy and R. Pierantozzi, J. Am. Chem. Soc., 98, 8054 (1976).

91. A.H. Janowicz and R.G. Bergman, J. Am. Chem. Soc., 105, 3929 (1983).

92. J.P. Collman and L.S. Hegedus, "Principles and Applications of Organotransition Metal Chemistry", University Science Books, Mill Valley, Calif., 1980.

93. M.A. Green, J.C. Huffman and K.G. Caulton, J. Am. Chem. Soc., 103, 695 (1981).

94. M.L.H. Green and S.J. Simpson, J. Organomet. Chem., 148, C27 (1978).

95. J.L. Graff and M.S. Wrighton, J. Am. Chem. Soc., 103, 2225 (1981).

96. N.S. Lewis, K.R. Mann, J.G. Gordon and H.B. Gray, J. Am. Chem. Soc., 98, 7461 (1976).

97. K.R. Mann, N.S. Lewis, V.M. Miskowski, D.K. Erwin, G.S. Hammond and H.B. Gray, J. Am. Chem. Soc., 99, 5525 (1977).

98. M.P. Brown, R.J. Puddephatt, M. Rashidi, and K.R. Seddon, Inorg. Chim. Acta , L27 (1977).

99. When this work was nearing completion, we learned that G.L. Geoffroy and co-workers were conducting an independent study of the photolysis of (Ia). Where common experiments were conducted the key results of the two groups are in agreement.[84]

100. Lj. Manojlovic-Muir and K.W. Muir, J. Organomet. Chem., 219, 129 (1981).

101. S.L. Murov, "Handbook of Photochemistry", Marcel Dekker, New York, 1973.

102. E. Clar and M. Zander, Chem. Ber., 89, 749 (1956).

103. I.B. Berlman, "Handbook of Fluorescence Spectra of Aromatic Molecules", 2nd edition, Academic, New York, 1971.

104. P.J. Wagner and I. Kocharar, J. Am. Chem. Soc., 90, 2232 (1968).

105. V. Balzani, L. Moggi, M.F. Manfrin, F. Bolleta and G.S. Lawrence, Co-ord. Chem. Rev., 15, 321 (1975)

106. M.L. Grossel, R.P. Moulding and K.R. Seddon, "The Multinuclear Approach to N.M.R. Spectroscopy", NATO Advanced Study Institute, Stirling, Scotland, 1982.

107. For example, we note that, if equation (3.5) applies and if $k_d(H) \sim k_d(D)$, then the ratios $k_r(H)/k_r(D) \sim 5(CH_3CN)$ and 2.5(py) can be calculated. If, as expected, $k_d(H) \geq k_d(D)$ these should be minimum values for $k_r(H)/k_r(D)$ but, if equation (3.5) does not apply, this interpretation is invalid.

108. J.K. Hoyano and W.A.G. Graham, J. Am. Chem. Soc., 104, 3273 (1982).

109. W.D. Jones and F.J. Feher, Organometallics, 2, 562 (1983).

110. D. Milstein, J. Am. Chem. Soc., 104, 5227 (1982).

111. J. Halpern, Acc. Chem. Res., 15, 332 (1982).

112. G. Erker, J. Organomet. Chem., 134, 189 (1977).

113. G. Phillips, R.J. Puddephatt and C.F.H. Tipper, J. Organomet. Chem., 131, 467 (1977).

114. F. Ozawa, A. Yamamoto, T. Ikariya and R.H. Grubbs, Organometallics, 1, 1481 (1982).

115. D.C.L. Perkins, R.J. Puddephatt and C.F.H. Tipper, J. Organomet. Chem., 166, 261 (1979)

116. D.C.L. Perkins, R.J. Puddephatt and C.F.H. Tipper, J. Organomet. Chem., 191, 481 (1980).

117. C. Bartocci, A. Maldotti, S. Sostero and O. Traverso, J. Organomet. Chem., 253, 253 (1983).

118. T.G. Appleton, M.A. Bennett and I.B. Tomkins, J. Chem. Soc., Dalton Trans., 439 (1976).

119. S.J. Cooper, M.P. Brown and R.J. Puddephatt, Inorg. Chem., 20, 1374 (1981).

120. The quantum yield is however much higher than in acetonitrile and probably 1.

121. K.A. Azam, M.P. Brown, S.J. Cooper and R.J. Puddephatt, Organometallics, 1, 1183 (1982).

122. H.B. Abrahamson and E. Dennis, J. Organomet. Chem., 201, C19 (1980).

123. J.W. Bruno, D.G. Kalina, E.A. Mintz and T.J. Marks, J. Am. Chem. Soc., 104, 1860 (1982).

124. R.J. Kazlauskas and M.S. Wrighton, J. Am. Chem. Soc., 102, 1727 (1980).

125. R. Severson and A. Wojcicki, J. Organomet. Chem., 157, 173 (1978).

126. P.W.N.M. van Leeuwen, C.F. Roobeek and R. Huis, J. Organomet. Chem., 142, 233 (1977).

127. R. Pierantozzi, C. McLaren and G.L. Geoffroy, unpublished work quoted in ref. 87.

128. J.Y. Chen and J.K. Kochi, J. Am. Chem. Soc., 99, 1450 (1977).

129. D.L. Morse and M.S. Wrighton, J. Am. Chem. Soc., 98, 3931 (1976).

130. J.C. Luong, R.A. Faltynek and M.S. Wrighton, J. Am. Chem. Soc., 101, 1597 (1979).

131. J.C. Luong, R.A. Faltynek and M.S. Wrighton, J. Am. Chem. Soc., 102, 7892 (1980).

132. D.S. .liger and H.B. Gray, J. Am. Chem. Soc., 102, 6761 (1980).

133. T.J. IcCarthy, R.J. Nuzzo and G.M. Whitesides, J. Am. Chem. Soc., 103, .676 (1981).

134. T.J. McCarthy, R.G. Nuzzo and G.M. Whitesides, J. Am. Chem. Soc., 103, 3396 (1981).

135. M.H. Chisholm, D.A. Haitko and C.A. Murillo, J. Am. Chem. Soc., 100, 262 (1978).

136. M.H. Chisholm and D.A. Haitko, J. Am. Chem. Soc., 101, 6784 (1979).

137. M.H. Chisholm, K. Folting, D.A. Haitko and J.C. Huffman, J. Am. Chem. Soc., 104, 2138 (1982).

138. R.J. Kazlauskas and M.S. Wrighton, J. Am. Chem. Soc., 104, 6005 (1982).

139. S.-C.H. Su and A. Wojcicki, Tenth International Conference on Organometallic Chem., Toronto, Abstract IC08, August 9-14, 1981.

140. S.-C.H. Su and A. Wojcicki, Organometallics, 2, 1296 (1983).

141. T.D. Miller, M.A. St. Clair, M.K. Reinking and C.P. Kubiak, Organometallics, 2, 767 (1983).

142. K.S.Y. Lau, P.K. Wong and J.K. Stille, J. Am. Chem. Soc., 98, 5832 (1976).

143. N. Dominelli and A.C. Oehlschlager, Can. J. Chem., 55, 364 (1977).

144. M.F. Lappert and P.W. Lendor, Chem. Comm., 948 (1973).

145. A.V. Kramer and J.A. Osborn, J. Am. Chem. Soc., 96, 7832 (1974).

146. A.V. Kramer, J.A. Labinger, J.S.Bradley and J.A. Osborn, J. Am. Chem. Soc., 96, 7145 (1974).

147. P.K. Monaghan and R.J. Puddephatt, Organometallics, 2, 1698 (1983).

148. G. Ferguson, M. Parvez, P.K. Monaghan and R.J. Puddephatt, J. Chem. Soc. Chem. Comm., 267 (1983).

149. N. Chaudhury and R.J. Puddephatt, J. Organomet. Chem., 84, 105 (1975).

150. E.G. Janzen and J. I-P. Liu, J. Mag. Res., 9, 510 (1973).

151. R.E. Dessy, T.J. Flautt, H.J. Jaffe and G.F. Reynolds, J. Chem. Phys., 30, 1422 (1959).

152. A.J. Bloodworth, "The Chemistry of Mercury", C.A. McAuliffe,Ed., Macmillan Co., Toronto, 1977.

153. M.K. DeArmond and J.E. Hillis, J. Chem. Phys., 54, 2247 (1971).

154. L.S. Forster, "Concepts of Inorganic Photochemistry", A.W. Adamson and P.D. Fleichauer, Eds., J. Wiley and Sons, New York, 1975.

155. S.M. Fredericks, J.C. Luong and M.S. Wrighton, J. Am. Chem. Soc., 101, 7451 (1979).

156. D.H.W. Carsons and G.A. Crosby, J. Mol. Spec., 34, 113 (1970).

157. R.J. Watts and G.A. Crosby, J. Am. Chem. Soc., 93, 3184 (1971).

158. D.M. Klassen and G.A. Crosby, Chem. Phys. Lett., 1, 127 (1967).

159. P.J. Giordano, S.M. Fredericks, M.S. Wrighton and D.L. Morse, J. Am. Chem. Soc., 100, 2257 (1978).

160. K.L. Rollick and J.K. Kochi, J. Am. Chem. Soc., 104, 1319 (1982).

161. W.J. Heilman, A. Rembaun and M. Szwarc, J. Chem. Soc., 1127 (1957).

162. A. Citterio, Tett. Lett., 30, 2701 (1978).

163. A. Citterio, A. Arnoldi and F. Minisci, J. Org. Chem., 44, 2674 (1979).

164. H.H. Storch, N. Golumbic and R.B. Anderson, "The Fisher-Tropsch and Related Synthesis", Wiley, New York, N.Y. (1951).

165. "Catalyst Handbook", Springer-Verlag, London, 1970.

166. L.S. Kassel, J. Am. Chem. Soc., 56, 1838 (1934).

167. C.-H. Cheng; D.E. Hendriksen, R. Eisenberg, J. Am. Chem. Soc., 99, 2791 (1977).

168. R.M. Lane, R.G. Rinker and P.C. Ford, J. Am. Chem. Soc., 99, 252 (1977).

169. R.B. King, C.C. Frazier, R.M. Hanes and D.D. King, Jr., J. Am. Chem. Soc., 100, 2925 (1978).

170. T. Yoshida, Y. Ueda and S. Otsuka, J. Am. Chem. Soc., 100, 3941 (1978).

171. C.P. Kubiak and R. Eisenberg, J. Am. Chem. Soc., 102, 3637 (1980).

172. H.C. Clark and W.J. Jacobs, Inorg. Chem., 9, 1229 (1970).

173. A.A. Frew, R.H. Hill, L. Manojlovic-Muir, K.W. Muir and R.J. Puddephatt, Chem. Comm., 198 (1982).

174. J. Chatt and P. Chini, J. Chem. Soc. A, 1538 (1970).

175. A. Albinati, G. Carturan and A. Musco, Inorg. Chim. Acta, 16, L3 (1976).

176. D.C. Moody and R.R. Ryan, Inorg. Chem., 16, 1052 (1977).

177. Tetranuclear and pentanuclear clusters are also known however. R.G. Vranka, L.F. Dahl, P. Chini and J. Chatt, J. Am. Chem. Soc., 91, 1574 (1969); R. Bender, P. Braunstein, J. Fisher, L. Ricard and A. Mitschler, Nouv. J. Chem., 5, 81 (1981).

178. A. Moor, P.S. Pregosin and L.M. Venazi, Inorg. Chim. Acta, 48, 153 (1981).

179. A. Moor, P.S. Pregosin and L.M. Venanzi, Inorg. Chim. Acta, 61, 135 (1982).

180. R.G. Vranka, L.F. Dahl, P. Chini and J. Chatt, J. Am. Chem. Soc., 91, 1574 (1969).

181. P.W. Frost, J.A.K. Howard, J.L. Spencer and D.G. Turner, J. Chem. Soc. Chem. Comm., 716 (1981).

182. M.A.A.F. de C.T. Carrondo and A.C. Skapski, Acta. Cryst., B34, 1857 (1978).

183. R.B. King, D.B. Yang and A.D. King Jr., J. Am. Chem. Soc., 103, 2699 (1981).

184. T. Yoshida, Y. Ueda and S. Otsuka, J. Am. Chem. Soc., 100, 3941 (1978).

185. E.C. Baker, D.E. Hendriksen and R. Eisenberg, J. Am. Chem. Soc., 10[illegible] 1028 (1980).

186. C.G. Hatchard and C.A. Parker, Proc. Roy. Soc. (London), A235, 519 (1956).

187. N. Chaudhury , Ph.D. Thesis, University of Liverpool,Liverpool (1976).

188. P.K. Monaghan, Ph.D. Thesis, University of Western Ontario, London, 1984.

189. The correction applied was that given in ref. 183 and results in multiplication by 2.08 from the equation

$$\frac{P_{CO_2}/P_{H_2}}{1-P_{CO_2}P_{H_2}} = (RT\ K(CO_2))^{-1}\left(\frac{V_g}{V_l}\right)$$

where $K(CO_2) = 1.55 \times 10^{-2}$ mol L^{-1} atm^{-1}.

END

2803185

FIN